# SINGLE-CELL ANALYSIS OF HEMATOPOIETIC STEM CELL IDENTITY AND BEHAVIOUR

by

David Jorg Hans Fraser Knapp

B.Sc., The University of British Columbia, 2005

A THESIS SUBMITTED IN PARTIAL FULFILLMENT OF

THE REQUIREMENTS FOR THE DEGREE OF

DOCTOR OF PHILOSOPHY

in

THE FACULTY OF GRADUATE AND POSTDOCTORAL STUDIES

(Experimental Medicine)

THE UNIVERSITY OF BRITISH COLUMBIA

(Vancouver)

December 2015

## Abstract

The concept of stem cell self-renewal was developed from clonal tracking of hematopoietic stem cell (HSC) divisions *in vivo* 50 years ago. However, protocols to expand these cells *in vitro* without loss of their stem cell properties have remained elusive. A number of factors contribute to this inability. Key among these is a lack of knowledge of the critical molecular characteristics that distinguish HSCs from hematopoietic progenitors as well as how the control of the fundamental biological programs of survival, division and differentiation are integrated in HSCs. Using a combination of single-cell tracking, transcriptomics, and *in vivo* readouts applied to highly enriched mouse HSCs, we now show that their survival, proliferation, and maintenance of stem cell properties are mechanistically dissociable. Discovery of a protocol that allows input numbers of functionally intact human HSC numbers to be maintained for 3 weeks *in vitro* using defined growth factors, was then leveraged to design single human HSC cell tracking and functional analyses. The results of these showed that for human HSC, as in the mouse model, survival, proliferation, and maintenance of stem cell status are mechanistically dissociable, and controlled in a combinatorial manner. We then developed a panel of mass cytometry detectors to enable >40 surface and intracellular proteins to be simultaneously measured at single cell resolution. Using this panel, we identified some of the signaling intermediates activated by growth factors that differentially control human HSC biological responses assessed in high-throughput assays. Correlation of the molecular properties, surface phenotypes and functional activities of CD34+ subsets have further revealed a surprising degree both of heterogeneity within each phenotype and overlap between phenotypes. In some cases, the results suggest a given phenotype contains distinct subsets and a broader scheme of differentiation pathways than suggested by current models of human hematopoietic cell

differentiation. Finally, we identify $CD33^{+}$ as a novel marker which demarcates the most potent human HSC within the current best phenotypic enrichment strategy. These results lay a foundation on which future HSC expansion strategies can be constructed, and have implications for the development of leukemia.

## Preface

Chapter 2 represents a study undertaken together with Stefan Wohrer that was published in Cell Reports in 2014 under the title "Distinct stromal cell factor combinations can separately control hematopoietic stem cell survival, proliferation, and self-renewal". Single clone transplants, LTC-IC split doublet analyses, growth kinetic experiments, cell processing and RNA extraction for affymetrix arrays, and growth factor survival screens were performed by Stefan and myself together. Conditioned medium washout experiments and limiting dilution transplants on previously published expansion protocols were performed by Stefan. Affymetrix hybridizations were performed by the Centre for Translational and Applied Genomics (CTAG; Vancouver, BC, Canada). I undertook all affymetrix data analyses and target identification, NGF+Col and F+S+3+6+E limiting dilution assays, and Annexin V staining for apoptosis studies. Stefan, Connie Eaves and I wrote the manuscript with approval and input from all co-authors. Stefan and I generated the figures and Stefan did the final figure arrangement. Stefan Wohrer, David Knapp, Michael Copley, Claudia Benz, Sonja Babovic, Keegan Rowe and Heidi Mader helped collect data and Stefan Wohrer, David Knapp, Michael Copley, Claudia Benz, and Sonja Babovic contributed to the interpretation of the data.

Chapter 3 has been submitted for publication under the title "Distinct molecular programs control human hematopoietic stem cell survival, proliferation and maintenance". Connie Eaves and I designed the experiments and wrote the manuscript. I performed all experiments assisted by Colin Hammond and Paul Miller. I performed the final data analysis. Paul Miller, Philip Beer, Alice Cheung, Keith Humphries, Guy Sauvageau, and Peter Zandstra assisted with experimental designs and interpretation. Nima Aghaeepour, Davide Pellacani and Karen Sachs helped with data analysis and interpretation. Gabrielle Rabu assisted with xenograft analyses. Marketa

Ricicova, Véronique Lecault, Daniel Da Costa, and Michael VanInsberghe assisted with microfluidics cell cultures. Sean Bendall and Garry Nolan assisted with the design of the CyTOF panel and experiments. Wendy Qiao and WeiJia Wang performed CyTOF experiments on alternative growth factor cocktails. James Piret and Carl Hansen assisted with the single-cell culture experimental design and interpretation of the results.

Chapter 4 is being prepared for publication. Connie Eaves and I designed the experiments and wrote the manuscript. I oversaw the execution of all experiments, collected the final data and performed the data analysis. Barcoding reagents were kindly provided by Fluidigm. Eli Zunder, Rachel Fink, and Greg Behbahani shared the barcoding protocol. Sean Bendall and Garry Nolan assisted with the design of the CyTOF panel. Nima Aghaeepour, and Davide Pellacani assisted with data analysis and interpretation. Paul Miller, Colin Hammond, Philip Beer, Carl Hansen, and Martin Hirst assisted with experimental designs and data interpretation.

# Table of Contents

**Abstract** ..... **ii**

**Preface** ..... **iv**

**Table of Contents** ..... **vi**

**List of Tables** ..... **xii**

**List of Figures** ..... **xiv**

**List of Abbreviations** ..... **xvii**

**Acknowledgements** ..... **xxii**

**Dedication** ..... **xxiv**

**Chapter 1: Introduction** ..... **1**

1.1 Historical origin and clinical relevance of transplantable of hematopoietic cells ..... 1

1.2 The hematopoietic hierarchy; classical approaches to compartment definitions ..... 4

1.3 HSC regenerative activity *in vivo* ..... 8

1.3.1 Origin, expansion and maintenance of steady state HSCs populations ..... 9

1.3.2 Hematopoietic cell types with variable regenerative properties in myeloablated recipients -mouse ..... 14

1.3.3 Hematopoietic cell types with variable regenerative properties in myeloablated recipients -human ..... 15

1.4 Heterogeneity in HSCs ..... 20

1.4.1 Mouse ..... 20

1.4.2 Human ..... 21

1.5 Regulation of HSC behaviour and heterogeneity ..... 22

1.5.1 Intrinsic control of HSC potential ..... 23
1.5.2 Extrinsic control of HSC functions ..... 27
1.5.3 Mechanisms of HSC control are interconnected ..... 32
1.6 Tools for the analysis of single cell molecular states and behaviour ..... 34
1.6.1 Flow cytometry and index sorting ..... 34
1.6.2 Proteomic analysis using mass cytometry ..... 35
1.6.3 Single cell sequencing ..... 39
1.6.4 Single-cell fate tracking ..... 40
1.7 Thesis objectives ..... 41
**Chapter 2: Survival, proliferation and stem cell identity can be differentially controlled in murine HSC ..... 47**
2.1 Introduction ..... 47
2.2 Methods ..... 49
2.2.1 Mice ..... 49
2.2.2 UG26 cells and CM ..... 50
2.2.3 ESLAM cell cultures ..... 50
2.2.4 HSC transplantation assays ..... 52
2.2.5 LTC-IC assays ..... 53
2.2.6 Microarray analyses ..... 54
2.2.7 Statistical analysis ..... 56
2.3 Results ..... 56
2.3.1 Stromal cell-derived factors enhance the output of DSR-HSCs *in vitro* in the presence of SF+IL-11 ..... 56

2.3.2 UG26 cells produce factors that in combination with SF+IL-11 enable all HSC differentiation programs to be sustained ..... 59
2.3.3 Different factors separately regulate HSC survival and mitogenesis ..... 62
2.3.4 NGF and Col 1 can partially replace UG26 CM in maintaining DSR activity during HSC expansion *in vitro* ..... 64
2.4 Discussion ..... 66
2.4.1 Stromal cells produce factors that synergize with SF and IL-11 to promote DSR-HSC self-renewal divisions *in vitro* ..... 66
2.4.2 The effects of stromal factors on HSC self-renewal in vitro are manifest within the first cell cycle and act to preserve the HSC lineage program as well as their DSR state ..... 69
2.4.3 Implications for future improvement of HSC expansion protocols ..... 71
**Chapter 3: Distinct programs control human hematopoietic stem cell survival, proliferation and maintenance ..... 87**
3.1 Introduction ..... 87
3.2 Methods ..... 89
3.2.1 Human CB cells ..... 89
3.2.2 *Ex vivo* HSC expansion experiments ..... 90
3.2.3 HSC quantification in immunodeficient mice ..... 91
3.2.4 Single-cell cultures ..... 92
3.2.5 Mass cytometric analysis ..... 94
3.2.6 Data analysis ..... 95
3.3 Results ..... 96
3.3.1 21-day *ex vivo* maintenance of serially transplantable human HSCs in 5 GFs ..... 96

3.3.2 HSC survival and proliferation are differentially controlled by specific GFs ..... 97
3.3.3 GF conditions that differentially support HSC survival and proliferation show equivalent maintenance of their regenerative activities ..... 99
3.3.4 Single GFs activate distinct signaling spectra, and additional pathways in combination ..... 99
3.3.5 Discussion ..... 101
**Chapter 4: Primitive human hematopoietic cells comprise a complex continuum of multiple functional states ..... 122**
4.1 Introduction ..... 122
4.2 Methods ..... 123
4.2.1 Umbilical cord blood ..... 123
4.2.2 Flow cytometry and index sorting ..... 124
4.2.3 Mass cytometric analysis ..... 124
4.2.4 *In vitro* assays of CFC and LTC-IC activity ..... 125
4.2.5 Repopulation assays ..... 126
4.2.6 Data analysis ..... 127
4.3 Results ..... 130
4.3.1 Data scaling reduces variability between samples and reveals differences between fresh, cryopreserved and briefly cultured cells ..... 130
4.3.2 Conventionally defined phenotypic subsets of $CD34^+$ CB cells are molecularly heterogeneous ..... 132
4.3.3 Cells with different myeloid and erythroid differentiation properties also show distinct but overlapping molecular profiles ..... 134

4.3.4 Identification of functionally and molecularly distinct subsets of HSCs in human CB ..... 136

4.3.5 The most primitive human HSC reside in the $CD33^{+}$ sub-fraction of $CD49f^{+}$ cells ..... 137

4.4 Discussion ..... 138

**Chapter 5: Conclusions/implications/future directions and opportunities .....167**

5.1 Major contributions ..... 167

5.2 Implications and future directions ..... 171

5.2.1 The utility and limitations of surface phenotype in identification of cell populations ..... 171

5.2.2 Towards a molecular description of lineage restriction in primitive human hematopoietic cells ..... 173

5.2.3 Implications for *ex vivo* human HSC expansion ..... 174

5.3 Concluding remarks ..... 178

**Bibliography .....179**

**Appendices .....209**

Appendix A ..... 209

A.1 REACTOME pathways (n=250) with significantly altered transcript expression in ESLAM cells maintained in S+11+UG26 CM. ..... 209

A.2 Secreted factor mRNAs (n=172) produced by UG26 cells with predicted interactions with the products of genes expressed by activated ESLAM cells. ..... 215

Appendix B ..... 220

B.1 Additional relative marker intensities of the nearest neighbours for each myeloid CFC type. ..... 221

B.2 Additional relative marker intensities of the nearest neighbours of highly proliferative LTC-IC compared to all others. ..... 223

## List of Tables

Table 2.1 Concentration of additives used in single ESLAM cell survival screens ..... 73

Table 2.2 Significantly affected pathways of ESLAM cells upon stimulation with UG26 CM and SF+IL-11. ..... 74

Table 3.1 Antibodies used for isolation of $CD49f^+$ cells. ..... 103

Table 3.2 Total numbers of cells produced from 1,000 $CD49f^+$ cells in 21-day cultures and cell numbers removed by EasySep$^{TM}$ selection steps performed on days 12 and 17. ..... 103

Table 3.3 Antibodies used for detecting human hematopoietic cells in the bone marrow of transplanted mice. ..... 103

Table 3.4 Antibodies and fluorophores used for assessing human hematopoietic progenitor content as well as total chimerism in the bone marrow of transplanted mice. ..... 104

Table 3.5 Antibodies used for the CyTOF analyses. ..... 105

Table 3.6 HSC frequencies in $CD49f^+$ cells and their progeny present in 21-day cultures (described in Figure 3.2A) derived by LDA of primary transplanted mice..... 106

Table 3.7 Numbers of cells/experiments included in the analysis of survival, proliferation and division kinetics. ..... 107

Table 4.1 Antibodies used in progenitor cell index sorts..... 143

Table 4.2 Antibody staining panel for bulk sub-setting of the CD49f compartment. ..... 143

Table 4.3 Antibodies used in HSC index sorts. ..... 143

Table 4.4 Sample cryo-preservation status, donor number, and palladium isotope labeling (1= presence, 0=absence) ..... 144

Table 4.5 Antibodies used in the mass cytometric analyses. ..... 145

Table 4.6 Number of cells for each $CD34^{+}CD38^{-}CD45RA^{-}CD90^{+}CD49f^{+}$ subset injected per mouse. ..... 146

Table 4.7 Cell numbers per progenitor population associated with each sample. ..... 147

## List of Figures

Figure 1.1 The classic model of the hematopoietic hierarchy. ..... 44

Figure 1.2 A revised model of the hematopoietic hierarchy. ..... 45

Figure 1.3 A further revision to the hematopoietic hierarchy. ..... 46

Figure 2.1 Comparison of the number of HSCs present in 7-day cultures of ESLAM cells containing different growth factor cocktails and supplements. ..... 75

Figure 2.2 Comparison of the different reconstitution kinetics obtained in mice transplanted with matched progeny outputs of ESLAM cells cultured for 7 days with different stimuli. ..... 77

Figure 2.3 Comparison of the effect of different supplements on the frequency of HSC-containing clones and their differentiation patterns in 7-day cultures initiated with single ESLAM cells. ..... 78

Figure 2.4 UG26 CM enhances the retention of DSR-HSC functionality in the first division progeny of single ESLAM cells. ..... 79

Figure 2.5 Comparison of the serial GM-, B-, and T-cell reconstituting activities of the 2 β-HSCs and their progeny produced from the first *in vitro* division of a single ESLAM cell. ..... 81

Figure 2.6 UG26 CM and SF+IL-11 support the frequent production of LTC-ICs in both progeny of single ESLAM cells stimulated to divide *in vitro*. ..... 82

Figure 2.7 Comparison of the different mitogenic and pro-survival activities of UG26 CM, SF+IL-11 and the combination on ESLAM cells in single cell cultures. ..... 83

Figure 2.8 Col 1 and NGF can substitute for UG26 CM to support DSR-HSC self-renewal *in vitro*. ..... 85

Figure 3.1 Examples of FACS profiles from LDA experiments. ..... 108

Figure 3.2 A defined medium supplemented with 5 GFs maintains fully functional human HSC numbers over a 21-day period *in vitro*. ..... 109

Figure 3.3 Survival and proliferative responses of $CD49f^+$ cells are independently and combinatorially regulated. ..... 111

Figure 3.4 Pair-wise significance testing of differences in survival, recruitment into division, and time to complete a first division..... 113

Figure 3.5 Multiple GF combinations sustain *in vivo* HSC functionality for 4 days *in vitro*. .... 115

Figure 3.6 Gating hierarchy for $CD49f^+$ cells from CyTOF data. ..... 117

Figure 3.7 Different GFs alone and in combination activate different signaling responses in $CD49f^+$ cells. ..... 118

Figure 3.8 Population distributions based on their molecular characteristics following stimulation with individual GFs..... 120

Figure 3.9 Signal activation in alternative GF cocktails. ..... 121

Figure 4.1 Gating for progenitor populations from CyTOF data..... 148

Figure 4.2 Molecular overlap between samples with and without data scaling. ..... 149

Figure 4.3 Molecular overlap between samples including cells exposed to culture. ..... 151

Figure 4.4 Phenotypic progenitor distribution across molecular space. ..... 153

Figure 4.5 Transcription factor levels across human progenitor molecular distribution. ..... 154

Figure 4.6 Relative levels intracellular proteins in phenotypic progenitor populations. ..... 155

Figure 4.7 Gating for CMP sub-populations..... 156

Figure 4.8 Differences in molecular markers between CMP sub-populations. ..... 157

Figure 4.9 Index sorted myeloid progenitor frequencies. ..... 158

Figure 4.10 Myeloid colony forming cell distribution in molecular space..... 159

Figure 4.11 Significant differences in surface and intracellular markers between myeloid colony forming cells. ..... 160

Figure 4.12 Index sorted long-term culture initiating cell frequencies. ..... 161

Figure 4.13 Long-term culture initiating cell distribution in molecular space. ..... 162

Figure 4.14 Significant differences in surface and intracellular markers between highly proliferative long-term culture initiating cells and others. ..... 163

Figure 4.15 Gating hierarchy for $CD49f^{+}$ subsets. ..... 164

Figure 4.16 Secondary repopulating activity is restricted to the $CD33^{+}$ sub-population of $CD49f^{+}$ cells. ..... 165

Figure 4.17 Waddington landscapes of the human progenitor hierarchy. ..... 166

## List of Abbreviations

| | |
|---|---|
| 5-FU | 5-fluorouracil |
| 4-HC | 4-hydroperoxycyclophosphamide |
| AGM | Aorta-Gonad-Mesonephros |
| Angptl | Angiopoietin-like |
| BM | Bone Marrow |
| BMP | Bone Morphogenic Protein |
| CADM | Congruence Among Distance Matrices |
| CB, UCB | Umbilical Cord Blood |
| CCD | Charge-Coupled Device |
| $CD49f^{+}$ | $CD34^{+}CD38^{-}CD45RA^{-}CD90^{+}CD49f^{+}$ |
| CFC | Colony-Forming Cell |
| CFU-S | Colony forming units-spleen |
| ChIP-seq | Chromatin Immuno-Precipitation sequencing |
| CLP | Common Lymphoid Progenitor |
| CM | Conditioned Medium |
| CMP | Common Myeloid Progenitor |
| Col | Collagen |
| CSB | Cell Staining Buffer |
| DAB | Data Above Background |
| DREMI | conditional-Density Resampled Estimate of Mutual Information |
| DSR | Durable Self-Renewal |
| EGFR | Epidermal Growth Factor Receptor |

| | |
|---|---|
| ELDA | Extreme Limiting Dilution Analysis |
| EPO | Erythropoietin |
| ESLAM | $CD45^{+}EPCR^{+}CD48^{-}CD150^{+}$ |
| FACS | Fluorescence Activated Cell Sorting |
| FBS | Fetal Bovine Serum |
| FDR | False Discovery Rate |
| FGF1 | Fibroblast Growth Factor 1 |
| FLT3L | Fms-like tyrosine kinase 3 ligand |
| FMO | Full-Minus-One |
| G-CSF | Granulocyte-Colony-Stimulating Factor |
| GEMM | granulocyte, erythrocyte, monocyte megakaryocyte |
| GFs | Growth Factors |
| GM | Granulocyte-Macrophage |
| GM-CSF | Granulocyte-macrophage colony-stimulating factor |
| GMP | Granulocyte-Macrophage Progenitor |
| GO | Gene Ontology |
| GVHD | Graft vs Host Disease |
| HLA | Human Leukocyte Antigen |
| HSBS | Hank's Balanced Salt Solution |
| HSC | Hematopoietic Stem Cell |
| ICP-MS | Inductively Coupled Plasma Mass Spectrometry |
| IdU | 5-iodo-2-deoxyuridine |
| IGFBP2 | Insulin Growth Factor-Binding Protein 2 |

| | |
|---|---|
| IGF2 | Insulin-like Growth Factor 2 |
| IL11, IL-11 | Interleukin-11 |
| IL3, IL-3 | Interleukin-3 |
| IL6, IL-6 | Interleukin-6 |
| IMDM | Iscove's Modified Dulbecco's Medium |
| IPSC | Induced Pluripotent Stem Cell |
| IQR | Interquartile Range |
| ITRC | Intermediate-Term Repopulating Cell |
| KEGG | Kyoto Encyclopedia of Genes and Genomes |
| LSR | Limited Self-Renewal |
| LT | Long-Term |
| LTC-IC | Long-Term Culture Initiating Cell |
| MEP | Megakaryocyte-Erythroid Progenitor |
| MHC | Major Histocompatibility Complex |
| miR | micro-RNA |
| MLP | Multi-Lymphoid Progenitor |
| mPB | Mobilized Peripheral Blood |
| MPP | Multi-Potent Progenitor |
| Msi2 | Musashi-2 |
| NA10hd | NUP98-HOXA10homeodomain |
| NGF | Nerve Growth Factor |
| NIA | National Institute of Aging |
| NK | Natural Killer cell |

| | |
|---|---|
| NOD | Non-Obese Diabetic |
| NRG | NOD.Cg-Rag1$^{tm1Mom}$ Il2rg$^{tm1Wjl}$/SzJ |
| NSG | NOD.Cg-Prkdc$^{scid}$Il2rγ$^{tm1Wjl}$/SzJ |
| PB | Peripheral Blood |
| PBS | Dulbecco's Phosphate Buffered Saline |
| PCA | Principal Component Analysis |
| PDGF | Platelet Derived Growth Factor |
| PDMS | polydimethylsiloxane |
| PFTE | polytetrafluoroethylene |
| PFA | paraformaldehyde |
| PRC | Polycomb Repressive Complexe |
| PSI | Pounds per Square Inch |
| qPCR | quantitative Polymerase Chain Reaction |
| RMA | Robust Multi-Array |
| SCE | Starting Cell Equivalent |
| SCID | Severe-Combined Immune Deficient |
| SEM | Standard Error of the Mean |
| SF, SCF, KIT-L | Steel Factor, Stem Cell Factor, c-kit-ligand |
| SFM | Serum-Free Medium |
| SPADE | Spanning-tree Progression Analysis of Density-Normalized Events |
| ST | Short-Term |
| STRC | Short Term Repopulating Cell |
| TF | Transcription Factor |

| | |
|---|---|
| TGF-β | Transforming Growth Factor-Beta |
| TPO | Thrombopoietin |
| t-SNE | t-distributed Stochastic Neighbor Embedding |
| UG26 | UG26-1B6 |
| VEGF | Vascular Endothelial Growth Factor |

## Acknowledgements

First and foremost I would like to thank Connie Eaves for her unwavering support and guidance. Her undying enthusiasm and ever-questioning mind is a beacon to us all. She is a true leader in the field, and scientific mother to all of us in her lab. It has been a privilage to be a member of the Eaves lab family.

To my commitee members, Vincent Duronio, Keith Humphries, and Carl Hansen, thank you for your guidance over these years. It has undoubtedly helped to see this project to fruition.

To all the members of the Eaves lab past and present. Paul, Philip, Davide, Colin, Nima, Gaby, Maisam, Raj, Mel, Lisas (little and big), Sonja, Sneha, Long, Alice, Mike, we may scatter to the ends of the earth but we'll always be scientific family. Thank you for making the lab such a great place to spend so much time! Thank you also to Glen Edin, Margaret Hale, and Darcy Wilkinson for your expert technical support and conversation. Also thank you to Daniel Da Costa, Michael VanInsberghe, Marketa Ricicova, and Véronique Lecault who put up with my constant questions and issues, and without whom the microfluidics data could never have been obtained.

To our collaborators Garry Nolan, Sean Bendall, James Piret, Peter Zandstra, Guy Sauvageau, and their teams, thank you for your useful discussions and the knowledge you have given me, without which this project could not have reached the levels it did.

To the wonderful support staff at the TFL including Alice Chau, Amanda Kotzer and Cynthia Wong. Without you the gears of TFL would grind to a screeching halt. Thanks to Wenbo Xu in the flow core, and particularly David Ko, both for flow support, motorocycling, and training. Thanks to ARC staff for keeping our mice happy and healthy. I would also like to acknowledge all the mice who gave their lives to better our own. Your sacrifices won't be forgotten. Thanks to Karen, Dianne, Cheryl, Helen, and Lorraine in the Stem Cell Assay Lab for always being willing to pull samples for us, answer our questions, and process cord blood.

Thank you to the UBC Experimental Medicine Program. Thank you to all of the generous funding agencies who have backed my work including UBC, Vanier CGS, the Canadian Cancer Society Research Institute, ISSCR, and the BC Foundation for non-animal reserach. Also thanks to DVS Sciences/Fluidigm who contributed reagents used in the pursuit of this work.

To my previous mentor Richard Harrigan, for giving me every possible opportunity and shaping me in my formative years as a scientist. You are an amazing PI and an excellent leader. Also thanks to Art Poon for getting me started on my bioinformatic journey; you really are a magic dragon.

Thank you to my friends Brian Pantaleo, Shane Gilmore, Kevin Kimoto, Mike Azzano, Lukas Oddy, and Brent James for always being there and understanding when I'm spending yet another night in the lab. Thank you to my friends and mentors at Tong Moo Do Joseph Jung, Arneil Ona, Ethan Stuart, Eddy Tang, MJ Somani, Tim Chang, Jamie Grewal, Evan Waterman. I would also like to thank my grandmother Erica Haug for her prayers and constant curiosity.

Thank you to my dogs Spike, Lily, and Basil. Your intellectual contributions to this project were immesurable. Without your support this work could never have been completed.

Finally, I would like to unreservedly thank my parents Arno and Rita Knapp for their constant love and support. One couldn't ask for better parents.

## Dedication

*To my pack. Woof.*

# Chapter 1: Introduction

## 1.1 Historical origin and clinical relevance of transplantable of hematopoietic cells

The existence of cells with high regenerative capabilities and responsible for tissue homeostasis was first speculated in 1909 by Alexander Maximow following his early morphological studies of blood cell development (Maximow, 1909). Experimental evidence of bone marrow (BM) cells capable of reconstituting the blood-forming system came some time later from work in the 1950s that first showed the radioprotective effects of infusions of donor BM (and spleen) cells in rodents (Jacobson et al., 1951; Lorenz et al., 1951). It was subsequently demonstrated that the reconstituted blood production in the host was derived from the transplanted cells (Ford et al., 1956; Nowell et al., 1956).

Baptism of the hematopoietic stem cell (HSC) concept, however, came later from studies reported by the group led by Till and McCulloch in the 1960's. This group demonstrated that the large (macroscopically visible) colonies that formed on the spleens of reconstituted irradiated mice were, in fact, derived from single cells (Becker et al., 1963; Till and McCulloch, 1961). They also showed that these cells (which they called colony forming units – spleen, CFU-S) were often multi-potent (Wu et al., 1967, 1968), predominantly quiescent in normal adult BM, but could be activated into cycle when appropriately stimulated (Becker et al., 1965; Bruce et al., 1966), and then produced progeny CFU-S in highly variable numbers (Siminovitch et al., 1963). This work gave birth to a working definition of stem cells based on their ability to proliferate without altering their “uncommitted” differentiated state; a retrospectively determined, operationally defined, behaviour referred to as “self-renewal”. Further, they introduced the important idea that these cells, though not identifiable *a priori* were, nevertheless, quantifiable.

In parallel to the birth of hematopoiesis as a quantitative science, clinical research on the use of BM transplants was evolving. The first clinically successful non-autologous BM transplant was reported in 1957. This trial described the transplantation of BM cells from one identical twin to another, thus avoiding the issue of rejection (Thomas et al., 1959). Despite this initial success, most subsequent early attempts at BM transplantation in humans failed (Bortin, 1970). This was primarily due to an incomplete understanding at that time of the many sources of immune incompatibility that can exist between different normal individuals and cause the development of a frequently intense and sometimes prolonged and fatal graft versus host disease (GVHD). An improved understanding of Human Leukocyte Antigen (HLA) matching in the 1960's and 70's resulted in a flurry of increasingly successful clinical activity in the BM transplant field, including applications for the treatment of leukemia following intensive radiation or chemotherapy (Buckner et al., 1970), as well as for various congenital immuodeficiency disorders (Bach et al., 1968; De Koning et al., 1969; Gatti et al., 1968). Subsequent advances in the development of drugs with potent immunosuppressive activity together with improvements in preparative regimens further expanded the clinical use of HSC transplantation to include much older patients (>60 years old) (Appelbaum et al., 2011). Currently it is estimated that, 55,000-60 000 patients worldwide, receive a hematopoietic cell transplant every year as part of treatments for a wide range of diseases. These diseases include chronic and acute leukemias, lymphomas, multiple myeloma, and various autoimmune and inherited genetic disorders (Appelbaum et al., 2011).

Recognition of the broad clinical utility of hematopoietic cell transplants has been accompanied by a diversification in the sources of the cells found to be useful. Thus, the use of BM harvested from anaesthetized donors has now been largely replaced by peripheral blood

(PB) cells harvested by leukapheresis from unanaesthetized donors pretreated with hematopoietic growth factors (GFs) such as granulocyte-colony-stimulating factor (G-CSF), and/or drugs such as Plerixafor that mobilize primitive hematopoietic cells to enter the blood from the BM (Devine et al., 2004; Liles et al., 2003; Powles et al., 2000). Cord blood (CB) harvested from normal births is also now a recognized rich source of transplantable hematopoietic cells of established utility in pediatric patients. Use in adults is more limited due to inadequate numbers of required cell types in single CB collections (Appelbaum et al., 2011). CB collections are a particularly attractive source of cells for clinical transplant applications for several reasons. They are widely available and can be obtained by non-invasive procedures following most births. Their widespread cryopreservation and storage has enabled large stocks of cells of many HLA and other genotypes to be available worldwide. CB grafts have also been found to be less likely to generate acute GVHD as compared to allogeneic sources of HLA-matched mobilized PB (mPB) or adult BM transplants (Appelbaum et al., 2011). CB contains a high *concentration* of primitive hematopoietic cells (Broxmeyer et al., 1989), but the *total* number of cells in a single CB collection is relatively low for administration to adult patients, particularly for cells thought to be responsible for rapid platelet and neutrophil outputs (Cheung et al., 2012). These issues likely explain the more frequently delayed time to platelet and neutrophil recovery and increased incidence of graft failure in adult recipients of CB transplants (compared to mPB and adult BM transplants (Appelbaum et al., 2011).

The very success of hematopoietic cell transplants has stimulated greater interest than ever before in the possibility of the broader, safer and improved utility of this treatment modality if methods of significantly expanding the number of required cells were possible. However, it is becoming increasingly clear that this is unlikely to be achieved until a more complete

understanding of this very complex and vital system, its components and their modes of regulation are elucidated in a more precise fashion than has yet been achieved.

## 1.2 The hematopoietic hierarchy; classical approaches to compartment definitions

Intrinsic to the concept of a stem cell is the derivative idea of a cellular hierarchy in which stem cell properties are irreversibly lost and expression of differentiated programs are activated. Early BM transplantation experiments identified rare hematopoietic cells in mice that were capable of repopulating the blood system in myeloablated recipients and revealed some of the properties of these cells. These and subsequent studies further revealed that cells with repopulating activity include multiple prospectively separable subsets with variable durations of differentiated cell output ability and associated differences in molecular properties (Akashi et al., 2000; Doulatov et al., 2010; Galy et al., 1995; Hao et al., 2001; Kent et al., 2009; Kondo et al., 1997; Manz et al., 2002; Morita et al., 2010; Notta et al., 2011; Osawa et al., 1996). In addition, a number of *in vitro* assays to analyze the differentiation potential and other properties of primitive hematopoietic cells have been developed. For these as well, the ability to quantify the outputs of single cells, as well as features of the initial cells themselves, have been critical.

A short term *in vitro* colony-forming cell (CFC) assay that detects progenitors able to make dozens to thousands of neutrophils and/or macrophages was the first assay of this type to be developed, initially for mouse cells and later for human cells (Bradley and Metcalf, 1966; Pluznik and Sachs, 1965; Senn et al., 1967). The discovery of conditions required to support the terminal differentiation into other types of mature blood cells led to the development of similar quantitative assays for clonogenic erythroid, megakaryocyte, eosinophil and basophil progenitor numbers as well as for clonogenic progenitors of variable mixtures of these lineages.

GF combinations that support the robust growth and complete differentiation of myeloid progenitors generally fail to support the generation and differentiation of lymphoid cells. This is due, in part, to the inability of such conditions to stimulate lymphoid progenitor differentiation, and, in part, because terminally differentiated neutrophils and macrophages produce factors that inhibit lymphoid cell differentiation. Analogous *in vitro* clonogenic assays for mouse B-lineage progenitors have been developed (Vieira and Cumano, 2004). However, detection of the first stages of mouse B-cell development and all stages of human B-lineage development require co-culture of the cells with BM stromal cells or derived cell lines (e.g., OP9, MS5, M2-10B4) with or without additionally provided GFs (Doulatov et al., 2010; Nakano et al., 1994; Vieira and Cumano, 2004; Yoshikawa et al., 1999). T-cell production from both species also requires stromal co-culture conditions but with the additional need for presentation of the Notch ligands Delta-like 1 or 4 (Motte-Mohs et al., 2005).

Analysis of the time course of differentiation of the cells produced in these assays coupled with the demonstration of different properties of the cells of origin led to a proposed stepwise differentiation hierarchy of progressively restricted progenitor subsets. The initial version of this model of hematopoietic cell differentiation held that hematopoietic cells able to generate *all* blood cell lineages undergo a progressively loss of self-renewal potential prior to a subsequent split between daughters that exclusively retained either granulopoietic/megakaryocyte/erythroid potential or lymphoid differentiation potential via separate common myeloid (Akashi et al., 2000; Manz et al., 2002) and common lymphoid (Galy et al., 1995; Hao et al., 2001; Kondo et al., 1997) progenitor populations. These were then envisaged to undergo further sequential lineage restrictive events (Figure 1.1) (Reya et al., 2001).

This simple myeloid/lymphoid bifurcation model, although conceptually attractive, has subsequently come under question with more recently acquired experimental data. Indeed, even the first reports of human common lymphoid progenitors (CLPs) defined either by their $CD34^{+}Lin^{-}CD10^{+}$ (Galy et al., 1995) or $CD34^{+}CD38^{-}CD7^{+}$ (Hao et al., 2001) phenotypes were confusing in their consistently demonstrable dendritic cell output potential. Moreover, evidence was provided at that time that human $CD34^{+}CD38^{-}CD10^{+}$ cells also have granulopoietic capabilities, even when analyzed at a clonal level using a 2-stage system – first a stromal cell co-culture and then a methyl-cellulose culture step (Hao et al., 2001). Cellular phenotypes with both granulopoietic and lymphoid but no megakaryocyte/erythroid potential (Adolfsson et al., 2005; Lu et al., 2002), or T-cell progenitor activity (Bell and Bhandoola, 2008; Wada et al., 2008) were also identified in mice. More refined analysis of the differentiation potential of additional human cellular phenotypes has now enabled a similar multi-lymphoid progenitor (MLP) population that retains monocyte, macrophage, and dendritic cell activity along with lymphoid activity to be identified (Doulatov et al., 2010). Together, these more recent data suggested an updated hierarchy as depicted in Figure 1.2 (Doulatov et al., 2010, 2012).

Very recent analyses of human cells have yielded additional findings suggesting a derivative linear branching model of hematopoietic differentiation (Görgens et al., 2013). This model is based on the finding that human neutrophil progenitors are separable from those that produce basophils and eosinophils and that erythroid/megakarypoietic activity is primarily a property of $CD133^{low/-}$ cells, while $CD133^{+}$ cells have primarily granulopoietic/macrophage potential. The resultant model is thus one in which granulocyte-macrophage progenitors (GMPs) appear within the lymphoid arm of the hematopoietic hierarchy, and cast doubt on the existence of common myeloid progenitors (CMPs) as a functionally distinct population originally

conceived to include neutrophil, as well as erythroid and megakaryocyter progenitors, (Figure 1.3).

Much of the confusion over the years for the acceptance of different branch points and their sequence in the proposed hierarchical differentiation process may be due to the choices of different functional assays used to validate them. Importantly, no assay in either the mouse or the human system is capable of detecting progenitor cells at any level of currently defined differentiation programs at a clonal level with high efficiency. Thus, for any given progenitor cell type, analysis of its differentiation potential is constrained by the particular system used as the detection system. This is an important issue for human hematopoietic cells as no human phenotype has, as yet, proven to contain a functionally homogeneous progenitor population (Doulatov et al., 2010; Görgens et al., 2013). Thus any activities derived from assessments of multiple cells might represent the combined results of multiple sub-populations that happen to share the phenotype of interest, rather than additional potentials of a given progenitor cell. Adding to this confusion is the fact that assays are often performed with different GF combinations or stromal feeder layers, thus making inferences difficult to standardize between different groups of investigators.

Each assay may also not be able to activate the full potential from the input cells being assessed, even for the activities they are intended to measure. For example, Manz *et al.* showed robust B/NK cell production from $Lin^-CD34^+CD38^+CD10^+IL7R\alpha^+$ in a stromal co-culture system but failed to show such potential for $Lin^-CD34^+CD38^-$ cells (Manz et al., 2002) despite the ability of these cells to repopulate B/NK cell lineages *in vivo*. Another example was shown by Doulatov *et al.* where pre-culture of the MLP population with OP9 stromal cells increased the

frequency of cells capable of producing monocyte clones (Doulatov et al., 2010), thus demonstrating that the initial assay underestimated the myeloid potential of MLPs.

The concept of a hematopoietic hierarchy is also based on the assumption that somatic cells undergo a fixed and unique series of irreversible changes that ultimately determine the final mature differentiated state their progeny will acquire. This concept, promoted by Waddington to describe developmental processes in the embryo (Waddington and others, 1957), has been embraced to describe mechanisms of tissue maintenance in the adult organism and has clearly had substantial utility in identifying some of the underlying mechanisms of blood formation (Graf and Enver, 2009). The entire foundation of the concept of cellular 'potential' that progenitor assays strive to measure may, however, be subject to serious caveats. The ability to induce pluripotency and thus turn any cell into an induced pluripotent stem cell (IPSC) reported by Yamanaka's group in 2006 (Takahashi and Yamanaka, 2006) has demonstrated the lack of universal validity in the classical assumptions of fixed, irreversible acquired states dictating the properties of somatic cells. These findings now raise important questions as to the entire basis of differentiation hierarchies.

### 1.3 HSC regenerative activity *in vivo*

The daily and lifelong output of blood cells is remarkable. Every day a total of $2x10^{11}$ red blood, $6x10^{10}$ neutrophils, and $2.5x10^{11}$ platelets are produced in an average adult human (Eaves and Eaves, 2006). The regenerative potential of the HSCs responsible for this process must therefore be correspondingly vast, despite the fact that, at any given time throughout adult life, most of the HSCs are quiescent (in $G_0$) (Becker et al., 1965; Bruce et al., 1966). The ability of HSCs to accomplish this magnitude of mature cell output is thought to be based on the ability of

HSCs to create transient amplifying progenitor cell populations which, in turn, are responsible for the bulk of the cell expansion, and on the abilityof HSCs to maintain their own numbers by executing self-renewal divisions.

### 1.3.1 Origin, expansion and maintenance of steady state HSCs populations

Multiple successive waves of hematopoiesis have been characterized by the production of cells with differing functional characteristics throughout the development and aging of many species including mice and humans. In mice, birds, and humans, the first hematopoietic cells are produced in the blood islands of the yolk sac and consist of multipotent progenitors capable of producing nucleated red blood cells and myeloid cells (Ciau-Uitz et al., 2014; Moore and Metcalf, 1970; Moore and Owen, 1965). Early studies in which quail embryos were transplanted into chicken eggs demonstrated that, definitive hematopoiesis characterized by the production of enucleated red blood cells arises from cells located within the embryo (Dieterlen-Lievre, 1975). Subsequent transplantation experiments comparing the types of cells present in the yolk sac and within the aorta-gonad-mesonephros (AGM) region of embryonic mice before circulation is initiated suggested that definitive hematopoiesis arises in the AGM region of the embryo and is absent from the yolk sac (Cumano et al., 2001; Medvinsky and Dzierzak, 1996). Life-long tracking of the progeny of hematopoietic cells marked in the yolk sac of mice with a cre-mediated Runx1-reporter, however, has complicated this picture by showing that some cells from the yolk sac may be responsible for partially seeding other hematopoietic organs (Samokhvalov et al., 2007). Yolk-sac cells, when cultured on AGM stroma, are also able to produce cells progeny that can engraft adult mice further supporting the notion that some of the primitive hematopoietic cells from the yolk sac may seed other hematopoietic tissues (Matsuoka et al.,

2001). Nonetheless, overall evidence indicates that, at least in the mouse, primitive and definitive hematopoiesis originate primarily independently from distinct sources of cells.

The developmental origin of HSCs defined by their transplantable long-term repopulating activity has also been a topic of continuing debate. The prevailing model is that HSCs are derived from cells with endothelial features that line the dorsal aorta of the AGM. The loss of definitive HSC formation upon conditional deletion of Runx1 in the early endothelium supports this view (Chen et al., 2009). Further evidence of such a process comes from lineage tracing studies in which a tamoxiphen-inducible VE-cadherin Cre was used to track the emergence of hematopoietic cells. This latter study showed that initial endothelial cell labeling resulted in label-positive cells later in the fetal liver, as well as in the BM that had HSCs properties (Zovein et al., 2008). However, whether these HSCs arise from precursors outside the aortic endothelium or from a predetermined lineage of cells separate from those that remain as aortic endothelial cells, is not yet clear.

Following initiation of definitive hematopoiesis, and the appearance of HSCs (with long-term self-sustaining activity), their properties continue to change. For example, the vast majority of HSCs in mice are actively cycling until 3 weeks after birth and show an accompanied accelerated regenerative activity upon transplantation into myeloablated adult recipients as compared to the largely quiescent adult BM HSCs (Bowie et al., 2006, 2007a; Fleming et al., 1993; Rebel et al., 1996). These differences may be due, at least in part, to an increased sensitivity of mouse fetal liver HSCs to respond to stem cell factor (SCF, also referred to as Steel Factor (SF) or c-kit-ligand (Kit-L)) (Bowie et al., 2007b). Interestingly, there is a developmental switch that takes place in mice between 3 and 4 weeks after birth, in which these HSC properties

change abruptly (Bowie et al., 2007a). Late in life there is an additional shift in mouse hematopoiesis wherein lymphoid potential decreases (Benz et al., 2012; Rossi et al., 2005).

Many of these developmentally-timed changes in hematopoietic cells observed in the mouse, appear to be shared by human hematopoietic cells. For example, primitive human fetal liver cells appear to be actively cycling (Cashman et al., 2002), and display greater cell output activities than their counterparts in adult BM (Babovic and Eaves, 2014; Holyoake et al., 1999; Nicolini et al., 1999). Interestingly, human CB HSCs, whose counterparts in the mouse have not been investigated, appear to possess self-renewal capabilities intermediate between adult BM and fetal liver (Holyoake et al., 1999). Primitive hematopoietic cells in human fetal liver may also have increased sensitivity to GFs (Oh et al., 2000). Additionally, primitive fetal HSC in human appear to show increased ability to produce erythroid progeny in xenografts (Holyoake et al., 1999; Nicolini et al., 1999). This difference in erythroid potential may be due in part to a greater sensitivity of fetal erythroid cells to erythropoietin (EPO), a GF which in the mouse has poor cross-reactivity on the human receptor (Nicolini et al., 1999). There is also some indirect evidence of an early post-natal switch in human HSC cycling activity ~1 year after birth. This latter inference is based on the abrupt and marked change at this time in the rate of telomere loss seen in circulating neutrophils (Robertson et al., 2000). Neutrophils have a very short half-life and an assumed constant, relatively rapid output from HSCs. Thus their rate of telomere loss should provide a relatively immediate reflection of the rate of turnover of their cells of origin. With age, in humans as in mice, there is also a selective reduction in the level of circulating lymphoid cells and their very early $CD34^{+}CD38^{+}CD127^{+}$ precursors. This finding is consistent with the possibility that human HSCs with retained myelod potential but reduced lymphoid potential (Pang et al., 2011) increasingly replace those with a more balanced lympho-myeloid

output potential in later life, although exactly how this population shift is achieved has not yet been elucidated. An additional, very recently recognized age-associated phenomenon in humans is the frequent appearance of dominant clones of normal blood cells marked by mutations typically found in leukemias but, without any clinical evidence of hematologic disease in these individuals, though they do show an increased risk for such malignancies later on in life (Genovese et al., 2014; Jaiswal et al., 2014; Xie et al., 2014b).

An extremely slow rate of turnover (~every 145 days) of HSCs with long-term repopulating ability (LT-HSC) has been estimated in mice during steady-state hematopoiesis using DNA labeling with pulse chase tracing (Wilson et al., 2008). More recent cre-recombinase mediated lineage tracing has further refined these measurements, suggesting that the LT-HSCs compartment give rise to short-term (ST) HSCs at a rate of ~1/110 cells per day (Busch et al., 2015). Nonetheless, given the estimate of 17,000 LT-HSCs per mouse (Busch et al., 2015), this represents a reasonable efflux from the LT-HSC compartment even in the steady-state. Efflux rates from each downstream compartment increased progressively (Busch et al., 2015), consistent with a cascading amplification of later progenitor types.

Similar evidence for the polyclonal maintenance of steady-state mouse hematopoiesis has been obtained by tracking clones marked by transiently activated Sleeping Beauty transposon insertion sites (Sun et al., 2014). These authors showed that in the steady state, mature granulocytes appeared to be highly polyclonal, with most insertion sites observable at only one time point (Sun et al., 2014). Contributions from HSCs were not directly detectable, but the threshold for detection in this experiment was not sufficiently sensitive to detect equal contributions from all HSCs (assuming 17,000 HSC per mouse as suggested in (Busch et al., 2015)). Indeed, most observed insertion sites occurred with frequencies near the detection

threshold (Sun et al., 2014). As such, clone detection likely had a substantial stochastic component. In contrast, all groups observed a strong recruitment of the LT-HSCs following treatment of mice with 5-fluorouracil (5-FU) to transiently arrest the production of mature blood cells being continuously derived from proliferating precursors (Busch et al., 2015; Wilson et al., 2008) or following transplantation of BM cells into irradiated hosts (Sun et al., 2014). Similar results were seen in mice given high doses of G-CSF, that stimulates the proliferation of primitive quiescent HSCs without toxicity to the terminal compartments (Morrison et al., 1997; Wilson et al., 2008);. Together these findings suggest that in the mouse, unperturbed steady-state neutrophil production is numerically maintained primarily by a large "intermediate" population that has significant downstream expansion capability thus diluting out the ability to detect accompanying, much smaller inputs from LT-HSCs. The LT-HSCs are, however, capable of responding to known stimuli and, in the case of severe damage to the system, these HSCs are essential for regenerating a renewed source of cells able to provide a lifetime output of mature blood cells.

It is interesting to speculate as to the implications of these mouse data may have for human hematopoiesis. Early studies of hematopoietic cells in females with X-linked G6PD heterzygosity indicated that in normal patients hematopoiesis is polyclonal (Fialkow et al., 1981a, 1981b, 1987). Insertion site analysis of blood cells obtained from patients in gene therapy trials has further suggested that clone representation stabilizes approximately one year following transplantation and is typically highly polyclonal thereafter (Aiuti et al., 2013; Biffi et al., 2013). Perhaps the shorter lifespan and smaller size of mice (and thus lower overall cell output needs) may create lower steady state requirements for an LT-HSC contribution. This is not without precedent, given that telomere deficient HSCs in the mouse have no defects until late generations

(Lee et al., 1998) or two rounds of serial transplantation (Allsopp et al., 2003), while in humans defects are observed within a single lifespan (Blasco, 2005).

### 1.3.2 Hematopoietic cell types with variable regenerative properties in myeloablated recipients -mouse

Early outputs of mature blood cells in transplanted, lethally irradiated mice is largely provided by a phenotypically distinct population of cells, as shown by cell separation and gene marking studies. These cells make up a relatively large subset of normal mouse BM, can home into the BM of the recipient, and can generate most of the mature blood cells detected in the subsequent 2-4 weeks post-transplant. These cells lack extensive self-renewal capability and hence their output of mature cells, although rapid in onset and life-saving, are not self-sustaining. Accordingly, these cells have been called short term repopulating cells (STRCs) (Harrison and Zhong, 1992; Okada et al., 1992; Siminovitch et al., 1963; Spangrude et al., 1988; Szilvassy et al., 1990; Yamamoto et al., 2013). Some STRCs are multi-potent, whereas others appear to be restricted to a subset of lineages or even a single lineage (Harrison and Zhong, 1992; Magli et al., 1982; Yamamoto et al., 2013). Rarer cells able to sustain a somewhat more prolonged wave of mature blood cell production are referred to as γ/δ-HSCs (Dykstra et al., 2007) or intermediate-term repopulating cells (ITRCs) (Benveniste et al., 2010; Yamamoto et al., 2013). Many of these latter cells are capable of multi-lineage repopulation for an extended period (sometimes up to 24 weeks), but eventually disappear and do not produce HSCs in sufficient numbers to demonstrate repopulation of secondary mice. LT-HSC represent a subset of cells that often do not make sufficient mature progeny for these to be detectable before 8 weeks post-transplant, but they are then capable of continuing to do so for the remaining lifespan of the mouse, and produce

progeny HSCs with similar lineage output properties (Benz et al., 2012; Dick et al., 1985; Dykstra et al., 2007; Keller et al., 1985; Lemischka et al., 1986; Yamamoto et al., 2013).

### 1.3.3 Hematopoietic cell types with variable regenerative properties in myeloablated recipients -human

Analysis of the repopulation kinetics displayed by different subsets of human hematopoietic cells transplanted into myelosuppressed humans or immunodeficient mice has suggested an analogous series of successive contributions from different cell types. The existence of LTRCs was readily established from the early success of allogeneic transplants where permanent donor-derived chimerism could be readily demonstrated due to the genetic differences between donor and recipient. Evidence for STRCs came initially from the use of autografts of human cells that were treated just prior to transplant with 4-hydroperoxycyclophosphamide (4-HC), with the goal of eliminating potential residual leukemic cells. However, the use of this protocol resulted in delayed recoveries of mature platelet and neutrophil production, without long-term graft failure (Yeager et al., 1986). Xenografting studies later showed that STRC activity is largely restricted to human $CD34^{+}CD38^{+}$ cells and were historically missed because of their selective sensitivity to the residual levels of natural killer (NK) cell activity present in non-obese diabetic (NOD) - severe-combined immunodeficiency (SCID) mice that was later removed when either the β2-microglobulin or the IL2-receptor gamma chain genes were knocked out in these mice (Glimm et al., 2001). Analysis of recipients of autologous transplants of retrovirally marked cells has provided further support for the existence of human STRCs. Here, the relevant observation is that many of the integration sites seen early (11 days) post-transplant did not persist beyond ~1 month (Glimm et al., 2005;

McKenzie et al., 2005). More recent characterization of the STRC numbers and phenotypes that contribute to platelet and to neutrophil outputs within 2-4 weeks in xenografted mice have shown that they are heterogeneous in their aldehyde dehydrogenase activity (and hence would be expected to vary accordingly in their sensitivity to 4-HC) as well as including multiple lineage-restricted, as well as multipotent cell types (Cheung et al., 2012). Evidence of human ITRCs has also been recently reported. This is based on the demonstration that the $CD45RA^{-}CD90^{-}(CD49f^{-})$ subset of human $CD34^{+}CD38^{-}$ CBcells will often repopulate transplanted immunodeficient mice for up to 20 weeks, but do not display more prolonged repopulating ability nor produce progeny able to repopulate secondary hosts (Majeti et al., 2007; Notta et al., 2011).

Interestingly, GFs have also been found to differentially affect the outputs of transplanted STRCs as compared to transplanted LT-HSCs. Injection of exogenous human GFs to SCID (Lapidot et al., 1992) and later NOD-SCID mice (Cashman and Eaves, 1999; Cashman et al., 1997) of human hematopoietic cells was found early on to elicit or increase the production of differentiating human progeny. Later studies demonstrated that both the human GFs and the extent of immunodeficiency appear to affect primarily the number of cells produced by each transplanted STRC (Glimm et al., 2001; Miller et al., 2013). However, even using the most permissive immunodeficient mice now available; i.e., NOD-*SCID-IL2rγ*$^{null}$ (NSG) (Hiramatsu et al., 2003; Ito et al., 2002) and NOD-*Rag1*$^{null}$ *IL2rγ*$^{null}$ (NRG) producing human IL-3, granulocyte-macrophage colony-stimulating factor (GM-CSF) and SF transgenically (NSG-3GS and NRG-3GS), transplants of human hematopoietic cells do not produce expected levels of mature blood cells in the blood. This suggests that the microenvironment of the BM of these mice is likely still unable to elicit the full differentiation potential of engrafted human hematopoietic cells.

The definition of what is a human HSC thus remains incompletely defined. Intially, a 6-10 week endpoint of human $CD45^+$ cell production in sublethally irradiated NOD-SCID mice was used. This endpoint was determined by the fact that most grafts could not be followed longer in these mice due to their universal spontaneous development of a fatal thyoma between 6 and 12 months of age (Christianson et al., 1997), although this could be followed by a secondary transplant of similar duration (Cashman and Eaves, 1999; Cashman et al., 1997; Hogan et al., 1997, 2002; Lapidot et al., 1992). Use of the more immunodeficient NSG or also more radio-resistant NRG mice as transplant hosts (Pearson et al., 2008), permits STRC readouts, improves the levels of human chimerism obtained, and importantly, removes the risk of endogenous thymomas and allows cell outputs to be monitore for at least a year.

HSC frequencies are thus now generally measured at or around 12-16 weeks post-transplant. This represents a dauntingly protracted endpoint from a practical perspective, however recent evidence suggests that even this period may not confer the discriminatory power that the same time frame offers in the mouse system. A recent study in rhesus macaques used insertion site analysis to track the clonal repopulation of marked CD34+ cells over a 12-year period following transplantation (Kim et al., 2014). This showed that the first year following transplantation was dominated by short-term clones, and that only after approximately one year did the clonal composition stabilize (Kim et al., 2014). As noted above, similar tracking of patients treated in recent gene therapy trials for X-linked Adrenoleukodystrophy (Cartier et al., 2009), Metachromatic Leukodystrophy (Biffi et al., 2013), Wiskott-Aldrich Syndrome (Aiuti et al., 2013), and β-thalassaemia (Cavazzana-Calvo et al., 2010) have all indicated that the clone complements did not stabilize until approximately one year after the cells had been transplanted and remained highly polyclonal. These data strongly suggest that the outputs of human ITRCs if

present rather than co-transplanted LT-HSCs can dominate mature blood cell outputs for at least a year in engrafted recipients.

The prolonged period of ITRC-derived clones derived from transplanted human and non-human primate cells suggests that even a 30-week endpoint in immunodeficient mice may give a poor estimate of LT-HSC numbers or activity when the input cells are not highly purified LT-HSCs to start with. Secondary transplantation may help discriminate outputs attributable to LT-HSCs and co-transplanted ITRCs, however, secondary transplantation experiments come with their own caveats. Harvesting the BM for secondary transplant assessments can capture only a fraction of the total BM in the primary mouse. Thus, a significant *in vivo* expansion of the input HSCs would be necessary to reliably detect an initial HSC in a secondary transplant experiment. However, LTC-IC yield (and hence presumably HSCs also) appear to be generally reduced, not amplified, at least in primary NOD-SCID recipients (Pflumio et al., 1996). Additionally, when BM is harvested from the primary recipient, co-transplantation of the mouse cells present may present an uncontrolled competition to the human HSCs being assessed. On the other hand, if an attempt is made to first purify the latter, this will inevitably cause additional losses of the cells of interest, thereby further decreasing the sensitivity of the experiment.

The addition of hypomorphic *Kit* mutations to existing highly immunodeficient mouse strains has recently been found to improve mouse modeling. KIT signaling has been previously shown to be critical for the detection of transplanted mouse CFU-S (McCulloch et al., 1965), and HSCs from mice with weak but demonstrable *Kit* mutations have a competitive disadvantage relative to HSCs from mice with intact KIT receptors (Geissler and Russell, 1983). The incorporation of either the $Kit^{Wv}$ or homozygous $Kit^{W41}$ alleles into the genome of NSG mice has recently been shown to improve the human chimerism obtained in them relative to parental NSG

(Cosgun et al., 2014; McIntosh et al., 2015) or NRG mice (Miller *et al*. personal communication). The increased chimerism affects all lineages including substantial increases in erythroid cell production and the regeneration of cells with a $CD34^{+}CD38^{-}$ phenotype. Additionally, these mice can become well engrafted with human cells even without prior irradiation (Cosgun et al., 2014; McIntosh et al., 2015) (Miller *et al*. personal communication). Given the increased outputs of human cells with a phenotype characteristic of primitive cells together with higher chimerism levels (and thus fewer competing mouse cells) and the innate competitive disadvantage of the remaining mouse cells, secondary transplantation from these mice is likely to be substantially improved. Indeed, both of the recent studies have demonstrated successful secondary transplantation of human cells produced in *Kit*-mutant NSG mice (Cosgun et al., 2014; McIntosh et al., 2015). However, quantitation of the extent of HSC expansion attained in the primary mice has yet to be determined.

Overall, substantial strides have been made in delineating the types of human cells responsible for repopulating a myeloablated compatible system and the kinetics of their output activities. Thus it is now seems clear that for usual clinical sources of hematopoietic transplants, the extent of early repopulation necessary for adequate patient recovery rates relies on the presence of adequate numbers of biologically different cells than those required for long-term repopulation. There is also growing evidence of an extended, but still transient, intermediate period of regenerated hematopoiesis in recipients of human cells. This could severely compromise conclusions drawn from even the most stringent criteria currently adopted in most mouse xenograft studies. These data suggest an urgent need for improved ways to differentiate LT-HSCs, ITRCs, and STRCs without resorting to increasingly unwieldy *in vivo* assays.

## 1.4 Heterogeneity in HSCs

### 1.4.1 Mouse

Single cell transplants have demonstrated substantial heterogeneity in the functional capabilities of mouse HSCs. Such experiments have been made possible through advanced sorting strategies (Kent et al., 2009; Morita et al., 2010; Osawa et al., 1996) and been facilitated by the use of highly permissive (Kit-mutant) recipients (Geissler and Russell, 1983). Such single-cell transplants have shown that HSCs can have differing repopulation kinetics, self-renewal ability, and ability to produce platelets, myeloid, and lymphoid cells (Benz et al., 2012; Dykstra et al., 2007; Lu et al., 2011; Muller-Sieburg et al., 2004; Sanjuan-Pla et al., 2013; Sieburg et al., 2006; Yamamoto et al., 2013). Further, this property appears to be largely intrinsically regulated, as indicated by the frequent retention of the initial mature cell output profile of clonally derived and assessed progeny HSCs (Benz et al., 2012; Dykstra et al., 2007).

Interestingly, the ability to produce platelets, appears to track strongly with mouse HSC self-renewal ability (Sanjuan-Pla et al., 2013; Yamamoto et al., 2013). In extreme cases, some HSCs able to produce only platelets long-term have been reported to retain secondary repopulating capability (Yamamoto et al., 2013). However, it is important to note that, despite their maintanined self-renewal ability, HSCs that produce almost exclusively erythroid, granulocyte-macrophage (GM) cells and platelets do not produce these in greater numbers than seen in clones containing large lymphoid outputs. Moreover, the former also display defects *at multiple levels* of B-lymphoid differentiation (Benz et al., 2012). These findings argue against a selection of “myeloid” programs *at the expense of* intact lymphoid programs.

Taken together, these results provide strong evidence that for mouse HSCs expanding *in vivo*, there is a mechanistic disconnect between the control of their self-renewal ability and their lineage potentialities.

### 1.4.2 Human

In the human system, heterogeneity in the HSC compartment remains less well understood. First, improved HSC enrichment strategies are still insufficient for large-scale analyses of single-cell HSC transplants. There is also additional confounding heterogeneity of human HSC numbers and behaviour due to their mixed genetic backgrounds. In addition, immunodeficient mouse xenograft models may themselves influence differentiation outcomes differently from how these might occur in an immunocompetent, albeit myeloablated, allogeneic or autologous host. For example, residual xenogeneic (host) macrophages may play a role in clearing platelets or erythrocytes (Cheung et al., 2012). Finally, the immunodeficient state of the recipient mice provides an enhanced and continuing impetus to produce cells of the lymphoid lineage.

Nevertheless, despite these many caveats, interesting heterogeneity of clonally-derived progeny from transplanted human cells has also been observed in xenotransplant experiments. Transplantation of HSC marked with a lentiviral genetic barcodes of random sequence has been used to successfully track the repopulation kinetics of many single clones simultaneously in a single host (Cheung et al., 2013). These data once confirmed a pattern of transient waves of regenerated clones dominating early time points post transplant with unexpected heterogeneity in the kinetics and mature cell outputs of clones that were detectable for up to 27 weeks. Nearly every conceivable combination of mature cell outputs, including many uni-lineage clones were

observed even after 27 weeks. This extreme level of heterogeneity highlights the need for clonal measurements to truly dissect the potentialities of primitive human hematopoietic cells with repopulating activity. Most long-term clones read out after an initial delay; however, some showed both transient early repopulation as well as late repopulation. This latter pattern could represent an early asymmetric division in which a LT-HSC generated one STRC and one daughter LT-HSC. Perhaps more disturbing was the presence of clones that were detected for the first time, as late as 27 weeks post-transplant, and the fact that most secondary repopulating cells were never observed in the primary mouse. Together these data add further support to the idea that the outputs of human LT-HSCs may require much longer periods of observation (i.e., >1 year) than currently used in most xenograft studies. They also highlight the need for more sensitive and efficient strategies for analyzing the content of regenerated clones on a large scale.

### 1.5 Regulation of HSC behaviour and heterogeneity

Regulation of HSC behaviour can be broadly separated into the functions being affected (viability, proliferative status, stability of the existing cell state, activation of poised programs, polarity and motility) and the intrinsic and extrinsic factors that target these functions. Cell intrinsic factors include the state of the chromatin across the genome and active/available transcription factor (TF) networks. Extrinsic factors include growth factors, adjacent cell surface components, molecular elements within the extracellular matrix and nutrients. In general cell-intrinsic factors could be considered as defining the competence of a cell activating one or more functions, whereas extrinsic factors tend to govern the activation of specific cellular programs that the cell is competent to execute. However, these distinctions are somewhat arbitrary and

likely over-simplified since there are clearly extrinsic factors that can also change a cell's apparent "competence".

### 1.5.1 Intrinsic control of HSC potential

Extensive chromatin immuno-precipitation sequencing (ChIP-seq) across the mouse hematopoietic heirarchy has shown large differences in enhancer use (inferred from H3K27ac and H3K4me1/2/3 and transcription levels of nearby genes) across lineages and at different differentiation points (Lara-Astiaso et al., 2014). This study showed identified enhancers were generally available in the most primitive cells analyzed and then inactive in populations that were undergoing terminal differentiation. In addition to a progressive loss of enhancer activity, a number of new enhancers were first observed when cells started to undergo a change in differentiation status, suggesting an accompanying process of sequential replacement of one transcriptional program by another. Coincident with these changes was the expression of new transcription factors that including various canonical TFs such as PU.1 with neutrophil differentiation, GATA1 with erythroid differentiation, C/EBPα associated with GMPs and downstream genes expressed in neutrophils, and PAX5 with B-lineage cells. Interestingly, even in mature populations the authors identify a number of poised enhancers which could reflect latent capabilities not active under normal homeostatic conditions.

Transcriptomes of the different phenotypes in the human hematopoietic hierarchy have also been generated. Transcripts for TFs thought to be required for lineage specification have been found to be expressed in very early cell types, but then show increases in the relevant committed progenitor populations (Chen et al., 2014). Of note, the same study showed that non-coding RNAs were enriched in the most primitive cell populations, suggesting these may be

involved in maintaining the likelihood of a self-renewal division by actively suppressing differentiation. The requirement to suppress lineage-specific genes is supported by mouse knock-out experiments which showed that Dnmt1, a factor necessary to maintain promoter CpG methylation, was necessary for the maintenance of HSC potential (Bröske et al., 2009; Trowbridge et al., 2009).

Further support for the importance of non-coding RNAs in human hematopoiesis comes from studies of several micro-RNAs (miRs). For example, miR-126 has been reported to be expressed at high levels in human HSCs and knock-down of this miR increased HSC cycling and the generation of cells able to repopulate secondary mice (Lechman et al., 2012). In contrast, over-expression of miR-126 decreased the levels of human chimerism attained in transplanted mice, and increased the quiescence and number of human cells with a primitive phenotype. Since the levels of miR-126 in freshly isolated human HSCs are already higher than other miRNAs, it seems unlikely that the presence of this miR in HSCs is promoting a loss of HSC properties by these cells. The over-expression of this miR decreasing the ability of HSC to proliferate, but simultaneously preventing differentiation would be consistent with this interpretation as detection of these cells in a xenograft assay is highly dependent on their having undergone extensive rounds of proliferation and differentiation.

The miR-99/100~let-7c~miR125b tricistron has also been implicated in HSC regulation. In mouse cells, its over-expression was reported to increase engraftment levels in both primary and secondary transplants and, in both mouse and human cells, over-expression decreased erythroid colony formation and increased megakaryocyte differentiation (Emmrich et al., 2014). Expression levels of the let-7 miR family (under the control of Lin28/HMGA2 transcription factors) have been associated with the transition between fetal and adult HSC behaviour in the

mouse (Copley et al., 2013; Yuan et al., 2012). Similar to miRs, RNA binding proteins can also affect HSC maintenance. For example, Musashi-2 (Msi2), has been shown to be important for HSC maintenance, and knockdown or knockout of Msi2 has been shown to increase symmetric differentiation and decrease engraftment potential (Kharas et al., 2010; Park et al., 2014).

Members of the polycomb repressive complexes (PRC), responsible for H3K27me3 maintenance and bivalent histone marking, have also been associated with maintenance of HSC capabilities. One of the better characterized members is Bmi1 (a member of PRC1). Bmi1 knockout HSCs exhibit an inability to repopulate mice transplanted with these cells (Park et al., 2003), likely due to the downstream activation of the Ink4a locus (encoding $p16^{Ink4a}$ and $p19^{arf}$) and subsequent growth arrest and apoptosis (Park et al., 2003). Similar effects on human $CD34^+$ cells have also been noted following lentiviral-mediated knockdown of BMI1 (including increased p16 and apoptosis, as well as decreased CFC and LTC-IC ability (Rizo et al., 2009).

Accumulation of H3K9me2 marks have been shown to occur during differentiation and this was associated with G9a methyltransferase activity (Chen et al., 2012). Small molecule inhibitors of G9a were also shown to improve maintenance of the $CD34^+$ phenotype in cultures, and induced a very slight increase in the engraftment levels of early NSG repopulating cells. Engraftment measurements were only carried to 8 weeks post transplants, however, so potential effects on HSCs remain unknown. Nevertheless, this example shows that epigenetic modification is an important aspect of human hematopoietic progenitor cell differentiation.

Expression of TFs, as suggested by their changing transcript levels across different cell populations, is also critical to the maintenance of cell identity. This concept has been demonstrated by the reprogramming of mature mouse blood cells into HSCs by dox-inducible over-expression of Hlf, Runx1t1, Pbx1, Lmo2, Zfp37 and Prdm5 (Riddell et al., 2014). Further,

the gene expression patterns measured on 151 lineage specific genes (including TFs, epigenetic regulators, surface markers, and cell cycle indicators) following reprogramming showed patterns in a subset of single cells analyzed similar to fresh HSCs (Riddell et al., 2014). This suggests that restoring expression of particular TFs, even temporarily, can re-establish transcriptional networks and re-adjust cell programming to an alternative (primitive) state. Given the observed changes in the epigenetic state of mouse cells during differentiation (Lara-Astiaso et al., 2014), this suggests that TF expression can also alter epigenetic states.

HSC self-renewal probabilities are also regulated by TFs. HOXB4 over-expression in mouse HSCs provided an early example of a TF that can strongly increase HSC self-renewal (Antonchuk et al., 2002; Sauvageau et al., 1995). NUP98-HOXA10homeodomain (NA10hd) fusion genes were later shown to exert even more potent self-renewal promoting activity forcing nearly every division to be a self-renewal division (Ohta et al., 2007). In human cells, however, these gene products have not shown the same potency (Buske et al., 2002; Sloma et al., 2013). Interestingly, primate models suggest that in HOXB4 may influence primarily short-term repopulating cells, while NA10hd likely influences long-term HSC (though less than in mouse) (Watts et al., 2011; Zhang et al., 2006b).

Other TFs with dual roles in differentiated lineages have also been reported to regulate this HSC function. For example, Gata3, a TF that regulate T-cell programs, has been shown to be highly expressed in the most primitive mouse HSCs, and functions to decrease the self-renewal of these cells when they are stimulated to proliferate (Frelin et al., 2013). Gata2 is another example of a TF that has a lineage-specific role (in regulating megakaryocyte differentiation) but is also necessary for both the emergence and continued survival and function of mouse HSCs (Pater et al., 2013). This role of Gata2 in HSC regulation is of particular interest, given the close

association of mouse HSC self-renewal capability with retention of megakaryocyte differentiation potential(Sanjuan-Pla et al., 2013; Yamamoto et al., 2013). Tal1 (aka Scl), is a TF associated with T-cell leukemias and erythropoiesis, that has also been shown to be important for the emergence (Robb et al., 1995; Shivdasani et al., 1995), quiescence, and long-term repopulating activity of mouse HSCs (Lacombe et al., 2010; Souroullas et al., 2009).

Regulators of HSC behaviour are not, however, restricted to TFs and epigenetic modifiers. The presence of CDK6 protein in phenotypically defined human HSCs, but not multi-potent progenitors (MPPs), appears to regulate the speed of HSC exit from a quiescence state (Laurenti et al., 2015). This conclusion was based on the observation that enforced expression of CDK6 in HSCs did not affect their lineage output or compromise their long-term repopulating capabilities, but did alter the speed at which they initiated divisions *in vitro*. Levels of the cytoskeleton regulator Cdc42 appears to affect lineage capability in mouse HSCs, with (age-dependent) increased levels having an association with poor B-cell differentiation ability and decreased cell polarization (Florian et al., 2012).

### 1.5.2 Extrinsic control of HSC functions

HSCs also remain responsive to many external factors in their environment. Perhaps the best studied extrinsic regulators of HSCs are GFs. The demonstration of defective regenerative activity of normal CFU-S transplanted into *Sl/Sl*$^{d}$ hosts (McCulloch et al., 1965) led ultimately to the identification of SCF, an important GF encoded by the *Sl* gene and expressed on the surface of BM cells that are not transplanted by IV injection (Martin et al., 1990; Zsebo et al., 1990a, 1990b). Additional evidence to support the concept of HSC dependence on GFs came from *in vitro* studies of enriched sources of primitive hematopoietic cells. These showed that neither

mouse nor human HSC function can be sustained *in vitro* in media (± serum) alone and that this situation can be greatly improved when the cells are appropriately co-cultured with BM-derived stromal cells (Dexter et al., 1977; Fraser et al., 1992; Gartner and Kaplan, 1980; Sutherland et al., 1991).

A number of GFs capable of promoting both mouse and human HSC functionality have now been identified. High concentration of SCF, Fms-like tyrosine kinase 3 ligand (FLT3L), and interleukin-3 (IL3) promote the survival, growth, and expansion of long-term culture initiating cell (LTC-IC),activity in cultures initiated with highly purified primitive human cells isolated from adult BM (Petzer et al., 1996a; Zandstra et al., 1997). Interestingly, these effects are also GF concentration-dependent, with higher concentrations being required to support LTC-IC outputs compared to CFC expansion (Zandstra et al., 1997). Thrombopoietin (TPO) has also been implicated in the support of LTC-IC production, although it's addition to a combination of SCF+FLT3L+IL3+interleukin-6 (IL6)+G-CSF+nerve growth factor (NGF) did not provide additional benefit (Petzer et al., 1996a). In the mouse, SCF and interleukin-11 (IL11) have been shown to promote survival and proliferation with maintenance of 4-month repopulating activity (Audet et al., 2002; Kent et al., 2008). A number of other GF combinations and additional additives have also been reported to promote maintenance of the HSC state in either the mouse, the human, or both, including fibroblast growth factor 1 (FGF1) (de Haan et al., 2003), insulin-like growth factor 2 (IGF2) (Zhang and Lodish, 2004), insulin growth factor-binding protein 2 (IGF2BP2) (Huynh et al., 2008), members of the angiopoietin-like (Angptl) family (Zhang et al., 2006a), Wnt3a (Reya et al., 2003), pleiotrophin (Himburg et al., 2010), and immobilized Delta1 (DL1, a notch ligand) (Suzuki et al., 2006). In all cases, however, the durability of the repopulating activity of the “HSCs” produced remains questionable.

A wide array of GFs have also been characterized to antagonize HSC function. GFs shown to antagonize primitive hematopoietic cell proliferation and potentially induce apoptosis include MCP-1, MIP-1α, SDF-1, RANTES, TNF-α, and TGF-β (Bonnet et al., 1995; Cashman et al., 1990, 1998; Zhang et al., 1995). Interestingly, dilution of inhibitory factors produced by the maturing progeny of the input cells using a continuous "fed-batch" culture protocol improved the output of repopulating cells and LTC-ICs (Csaszar et al., 2012). This result highlights the negative effects of paracrine signaling resulting from of the large numbers of differentiated cells produced from GF-stimulated HSCs and/or their immediate progeny, and may represent an important mechanism of negative feedback control of HSCs *in vivo*.

It is important to note, however, that GFs can have opposite effects depending on the concentration of GF to which the target cell is exposed and the presence of other GFs. Early examples were obtained from studies of purified mouse or human HSCs exposed to excessive concentrations of SCF or IL3 (Audet et al., 2002; Ogawa et al., 1991; Zandstra et al., 1997). Even relative GF concentrations were found to affect cell responses, as shown by the fact that normally beneficial IL3 concentrations were harmful when SCF/FLT3L levels were lowered (Zandstra et al., 1997). Similarly, a number of studies have indicated that TGF-β, or signaling molecules downstream of it, can promote maintenance of primitive cell capabilities (Karlsson et al., 2007; Sitnicka et al., 1996; Yamazaki et al., 2009). Interestingly, one mechanism by which TGF-β appears to exerts its effects is by modulating cell responsiveness to other GFs, like SCF (Jacobsen et al., 1995), possibly by inhibiting GF-stimulated clustering of lipid rafts (Yamazaki et al., 2009). Extremely low concentrations of TGF-β have also been shown to promote the proliferation of mouse HSCs with primarily myeloid repopulation capabilities, although an inhibitory effect was again seen at higher concentrations (Challen et al., 2010). A similar

bimodal dose-response of human $CD34^+$ colony–forming cells to TGF-β has also been demonstrated (Kale, 2004). Subsequent molecular analyses on cell lines have suggested that very low (picogram/mL) doses of TGF-β activate MAPK/AKT and STATs, while higher doses act primarily via SMAD3 and p38 (Kale, 2004; Kale and Vaidya, 2004). These seemingly contradictory effects of TGF-β on HSCs may reflect a combination of different effects on individual cells/cell subtypes, bimodal dose-responses, and interaction between TGF-β and other GFs thus serving to highlight a need for their examination at the single cell level.

In addition to GF-mediated control of HSC survival and proliferation, recent evidence suggests that GFs can play a deterministic role in activating a particular downstream lineage. Exposure of highly enriched mouse HSCs to M-CSF, for example, was shown to increase the frequency of divisions producing $PU.1^+$ progeny (Sarrazin et al., 2009). Video tracking of single highly enriched PU.1-reporter mouse HSCs further showed that M-CSF induces PU.1 expression even in the absence of cell division, thus arguing against a selection-based lineage choice mechanism (Mossadegh-Keller et al., 2013). HSCs with decreased TF MafB showed an increased sensitivity to M-CSF and an increased myeloid output (Sarrazin et al., 2009). Together these suggest that M-CSF is capable of causing the progeny of HSCs to favor activating a granulopoietic program, although exactly how this is achieved at a molecular level is still unclear. Similar to M-CSF, Rantes (aka. Ccl5) has also been suggested to have granulopoiesis instructing capabilities (Ergen et al., 2012). Even a 4-hour pre-treatment with Rantes was sufficient to result in a decreased output of T-cells 16 weeks later, with no significant effects on the outputs of cells in other lineages (Ergen et al., 2012). Viability following the pre-treatment was, however, not assessed. Thus the possibility that Rantes eliminated T-cell competent HSCs

rather than suppressing a potential T-cell program in initially multi-potent HSCs cannot yet be ruled out in this case.

The effects of GFs on HSCs have been extensively studied because of their anticipated importance in HSC expansion strategies. However, other mechanisms of HSC regulation have also been identified. DNA damage has been shown to induce lymphoid differentiation in mouse HSCs in a Batf, G-CSF/Stat3 dependent fashion (Wang et al., 2012). This finding may be particularly interesting given the evidence that mouse HSC cycling induced by hematopoietic challenge results in the accumulation of DNA damage in these cells (Walter et al., 2015).

Metabolism is another mechanism by which HSC functions are regulated. Inhibition of the nutrient sensor mTOR, combined with activation of β-catenin, allowed maintenance of 8 month repopulation potential (4 months in primary, 4 months in secondary recipients) *ex vivo* for 7 days (Huang et al., 2012). In addition to its role as a nutrient sensor, mTOR can also be activated downstream of GF signaling networks (Inoki et al., 2002) suggesting that it may be an integration point for nutrient sensing and GF signaling. However, decreasing mitochondrial aerobic metabolism (and consequently hyper-activation of Ampk, and glycolysis/fatty acid metabolism) in mouse HSCs decreased their propensity to differentiate *ex vivo* (Liu et al., 2015). Signaling from fatty acid oxidation via the Pml-Ppar complex has also been linked to the maintenance of HSC capabilities, with inhibition of Pml-Ppar reported to enhance symmetric *in vitro* differentiation divisions by mouse HSC with accompanying loss of their quiescence *in vivo* and activation of Pml-Ppar giving rise to an increase in asymmetric divisions *in vitro* (Ito et al., 2012).

A number of small molecules have also demonstrated the ability to regulate HSC function. Inhibition of the aryl hydrocarbon receptor, for example has been shown to inhibit

differentiation of primitive human cells, together with GF stimulation allowing expansion of some types of NSG repopulating cells (Boitano et al., 2010). Another compound, UM171, has also been shown to reduce HSC differentiation *in vitro*, to enable greater expansions of NSG repopulating cells in the presence of GFs (Fares et al., 2014). While the target for this compound was not identified, it was shown to not act via the aryl hydrocarbon receptor, and indeed, showed additive effects in terms of progenitor outputs (though interestingly not in repopulating cell outputs) (Fares et al., 2014). The signaling intermediate, p38, has also been implicated in regulating HSC differentiation, with inhibition of this pathway improving early/intermediate-term repopulating cell expansion in culture (Baudet et al., 2012). Interestingly, this fits with mouse data showing that activation of p38 results in GATA3 nuclear localization and HSC differentiation (Frelin et al., 2013). Overall, these demonstrate that HSC differentiation can be activated by multiple different pathways.

HSC behaviour is thus intimately linked to the particular conditions of the external environment in which these cells are located. Both cell and matrix-bound GFs are important players, but a number of other external factors such as nutrients and DNA damage, can also affect multiple HSC functions. These include regulation of survival, cell cycling, lineage instruction, and maintenance of repopulation potential.

### 1.5.3 Mechanisms of HSC control are interconnected

Aspects of many cell-intrinsic as well as extrinsic mechanisms of HSC control have been identified and, as has been delineated in other systems, evidence that these overlap in their effects on different bio-endpoints has emerged. At a molecular level, examples of cross-talk between the signaling events activated by different GFs include activation of p38 (a part of the

MAPK signaling cascade), leading to the nuclear accumulation of GATA3 in highly enriched mouse HSCs, and an increased probability of HSCs choosing a differentiation fate (Frelin et al., 2013). Another possible link was identified in studies of mouse BM mast cells where Stat5 was shown to bind directly to the Gata2 promoter, inducing its expression (Li et al., 2015). Akt, a common downstream signaling molecule of many GFs, has been shown to phosphorylate Bmi1 in mouse embryonic fibroblasts (Liu et al., 2012), resulting in an inability to inhibit expression of the Ink4a locus (encoding $p16^{Ink4a}$ and $p19^{arf}$) (Liu et al., 2012). Expression of a mutant Bmi1 lacking the Akt phosphorylation site improved mouse CFC re-plating ability, suggesting that this pathway may be relevant *in vivo* as well (Liu et al., 2012).

Regulation of RNA expression represents another mechanism used by HSCs to integrate extrinsic and intrinsic factors that control their state. For example, miR-126, which is highly expressed in human HSCs, has been shown to suppress *AKT* expression, thus regulating the ability of these cells to respond to GFs and promoting their quiescence (Lechman et al., 2012). Another example is the miR99/100/125b tricistron that targets multiple activators of TGF-β, as well as negative regulators of Wnt, thus helping to promote activation of HSCs (Emmrich et al., 2014). The RNA binding protein Msi2, also implicated in mouse HSCs maintenance, is similarly is involved in repression of TGF-β signaling (Park et al., 2014).

In fact, the number of mechanistic elements that appear to be involved in HSC control appears large include both extrinsic and intrinsic factors whose effects are influenced by many context parameters. Together thes pose daunting challenges to elucidating how different outcomes are actually controlled at both the single cell and cell population level.

## 1.6 Tools for the analysis of single cell molecular states and behaviour

### 1.6.1 Flow cytometry and index sorting

Flow cytometry (frequently also called fluorescence activated cell sorting [FACS] even when restricted to cell analytical as opposed to cell isolation applications), represents one of the most commonly used platforms for obtaining molecular information on single cells. Most frequently, flow cytometry is used to determine cell surface phenotypes using fluorescently labeled antibodies with or without their isolation based on these parameters. Index sorting, is similar to standard single-cell flow sorting, but the fluorescence profile of the sorted cell is saved in association to its sort position (Osborne, 2011). This allows any downstream measurements of the cell to be linked back to the specific molecular characteristics it displayed in the FACS run used for its isolation. Such a strategy was recently applied to mouse HSCs, where single-cell quantitative polymerase chain reaction (qPCR) and RNA-seq were linked back to initial surface profiles using a combination of different HSC sort strategies (Wilson et al., 2015). Cells common to the HSC sort strategies were then identified and mapped back both to their molecular profile and their initial surface profile. This strategy enabled additional differences in the surface marker profiles of HSC-enriched populations that could then be used to subset the populations by molecular characteristic and functional phenotype.

In addition to viable, live-cell sorting, adapted protocols can allow measurement of a wide variety of parameters including DNA (Crissman and Steinkamp, 1973; Kraemer et al., 1971), RNA (Crissman et al., 1985), apoptosis (Vermes et al., 1995), intracellular proteins (Jacobberger et al., 1986), enzyme activity (Jones et al., 1995), reactive oxygen species (Bass et al., 1983), telomere length (Rufer et al., 1998), protein phosphorylation levels (Krutzik and Nolan, 2003; Krutzik et al., 2005), and others. Many of these protocols require fixation and/or

permeabilization, and thus cannot be performed on viable cells. They do, however, allow molecular analysis of rare cells at a single cell level, often inaccessible to analysis by any other currently available strategy.

While flow cytometry is a powerful method of analysis, the number of parameters that can be analyzed simultaneously per cell is limited. Current machines can detect upwards of 20 channels, but complexities in panel design such as epitope abundance, fluorophore brightness, antigen stability, clone specificity, and particularly spectral overlap (O'Donnell et al., 2013; Roederer, 2001) mean that most panels are practically restricted to 10-15 parameters. Additionally, marker detection depends on the panel and cellular context in which the experiment was performed.

### 1.6.2 Proteomic analysis using mass cytometry

An adapted version of flow cytometry termed mass cytometry that allows many more parameters per cell to be measured has recently been introduced. This technology uses antibodies tagged with stable heavy metal isotopes (Lou et al., 2007) rather than fluorophores to increase the number of parameters that can be resolved. Inductively coupled plasma mass spectrometry (ICP-MS) is then used to detect the mass and abundance of all tags as single cells are passed one at a time through the device (Bandura et al., 2009). Spillover between channels is thus reduced to negligible levels in most cases, theoretically allowing as many as 100 channels to be separated, although most analyses to date have been limited to <50 (Bandura et al., 2009; Bendall et al., 2011a, 2014; Krishnaswamy et al., 2014; Lujan et al., 2015; Mingueneau et al., 2014; Zunder et al., 2015a). DNA can also be measured using metal labeled intercalating agents (Tanner et al., 2007) and cell viability using a cisplatin-based labeling approach (Fienberg et al., 2012). S-phase

entry can be measured by direct measurement of 5-iodo-2-deoxyuridine (IdU) incorporation, and together with measurement of other cell cycle regulators can allow discrimination of all stages of the cell cycle (Behbehani et al., 2012). A unique collection of palladium isotope-labeled amine-reactive dyes have also been developed to allow sample barcoding (Behbehani et al., 2012; Zunder et al., 2015b). This improves staining reproducibility by allowing all samples to be treated simultaneously in the same tube. It also increases the ease and efficiency of downstream analysis protocols.

Mass cytometry has been used primarily to combine deep surface phenotyping with analysis of intra-cellular signaling events to identify new cellular subsets and their regulation. The flagship paper for this method analyzed the signaling responses of most previously described subsets of human BM cells (Bendall et al., 2011a). Other examples of the power of this technology in the hematopoiesis arena include a high-throughput mapping of drug responses across known cell compartments in the peripheral blood (Bodenmiller et al., 2012); a more comprehensive analysis of the human B-cell differentiation cascade than was previously possible, (Bendall et al., 2014); and a delineation of the  different behaviours of cytotoxic T-cell subsets with different antigen specificities using major histocompatibility complex (MHC) peptide tetramers (Newell et al., 2012).

Understanding the structure and dynamics of cell signaling networks and how they respond to external stimuli is another field where mass cytometry (and even standard flow cytometry) has proven useful. Single-cell data is highly suited to network analysis by enabling analyses of rare cell types and avoiding the pitfalls of population averaging thereby improving the ability to predict underlying relationships. The utility of such data has been demonstrated even using standard flow cytometry, showing a reconstruction of key parts of the T-cell signaling

network (Sachs et al., 2005). Standard statistical tools for network analysis require that measurements be made on the same cell. Thus standard flow cytometry is more limited in the number of interactions that can be studied, particularly where multiple markers are necessary to identify the cell population of interest. The corresponding advantages of mass cytometry were recently illustrated with the introduction of a new algorithm that uses the stochastic distribution of single cells across parameters to obtain a quantifiable estimates of signal strength (Krishnaswamy et al., 2014). This algorithm, termed "conditional-Density Resampled Estimate of Mutual Information (DREMI)" was used to determine signal strength dynamics over time and further allowed comparison between different T-cell subsets, showing differences in naive and memory T-cell signaling responses (Krishnaswamy et al., 2014). This method has also been successfully applied to the mechanistic analysis of defective T-cell signaling in NOD mice, showing that subtle changes in early signaling events can result in large changes both in signal output and downstream cellular responses (Mingueneau et al., 2014).

While mass cytometry represents a powerful new tool in the analysis of single-cell proteomics and molecular biology, the technology is not without limitations. One of these, inherent in the use of ICP-MS, is the fact that the analysis is a destructive process (the cells are vaporized by 5500 K plasma). It is therefore not possible to sort the cells being analyzed. Additionally, while spectral overlap is generally reduced to negligible levels, some signal interference can still occur due to oxidation of the reporters (+16 Da), or from impurities present in the isotopes themselves (usually ±1 Da) (Bendall et al., 2012). Additionally, the sensitivity of lanthanide metal-labeled antibodies is still lower than that provided by bright fluorophores, although the differential sensitivity across available channels is much lower for mass cytometry, and the decreased background (due to lack of autofluorescence) also helps alleviate the

sensitivity deficit to some extent (Bendall et al., 2012). Finally, machine limitations such as inefficiencies in cell nebulization, mean that mass cytometry is limited to analyzing cells at a rate of ~1000 cells per second, and allows measurement of only ~30% of the total cells in a given sample (Bendall et al., 2012).

Technical limitations aside, mass cytometry is, in many ways, becoming a victim of its own success, as the increasing dimensionality of the data is confounding traditional analysis methods inherited from flow cytometry. Primary among emerging algorithms are those that allow for dimensionality reduction of how the data is visualized while still preserving all cell relationships. One of the first released for the analysis of CyTOF data was spanning-tree progression analysis of density-normalized events (SPADE), where k-means based clustering were used to create a minimum spanning tree between clusters to map cell relationships (Qiu et al., 2011). A variety of dimensionality reduction algorithms are potentially applicable to mass cytometry data as well, and these have the benefit of retaining single-cell data. Principal component analysis (PCA) is perhaps the most commonly used method for dimensionality reduction, however, this method depends on a linear relationship existing between the dimensions to be reduced. Most algorithms currently being applied to mass cytometry data use local distances to map intervals between events, thus eliminating the need for linearity. t-distributed stochastic neighbor embedding (t-SNE) is one such dimensionality reduction algorithm (Van der Maaten and Hinton, 2008) and has been specifically implemented for mass cytometry data in the form of viSNE (Amir et al., 2013). viSNE has been successfully applied to the identification of both normal and cancerous cell subsets (Amir et al., 2013). Other algorithms include 'wanderlust' which uses local distances to place cells in order and was used in the

dissection of B-cell differentiation (Bendall et al., 2014), and DREMI which was used in the mapping and quantification of mouse T-cell signaling (Krishnaswamy et al., 2014).

Overall, mass cytometry, despite its limitations, is proving a highly valuable analysis tool as it gives direct protein level measurements with high dimensionality. With the continued advent of additional computational tools and improvements in technical aspects, this technique will undoubtedly see increasing use in the coming years.

### 1.6.3 Single cell sequencing

Analysis of cellular RNA has proven to be extremely useful in multiple systems. Until recently, however, such analysis required very large cell numbers, and thus represented only an average value from often highly impure populations. Single-cell qPCR has already proven to be valuable in identifying transcriptional networks in rare and heterogeneous populations including mouse HSCs (Moignard et al., 2013). Unbiased methods such as RNA-Seq are preferable as they eliminate the need to select specific markers. Initial reports of successful single-cell RNA-seq were low-throughput and included known biases in read depth compared to transcript position (Tang et al., 2009). However, a number of additional tools have now become available. Improvements in throughput are achieved via cell multiplexing using unique primer sequences to allow subsequent de-convolution (Islam et al., 2011). The introduction of template switching PCR to selectively amplify whole length sequences has also helped to reduce transcript position biases (Picelli et al., 2014; Ramsköld et al., 2012). Meanwhile the use of *in vitro* transcription rather than PCR to amplify starting RNA has lead to further decreases in noise (Hashimshony et al., 2012; Jaitin et al., 2014). Recent methods have also begun to implement the use of unique molecular identifiers which tag each individual template molecule during initial reverse-

transcription, thus allowing template quantification independent of subsequent amplification biases (Grün et al., 2014; Islam et al., 2014; Kivioja et al., 2012). As technical improvements in single-cell RNA sequencing continue to be made, these technologies will undoubtedly be used increasingly in the field of HSC biology.

### 1.6.4 Single-cell fate tracking

An understanding of the molecular features of cells is important, however, a delineation of their kinetic behaviour also at a single-cell level is essential to obtaining a detailed understanding of the mechanisms controlling their biological outcomes. Early experiments with adult mouse BM HSCs demonstrated that cells with long-term *in vivo* repopulating activity showed delayed recruitment into division (Dykstra et al., 2006; Ema et al., 2000) and absence reduced display of uropodia (Dykstra et al., 2006). A later study of single mouse HSCs tracked in hydrogel microwells revealed differential effects of Wnt3a and N-Cadherin compared to TPO on HSC proliferation rates and maintenance of *in vivo* repopulating capability (Lutolf et al., 2009). Tracking the behaviour of single cells was also used to demonstrate a definitive lineage relationship between mouse HSC and endothelial cells (Eilken et al., 2009). Dynamic control of media composition combined with cell tracking on a microfluidics chip has also been performed, and showed that mouse HSC survival could be maintained following exposure of the cells to low SF concentrations, but only for up to 24 hours (Lecault et al., 2011). The fact that division was initiated within this period (Lecault et al., 2011) suggests that SF control of survival may have a cell cycle-dependent checkpoint. The ability to combine dynamic exposure to external factors with high-resolution, high-throughput monitoring, will undoubtedly help further our knowledge of HSC behaviour in response to extrinsic factors.

High throughput methods to track the *in vivo* outputs of single cells are also desirable. Single-cell transplants of essentially pure populations of HSCs are possible with mouse cells (Benz et al., 2012; Dykstra et al., 2007; Kent et al., 2009; Yamamoto et al., 2013) and are getting close with human cells (Notta et al., 2011), but are both expensive and labour-intensive. Analysis of viral insertion sites following infection has long enabled the tracking of multiple HSC-derived clones in a single recipient, however, the sensitivity of these sequencing methods tends to be low due to the stochastic distribution of digestion sites in the first stages of the protocol (Cornils et al., 2013; Dick et al., 1985; Guenechea et al., 2001; Harkey et al., 2007; Lemischka et al., 1986; Schmidt et al., 2007; Wu et al., 2013). Recently, the advent of lentiviral barcodes which label cells with unique sequences has allowed targeted sequencing of the vector to identify clones (Bystrykh et al., 2014; Cheung et al., 2013; Grosselin et al., 2013; Lu et al., 2011; Nguyen et al., 2014; Porter et al., 2014). Using this method, large-scale clonal tracking of transplanted HSC outputs can be replicated in very low numbers of recipients, enabling the extreme heterogeneity of human HSC outputs to be revealed (Cheung et al., 2013).

## 1.7 Thesis objectives

The primary objective of my work was to elucidate cellular and molecular mechanisms underpinning HSC survival, proliferation, and the maintenance of their stem cell potential. In pursuit of this goal, the specific hypothesis tested was "The survival, proliferation, and maintenance of stem cell potential are regulated independently in HSC". A deeper understanding of these programs and how they're regulated would allow the rational design of HSC expansion strategies.

In the work described in Chapter 2, I worked closely with Stefan Wohrer to investigate the dissociability of survival, proliferation, and maintenance of stem cell potential in mouse HSCs. This model was chosen because of the numerous advantages it offers for making definitive investigations tractable. These included effective sort strategies which allow mouse HSCs to be prospectively isolated at 30-50% functional purity (Kent et al., 2009), historical knowledge of GFs able to promote mouse HSC proliferation *in vitro* (Huynh et al., 2008; Kent et al., 2008; Miller and Eaves, 1997) and a stromal cell line known to promote the maintenance of their stem cell capabilities (Oostendorp et al., 2002, 2005). I therefore chose to exploit these advantages in combination with planned analysis of transcriptional data and functional assays to screen for candidate regulators and demonstrate the dissociability of key cellular programs in mouse HSCs.

Having shown that survival, proliferation, and maintenance of stem cell ability could be dissociated in mouse HSCs, in Chapter 3 I sought to determine whether these findings would extend, at least in principle, to human HSCs. I adopted a combination of 5 GFs that had been previously implicated in our lab as able to maintain human HSCs *in vitro* (Zandstra et a l., 1997). The next step was to combine these with recent findings that HSC maintenance could be improved by removing the paracrine effects of mature cells (Csaszar et al., 2012). I then chose to use a combination of single cell tracking tools (Lecault et al., 2011), and functional assays to test the role of individual factors and examine the mechanistic dissociability of their control of human HSC survival, proliferation and stem cell ability. Finally, I developed an antibody panel to simultaneously detect levels of >40 key surface and intracellular proteins at the single cell level using mass cytometry (Bendall et al., 2011a), which was then applied to identify some of the key molecular effectors of individual and combined GF activation.

Given that even the best phenotypic sort strategies tend to give relatively low human HSC purities (~10%) starting from CB (Doulatov et al., 2010; Notta et al., 2011), in Chapter 4 I sought to relate the molecular state of cells with differing functional capabilities and surface phenotypes. For this, I applied a combination of mass cytometric single cell protein analysis and functional assays across the spectrum of cell types found within the $CD34^+$ compartment of CB cells. I then used this data to examine molecular differences across the subsets used conventionally to define the human hematopoietic hierarchy, determine the correlation between functional progenitors and the phenotypes used to isolate them, and identify additional surface markers that could aid in their purification.

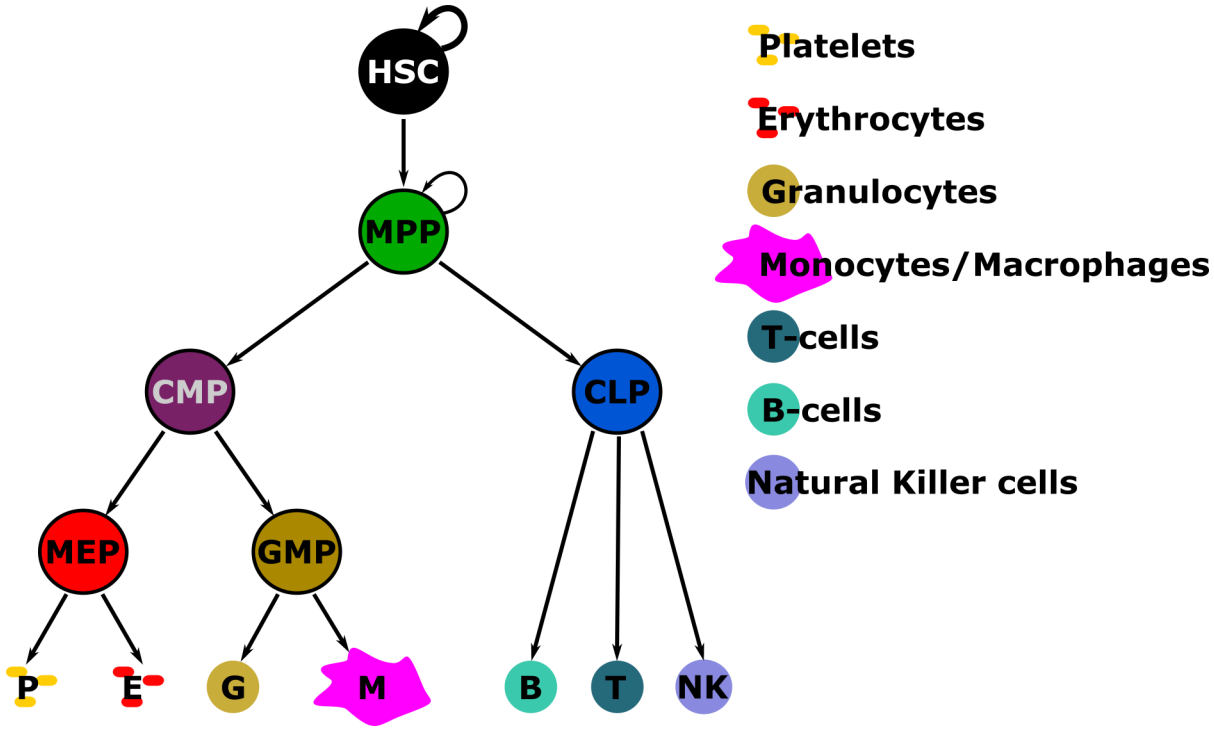


**Figure 1.1 The classic model of the hematopoietic hierarchy.**

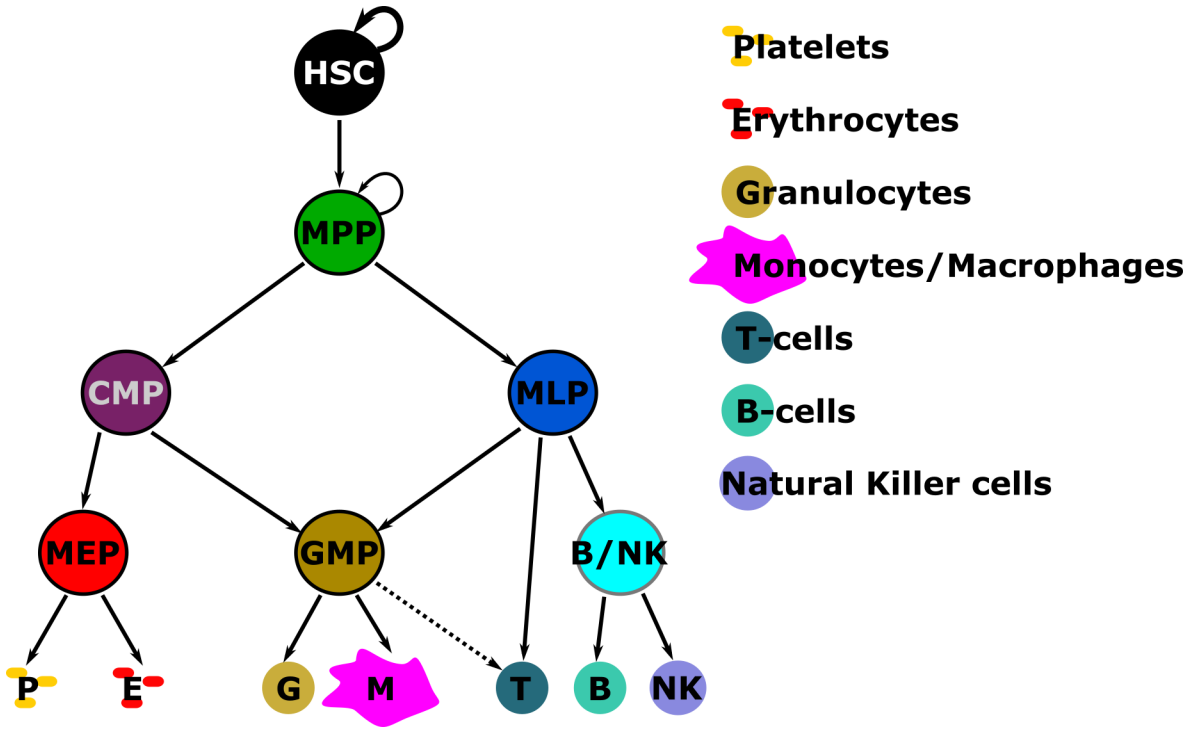


**Figure 1.2 A revised model of the hematopoietic hierarchy.**

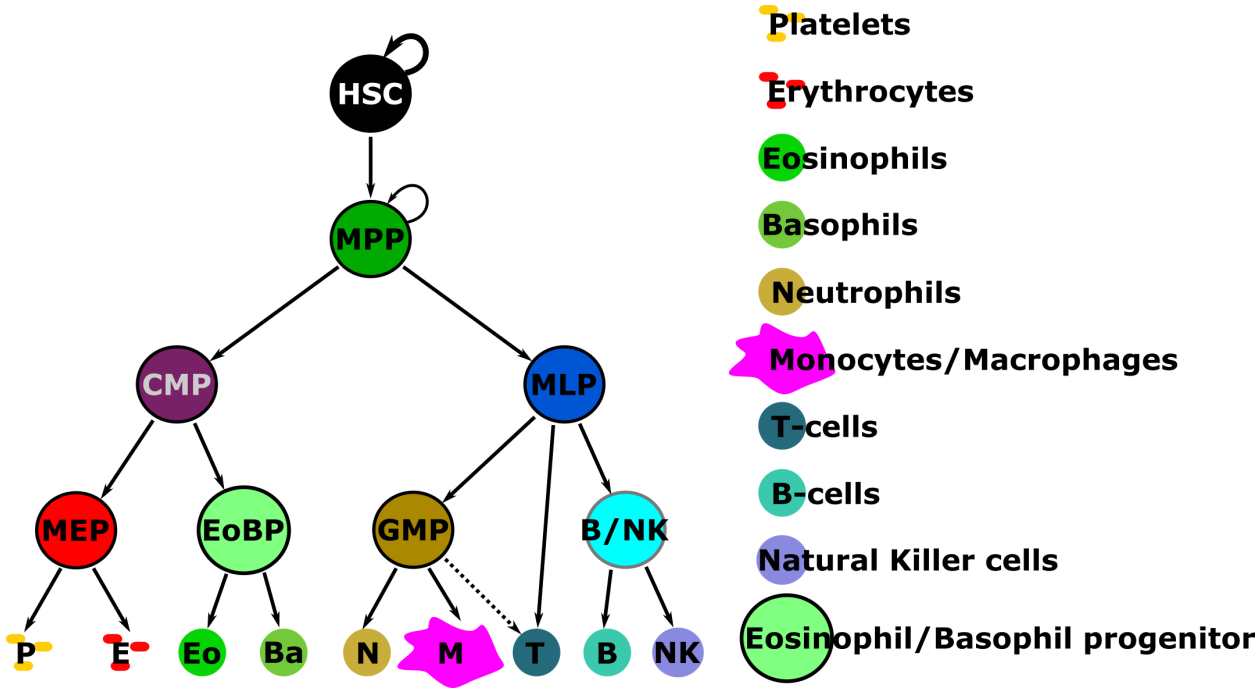


**Figure 1.3 A further revision to the hematopoietic hierarchy.**

# Chapter 2: Survival, proliferation and stem cell identity can be differentially controlled in murine HSC

## 2.1 Introduction

HSCs represent a rare subset of undifferentiated precursors of blood cells, historically recognized by their ability to regenerate large, self-sustaining clones of mature progeny in transplanted irradiated hosts. This property has been successfully exploited experimentally to interrogate molecular mechanisms that regulate the acquisition and maintenance of the HSC state during development, injury, aging and transformation. It is also the basis of widely used hematopoietic cell transplants in patients given therapies that require external hematopoietic support or replacement. Not surprisingly, therefore, is the intense interest in defining conditions that would allow significant HSC expansion to be obtained *in vitro*. Efforts to date have led to the identification of many genes important to HSC proliferation and self-renewal (Xie et al., 2014a). However, these have not yet provided a molecular signature that specifically defines the functional state of HSCs, nor the identification of culture conditions that support significant net expansions of normal HSCs with lifelong cell output activity.

One limitation lies in the recently appreciated heterogeneity that characterizes populations historically classified as HSCs. Current evidence now indicates that cells able to produce mature blood cells for at least 4 months in transplanted hosts still comprise biologically distinct and physically separable subsets of HSCs that sustain self-renewal ability over different periods of time and numbers of divisions (Benveniste et al., 2010; Benz et al., 2012; Dykstra et al., 2007; Kent et al., 2009; Morita et al., 2010;

Sanjuan-Pla et al., 2013; Yamamoto et al., 2013). Serial transplants of clonally tracked HSCs has shown that only about half of HSCs thus defined will produce sufficient daughter HSCs in transplanted primary hosts to regenerate long-term hematopoiesis in secondary mice. HSCs possessing this durability of self-renewal activity (hereafter referred to as DSR-HSCs) are selectively enriched in the lineage marker-negative ($Lin^-$) $CD45^+EPCR^+Sca1^+CD34^-CD49b^{low}CD48^-CD150^{++}$ fraction of adult mouse BM. Biologically, they are also distinguished by a continuing robust ability to produce mature myeloid cells independent of their lymphopoietic activity (Benveniste et al., 2010; Benz et al., 2012; Dykstra et al., 2007; Kent et al., 2009; Morita et al., 2010). This includes most HSCs subclassified as α- or β-HSCs and a few classified as γ-HSCs based on the deficient, balanced or more persistent lymphoid programs their progeny display in primary recipients. Conversely, more limited self-renewal (LSR) activity (indicated by a failure to produce sufficient HSCs to repopulate secondary mice), is a property of most other HSCs (all HSCs subclassified as δ-HSCs and many γ-HSCs based on their inability to sustain a strong granulopoietic potential for 16 weeks) and found to be enriched in the $CD45^+EPCR^+Sca1^+CD34^-CD49b^{hi}CD48^-CD150^{+/-}$ fraction of adult mouse BM.

Survival, proliferation and self-renewal are all actively regulated states of HSCs and hence likely to be important determinants of the numbers of HSCs obtained after culture. These states are also known to be subject to regulation by external cues, at least some of which appear to be locally provided *in vivo* (Mercier et al., 2012). Numerous experiments have reported that HSCs can survive and execute self-renewal divisions to a limited degree *in vitro* in the presence of supportive BM stromal cells (Dexter et al., 1977; Fraser et al., 1992) or various stromal cell-derived factors including SF, IL-11,

Flt3-ligand, Wnt3a, Angptl, TPO, FGF1, and IGFBP2 (Audet et al., 2002; Huynh et al., 2008; Kent et al., 2008; Miller and Eaves, 1997; Reya et al., 2003; Zhang et al., 2006a). However, to date, large net expansions of DSR-HSCs *ex vivo* have not been achieved using defined factors and the relative roles of different factors in promoting DSR-HSC viability, proliferation and self-renewal is not understood. To elucidate the mechanisms by which stromal cells regulate key functions of HSCs, we used urogenital ridge-derived UG26 cells because they were found to be exceptionally potent in supporting HSCs cell contact independently (Oostendorp et al., 2002, 2005).

Here we used highly purified adult mouse HSCs (~40% pure) to reveal the ability of different defined *in vitro* conditions to directly and differentially regulate the survival, proliferation and self-renewal of DSR-HSCs. We identify NGF and collagen 1 (Col 1) as additives that can optimize DSR-HSC survival in a defined serum-free medium (SFM), and also synergize with the mitogenic and self-renewal-promoting activity of SF and IL-11 to achieve an unprecedented expansion of total HSCs while maintaining input DSR-HSC numbers.

## 2.2 Methods

### 2.2.1 Mice

C57Bl/6J (B6)-*Ly5.1* or -*Ly5.2* mice and congenic B6-*W41/W41-Ly5.1* and -*Ly5.2* (*W41-5.1* and *W41-5.2*) mice were bred and maintained in our Animal Resource Center in microisolator cages and provided continuously with sterile food, water, and bedding. ESLAM cells were isolated from 6 to 16 week-old adult B6 BM cells as previously described (Benz et al., 2012; Kent et al., 2009). Recipient mice were 8 to 12-week old

Ly5 congenic *W41* mice. All procedures were carried out with approval from the University of British Columbia Animal Care Committee.

### 2.2.2 UG26 cells and CM

UG26-1B6 (UG26) stromal cells were cultured as previously described (Oostendorp et al., 2002) and conditioned medium (CM) obtained from confluent UG26 cells X-irradiated with 30 Gy and then incubated for 3 days with SFM after removal of the UG26 culture medium and rinsing the cultures several times with Dulbecco's Phosphate Buffered Saline (PBS). The CM was then filtered through a 40 μm cell strainer (Becton Dickinson, BD, San Jose, CA, USA) and stored frozen at -20$^{o}$ C.

### 2.2.3 ESLAM cell cultures

ESLAM cells were deposited into the round bottomed wells of 96-well plates using the single-cell deposition unit of the sorter, each well having been preloaded with 100 μl of SFM. SFM consisted of Iscove's Modified Dulbecco's Medium (IMDM) supplemented with 10 mg/ml bovine serum albumin, 10 μg/ml insulin, and 200 μg/ml transferrin, 40 μg/ml low-density lipoproteins, 100 U/ml penicillin, 100 μg/ml streptomycin (all from STEMCELL Technologies), and $10^{-4}$ M β-mercaptoethanol (Sigma-Aldrich). For cultures initiated with 30 ESLAM cells, we then added another 100 μl of SFM containing the supplements indicated. For single-cell cultures, each well was first visually inspected to identify those wells that contained 1 viable (refractile) cell. Cells were then incubated at 37$^{o}$C in a humidified atmosphere of 5% $CO_2$ in air and then evaluated as described in the Results.

Additives tested were as follows: recombinant mouse SF and IL-3, and recombinant human EPO and Col 1 were purchased from STEMCELL Technologies (Vancouver, BC, Canada), recombinant human IL-11 and M-CSF were gifts from Genetics Institute (Cambridge, MA, USA), recombinant mouse Wnt3a, mouse Angptl3 and IGFBP2, and recombinant human NGF, pleiotrophin, BMP4, Activin A, TGF-β, and PDGF-BB were purchased from R&D Systems (Minneapolis, MN, USA), recombinant mouse TPO was a gift from Genentech (San Francisco, CA, USA) human FGF-1 was purchased from Invitrogen (Carlsbad, CA, USA), heparin, fibronectin, recombinant human EGF, and and mouse laminin were purchased from Sigma-Aldrich (St. Louis, MO), recombinant human IL-6 was a gift from Cangene (Winnipeg, MA, Canada), Reduced Growth Factor Matrigel was purchased from Becton Dickenson Biosciences, San Jose, CA, USA), and SDF-1 was a gift from Ian Clark Lewis, University of British Columbia, Vancouver, BC, Canada). Concentrations of additives used in survival screen are listed in Table 2.1.

Cultures initiated with 30 cells were assessed for HSC content after 7 days of incubation. To measure the formation of apoptotic cells in these cultures, cells were harvested after 36 hours, washed, resuspended in Binding Buffer (eBioscience, San Diego, CA, USA), and stained with Annexin V eFluor® 450 as per the manufacturer's instructions and also with (FITC)–conjugated anti-CD45 (both from eBioscience, San Diego, CA, USA) to help discriminate ESLAM cells from debris. Cells were then analyzed on a BD LSRFortessa cell analyzer (Becton Dickinson, BD, San Jose, CA, USA).

For analysis of first division progeny in cultures initiated with single ESLAM

cells, cultures were examined microscopically every 4 hours starting 12 hours after initiation of the culture. The entire volume of culture medium in wells found to contain 2 cells after at least 32 hours of incubation (but not 4 hours previously) was individually harvested with a 250 μl pipette and then distributed into 3 separate wells. If the 2 starting cells ended up in different wells they were separately picked up with an insulin syringe and put on ice for up to 2 hours before being injected into irradiated recipient mice or used to initiate LTCs as described below. If 2 cells ended up in the same well, the process was repeated, and if only one cell could be found after the splitting process, the cell was discarded and not included in the transplantation analysis. For analysis of input ESLAM cell viability and division kinetics, cultures initiated with single ESLAM cells were monitored starting 12 hours later and then at the intervals indicated. The first appearance of 2 refractile cells was used to indicate completion of a first division. Following the addition of a medium containing 15% fetal bovine serum (FBS)+IL-3+IL-6+EPO to each well after 4½ days of incubation, evidence of a clone formation was inferred from the detection of >7 refractile cells.

### 2.2.4 HSC transplantation assays

Cells were transplanted by tail vein injection into sublethally irradiated Ly5-congenic *W41* mice and PB follow-up analyses of donor contributions to the B-, T- and GM lineages were then performed 8, 16, and 24 weeks later as previously described (Kent et al., 2007) using both anti–CD45.1-APC (eBiosciences) and anti–CD45.2-FITC (BD) to enable donor and recipient cells to be distinguished and to ensure that any double positive CD45.1 and CD45.2 events were excluded. Staining with anti–Ly6g-PE and

anti–Mac1-PE was used to detect GM cells, anti–CD19-PE for B-cells, and anti–CD5-PE for T-cells (all antibodies from BD). Secondary transplantations were performed 24 weeks after the primary transplantations. The subtype of the original HSC(s) transplanted was first determined 16 weeks post transplantation and reconfirmed either within one week before or on the day cells were harvested to perform secondary transplantations. For the latter, BM cells were harvested from both femurs, tibiae and the pelvis of primary mice, red blood cells lysed, and $10^7$ cells then injected into each secondary recipient. HSC frequency values were calculated from limiting dilution transplant results using an on-line program (http://bioinf.wehi.edu.au/software/elda/) and a positive read-out of >1% contribution to the total PB white blood cell pool at 16 weeks. HSCs were subclassified as DSR-HSCs when they produced >1% of the PB GM cells and as LSR-HSCs when they contributed <1% of the GM cells 16 weeks after transplantation. Differentiation patterns of HSCs were subclassified as α, β, γ, and δ based on the following ratios of their contributions to the total PB GM vs (T+B)-cell pools in recipient mice assessed 16-24 weeks post-transplant (i.e., >2.0; 0.25-2.0, <0.25 with >1% contribution to the myeloid lineage, and <0.25 with <1% contribution to the myeloid lineage, respectively), as described previously (Dykstra et al., 2007).

### 2.2.5 LTC-IC assays

LTC-IC assays were performed by plating visually confirmed single cells onto irradiated UG26 feeder cells in flat-bottomed wells containing 200 µl of Myelocult (STEMCELL Technologies) supplemented with $10^{-6}$ M hydrocortisone (Sigma-Aldrich) in 96-well plates. The co-cultures were maintained for 6 weeks at 37°C with weekly half-medium changes (Woehrer et

al., 2013). After 6 weeks of culture, fresh SFM medium containing 15% FBS, 50 ng/ml SF, 10 ng/ml recombinant mouse IL-3, 10 ng/ml recombinant human IL-6 and 3 U/ml recombinant human EPO was added to the wells. Wells that contained clusters of >25 nonadherent cells 12 days later were counted as positive.

### 2.2.6 Microarray analyses

Between 2,000 (cultured cells) and 6,000 (freshly isolated adult BM) ESLAM cells were collected and mRNA was extracted with RNAeasy (Qiagen, Inc, Toronto, ON, Canada). mRNA from three independent experiments was pooled, reverse transcribed and amplified with Nanokit following the manufacturer's instructions (Agilent Technologies, Mississauga, ON, Canada). cRNA was hybridized onto 2 gene chips (GeneChip Mouse Gene 1.0 ST Array, Affymetix, Santa Clara, CA, USA) per condition. All arrays were robust multi-array averaged (RMA) normalized using the Bioconductor package 'xps' in R (http://www.R-project.org/) including the metacore probesets grouped by exon (Gentleman et al., 2004). Gene annotation data was added using a combination of the NetAffx (Release 31) annotation files as well as the Bioconductor packages 'mogene10sttranscriptcluster.db' and 'Org.Mm.eg.db'. All probe sets that were not mapped to an Entrez Gene identifier were discarded. Data Above Background (DAB) scores were calculated for each probe set and those probe sets with a DAB p-value $\leq 0.05$ in both technical replicates of at least one condition were retained. In the case of multiple probe sets mapping to the same Entrez Gene identifier, the probe set with the highest maximum absolute deviation across all chips was retained. This was done in order to maximize power in later statistical tests as it reduces multiple testing while retaining the

probes with the greatest signal. Expression values were then normalized between the arrays by quantile normalization (Smyth et al., 2005) using the R package 'limma'.

Publicly available microarray data for the UG26-1B6 cell line (Gene Expression Omnibus, GSE11589) was used together with the data for the freshly isolated ESLAM cells (from above) in order to generate a list of potential secreted factors. This data (from the mouse 4302 chip) was RMA-normalized and transcripts called as present if at least one probe set had a MAS5 p-value of 0.05 or less using the R package 'affy'. Transcripts that were defined as present and that also had the gene ontology (GO) term "extracellular region" (GO:0005576) were compared to transcripts with the GO term "receptor activity" (GO:0004872) present in transcripts of fresh ESLAM cells (as defined above). "Extracellular region" transcripts from UG26 which had transcripts with "receptor activity" in fresh ESLAM cells predicted or shown to interact in either the National Institute of Aging (NIA) mouse protein-protein interaction database (Yellaboina et al., 2008), the BioGRID database (Stark et al., 2006) or the Cytokine-cytokine receptor interaction (mmu04060) or ECM-receptor interaction (mmu04512) entries from the Kyoto Encyclopedia of Genes and Genomes (KEGG) Pathway database (www.genome.jp/kegg/pathway.html) were retained as potential secreted factors, and their median expression and putative receptors (interacting "receptor activity" transcripts) recorded.

For pathway analysis, arrays from extracts of cells exposed to CM were grouped and compared against extracts from fresh ESLAM cells and from cells exposed to SF+IL-11 only in order to provide biological replication and minimize differences due only to differential cell cycle status. The 'romer' algorithm (a rotation based modification of the

GSEA algorithm (Subramanian et al., 2005)) was used to test for differential expression of genes in pathways from the REACTOME database (Croft et al., 2011) (taken from the R version of the molecular signatures database, http://bioinf.wehi.edu.au/software/MSigDB/) using a mixed alternative hypothesis (i.e., the differential expression can be in both directions) with the "floor mean" test statistic and 100,000 rotations, correcting for correlation between technical replicates (Smyth et al., 2005).

### 2.2.7 Statistical analysis

GraphPad Prism version5 or R (http://www.R-project.org/) was used to perform basic statistical analyses including calculation of mean ± SEM values, and Student's t-tests. Extreme limiting dilution analysis (ELDA) (http://bioinf.wehi.edu.au/software/elda/) or the 'elda' function in the R package 'statmod' was used to perform the limiting dilution analyses and to evaluate the significance of differences obtained using different culture conditions.

## 2.3 Results

### 2.3.1 Stromal cell-derived factors enhance the output of DSR-HSCs *in vitro* in the presence of SF+IL-11

In a first series of experiments, we set out to compare the DSR-HSC stimulating activity of various culture additives reported to support adult mouse BM HSC expansion *in vitro.* To focus on the identification of direct-acting external factors that contribute to this response, we initiated each test culture with highly purified HSCs (30

$CD45^+EPCR^+CD48^-CD150^+$ - ESLAM - cells isolated from adult mouse BM) suspended in SFM and then incubated the cells for 7 days prior to harvesting all the cells and determining their content of total and DSR-HSCs by performing limiting dilution transplant assays (Figure 2.1A). We defined HSCs as cells whose *in vivo*-regenerated progeny constituted >1% of all the nucleated PB cells 16-24 weeks post-transplant. DSR-HSCs were defined as the HSCs that generated >1% of all the circulating GM cells at 16-24 weeks post-transplant (and LSR-HSCs as all the rest). Single-cell transplants of 50 freshly isolated ESLAM cells indicated that each culture was initiated with, on average, 12 total HSCs of which 8 were DSR-HSCs. The results pooled from a total of 3 to 5 experiments per condition showed that the number of DSR-HSCs increased significantly (29-fold, p<0,001) in cultures that contained UG26 cells as well as SF+IL-11 and to a slightly, but not significantly, lesser extent (15-fold, p=0.19) when the UG26 cells were replaced with CM prepared from them. Total HSC numbers were also significantly increased in both of these cultures, (20-fold and 11-fold, respectively, P<0.001), and again not to significantly different extents (P=0.19, Figure 2.1B, left and middle panels). Representative FACS profiles of recipients of cells cultured in SF+IL-11 plus UG26 cells are shown in Figure 2.1C and full time course plots of the lineage-specific reconstitution kinetics of donor cells in recipients of equivalent fractions of cultures that contained SF+IL-11 plus UG26 cells, or SF+IL-11 plus CM, or SF+IL-11 only are shown in Figure 2.2. Interestingly, ESLAM cells cultured in UG26 cells alone showed maintenance but not expansion of DSR-HSCs (and total HSCs, Figure 2.1B). In contrast, DSR-HSC numbers showed a net decrease when cultured in any of the 4 other

conditions tested although in some, total HSC numbers were maintained at, or close to, input levels (Figure 2.1B).

To evaluate more stringently the DSR property of the *in vitro* expanded HSCs, we determined the number of daughter HSCs generated in the primary recipient mice. This involved performing another set of limiting dilution HSC transplant assays on BM cells harvested from each group of primary recipients 24 weeks after they had been initially transplanted with cells harvested from the 7-day cultures. The results showed that cultures to which either UG26 cells or UG26 CM had been added to the SF+IL-11 cocktail produced HSCs *in vitro* that were capable of extensive further expansion in the primary hosts (Figure 2.1B, right panel) and hence gave a high level of repopulation of the secondary mice (Figure 2.1C, lower panels). Thus, the overall expansion of DSR-HSCs achieved (first *in vitro*, and then in the primary recipients) when UG26 cells were present together with SF+IL-11 in the cultures was 130-fold, and 360-fold when UG26 cell CM was added (assuming 1 femur represents 5% of the total BM of a mouse (Colvin et al., 2004)). These expansions were again not significantly different from each other ($p=0.13$). In contrast, no secondary repopulating activity was detected in comparable assays of BM cells from primary recipients of cells cultured with any of the defined growth factor cocktails.

These findings document the ability of factors produced by UG26 cells to synergize with SF+IL-11 to produce a rapid and significant net expansion *in vitro* of serially transplantable HSCs. They also demonstrated that this effect can be mediated by a mechanism that is cell contact-independent.

### 2.3.2 UG26 cells produce factors that in combination with SF+IL-11 enable all HSC differentiation programs to be sustained

We then designed experiments to determine the frequency of ESLAM cells from which the HSCs are derived when SF+IL-11 plus UG26 cells or UG26 CM is present, as compared to cultures of ESLAM cells exposed to SF+IL-11 alone and the differentiation programs displayed by their clonal progeny. This involved setting up a similar series of 7-day cultures but, this time, each culture was initiated with a single ESLAM cell and each culture was then assessed by transplanting its entire contents (irrespective of how many cells it contained) into a single irradiated recipient (Figure 2.3A). Analysis of the PB of these mice 16-weeks later showed that $\alpha$ or $\beta$ patterns of differentiation (see Experimental Procedures for their definition) were obtained from 18% of the cultures to which UG26 cells had been added, a frequency that is not significantly different ($p=0.12$) from the frequency of $\alpha$ and $\beta$-HSCs in the input ESLAM cells (28%, Figure 2.3B). However, it is notable that the proportion of cultures that contained any type of HSC was significantly higher than the frequency of total HSCs in the original ESLAM cells (72% versus 40%, $P<0.001$, Figure 2.3B). Thus, some ESLAM cells that are not directly detectable as HSCs can, nevertheless, generate progeny that have the functional properties of HSCs *in vivo*. In contrast to the cultures that contained SF+IL-11 plus UG26 cells, only 13% of the cultures that contained only SF+IL-11 contained any HSCs (a value significantly <40%, the input HSC frequency, $p<0.001$) and all of these appeared restricted to produce a $\delta$ pattern of reconstitution.

As a more direct test of the frequency of ESLAM cells that are responsive to the factors produced by UG26 cells in concert with SF+IL-11, we set up another series of single-cell cultures, in this case with SF+IL-11 ± UG26 CM (36 with and 12 without UG26 CM, Figure 2.4A). Each of these cultures were then monitored for 4½ days until a first division occurred and then the pair of daughter cells obtained were separated and each cell then individually transplanted into an irradiated recipient. 17 (47%) of the 36 pairs of cells produced in the cultures containing SF+IL-11 plus UG26 CM included at least one HSC and 9 of these (25% of the 36 pairs) included at least one α- or β-HSC (Figure 2.4B). Overall the frequencies and distributions of HSCs subtypes in the first division progeny of ESLAM cells generated under conditions that give net expansions of DSR-HSCs after 7 days are similar to the frequencies of the HSCs in the starting ESLAM populations and in the 7-day clones generated under similar conditions (Figure 2.4C). Secondary limiting dilution transplantation assays of the cells regenerated from these first division daughter cells confirmed their DSR and LSR attributes assigned on the basis of their clonal GM contributions in the primary mice (Figure 2.4D and Figure 2.5). Consistent with previous evidence of the reduced supportive activity of SF+IL-11 only, none of the 24 mice injected with the first division progeny of cells that had been cultured under these conditions were repopulated.

Because each well from which the paired daughter cells were obtained had been tracked visually to identify the timing of the first division, we could also ask whether there was a relationship between the time taken for an input ESLAM cell to complete a first division and whether it yielded HSC progeny. This analysis showed that the frequency of HSC-containing daughter pairs was significantly higher ($p=0.007$) for cells

that underwent their first division more than 48 hours after being placed in culture (67%), as compared to those that completed a first cell cycle in less than 48 hours (16%) and reached 100% for cells that did not divide until after 96 hours.

In previous studies we had found that cells able to generate hematopoietic progeny for 7 weeks in clonal LTC-ICs are present in the ESLAM population at a similar frequency to HSCs (Kent et al., 2009). It was therefore of interest to evaluate the effect of adding UG26 CM to SF+IL-11 on the proportion of first division progeny of ESLAM cells that would display LTC-IC activity (Figure 2.6A). In the present study, we used a 6-week LTC-IC assay, but the frequency of LTC-ICs measured in the starting ESLAM cells (89/213=42%, Figure 2.6B) again proved similar to the frequency of total HSCs (40%, p=0.87, Figure 2.3B). In addition, we found the frequency of ESLAM cells that produced at least one daughter (6-week) LTC-IC (70/96=73%) was higher than the input LTC-IC frequency ($p<0.001$) and also higher than the frequency of ESLAM cells that generated at least one daughter HSC (47%, $p<0.001$, Figure 2.3D). The frequency of pairs in which both daughter cells were LTC-ICs (28%) was also higher than the frequency of pairs containing 2 HSCs (14%, p=0.023). These disparities in the apparent effects of UG26 CM plus SF+IL-11 on LTC-IC and HSCs could be due in part to the selective inability of HSCs to engraft when they are in $S/G_2/M$ phases of the cell cycle (Bowie et al., 2006) but may also reflect a broader specificity of the LTC-IC assay used here.

### 2.3.3 Different factors separately regulate HSC survival and mitogenesis

We next designed a series of experiments to interrogate the biological mechanism(s) by which the factors produced by UG26 cells might enable an *in vitro* expansion of DSR-HSC numbers. Possibilities included differential effects on HSC survival and/or their rate or frequency of activation into cycle, and/or their self-renewal potential. To distinguish between these possibilities, we initiated another set of single-cell cultures with ESLAM cells and then monitored them visually at intervals over the next 4½ days (108 hours) to track the persistence of viable (refractile) cells and their rate of entry into a first division during that period (Figure 2.7A). At the end of 4½ days, we added medium containing FBS+SF+IL-3+IL-6+Epo as a further stimulus to promote the formation of readily detectable differentiating clones from persisting viable cells.

In the presence of SF+IL-11 plus UG26 CM, 97% of the input cells (279/288 cells monitored in a total of 3 independent experiments) survived and executed a first division between 24 and 108 hours after being placed *in vitro*. Single ESLAM cells incubated in FBS+SF+IL-3+IL-6+Epo medium from the initiation of the cultures showed the same full survival (160/168=96%), proliferation kinetics and subsequent clone formation as the cells incubated for the first 4½ days in SF+IL-11 plus UG26 CM in spite of their inability to support the retention of DSR-HSC activity (Figure 2.1A). In contrast, 64% (184/288) of the single ESLAM cells cultured in SF+IL-11 alone could no longer be visualized at the end of the first 12 hours *in vitro*. However, the remaining 36% of these cells remained refractile and appeared viable for the first 18 hours and then began to divide with the same kinetics as the cells maintained in SF+IL-11 plus UG26 CM. These (and none of the apparently dead cells) also all went on to produce large colonies when the

FBS+SF+IL-3+IL-6+Epo cocktail was added at the end of the first 4½ days. Interestingly, 90% (259/288) of the cells initially cultured in UG26 CM alone (without SF+IL-11) did not divide and most also became smaller over time and appeared of questionable viability. Nevertheless, at the end of the first 4½ days, all of these cells plus another 12 thought to be dead (i.e., a total of 271 of the original 288) could still be stimulated to produce readily detectable colonies upon the addition of the FBS+SF+IL-3+IL-6+Epo cocktail.

To determine whether the survival advantage afforded by factors present in UG26 CM might be restricted to cells that are quiescent, we set up new single ESLAM cell cultures in SF+IL-11 plus UG26 CM for 4½ days (by which every cell had completed at least one division) and then switched the medium to SFM with SF+IL-11 only for a second 4½ days. Continued monitoring of each of these wells over the second 4½ days, showed that 97% (279/288) of the wells contained cells that continued to divide and the range of times taken to complete the next division was the same as for the first division initiated in SF+IL-11 plus UG26 CM, discounting the initial lag (Figure 2.7C). Moreover, addition of FBS+SF+IL-3+IL-6+Epo medium at the end of the second period of monitoring showed that 97% of the cultures again contained a very large clone when assessed another 7 days later.

These results indicate that SFM containing SF+IL-11 only is unable to support the survival of a large proportion of quiescent adult HSCs, although once these are activated, both their viability and their proliferation can be efficiently sustained by continued exposure to SF+IL-11 supplemented SFM. The initial loss of quiescent adult BM ESLAM cells that occurs when these cells are first isolated can, however, be circumvented by exposing them to other

factors. These are present in both UG26 CM and in the FBS+SF+IL-3+IL-6+Epo cocktail, although these 2 sources of pro-survival factors clearly differ in their mitogenic activities and in their abilities to sustain self-renewal activity (Figure 2.1A). Interestingly, the overall rate at which initially quiescent ESLAM BM cells enter the cell cycle appeared independent of any of these conditions of stimulation.

### 2.3.4 NGF and Col 1 can partially replace UG26 CM in maintaining DSR activity during HSC expansion *in vitro*

As a first step towards identifying the mediators of the biological effects of UG26 cells, we looked for pathways that they differentially activate as well as related candidate effectors secreted by UG26 cells and their possible receptors in purified adult BM ESLAM cells. To undertake these cross comparisons, we generated gene expression profiles for adult BM ESLAM cells before, and 6 hours after they had been placed in culture with or without UG26 CM and with or without SF+IL-11 (as described in the Experimental Procedures). The 6-hour time point was chosen to obtain cells before evidence of their death is obvious when they are cultured in SF+IL-11 alone (Lecault et al., 2011). We then compared these profiles with each other, as well as with a published gene expression profile for UG26 cells (Ledran et al., 2008) (Figure 2.8A).

Analysis of the profiles obtained for ESLAM cells stimulated with UG26 CM (with or without SF+IL-11) compared to fresh ESLAM cells and ESLAM cells stimulated with SF+IL-11 identified a total of 250 (of 430 tested) REACTOME pathways for which some members showed significantly altered transcript expression ($p<0.05$) in cells maintained in UG26 CM with or without SF+IL-11 (Appendix A.1). These

pathways included cell cycle progression and metabolic pathways, signaling pathway activation, apoptosis-related pathways, and RNA processing/splicing pathways (Appendix A.1). To identify specific candidate factors, we used Gene Ontology annotations to select transcripts present in UG26 cells that were categorized as encoding proteins in the "extracellular region" and that had anticipated interactions with expressed genes annotated as having "receptor activity" in the ESLAM cells (Table 2.2). From this analysis, we identified 172 candidate factors (Appendix A.2). From a survey of the current stem cell literature, a comparison of candidate factors to the differential expression of downstream pathways, and factor availability, we then selected a subset of 12 of the 172 candidate proteins for further testing of their ability to block the death of HSCs as previously shown for UG26 CM (Figure 2.8A). Among the 12 candidates tested, we found NGF and Col 1 to be the most effective substitute for UG26 CM (Figure 2.8B). Moreover, when both NGF and Col 1 were present together, 97% of the input ESLAM cells remained viable. Both NGF and Col 1 also mimicked the complete lack of mitogenic activity of the UG26 CM (data not shown).

To assess whether the mechanism of cell death being blocked was apoptosis, we measured the proportion of Annexin $V^+$ ESLAM cells present after 36 hours in cultures containing SF+IL-11 with or without the various pro-survival factors identified (UG26 CM, NGF and Col 1, and FBS+SF+IL-3+IL-6+Epo). The results shown in Figure 2.8C indicate a high frequency of Annexin $V^+$ cells in the cultures containing only SF+IL-11 (20%), only slightly less than the proportion of dead cells determined by visual inspection and subsequent failure to form colonies in the presence of added growth factors (Figure

2.8B). In contrast, all 3 pro-survival additives, including NGF+Col 1, caused a significant decrease in Annexin $V^+$ cells ($p \leq 0.03$).

To determine whether NGF and Col 1 can replace the ability of UG26 CM to promote HSC self-renewal divisions *in vitro* in the presence of SF+IL-11, we set up a final series of 7-day cultures with 1 or 30 ESLAM cells each and assayed the HSC output using the same protocol as in Figure 2.1. Primary recipients of these cultured cells showed that the addition of NGF+Col 1 to SF+IL-11 maintained DSR-HSC numbers in the 7-day cultured cells compared to input levels and produced a 4-fold expansion of total HSCs ($p=0.48$ and $<0.001$, respectively, Figure 2.8D). Although these values were nevertheless not as high as those achieved with UG26 CM ($p<0.001$ and $=0.01$, respectively, Figure 2.1B), secondary transplant assays confirmed the continuing DSR activity of the HSCs maintained using NGF+Col 1 instead of UG26 CM (Figure 2.8D). Analyses of another 23 mice each transplanted with a separate clone generated from a single ESLAM cell cultured for 7 days in SFM containing SF+IL-11 plus NGF+Col 1, showed that 17 of the clones (74%) had produced HSCs and 3 of these (13%) contained DSR-HSCs that included the DSR-HSC-associated β-pattern of differentiation (Figure 2.8E).

## 2.4 Discussion

### 2.4.1 Stromal cells produce factors that synergize with SF and IL-11 to promote DSR-HSC self-renewal divisions *in vitro*

Evidence that HSCs are regulated by non-hematopoietic stromal cells *in vivo* dates back many decades to transplantation experiments performed with *Sl/Sl*$^d$ mice

(McCulloch et al., 1965; Sutherland et al., 1970). Many products of stromal cells and related cell types have now been implicated in the regulation of the HSC compartment *in vivo* (Mercier et al., 2012). Likewise, the most successful strategies for maintaining HSCs long term *in vitro* have involved their co-culture with primary stromal cells or stromal cell lines from various sources (Dexter et al., 1977; Fraser et al., 1990, 1992; Moore et al., 1997; Ploemacher et al., 1989; Wineman et al., 1996). However, the specific stromal-derived factors that support the net expansion of HSCs that takes place during development, or after irradiation or myelosuppressive chemotherapy and the molecular and biological mechanisms targeted remain poorly characterized. The recent identification of distinct subsets of stromal cells with variable roles in regulating different HSC functions in adult BM now raises the interesting possibility that they regulate HSC via non- (or incompletely) overlapping mechanisms (Ding and Morrison, 2013; Guezguez et al., 2013; Kunisaki et al., 2013).

Here we identify different combinations of factors secreted from stromal cells that differentially support biologically distinct HSC functions. These functions are controlled intrinsically by separate, albeit likely interconnecting pathways, although all are important to the speed and extent to which HSC can expand their numbers. Specifically, they are responsible for the maintenance of HSC viability, the response of HSCs to factors that control their cycling state and the maintenance in HSCs of a continuing poised, but undifferentiated state. Clonal analysis and secondary transplant assays of the cells produced *in vitro* under conditions that support all 3 of these functions (i.e., SF+ L-11 plus UG26 cells, or UG26 CM, or NGF+Col 1) demonstrated a significant net expansion of adult mouse HSCs with either maintenance or expansion of HSCs with

DSR properties. In contrast, in the absence of UG26 cells, or UG 26 CM or NGF+Col even full maintenance of ESLAM (and hence HSC) survival and mitogenesis, as could be achieved with exposure to FBS+SF+IL-3+IL-6+Epo, was not sufficient to prevent a rapid and significant loss of DSR activity. In addition, we found the kinetics of mitogenesis to be unaltered under conditions where >50% of the ESLAM cells failed to survive the first 24 hours *in vitro* (i.e., in SF+IL-11). We also used analysis of split doublets to formally document the execution of first divisions that produce 2 DSR-HSC under conditions where survival, proliferation and self-renewal were all well supported. These findings thus represent a major advance over previously reported results with "optimal" cytokine cocktails (SF+IL-11, SF+TPO+Angptl3+I+FGF+H, SF+Wnt3A) that we now show result in a net and rapid loss of total input DSR-HSCs.

Until recently, the speed with which many adult mouse BM HSCs die (in the first 12 hours) when they are incubated under conditions generally used to stimulate their rapid entry into the cell cycle had not been widely appreciated. However, in retrospect, this finding may account for historic difficulties in obtaining pure mouse HSC populations and the low yields accompanying more promising approaches. Surprisingly little is known about the specific regulation of HSC viability beyond the level of expression of particular genes with identified roles in general cell survival control and evidence of their activation in leukemia (Jordan and Guzman, 2004). A notable exception was an early study suggesting an ability of Bcl-2 to delay HSC apoptosis and synergize with SF to maintain HSC survival (Domen et al., 2000). We did not find evidence of up-regulated Bcl2 in the HSCs treated with UG26 CM, but this is not surprising as Bcl-2 has not been implicated in the physiological control of HSCs. It is thus inviting to speculate

that NGF+Col 1 and UG26 CM may modulate similar downstream pathways to block apoptosis, as suggested by our finding of a differential expression of genes in the 'Apoptosis' REACTOME pathway following UG26 CM exposure, and the similar relative decrease in Annexin V staining of ESLAM cells incubated with either of these additives.

### 2.4.2 The effects of stromal factors on HSC self-renewal in vitro are manifest within the first cell cycle and act to preserve the HSC lineage program as well as their DSR state

Of note, the early death of HSCs appeared complete, even before they entered the cell cycle – consistent with a significant dissociation in the signaling pathways that promote survival and mitogenesis. This inference was further supported by the finding that both UG26 cells, and NGF+Col 1, have potent pro-survival HSC activity in the absence of any mitogenic effect on the HSCs thus "protected". The maintenance of DSR potential also appears to be regulated independent of the control of this early pro-survival effect on initially isolated quiescent adult HSCs, as the FBS+SF+IL-3+IL-6+Epo cocktail was similarly able to prevent early death of HSCs, but induced a rapid loss of their self-renewal property. Analysis of paired daughter cells of individual input ESLAM cells further showed that they required early exposure to UG26 CM (in their first cell cycle) to retain a DSR-HSC state. This is an important extension of our previous observation that abrogation of all HSC activity can be obtained even before the cells complete a first cell cycle if they are exposed to suboptimal concentrations of SF (Kent et al., 2008). These results suggest that survival and maintenance of DSR competence in quiescent HSCs

depend on their continuous exposure to different external factors that act via pathways (or pathway elements) that do not require, nor involve, entry into cell cycle.

Of additional interest is the observation that the time taken for mitogenically stimulated ESLAM cells to reach a first metaphase is positively associated with the likelihood that at least one of their 2 daughter cells will retain HSC functionality. This is consistent with previous evidence that longer cell cycle transit times correlate with the most primitive HSCs (Dykstra et al., 2006; Lutolf et al., 2009; Yamazaki et al., 2009). Such associations suggest the possibility that cell cycle control, like retention of GM differentiation potential, may be mechanistically linked to DSR competence in adult mouse BM HSCs.

Our findings are also potentially relevant to understanding the role of transplantation assays in detecting cells with the molecular machinery required for HSC activity. Single-cell transplantation experiments, confirmed here, have consistently shown that approximately half of these cells are detectable as HSCs whereas the other half are not. However, as now revealed, nearly all FACS-purified ESLAM cells can display extensive proliferative potential *in vitro*, even though only half are detectable as LTC-ICs in a 6 to 7-week assay (Kent et al., 2009). Moreover, the frequency of ESLAM cells that can respond to SF+IL-11 in the presence of UG26 CM *in vitro* by generating progeny HSCs that are functional *in vivo* is significantly higher than the 40% of freshly isolated ESLAM cells that are directly detectable *in vivo* as HSCs. Taken together, this raises the possibility that most adult BM ESLAM cells have not irreversibly lost the molecular status of HSCs. Both, the *in vitro* as well as the *in vivo* experiments suggest

that a critical phase for cells to be detected as HSCs is when they are exiting a quiescent state.

Overall, these data suggest that several core HSC behavioral programs can be functionally uncoupled, allowing their differential and combinatorial activation by an array of external factors. This differential program activation could result from activation of multiple independent signaling pathways (a combinatorial switch mechanism), by different levels of activation in few common pathways (a cellular rheostat-like mechanism), or by some combination of these two. Furthermore, in either case additional molecular interaction downstream of these pathways is likely. The various genes and pathways previously implicated in HSC maintenance/expansion are consistent with a combinatorial mechanism operating to control HSCs (Reya et al., 2003). Similarly, previous findings by our group that low concentrations of SF provide HSC survival benefits but maintenance of some repopulation potential requires high levels of SF provides some preliminary support for the existence of mechanisms that depend on different signaling thresholds in these cells (Kent et al., 2008). It will be of significant interest to determine the molecular underpinnings of these programs and their relevance to human HSC regulation.

### 2.4.3 Implications for future improvement of HSC expansion protocols

Our findings have several significant implications. First, they further underscore the deficiency of 4- to 6-month PB repopulation endpoints that do not specifically measure the output of donor-derived GM cells in order to distinguish between HSC that have retained or lost DSR activity, as recently highlighted by others (Yamamoto et al.,

2013). Second, they indicate that mouse DSR-HSC self-renewal divisions can be achieved under defined conditions *in vitro* and in the absence of any other cells. However, to achieve this response, multiple extrinsic factors are required. Third, it is now clear that at least some of the factors required (exemplified by Col 1 (Hu et al., 2011) and NGF (García et al., 2004)) may be ubiquitously prevalent extracellular matrix components of the interstitial space within hematopoietic tissue. Notably, recent studies have highlighted a differential expression on the surface of HSCs and their closely related downstream derivatives (Benveniste et al., 2010; Notta et al., 2011; Wagers and Weissman, 2006) of several integrins, which are receptors for such proteins. Thus, factors that activate these receptors may constitute an additional strategy for enhancing HSC expansion, as has also been suggested by others (Celebi et al., 2011; Kurth et al., 2011; Umemoto et al., 2012). Finally, the demonstrated ability of a combination of defined soluble proteins to replace contact with stromal cells to promote HSC maintenance and expansion refutes the hypothesis that cell contact is required to mediate such responses and provides a new and powerful platform for interrogating the mechanisms involved in the maintenance of the DSR state and its retention by HSCs when they are stimulated to proliferate.

**Table 2.1 Concentration of additives used in single ESLAM cell survival screens**

| Additive | Concentration |
|---|---|
| TGF-β | 5 ng/mL |
| Fibronectin | 10 µg/mL |
| EGF | 1 ng/mL |
| Laminin | 50 µg/mL |
| M-CSF | 100 ng/mL |
| SDF1 | 300 ng/mL |
| BMP4 | 20 ng/mL |
| PDGF | 50 ng/mL |
| Activin A | 5 ng/mL |
| PTN | 250 ng/mL |
| Collagen | 300-600 µg/mL |
| Reduced GF Matrigel | 10 % |
| NGF | 250 ng/mL |
| Col + NGF | 300 µg/mL, 250 ng/mL |
| Matrigel | 5-10 % |

**Table 2.2 Significantly affected pathways of ESLAM cells upon stimulation with UG26 CM and SF+IL-11.**

| Signaling pathways | Number of involved genes | Regulation of HSC | References |
|---|---|---|---|
| NGF | 208 | AGM HSC activity | (Durand et al., 2007) |
| PDGF | 63 | HSC expansion | (Su et al., 2002) |
| WNT | 54 | HSC proliferation | (Reya et al., 2003; Willert et al., 2003) |
| EGFR | 46 | HSC migration | (Ryan et al., 2010) |
| ROBO Receptor | 32 | HSC-niche interaction | (Shibata et al., 2009; Smith-Berdan et al., 2011) |
| BMP | 23 | AGM HSC activity | (Durand et al., 2007) |
| Integrin Signaling | 23 | HSC adhesion | (Benveniste et al., 2010; Notta et al., 2011) |
| TGF-ß | 15 | HSC subtype regulation | (Challen et al., 2010) |
| Notch | 14 | HSC *de novo* generation | (Kumano et al., 2003) |
| VEGF | 11 | HSC survival | (Gerber et al., 2002) |

NGF: nerve growth factor, AGM: aorta-gonad-metanephron, PDGF: platelet derived growth factor, EGFR: epidermal growth factor receptor, ROBO: roundabout family, BMP: bone morphogenic protein, TGF-ß: transforming growth factor-beta, VEGF: vascular endothelial growth factor.

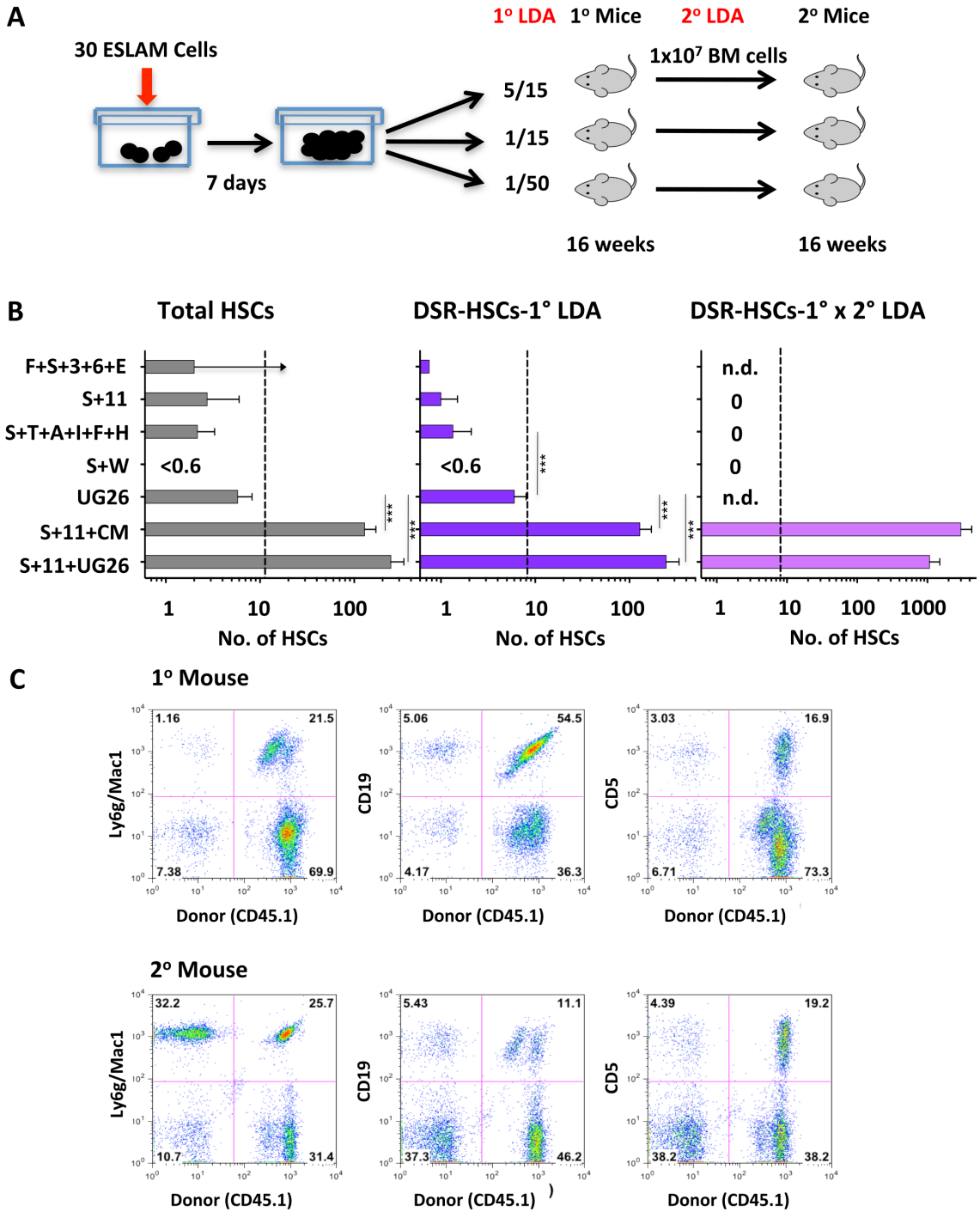


**Figure 2.1 Comparison of the number of HSCs present in 7-day cultures of ESLAM cells containing different growth factor cocktails and supplements.** A. Schematic showing the experimental design used. B. Results of 16-week limiting dilution transplant assays used to determine the outputs of HSCs and DSR-HSCs, as defined

in the text and Experimental Procedures (left 2 panels), and the overall DSR-HSC expansion obtained *in vitro* and then in primary ($1^o$) recipients (right panel) (12 mice/condition/experiment, 3-5 experiments/condition). In each panel, the dotted line: shows the corresponding total or DSR-HSCs present in the initial 30 ESLAM cells based on the results of transplants of 50 single ESLAM cells. Each bar shows the mean and standard error of the mean (SEM) for a given test culture condition. Holm-corrected pair-wise significance values are shown with * representing p=0.05, ** representing p=0.01, and *** representing p<0.001. Where a limiting dilution was not reached, the bar indicates the minimal HSC value detectable with an upward arrow on the bar to indicate this. Supplements were as follows: F+S+3+6+E = 15% FBS+50 ng/mL SF+10 ng/mL IL-3+10 ng/mL IL-6+3 U/mL EPO; S+11 = 100 ng/mL SF+20 ng/mL+IL-11; S+T+A+I+F+H = 10 ng/mL SF+20 ng/mL TPO+100 ng/mL Angptl3+500 ng/mL IGFBP2+10 ng/mL FGF1+10 μg/mL heparin (H); S+W = 30 ng/mL SF+100 ng/mL Wnt3a; UG26 = UG26 cells; CM = 50% UG26 CM; and S+11+CM = SF+IL-11+ 50% UG26 CM. C. Representative FACS profiles of PB cells obtained 16 weeks after transplanting primary and secondary mice with cells harvested from cultures containing UG26 cells plus SF+IL-11, described in Panel B. The following markers were used to investigate donor chimerism: Ly6g/Mac1 (GM cells), CD19 (B-cells), CD5 (T-cells).

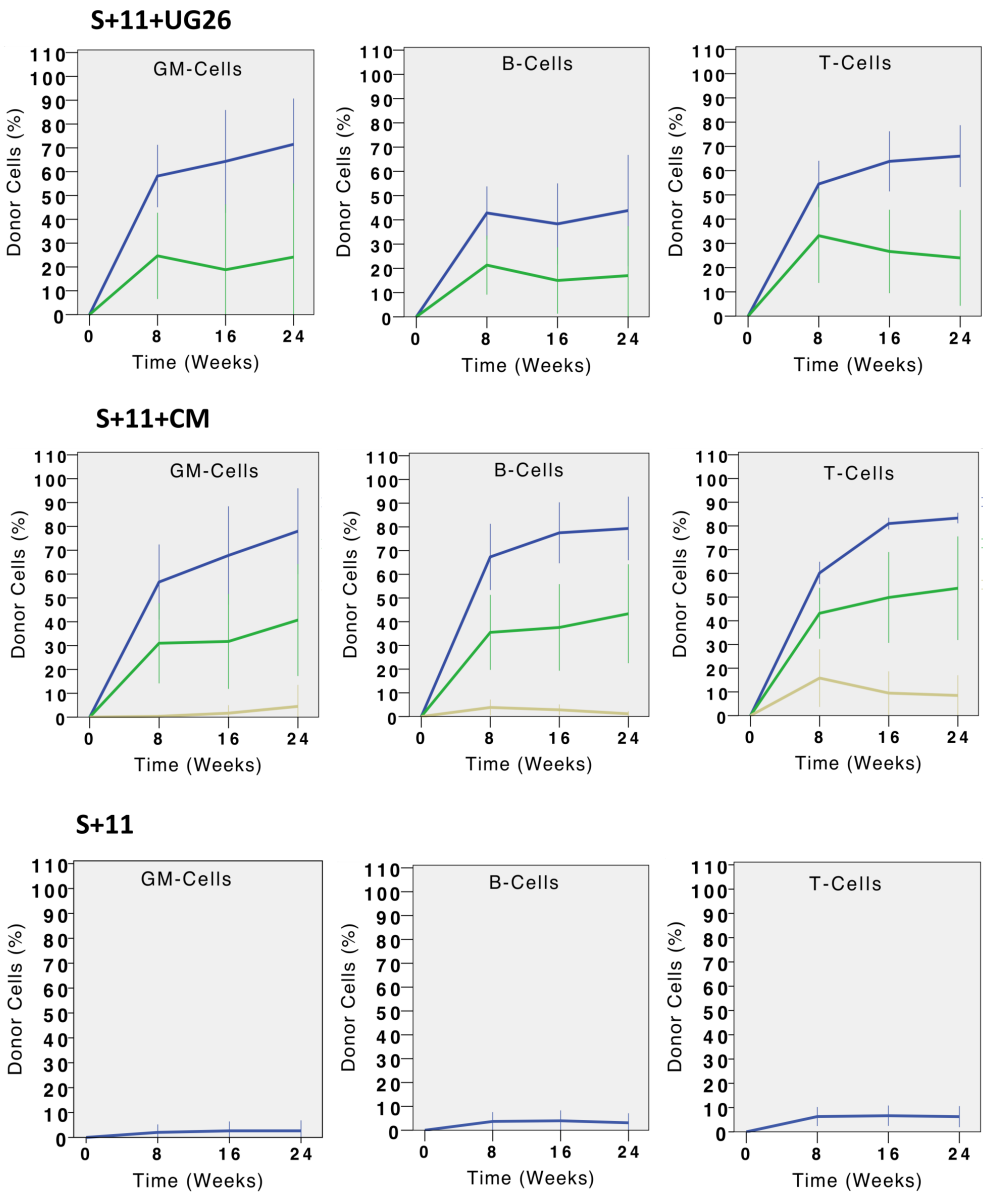


**Figure 2.2 Comparison of the different reconstitution kinetics obtained in mice transplanted with matched progeny outputs of ESLAM cells cultured for 7 days with different stimuli.** Depicted are the geometric mean percentages of donor cells in the total circulating GM-, B-, and T-cells measured at different times after transplanting groups of mice with the progeny of 30 ESLAM cells cultured under the conditions indicated and described in Figure 2.1. Error bars indicate the range defined by ±2 SEM. Blue lines indicate mice that received 1/15$^{th}$ of a culture each; green lines indicate mice that received 1/50$^{th}$ of a culture each and brown lines indicate mice that received 1/90$^{th}$ of a culture each.

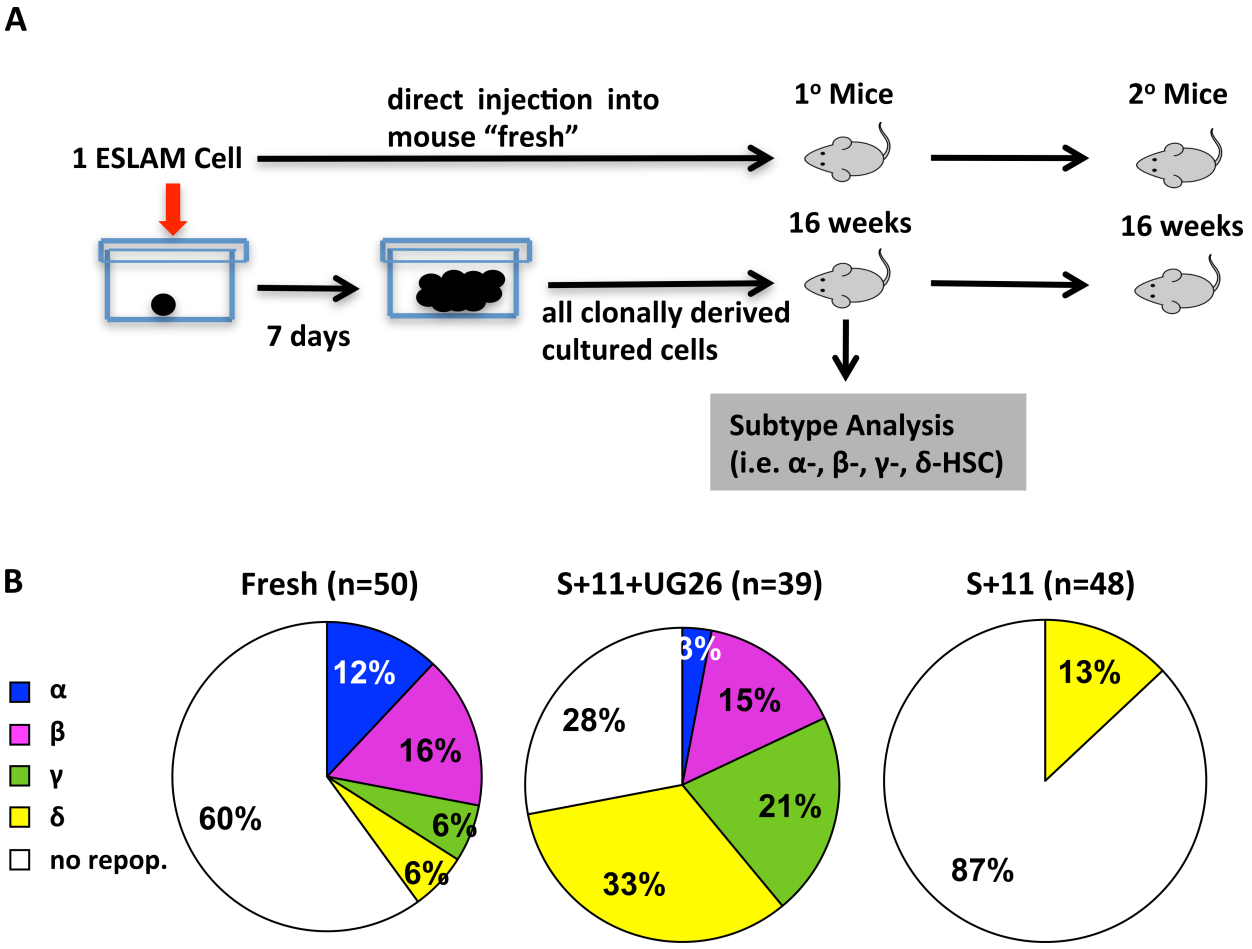


**Figure 2.3 Comparison of the effect of different supplements on the frequency of HSC-containing clones and their differentiation patterns in 7-day cultures initiated with single ESLAM cells.** A. Schematic showing the experimental design used. B. Pie charts showing the frequency of HSCs in the input ESLAM population (50 cells tested) and the distribution of the different differentiation patterns obtained from them (left), as compared to the frequency of HSC-containing clones and the differentiation patterns they generated in transplanted recipients for clones generated in 7-day cultures initiated with single ESLAM cells stimulated with UG26 cells plus SF+IL-11 (middle, 39 clones tested) or SF+IL-ll only (right, 48 clones tested). The definitions used to distinguish α, β, γ, and δ patterns of differentiation are given in the Experimental Procedures. The results are pooled from 3-6 experiments.

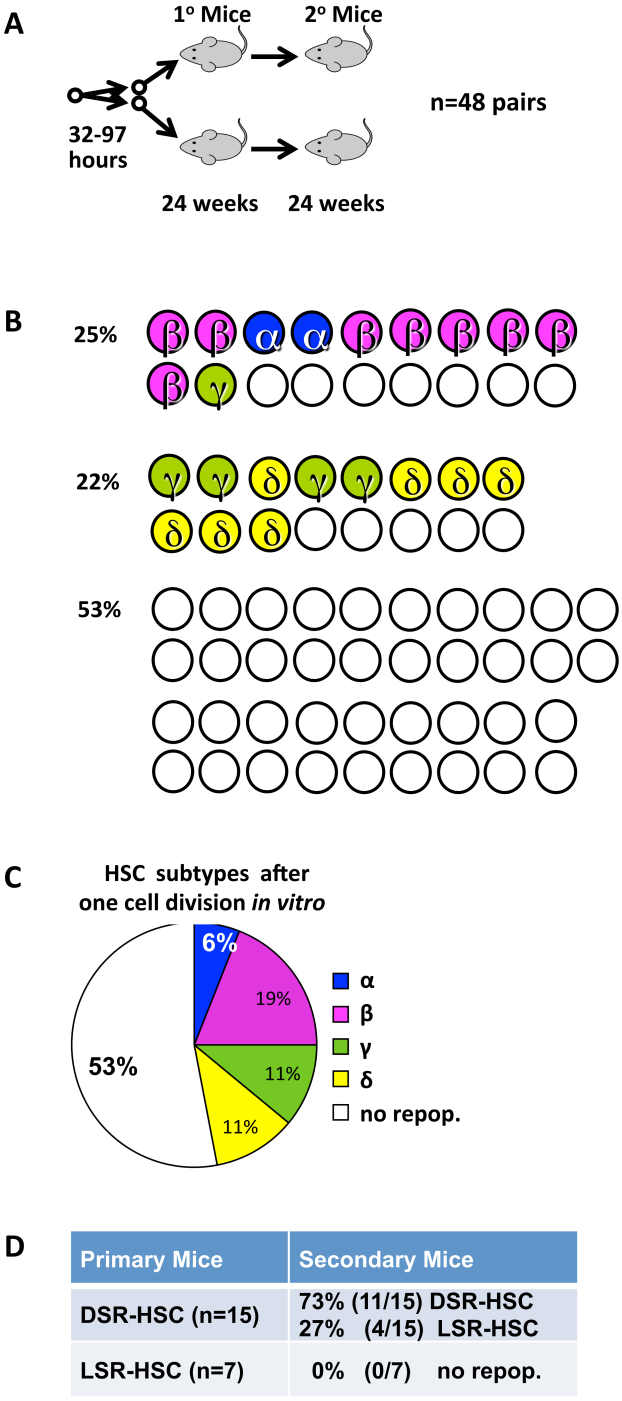


D

| Primary Mice | Secondary Mice |
|---|---|
| DSR-HSC (n=15) | 73% (11/15) DSR-HSC<br>27% (4/15) LSR-HSC |
| LSR-HSC (n=7) | 0% (0/7) no repop. |

**Figure 2.4 UG26 CM enhances the retention of DSR-HSC functionality in the first division progeny of single ESLAM cells.** A. Experimental design. 36 ESLAM cells were cultured as single cells in UG26 CM plus SF+IL-11, and 12 in SF+IL-11 only. Doublets produced from cells that divided between 32 and 97 hours after the

cultures were initiated were transferred into separate wells and then each cell of each pair was injected into a separate mouse. After 16 weeks the PB was analyzed to determine whether the injected cell was an HSC and its α, β, γ, or δ subtype as well as its DSR or LSR subtype. After 24 weeks, BM cells from DSR-HSC-repopulated primary mice were harvested and secondary transplantations performed. Sixteen weeks later the PB cells from these secondary mice were analyzed. B. Identified α, β, γ, or δ HSC-subtypes in each first generation pair of ESLAM daughter cells in which at least one daughter cell was an HSC of any type. Since none of the 24 mice that received a cell cultured in SF+IL11 showed engraftment, only data of cells cultured in UG26CM+SF+IL11 is shown. C. Distribution of the types of inferred input ESLAM cells classified according to the α, β, γ, or δ HSC-subtypes that they produced in their first generation progeny, as shown in Panel B. When both progeny were HSCs, the initial ESLAM cell was classified as the more primitive subtype (α, β, γ, δ – in that order). D. Representation of DSR- and LSR-HSC subtypes in the first generation progeny of ESLAM cells as determined from their reconstituting properties (same progeny shown in Panel B) and the DSR activity seen in secondary recipients of cells transplanted with BM harvested from the primary mice.

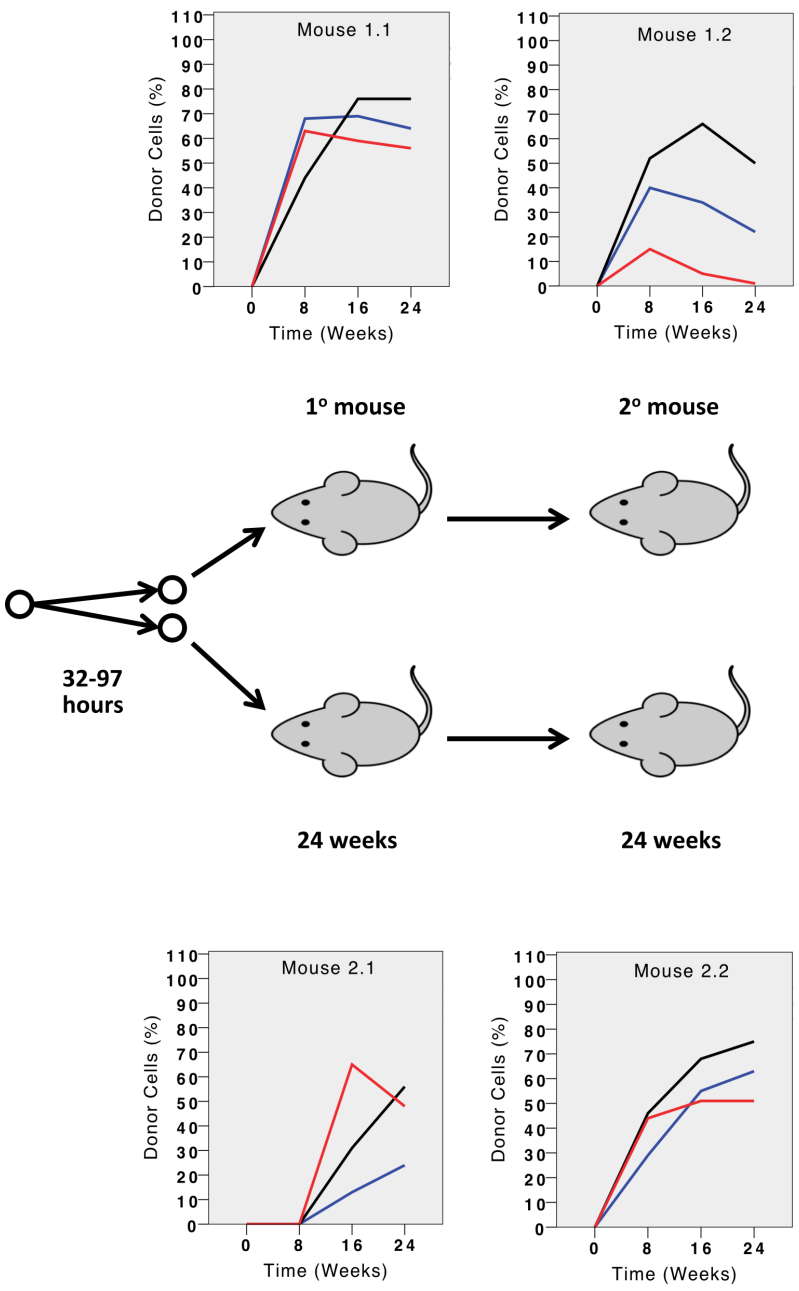


**Figure 2.5 Comparison of the serial GM-, B-, and T-cell reconstituting activities of the 2 β-HSCs and their progeny produced from the first *in vitro* division of a single ESLAM cell.** Donor-derived contributions to the PB GM cells are shown in red, to the PB B-cells in blue, and to the PB T-cells in black.

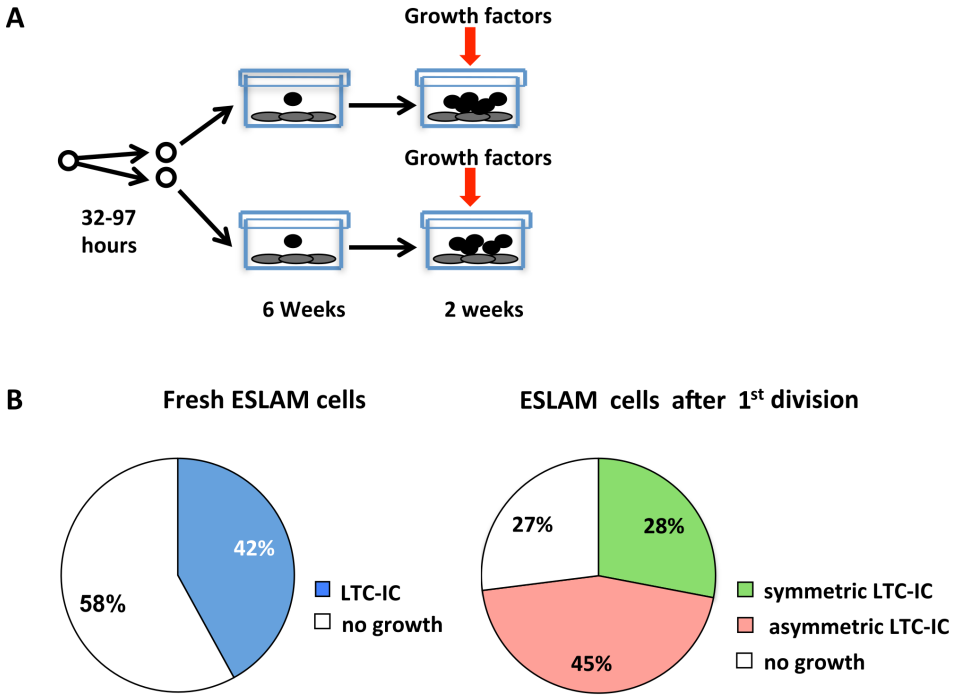


**Figure 2.6 UG26 CM and SF+IL-11 support the frequent production of LTC-ICs in both progeny of single ESLAM cells stimulated to divide *in vitro*.** A. Experimental design. 96 ESLAM cells were cultured as single cells in UG26 CM and SF+IL-11 until they divided a first time as in Figure 2.4. The doublets produced were then transferred into 192 separate wells containing UG26 cells and assayed for LTC-IC activity in a 6-week assay as described in the Methods. B. Pie charts showing the frequencies of LTC-ICs (light blue fraction) as determined from assays of single freshly isolated ESLAM cells (left), and the frequencies of ESLAM cells that produced 2, 1 or no LTC-ICs in their first division progeny (right).

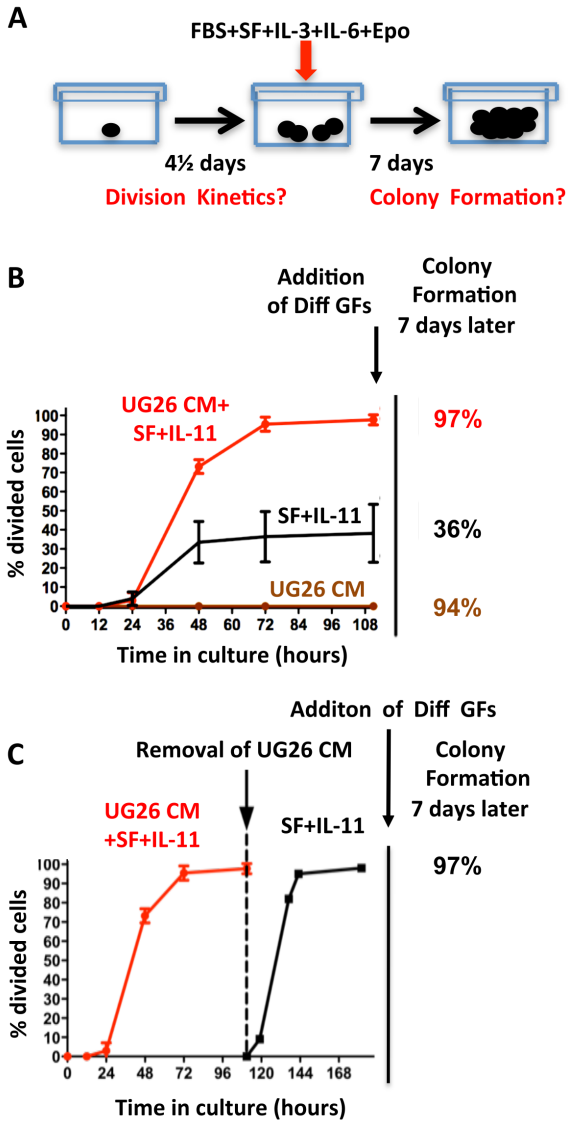


**Figure 2.7 Comparison of the different mitogenic and pro-survival activities of UG26 CM, SF+IL-11 and the combination on ESLAM cells in single cell cultures.** A. Experimental design used. Mitogenic activity was measured by monitoring the proportion of initially plated single ESLAM cells that completed a first division over a period of 4½ days *in vitro* under different conditions as assessed by visual inspection of the first appearance of a doublet. Pro-survival activity was measured by adding FBS+SF+IL-3+IL-6+EPO at the end of the 4½ days and determining whether a clone of >7 cells was present 7 days later. B. Cumulative plots of the kinetics with which single ESLAM cells completed a first division when cultured either in UG26 CM plus SF+IL-11 (CM+SF+IL11), or SF+IL-11 only, or UG26 CM (CM) only. Results

are pooled from 5 experiments in which 96 individual cells were examined in each experiment. Error bars show 95% CI. C. Plot showing the kinetics with which single ESLAM cells completed a second division when they were cultured for an initial 108 hours in UG26 CM plus SF+IL11 (until each cell divided at least once), and then the SFM and SF+IL11 was substituted for UG26 CM plus SF+IL11 (after washing the cells twice with SFM). Results are pooled from 3 experiments; 96 individual cells examined per experiment.

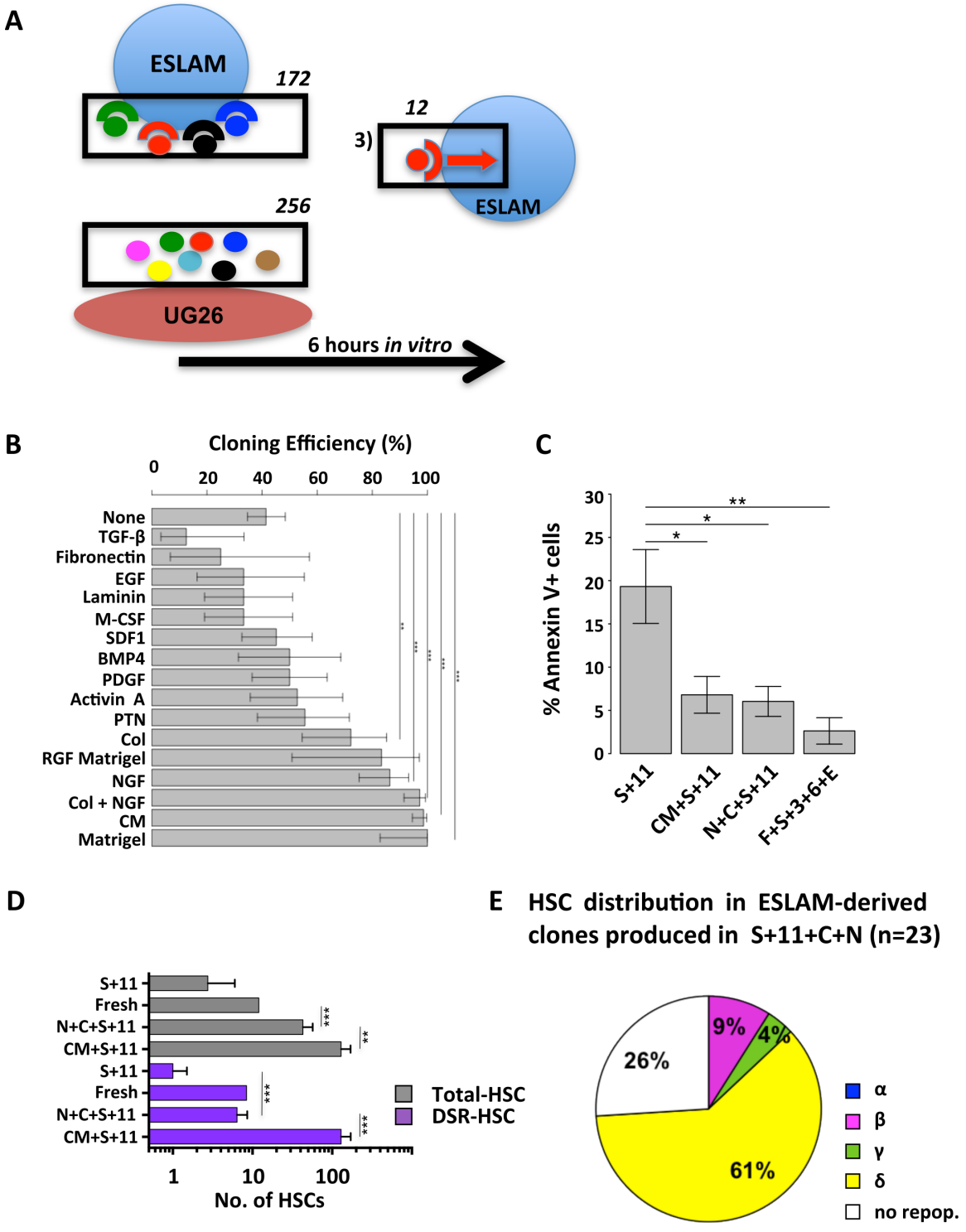


**Figure 2.8 Col 1 and NGF can substitute for UG26 CM to support DSR-HSC self-renewal *in vitro*.** A. Graphical display of the algorithm used to identify significantly changed pathways from Affymetrix gene chip data obtained on stromal cells and input and responding ESLAM cells. Numbers above the boxes indicate the number of

sequentially identified genes. Additional details are provided in the text and Supplementary Material. B. Comparison of the ability of different factors to enhance the survival and mitogenesis of isolated ESLAM cells cultured in SFM with 100 ng/ml SF + 20 ng/ml IL-11. Cultures were incubated for 7 days and scored as positive for clone formation if they contained >7 refractile cells. 12-144 cells were analyzed per test condition. Holm-corrected pair-wise significance values are shown with * representing p=0.05, ** representing p=0.01, and *** representing p<0.001. 95% CI were generated using the R function 'prop.test'. C. Proportion of Annexin $V^+$ cells in 36-hour cultures of ESLAM cells incubated in SFM plus the additives shown. Values indicated are the mean±SEM for data from 4 independent experiments. D. Outputs of HSCs from 7-day cultures initiated with 30 freshly isolated ESLAM cells as compared to input values using the same experimental design as shown in Figure 1A with HSCs and DSR-HSCs assessed by 16-week limiting dilution transplantation assays (12 mice/condition/experiment, 3-5 experiments/condition). White bars: total HSCs; purple bars: DSR-HSCs. Values shown are the mean ± SE. Additions were SF+IL-11 (= S+11); NGF+Col 1+SF+IL-11 (= N+C+S+11) or UG26 CM+SF + IL-11 (=CM+S+11) at same concentrations as in Figure 1. E. Distribution of HSC activity in clones derived from 23 single ESLAM cells cultured in SF+IL-11 plus Col 1+NGF for 7 days as determined from 16-week transplantation assays of single clones transplanted into individual mice.

# Chapter 3: Distinct programs control human hematopoietic stem cell survival, proliferation and maintenance

## 3.1 Introduction

The discovery of transplantable hematopoietic cells with stem cell properties in mice half a century ago (Siminovitch et al., 1963; Till and McCulloch, 1961; Wu et al., 1967) was rapidly translated into a clinical therapeutic modality. Transplants of human hematopoietic stem cell (HSC)-containing products now form a key component of curative treatments for many diseases (Thomas, 1993). Recently, a rare subset of human $CD34^{+}CD38^{-}CD45RA^{-}CD90^{+}CD49f^{+}$ CB cells (hereafter referred to as $CD49f^{+}$ cells) has been identified as being highly enriched (10% pure) HSCs, as shown by their ability to regenerate long-term (>6 months) hematopoietic activity in sub-lethally irradiated immunodeficient mice (Notta et al., 2011).

In mice, it has been possible to show that individual HSCs can be greatly expanded *in vivo* with lifetime retention of their original functional potential (Dykstra et al., 2007; Harrison, 1979; Iscove and Nawa, 1997; Keller et al., 1985). Years of persisting hematopoiesis in patients given allografts or gene-marked autologous cells (Aiuti et al., 2013; Biffi et al., 2013; Cartier et al., 2009; Cavazzana-Calvo et al., 2010) has supported the idea that the same biology applies to transplanted human HSCs. These findings have led to the expectation that large and sustained expansions of human HSCs should ultimately be achievable *in vitro*.

This goal has recently attracted further attention both to extend the use of CB collections, and to take advantage of newer gene-targeting strategies (Hsu et al., 2014). A number of strategies have been employed to improve the maintenance of HSCs and expansion of transplantable cell types in GF-supplemented cultures. These include over-expression of

transcription factors (Sloma et al., 2013), fed-batch culture systems (Csaszar et al., 2012), small molecules (Baudet et al., 2012; Boitano et al., 2010; Fares et al., 2014), less well understood GFs (Goessling et al., 2011; North et al., 2007; Ohishi et al., 2002; Suzuki et al., 2006), and co-culture with fibroblasts (de Lima et al., 2012). However, the results of these studies have not lived up to predictions from analogous experiments with mouse HSCs (Antonchuk et al., 2002; North et al., 2007; Ohta et al., 2007; Wohrer et al., 2014).

Combinations of human SCF, FLT3L, IL3, IL6, and G-CSF have been used extensively to expand primitive human HSCs *in vitro* . However, specific cell types and sources respond differently to these 5GFs, and their responses are also affected by the concentrations and combinations of these GFs to which they are exposed (Petzer et al., 1996a, 1996b; Zandstra et al., 1997, 1998). For example, beneficial concentrations of IL3 can be detrimental to the maintenance of long-term culture-initiating cells when SCF and FLT3L levels are reduced without affecting the concomitant expansion of colony-forming cells (Zandstra et al., 1997). These variables, together with the failure of current human HSC expansion strategies to meet expectations predicted from studies of mouse HSCs, highlight the need to investigate the mechanisms necessary for human HSC expansion directly in these cells.

We therefore designed a study to analyze the cellular and molecular effects of these 5 GFs alone and in combination on the purest source of human HSCs thus far described (Notta et al., 2011). The results show that these 5 GFs in combination can maintain input HSC numbers while simultaneously promoting huge outputs of differentiating cells when anticipated negative effects of co-produced myeloid cells are minimized. They also demonstrate that these GFs regulate the survival and proliferation of human HSCs in a direct and combinatorial fashion through mechanisms that are independent both from one another, and from the maintenance of

HSC status. Finally we identify specific molecular intermediates that are differentially activated by these factors including some that are activated only when all 5 GFs are present. These findings offer new insights into the control of HSC behavior, and open the way for rationally designed *ex vivo* HSC expansion strategies.

## 3.2 Methods

### 3.2.1 Human CB cells

Anonymized heparinized CB was obtained from normal full-term cesarian section deliveries in accordance with procedures approved by the Research Ethics Board of the University of British Columbia and samples from a single day pooled for further processing. Bulk low-density (<1.077g/ml) cells were then isolated by centrifugation on Lymphoprep (STEMCELL Technologies), or $CD34^+$ cells (>50%) were directly isolated by a 2-step procedure using reagents from STEMCELL Technologies, first to remove the bulk of the $CD11b^+$ monocytes, $CD3^+$ T-cells and $CD19^+$ B-cells along with the neutrophils and red blood cells using RosetteSep™, followed by a positive EasySep™ selection of the enriched $CD34^+$ cells according to protocols recommended by the supplier. The cells recovered in either case were then viably cryopreserved in DMSO and FBS (STEMCELL Technologies) for later use.

Cells were thawed by drop-wise addition of IMDM (STEMCELL Technologies) supplemented with FBS and 10 µg/mL DNase (Sigma-Aldrich). Cells were then re-suspended in blocking buffer consisting of Hank's Balanced Salt Solution (HSBS) supplemented with 5% human serum and 1.5 µg/mL anti-human CD32 antibody (Clone IV.3; STEMCELL Technologies) and stained for 1-2 hours with the antibodies listed in Table 3.1. $CD49f^+$ CB cells

were then isolated by sorting on a BD Influx II, BD FACSAria II, III or Fusion sorter (Becton Dickenson) using purity or single cell modes (as relevant).

### 3.2.2 *Ex vivo* HSC expansion experiments

All CB suspension cultures were performed using IMDM supplemented with 10 mg/mL bovine serum albumin, 10 µg/mL insulin, 200 µg/mL transferrin, 40 µg/mL low-density-lipoprotein, 100 U/mL penicillin, 100 µg/mL streptomycin, 2 mM glutamine (STEMCELL Technologies), and $10^{-4}$ M β-mercaptoethanol (Sigma), referred to as SFM, with other additives as indicated. All cultures were incubated in a humidified atmosphere at 37˚C in room air supplemented with $CO_2$ to achieve a final concentration of 5%.

For each 21-day HSC expansion culture, 1,000 $CD49f^+$ CB cells were delivered by the FACS machine directly into 1 mL of SFM supplemented with a cocktail of 5 recombinant human GFs. These consisted of SCF (gifted by Amgen) at 100 ng/mL, FLT3L (gifted by Immunex) at 100 ng/mL, IL3 (gifted by Novartis) at 20 ng/mL, IL6 (gifted by Cangene) at 20 ng/mL, and G-CSF (from STEMCELL Technologies) at 20 ng/mL. 1 mL of fresh medium containing the same 5-GF supplement was added on days 9, 10, 11, 16, and 20. EasySep™ positive selection of the $CD34^+$ cells was performed on days 12 and 17 of culture with 3 washes of the selected $CD34^+$ cells followed by their re-suspension in 3 mL fresh medium containing 5 GFs. Analysis of small samples collected pre-EasySep™ and from cell washes showed that, on average, 6% (SD = 3%) of the input-derived $CD34^+$ cells were lost in each of the $CD34^+$ cell enrichment steps undertaken on days 12 and 17 (Table 3.2).

For the 4-day cultures, $CD49f^+$ cells were sorted into SFM and then split by volume into each media condition such that each condition had 330 total starting cells in 0.5 mL. Individual GF concentrations were the same as used in the 5-GF cocktail.

### 3.2.3 HSC quantification in immunodeficient mice

Test cell suspensions were injected intravenously into NOD.Cg-$Prkdc^{scid}Il2r\gamma^{tm1Wjl}$/SzJ (NSG) mice pretreated with 315 cGy whole body $^{137}Cs$ γ-irradiation. Mice were bred and maintained in the Animal Resource Centre of the British Columbia Cancer Research Centre under SPF conditions and used according to protocols approved by the Animal Care Committee of the University of British Columbia. For transplants of freshly isolated $CD49f^+$ cells, aliquots of the required number of these were sorted into 100 µL SFM in a 96-well plate followed by injection of the contents of each well into a single NSG mouse. Post-culture doses were calculated as starting cell equivalent (SCE) proportions of the final culture (e.g., from 1,000 starting cells, 1/10th of the final volume would be 100 SCE). Bone marrow aspirates were performed 12, 20, and 30 weeks post-transplant and evidence of human hematopoietic cells tracked by flow cytometric analysis (using a BD LSR Fortessa analyzer, Becton Dickenson) of antibody-stained cells using a detection threshold of 10 cells that showed positive staining with each of 2 independent anti-human CD45 antibody clones and various lineage-specific antibodies (Table 3.3). This enabled a threshold of human cell chimerism of ~0.005% to be used reproducibly for the identification of “positive” mice (Figure 3.1). All LDA calculations were performed using the 'elda' function in the package 'statmod' in R.

After 33-42 weeks, all primary recipients were sacrificed. FACS-purified human $CD34^+CD38^{lo/-}$ cells were then isolated from pooled cells harvested from the pelvis, femurs, and

tibiae of all mice in the same group, and transplanted intravenously into NOD.Cg-Rag1$^{tm1Mom}$ Il2rg$^{tm1Wjl}$/SzJ (NRG) mice pretreated with 900 cGy whole body $^{137}$Cs γ-irradiation delivered over 3 hours (based on preliminary experiments showing that this gives equivalent reconstitution of all lineages from transplanted human CD34$^{+}$ CB cells as is obtained in NSG mice given 315 cGy, unpublished data). Bone marrow aspirates were obtained from these secondary NRG recipients another 3, 16, and 30 weeks later and levels of human chimerism determined using a Fortessa analyzer to quantify cells stained with the antibodies shown in Table 3.3.

For short term (4-day) cultures and associated day 0 controls, 100 SCE by volume were injected intravenously into NRG recipient mice pretreated with 900 cGy whole body $^{137}$Cs γ-irradiation. An additional 5 SCEs from each culture were put into a Terasaki plate and counted to estimate the cell output from each culture. Bone marrow aspirates were performed at 16 and 24 weeks post-transplant and the level of human chimerism and bone marrow progenitor content determined by flow cytometry using the antibodies shown in Table 3.4.

### 3.2.4 Single-cell cultures

Custom polydimethylsiloxane (PDMS) microfluidics chips were produced using multilayer soft lithography with layers bound by oxygen plasma treatment (Duffy et al., 1998; Thorsen et al., 2002; Unger et al., 2000). These devices combine an inverted well geometry for gravity-based cell capture with a 6 mL capacity open topped iso-osmotic bath layer similar to the devices previously reported for the culture of mouse HSCs (Lecault et al., 2011). Our chips contained 8,192 wells with each well having a volume of 2.9 nL. Each of these chips contained 4 individually addressable arrays with 2,048 wells. In later experiments, we also added a multiplexor (Lecault et al., 2011; Thorsen et al., 2002) to each arrays to further sub-divide each

into 16 sub-arrays of 128 wells. These devices were mounted on an inverted microscope (Nikon Ti-E w/ Perfect Focus System or Axiovert 200, Carl Zeiss) with a motorized stage (ASI MS-2500 XY Flat-Top Extended Travel Stage, Applied Scientific Instrumentation, or ProScan II, Prior Scientific) and maintained in an incubation chamber at 37˚C in 5% $CO_2$ in air with water dishes to ensure a high humidity.

All microfluidics devices were loaded with SFM and maintained at 37˚C overnight prior to loading the cells into the array. This was accomplished using a forward pressure of 4-6 pounds per square inch (PSI) and back pressure of 3 PSI. Valve pressure was maintained at 45 PSI when activated. Cells were sorted into SFM in Protein LoBind 1.5 mL Eppendorf tubes, spun down, and the volume reduced to ~10 µL. This volume was then taken up into polytetrafluoroethylene (PFTE) tubing (Cole-Parmer or Alpha Wire, Allied Electronics) pre-coated with SFM, and loaded into the microfluidics device as described in (Lecault et al., 2011). SFM supplemented with specified GFs was then flowed into the arrays for 2-20 minutes. The minimum time to complete a medium exchange was determined empirically by tracking the time taken to remove a loading of a fluorescent dye. For short term (48-hour) cultures, the medium was added only once, at the start of the experiment. For 4-day experiments, media was changed every 8-12 hours. Time 0 for each culture arm was set as the time at which media was added to that array/sub-array.

A charge-coupled device (CCD) camera (Grasshopper3 2.3 MP Mono USB3 Vision (Sony Pregius IMX174), Point Grey, or Orca, ER, Hamamatsu) with a 20x objective was used for image acquisition. Bright-field images were obtained every 30 minutes, and fluorescent images were obtained daily with automated chamber alignment and focus setting as described in Lecault *et al.* 2011 (Lecault et al., 2011). Images were scored manually for cell survival and proliferation.

Single-cell cultures of $CD49f^+$ CB cells were also performed in Terasaki plates. In this case, the cells were deposited directly as single cells into 20 µL SFM with indicated GFs into the wells of a 72-well Terasaki plate (Robbins Scientific or Greiner Bio-One). The plates were assessed an hour later to identify all wells that contained at least and only one viable-appearing (refractile) cell. The duration of survival of each input cell in these cultures over the next 4 days was determined by visual examination of each well once or twice each day. The (minimum) number of divisions executed during that period was calculated as follows: one division inferred from the detection of 2 cells, 2 divisions from the detection of 3 cells, 3 divisions from 5, etc. The first observation of 2 viable cells was used to denote the timing of a first cell division When 2 or more divisions occurred between observations, division timing was linearly interpolated with the final division occurring at the observation point and other divisions occurring at equal intervals between adjacent observation points.

### 3.2.5 Mass cytometric analysis

CB cells enriched in $CD34^+$ cells were thawed in IMDM with 10% FBS and 10 µg/mL DNase I (Sigma Aldrich), centrifuged, suspended at $10^6$ cells/mL SFM and exposed to 10 µM Cisplatin (Sandoz) for 1 minute at 37˚C followed by centrifugation and suspension of the cells in fresh SFM with 1 µM IdU ( Sigma Aldrich) at a concentration of 0.5-1x$10^6$ cells/mL. Cells were then incubated at 37˚C in the presence of 5% $CO_2$ in air usually for a total of 3 hours with 5GFs added as indicated for the final 5-120 minutes. In one experiment, cells were instead left in SFM for 60 minutes followed by GF stimulation for 5, 15 or 120 minutes.

At the end of the stimulation period, cells were fixed with 1.6% paraformaldehyde (PFA; Electron Microscopy Sciences) for 10 minutes at room temperature. Cells were washed twice in

PBS (STEMCELL Technologies) with 2% FBS and re-suspended in blocking buffer consisting of HSBS supplemented with 5% human serum and 1.5 µg/mL anti-human CD32 antibody (Clone IV.3; STEMCELL Technologies) at a concentration of 1.5-3x$10^6$ cells/100 µL. Cells were then stained for 1 hour on ice with antibodies against surface antigens listed in Table 3.5 and each tube mixed every 15 minutes within this period. The cells were then washed with PBS with 2% FBS, permeabilized by the addition of -80˚C methanol while vortexing to prevent clumping, immediately spun again and washed twice more in PBS with 2% FBS to remove residual methanol. Cells were then stained with antibodies against intracellular markers (Table 3.5) for 1 hour on ice with mixing every 15 minutes. At the end of this period cells were washed with PBS with 2% FBS, and re-suspended in 0.5 µM $^{103}$Rh in PBS with 2% FBS at a cell concentration of $10^6$ cells/mL and left overnight at 4 ˚C in the dark. Cells were washed twice with milli-Q 'ultrapure' $H_2O$ (Millipore). EQ™ Four Element Calibration Beads (DVS Sciences) were added at a concentration of 3.3x$10^4$ beads/mL to the cells in milli-Q $H_2O$ at a cell concentration not exceeding 0.5x$10^6$ cells/mL. Cells were then filtered and run on a CyTOF 2 with a flow speed of 0.045 mL/minute, a 30 second acquisition delay, and 10 second detector stability delay.

### 3.2.6 Data analysis

All statistical testing and data analysis was performed in R. Analysis of survival was performed using the package 'survival'. Flow cytometric and CyTOF data were analyzed using the package 'flowCore' together with custom scripts. t-SNE analysis was performed using the package 'Rtsne' with the perplexity parameter set to 30. For significance testing of differences in levels of individual intracellular parameters, empirical null distributions for median values were

created by bootstrap re-sampling (with replacement) the unstimulated $CD49f^+$ cells (pooled from all experiments; 100,000 bootstrap re-samplings performed on 50 sampled cells each time). p-values were not approximated for distributions in which >20% of the medians in the corresponding null distribution were ties, as these precluded making accurate estimates of p-value. A false discovery rate (FDR) correction for multiple testing was performed following p-value estimation.

## 3.3 Results

### 3.3.1 21-day *ex vivo* maintenance of serially transplantable human HSCs in 5 GFs

Figure 3.2A shows the culture protocol we designed to optimize the expansion of human CB HSCs in a defined culture medium supplemented with 100 ng/mL SCFand FLT3L and 20 ng/mL of IL3, IL6 and G-CSF. To delay the production of mature cells as long as possible, we initiated the cultures with $CD49f^+$ cells. Limiting dilution transplants confirmed that ~10% of the input cells were HSCs with 30-week serial transplantable repopulating activity in immunodeficient mice (Figure 3.2B, Table 3.6). We also increased the culture volume as differentiated cells appeared, in addition to positively selecting the $CD34^+$ cells present twice and then transferring them each time into fresh GF-containing culture medium. The total cell expansion measured over the full 21 days that the cells were cultured in this way in 2 independent experiments was >17,000-fold (Figure 3.2, Table 3.2). Limiting dilution analysis (LDA) of the human HSC numbers present in the 21-day culture harvests showed these were comparable to in the numbers measured in the input $CD49f^+$ cells (Figure 3.2B; Table 3.6). Secondary recipients of transplants of human $CD34^+CD38^{low/-}$ cells harvested from the primary

mice showed the culture-derived HSCs continued to maintain the same or better functional activity as the input cells (Figure 3.2C).

### 3.3.2 HSC survival and proliferation are differentially controlled by specific GFs

HSC numbers are determined by a combination of their survival, proliferation, and self-renewal responses to ongoing stimuli. To determine how these responses are affected by the 5 GFs added to the medium of the 21-day cultures, we set up a series of 4-day single-cell cultures to track the survival and growth kinetics of individual $CD49f^+$ cells under different GF conditions. In these experiments, we monitored a total of 2,625 single $CD49f^+$ cells in microfluidic culture arrays or terasaki plates. Since the results obtained in these 2 systems were indistinguishable, they were then pooled (Figure 3.3A, Figure 3.4A, Table 3.7). In the presence of all 5 GFs, 84% of the $CD49f^+$ cells were still alive at the end of 4 days. This outcome was not significantly reduced by the removal of any single GF (FDRs $\geq$0.18). In contrast, 97% of the $CD49f^+$ cells died within 4 days when none of the 5 GFs was present. Interestingly, 4 of the GFs alone (all except G-CSF) increased the survival of $CD49f^+$ cells significantly above the no GF condition (FDRs <0.01), with SCF and FLT3L having the most prominent pro-survival effects (39% and 44% surviving cells after 4 days, respectively). In addition, the combination of any 2 of FLT3, SCF, IL3 and IL6 had even greater pro-survival effects than any of these on their own (FDRs $\leq$0.03), but still less than the level of survival obtained with all 5 GFs together (FDRs $\leq$0.02).

Simultaneous analysis of the rate of passage of the $CD49f^+$ cells through a first and second mitosis showed the 5-GF combination also stimulated most, but not all, (82%) of the surviving cells to complete a first division within 4 days (median = 66 hours, IQR = 58-72 hours,

Figure 3.3B/C, Figure 3.4B/C, Table 3.7). Interestingly, this response is similar to that recently reported for the same phenotype of cells stimulated with a somewhat different GF cocktail (Laurenti et al., 2015). Here, we noted that 48% of the cells able to complete a first division when exposed to 5 GFs also completed a second cell division within the 4-day period (median = another 25 hours later, IQR = 19-28 hours later). In contrast, the mitogenic response to any single GF was very low, with the strongest effects elicited by either SCF or IL3 (~10% divided cells). Interestingly, the mitogenic response to SCF+IL3 was equivalent to that elicited by all 5 GFs (FDR = 0.63 and 0.24 for $1^{st}$ and $2^{nd}$ division, respectively), although the timing of the divisions stimulated by every 2-GF combination, including SCF+IL3, was significantly delayed compared to those obtained with the 5-GF cocktail (FDRs $\leq$0.01 except for IL3+IL6 where Ns were too low for significance, Table 3.7). Unexpectedly, removal of G-CSF increased the proportion of $CD49f^+$ cells that were recruited into division (by 1.2- and 1.9-fold for the first and second divisions with FDRs of 0.006 and <<0.001, respectively). This latter finding suggests that G-CSF may actually inhibit human HSC proliferation.

Conversely, elimination of SCF from the 5-GF cocktail significantly reduced the proportion of cells that divided (once by 1.8-fold, and twice by 3.1-fold, FDRs <<0.001), but without diminishing the high survival obtained with 5 GFs or changing the time to complete a first division (FDR = 0.11). Removal of IL3, IL6, or FLT3L from the 5-GF cocktail, on the other hand, had no significant effect on the recruitment of $CD49f^+$ cells into division. Taken together, these findings indicate that the mitogenic activity of IL3 on these cells can be replaced by a combination of other GFs. Removal of IL3 did, however, result in a slight delay in the time taken to complete a first division (median = 71.6 hours, IQR = 64.8-77.9 hours, FDR = 0.008) and removal of FLT3L had a similarly effect (median time to complete a first division = 70.6 hours,

IQR = 62.5-77.9, FDR = 0.009). Thus the 5 GFs alone and in combination differentially activate (or suppress) mechanisms that control not only the survival and mitogenesis of very primitive human hematopoietic cells, but also their rate of entry into (or passage through) the cell cycle.

### 3.3.3 GF conditions that differentially support HSC survival and proliferation show equivalent maintenance of their regenerative activities

We then tested the *in vivo* regenerative activity present in $CD49f^+$ cells cultured for 4 days with many of the same combinations of GFs used in the single-cell tracking experiments. Surprisingly, the results showed equivalent levels of multi-lineage human chimerism in the bone marrow of mice transplanted 6 months earlier with equivalent numbers of either the input $CD49f^+$ cells or their 4-day cultured derivatives for all GF combinations tested (Kruskal-Wallis rank sum test p = 0.91, Figure 3.5A/B). The bone marrow of all groups of recipients also contained similar numbers of human $CD34^+CD19^-CD38/CD45RA^-$ cells (p = 0.97, Figure 3.5C) suggesting similar numbers of secondary repopulating cells had also been regenerated from each of the original groups of cells transplanted. The contrast between these similar effects on HSC activity with GF combinations that differentially regulate $CD49f^+$ cell survival and mitogenesis points to differences in the mechanisms by which these programs are controlled within the HSC compartment.

### 3.3.4 Single GFs activate distinct signaling spectra, and additional pathways in combination

To gain insight into the mechanisms mediating these different GF actions on purified $CD49f^+$ cells, we used single-cell mass cytometry to analyze changes in their individual cell

content of 28 signaling intermediates following stimulation with each of the 5 GFs alone or together. Analysis of 11,742 $CD49f^+$ cells in a starting population of 1.2 x $10^6$ $CD34^+$ CB cells (Figure 3.6) showed a rapid and strong activation of several signaling intermediates (Figure 3.7A) with very consistent kinetics (Figure 3.7B). For example, maximum ERK1/2 phosphorylation always occurred within 5 minutes of stimulation and was then substantially reduced another 10 minutes later, whereas STAT3 was not maximally activated until 15 minutes after stimulation. To analyze the kinetics of $CD49f^+$ cell activation across all conditions, we subjected the $CD49f^+$ data to t-SNE dimensionality reduction (Van der Maaten and Hinton, 2008). The results confirmed an overall pattern of large-scale changes at 5 and 15 minutes post-stimulation, followed by a return within 120 minutes to a state similar to, but still distinct from, the unstimulated cells (Figure 3.7C, Figure 3.8B). In addition, this analysis revealed a minor $CD34^{low}CD133^-$ population (likely a mature subset of $CD34^+$ cells) that appeared unresponsive to GF exposure (median = 3.6%, IQR = 1.3-10%, across all stimulations/time points/samples).

Both SCF and FLT3L alone elicited similar signaling profiles that included common downstream MAPK pathway members (ERK1/2, AKT, CREB, and S6, Figure 3.7). In contrast, IL3 alone activated STAT5 and to a lesser extent S6. Both IL6 and G-CSF alone caused a rapid and strong activation of STAT3. IL6 also showed later activation of several additional pathways. These rapid responses to IL6 were unexpected since the alpha subunit of the IL6 receptor has been reported to be poorly detectable in quiescent HSCs (Tajima et al., 1996).

In combination, the 5 GFs elicited a signaling profile that reflected the sum of the effects of the individual GFs (Figure 3.7). Preliminary tests using 2 other commonly used GF cocktails for HSC expansion (Boitano et al., 2010; Csaszar et al., 2012; Fares et al., 2014) also showed activation of some of these (Figure 3.9). Interestingly, exposure of the $CD49f^+$ cells to all 5 GFs

together also elicited molecular responses not predicted by the effects of the single GFs alone. Notably, amongst these was a significant accumulation of active β-catenin exclusively in the $CD49f^+$ cells stimulated with all 5 GFs together (Figure 3.7A). In mouse HSCs, this molecular response has been associated with activation of a proliferative response (Reya et al., 2003). We also noted a decreased level of the apoptotic marker, cleaved PARP, in the cells stimulated with 5GFs. Although this latter effect did not reach significance, it is consistent with the improved survival also observed under this condition (Figure 3.3A). Interestingly, the 5 GF-specific responses occurred primarily at later times suggesting that they are secondarily activated by multiple upstream pathways.

### 3.3.5 Discussion

Recent HSC expansion culture systems containing soluble GFs have reported promising improvements in HSC yields using small molecule additives (Boitano et al., 2010; Fares et al., 2014). These strategies did not, however, optimize the GF milieu of the cultures. They also used relatively heterogeneous $CD34^+$ cell populations to initiate the cultures which results in the rapid accumulation of large numbers of mature myeloid cells with known negative effects on human HSCs (Csaszar et al., 2012). It is therefore not surprising that the results obtained with the small molecules thus far tested also fail to achieve substantial net HSC expansions. We now show that when these effects are minimized, the combination of 5 well-known GFs, alone, can directly stimulate extensive self-renewal divisions in human HSCs with full retention of long-term (>1-year) *in vivo* repopulating activity.

In addition, we provide the results of direct analyses of the cellular and molecular mechanisms involved. These demonstrate that the control of survival, proliferation, and

maintenance of stem cell capabilities can be both dissociated and combinatorially activated. They also provide evidence of synergistic effects on the signaling intermediates activated. For example, we show that maintenance of transplantable *in vivo* hematopoietic regenerative activity in purified human HSCs can be controlled independently from an activation of their proliferative and survival programs. Given that all GF combinations tested maintained HSC regenerative activity for at least 4 days, the loss of transplantable HSC observed previously in 9-day expansion cultures that contained similar GFs (Bhatia et al., 1997) is more likely explained, in retrospect, by an excessive production of negative factors by the maturing progeny of the input cells, rather than a failure of the GFs to stimulate HSC self-renewal divisions. This explanation would be consistent with the more recent improvements afforded by dilution-based culture protocols (Csaszar et al., 2012). The successful maintenance of fully functional HSC capabilities in the 21-day cultures described in the present study provide further support for this idea. These results thus extend to human HSCs principles of HSC control predicted by previous studies of mouse HSCs (Wohrer et al., 2014).

Our finding that GFs can independently activate human HSC survival, proliferation, and self-renewal suggests that stimulation of their maximal expansion will require the balanced optimization of each of these programs. Such optimization may be facilitated through the delineation and specific targeting of signaling pathways, such as β-catenin observed in our 5 GF mix, which are likely important convergent control points for these programs. Together with strategies to abrogate the negative influence of mature cell outputs, our results help lay a new foundation for the development of improved *ex vivo* human HSC expansion strategies.

**Table 3.1 Antibodies used for isolation of CD49f$^+$ cells.**

| Antigen | Clone | Supplier | Channel |
|---|---|---|---|
| CD49f | GoH3 | eBiosciences | eFluor450 |
| CD38 | HIT2 | BD Pharmingen | FITC |
| CD45RA | HI100 | eBiosciences | FITC |
| CD90 | 5E10 | eBiosciences | PE |
| CD34 | 581 | BioLegend | AF647 |

**Table 3.2 Total numbers of cells produced from 1,000 CD49f$^+$ cells in 21-day cultures and cell numbers removed by EasySep™ selection steps performed on days 12 and 17.**

| | | Cell number per culture | | Cell number removed by EasySep | | Cells removed by EasySep (%) | |
|---|---|---|---|---|---|---|---|
| Experiment | Time in culture (days) | Total | CD34$^+$ | Total | CD34$^+$ | CD34$^-$ | CD34$^+$ |
| 1 | 12 | 6.02E+06 | 6.92E+05 | 3.78E+06 | 3.46E+04 | 70 | 5 |
| | 17 | 1.68E+07 | 1.09E+06 | 1.09E+07 | 9.64E+04 | 69 | 9 |
| | 21 | 1.76E+07 | ND | NA | NA | NA | NA |
| 2 | 12 | 5.25E+06 | 3.52E+05 | 4.08E+06 | 2.16E+04 | 83 | 6 |
| | 17 | 2.30E+07 | 2.14E+06 | 1.24E+07 | 4.56E+04 | 59 | 2 |
| | 21 | 1.94E+07 | ND | NA | NA | NA | NA |

**Table 3.3 Antibodies used for detecting human hematopoietic cells in the bone marrow of transplanted mice.**

| Antigen | Clone | Supplier | Channel |
|---|---|---|---|
| CD3 | OKT3 or SK7 | eBiosciences | eFluor605NC or FITC |
| CD19 | SJ25C1 | eBiosciences | PE, PerCP-Cy5.5, or APC-eFluor780 |
| CD33 | WM53 | eBiosciences | PE-Cy7 |
| CD34 | 581 | BD Biosciences or BioLegend | AF700 or BV421 |
| CD45 | 2D1 | eBiosciences | APC |
| CD45 | HI30 | eBiosciences or BioLegend | PE or Pacific Blue |

**Table 3.4 Antibodies and fluorophores used for assessing human hematopoietic progenitor content as well as total chimerism in the bone marrow of transplanted mice.**

| Antigen | Clone | Supplier | Channel |
|---|---|---|---|
| CD49f | GoH3 | eBiosciences | eFluor450 |
| CD45RA | HI100 | eBiosciences | eFluor605NC |
| CD38 | HIT2 | BioLegend | Brilliant Violet 711 |
| CD3 | SK7 | eBiosciences | FITC |
| CD19 | SJ25C1 | eBiosciences | PE |
| CD33 | WM53 | BD Biosciences | PE-CF594 |
| CD90 | 5E10 | BD Pharmingen | PE-Cy7 |
| CD45 | 2D1 | eBiosciences | APC |
| CD45 | HI30 | eBiosciences | APC-eFluor780 |
| CD34 | 581 | BD Biosciences | AF700 |

**Table 3.5 Antibodies used for the CyTOF analyses.**

| Antigen | Clone | Supplier | Isotope | Concentration in 100 µL ($3x10^6$ cells) |
|---|---|---|---|---|
| **Intracellular** | | | | |
| PARP1 (Cleaved) | HLNC4 | eBioscience | 139La | 0.05 µg |
| pSHP2 (Y580) | D66F10 | DVS Sciences | 141Pr | 1 µL |
| GATA3 | D13C9 | CST | 142Nd | 0.4 µg |
| CRKL (pY207) | Polyclonal | DVS Sciences | 143Nd | 1 µL |
| SRC (pY418) | K98-37 | BD Biosciences | 145Nd | 0.05 µg |
| Acetyl-CoA Carboxylase (pS79) | Polyclonal | CST | 146Nd | 0.1 µg |
| Cyclin B1 | D5C10 | CST | 147Sm | 0.1 µg |
| PAX5 | D19F8 | CST | 148Nd | 0.2 µg |
| PU.1 | 9G7 | CST | 149Sm | 0.4 µg |
| STAT5 (pY694) | 47 | DVS Sciences | 150Nd | 1 µL |
| AKT (pS473) | D9E | DVS Sciences | 152Sm | 1 µL |
| STAT1 (pY701) | 58D6 | DVS Sciences | 153Eu | 1 µL |
| SMAD2/3 (pS465/S467)/(pS423/S425) | D6G10 | CST | 154Sm | 0.4 µg |
| p38 (pT180/Y182) | D3F9 | DVS Sciences | 156Gd | 1 µL |
| STAT3 (pY705) | 4/P-Stat3 | DVS Sciences | 158Gd | 1 µL |
| MAPKAPK2 (pT334) | 27B7 | DVS Sciences | 159Tb | 1 µL |
| IκBα | L35A5 | DVS Sciences | 164Dy | 1 µL |
| CREB (pS133) | 87G3 | DVS Sciences | 165Ho | 1 µL |
| β-Catenin (Non-phospho S33/S37/T41) | D13A1 | CST | 166Er | 0.4 µg |
| ERK1/2 (pT202/Y204) | D13.14.4E | DVS Sciences | 167Er | 1 µL |
| Ki67 | Ki67 | DVS Sciences | 168Er | 1 µL |
| pZAP70 (pY319)/SYK (pY352) | 17a | DVS Sciences | 171Yb | 1 µL |
| TAL1 | 5H1 | Abcam | 173Yb | 0.4 µg |
| C/EBPα | D56F10 | CST | 174Yb | 0.2 µg |
| S6 (pS235/S236) | N7-548 | DVS Sciences | 175Lu | 1 µL |
| GATA1 | D52H6 | CST | 176Yb | 0.4 µg |
| eEF2 (pT56) | Polyclonal | CST | 209Bi | 0.4 µg |
| **Surface** | | | | |
| CD45 | HI30 | eBioscience | 115In | 0.2 µg |
| CD114 (GCSFR) | LMM741 | eBioscience | 144Nd | 0.4 µg |
| CD123 (IL3Ra) | 6H6 | eBioscience | 151Eu | 0.4 µg |
| CD34 | 4H11 | eBioscience | 155Gd | 0.2 µg |
| CD33 | WM53 | eBioscience | 157Gd | 0.4 µg |
| CD49f | eBioGoH3 | eBioscience | 160Gd | 0.1 µg |
| CD10 | SN5c | eBioscience | 161Dy | 0.2 µg |
| CD135 (FLT3) | BV10A4H2 | eBioscience | 162Dy | 0.4 µg |
| CD38 | HIT2 | eBioscience | 163Dy | 0.2 µg |
| CD90 | 5E10 | eBioscience | 169Tm | 0.4 µg |
| CD202b | 33.1 | eBioscience | 170Er | 0.4 µg |
| CD133 | AC133 | Miltenyi Biotec | 172Yb | 0.2 µg |
| CD45RA | HI100 | eBioscience | ef605NC | 1 µL |

**Table 3.6 HSC frequencies in CD49f$^{+}$ cells and their progeny present in 21-day cultures (described in Figure 3.2A) derived by LDA of primary transplanted mice.**

| Culture Condition | Weeks Post-transplant (weeks) | Cell Dose | Engrafted/Total | HSC Frequency | p Value |
|---|---|---|---|---|---|
| Day 0 | 12 | 200 | 6/6 | 1 in 14 (30-6.4) | 0.32 |
| | | 50 | 8/8 | | |
| | | 10 | 3/7 | | |
| 5GF | 12 | 175 | 8/8 | 1 in <17 (30-<17) | |
| | | 35 | 8/8 | | |
| Day 0 | 20 | 200 | 6/6 | 1 in 14 (32-6.4) | 0.78 |
| | | 50 | 7/7 | | |
| | | 10 | 3/7 | | |
| 5GF | 20 | 175 | 8/8 | 1 in 17 (41-7) | |
| | | 35 | 7/8 | | |
| Day 0 | 30 | 200 | 6/6 | 1 in 8.8 (22-3.5) | 0.28 |
| | | 50 | 7/7 | | |
| | | 10 | 4/6 | | |
| 5GF | 30 | 175 | 5/5 | 1 in 18 (46-7.1) | |
| | | 35 | 6/7 | | |

**Table 3.7 Numbers of cells/experiments included in the analysis of survival, proliferation and division kinetics.**

| | Survival | | Division Recruitment | | Division Timing | |
|---|---|---|---|---|---|---|
| **Condition** | **Cell Number** | **Number of Experiments** | **Cell Number** | **Number of Experiments** | **Cell Number** | **Number of Experiments** |
| SCF | 183 | 5 | 61 | 4 | NA | NA |
| FLT3L | 219 | 5 | 87 | 4 | NA | NA |
| IL3 | 291 | 5 | 76 | 4 | NA | NA |
| IL6 | 131 | 5 | 21 | 4 | NA | NA |
| GCSF | 124 | 5 | 17 | 4 | NA | NA |
| no GF | 133 | 5 | 3 | 2 | NA | NA |
| 5GF | 295 | 8 | 223 | 7 | 182 | 7 |
| 5GF-SCF | 147 | 5 | 85 | 4 | 39 | 4 |
| 5GF-FLT3L | 112 | 4 | 58 | 3 | 47 | 3 |
| 5GF-IL3 | 102 | 4 | 53 | 3 | 42 | 3 |
| 5GF-IL6 | 108 | 5 | 71 | 4 | 58 | 4 |
| 5GF-GCSF | 90 | 4 | 58 | 3 | 56 | 3 |
| SCF+FLT3L | 111 | 5 | 55 | 4 | 19 | 4 |
| SCF+IL3 | 118 | 5 | 72 | 4 | 56 | 4 |
| SCF+IL6 | 107 | 3 | 46 | 2 | 26 | 2 |
| FLT3L+IL3 | 127 | 5 | 66 | 4 | 31 | 4 |
| FLT3L+IL6 | 119 | 3 | 48 | 2 | 9 | 1 |
| IL3+IL6 | 108 | 3 | 48 | 2 | 5 | 1 |

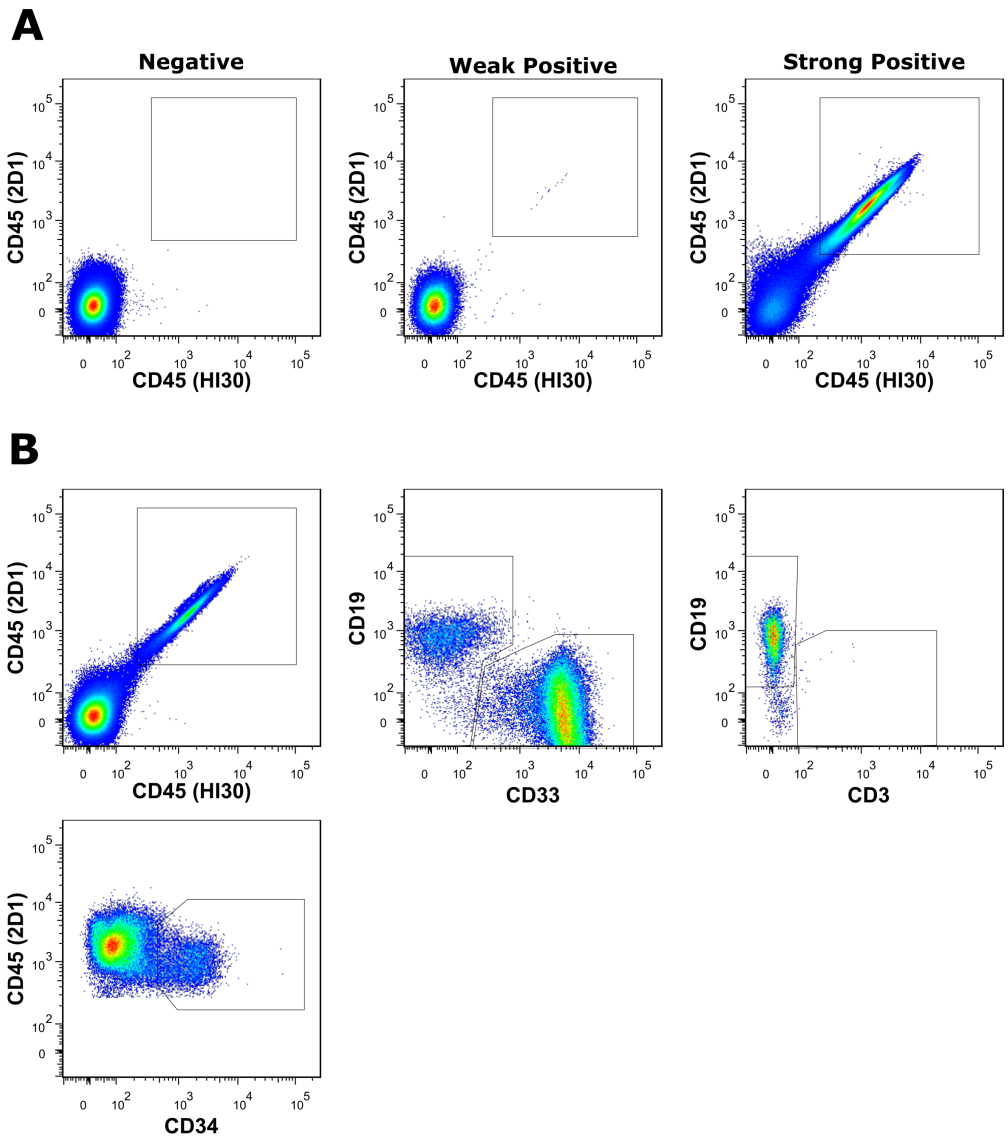


**Figure 3.1 Examples of FACS profiles from LDA experiments.** A) Examples of FACS profiles of absent, low and high levels of human cell chimerism in transplanted primary mice assessed 30 weeks post-transplant. B) Example of the lineage gating used for flow cytometric analysis of the chimerism levels measured in (A).

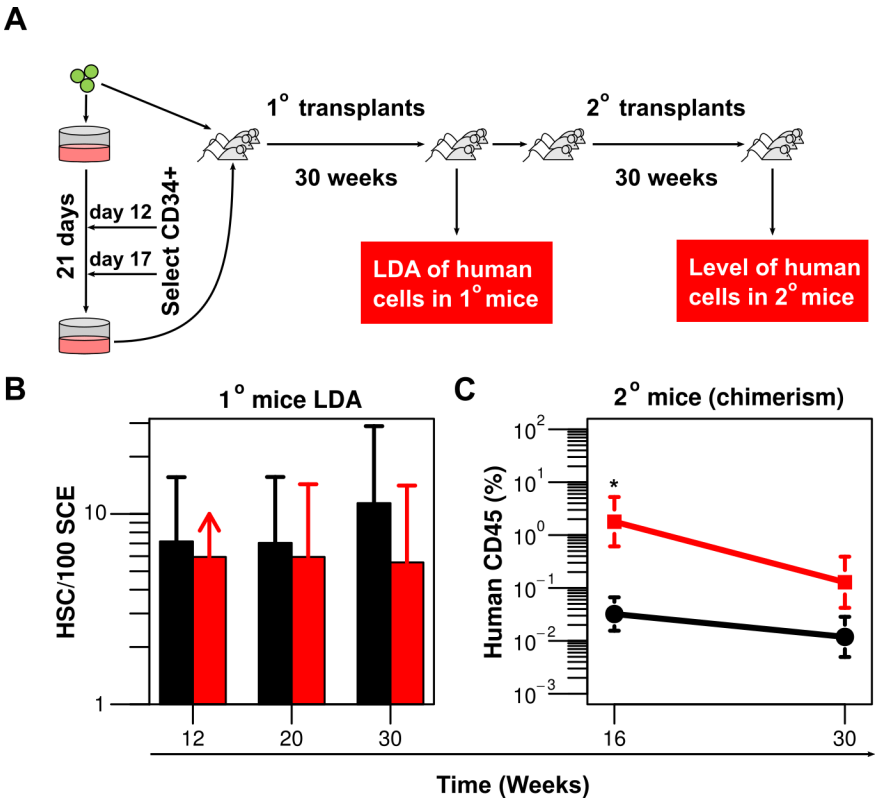


**Figure 3.2 A defined medium supplemented with 5 GFs maintains fully functional human HSC numbers over a 21-day period *in vitro*.** A) Experimental design. One-mL cultures were initiated with 1,000 freshly isolated $CD49f^+$ cells in SFM containing 5 GFs. An additional 1 mL of GF-supplemented medium was added on days 9, 10, 11, 16, and 20. On days 12 and 17, CD34+ cells were isolated immunomagnetically (thereby removing $CD34^-$ cells) and used to initiate further cultures in fresh SFM plus the 5GFs. The input $CD49f^+$ cells were injected into sub-lethally irradiated NSG mice at doses of 10, 50 and 200 cells each (black). Cultured cells were injected at doses equivalent to the output of 35 and 175 initial $CD49f^+$ cells (red). B) HSC numbers per 100 starting $CD49f^+$ cells were derived by LDA of the proportions of primary recipients in 2 independent experiments in which human chimerism in the bone marrow was below the limit of detection (<0.005%). Error bars show 95% confidence intervals. None of the primary recipients of the cultured cells were negative 12 weeks post-transplant, hence minimum values at this time were calculated assuming 1 of the primary recipients of the minimum cell dose tested was negative. C) Levels of total human $CD45^+$ cell chimerism in the bone marrow of secondary mice transplanted with human cells regenerated from the equivalent of 450 freshly isolated cells $CD49f^+$ cells or the corresponding

cells regenerated from the cultured progeny of the equivalent of 362 initial CD49f$^{+}$ cells (3 mice per arm). * at 16 weeks indicates p=0.04, and at 30 weeks, p=0.17 (Student's t-test).

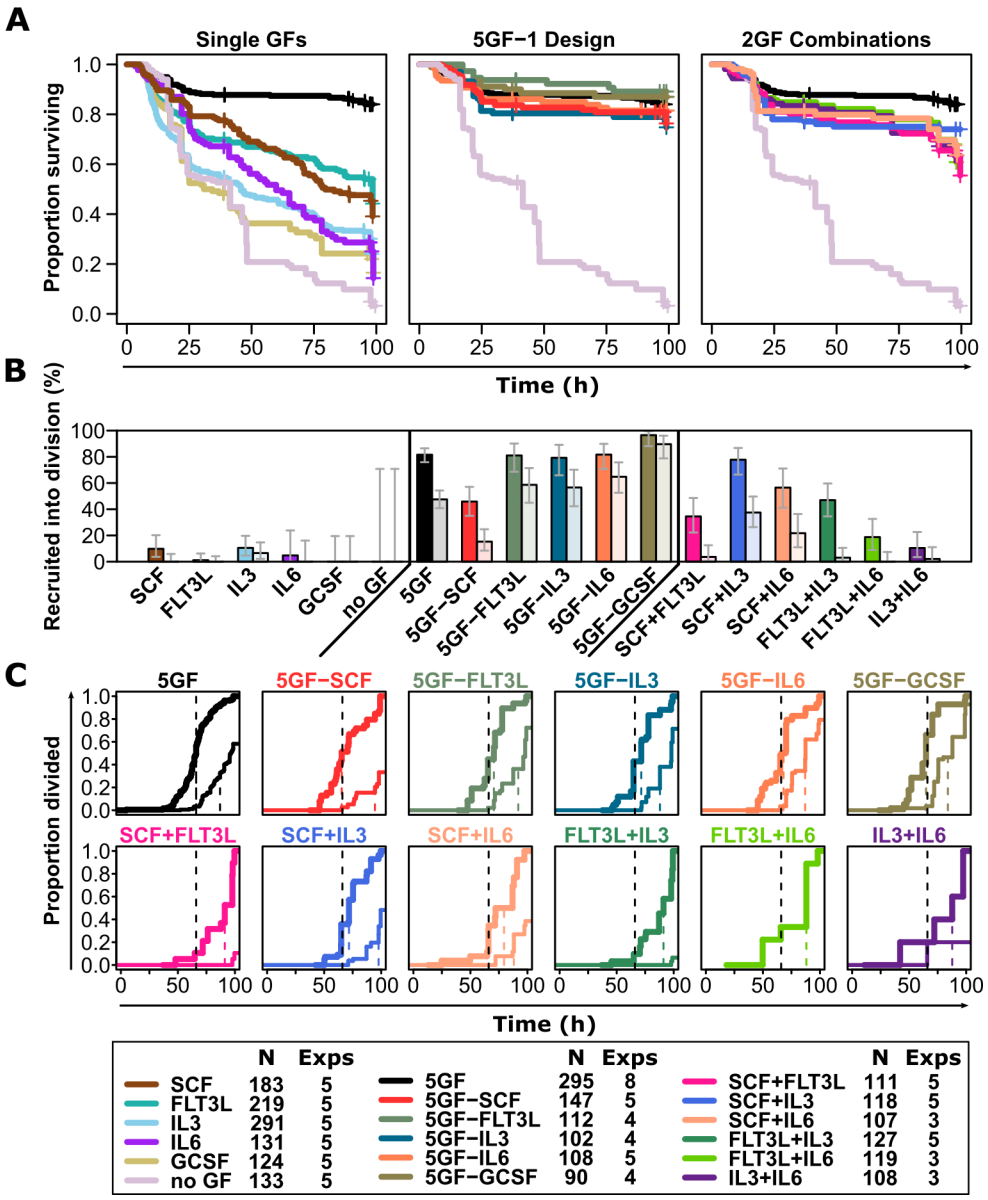


**Figure 3.3 Survival and proliferative responses of CD49f$^{+}$ cells are independently and combinatorially regulated.** A) Kaplan–Meier survival curves for FACS-purified CD49f$^{+}$ CB cells tracked over 4 days in single-cell cultures containing a single GF (left), 4 of the 5 GFs tested (middle), or combinations of 2 GFs (right). Survival of the cells in the 5-GF cocktail (black), or no GFs (thistle), are shown for reference. Censoring times for censored cells are shown as "+" signs. B) Percent of surviving single cells observed to undergo 1$^{st}$ and 2$^{nd}$ cell divisions (with binomial 95% confidence intervals). C) Cumulative distribution functions for 1$^{st}$ and 2$^{nd}$ cell divisions over time for each GF combination. The median first division time for cells cultured in 5 GFs is shown as a black dotted line in all

plots. First division distributions are shown in thick lines and second divisions as thinner lines. Dotted lines represent median times for first and second divisions, respectively. At the bottom of the figure are shown the total number of cells tracked per condition (with color coding), and the total number of experiments performed with each.

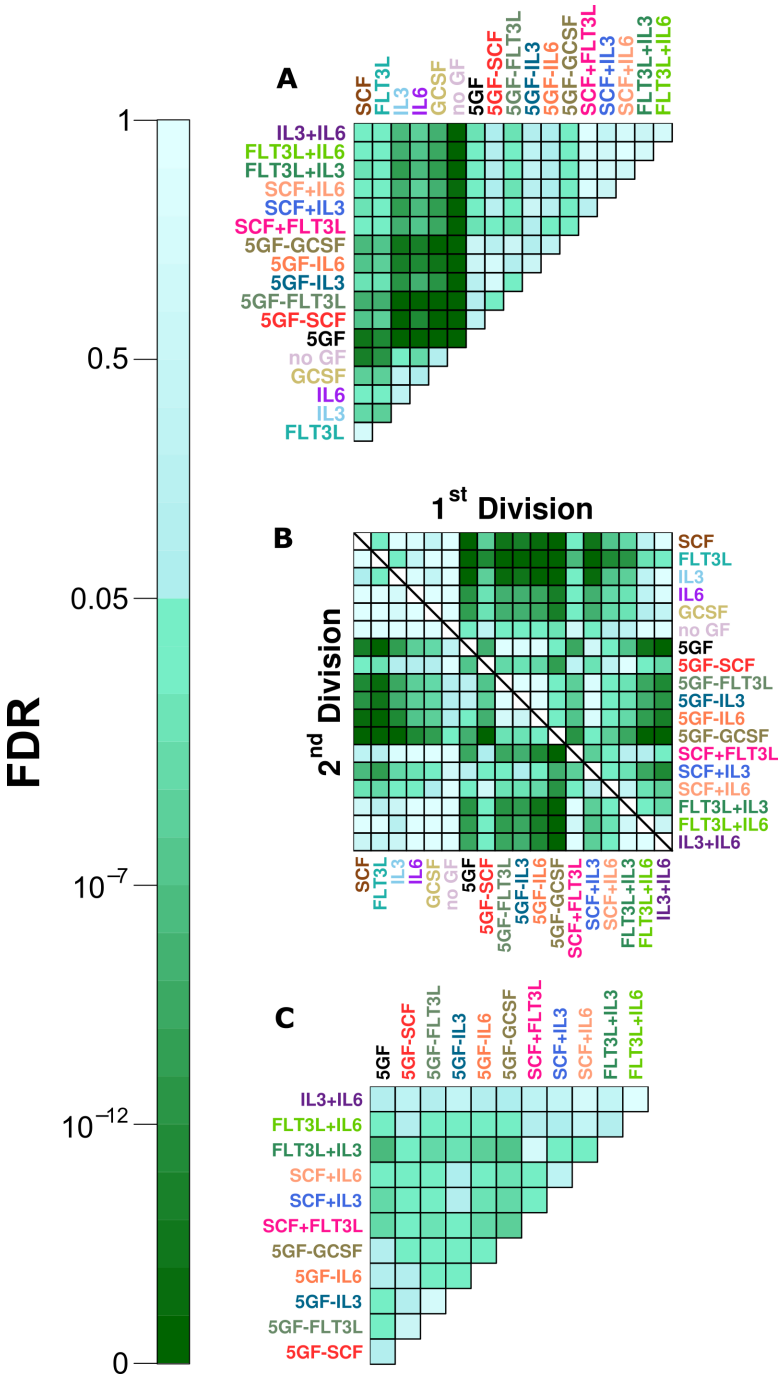


**Figure 3.4 Pair-wise significance testing of differences in survival, recruitment into division, and time to complete a first division.** Results of all tests have been corrected using a FDR correction for multiple testing. Colors indicate levels of significance corrected for multiple testing. A) Pair-wise survival curve comparison. B) Pair-wise Fisher's test for differences in the proportion of cells recruited into a 1st (top right triangle), or a 2nd

division (bottom left triangle). C) Pair-wise Kolmogorov-Smirnov test of equivalence in a 1st division cumulative distribution function.

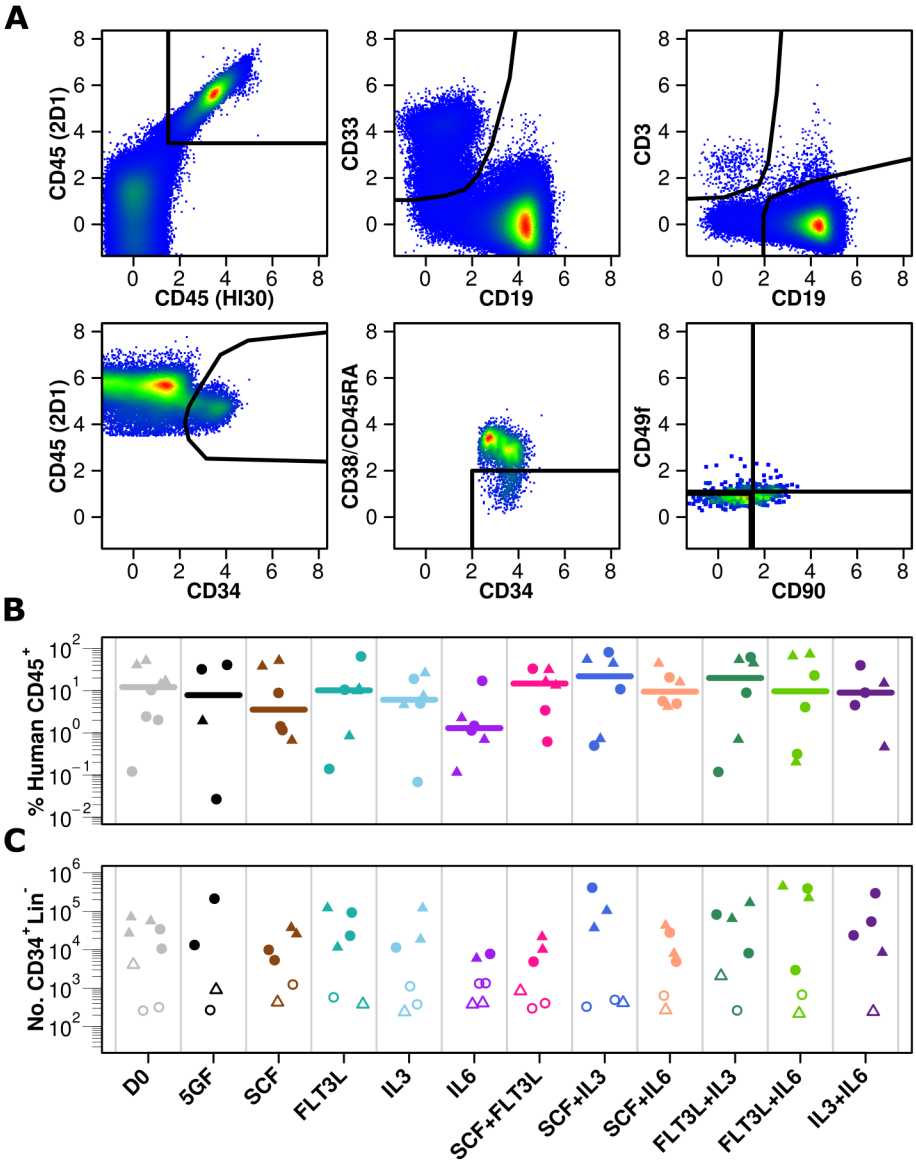


**Figure 3.5 Multiple GF combinations sustain *in vivo* HSC functionality for 4 days *in vitro*.** A) Representative FACS analysis showing human chimerism, lineages present and progenitor numbers in the bone marrow of a primary mouse transplanted 6 months previously with the progeny of 100 $CD49f^+$ cultured for 4 days in FLT3L+IL3. B) Total human $CD45^+$ cell chimerism levels in the bone marrow of mice assessed 6 months post-transplant with $CD49f^+$ derivatives obtained from 4-day cultures in the GFs indicated. Each point indicates an individual recipient. Results from 2 different experiments are shown as circles and triangles. C) Total number of human $CD34^+CD19^-CD38/CD45RA^-$ cells per mouse (assuming $2x10^8$ total bone marrow cells per mouse). Filled

and empty points distinguish mice in which at least 5 human cells with this phenotype were, or were not detected, respectively (ELDA p=0.97).

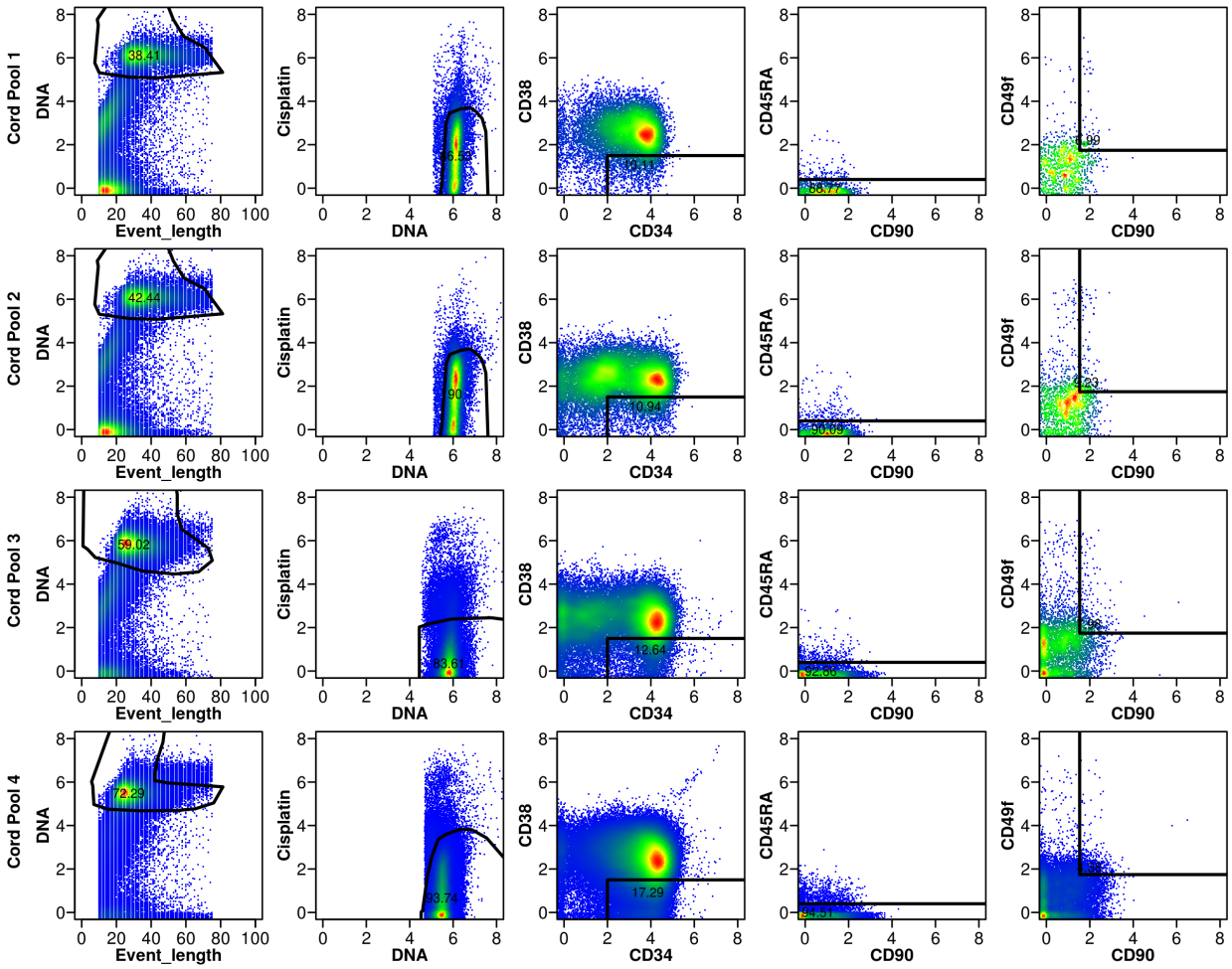


**Figure 3.6 Gating hierarchy for CD49f$^+$ cells from CyTOF data.** Gating hierarchy is shown for each experiment. A random sample of 10% of the events from each condition/time point is shown for each level of the gating hierarchy. Zero values were given a random jitter under zero to improve visualization.

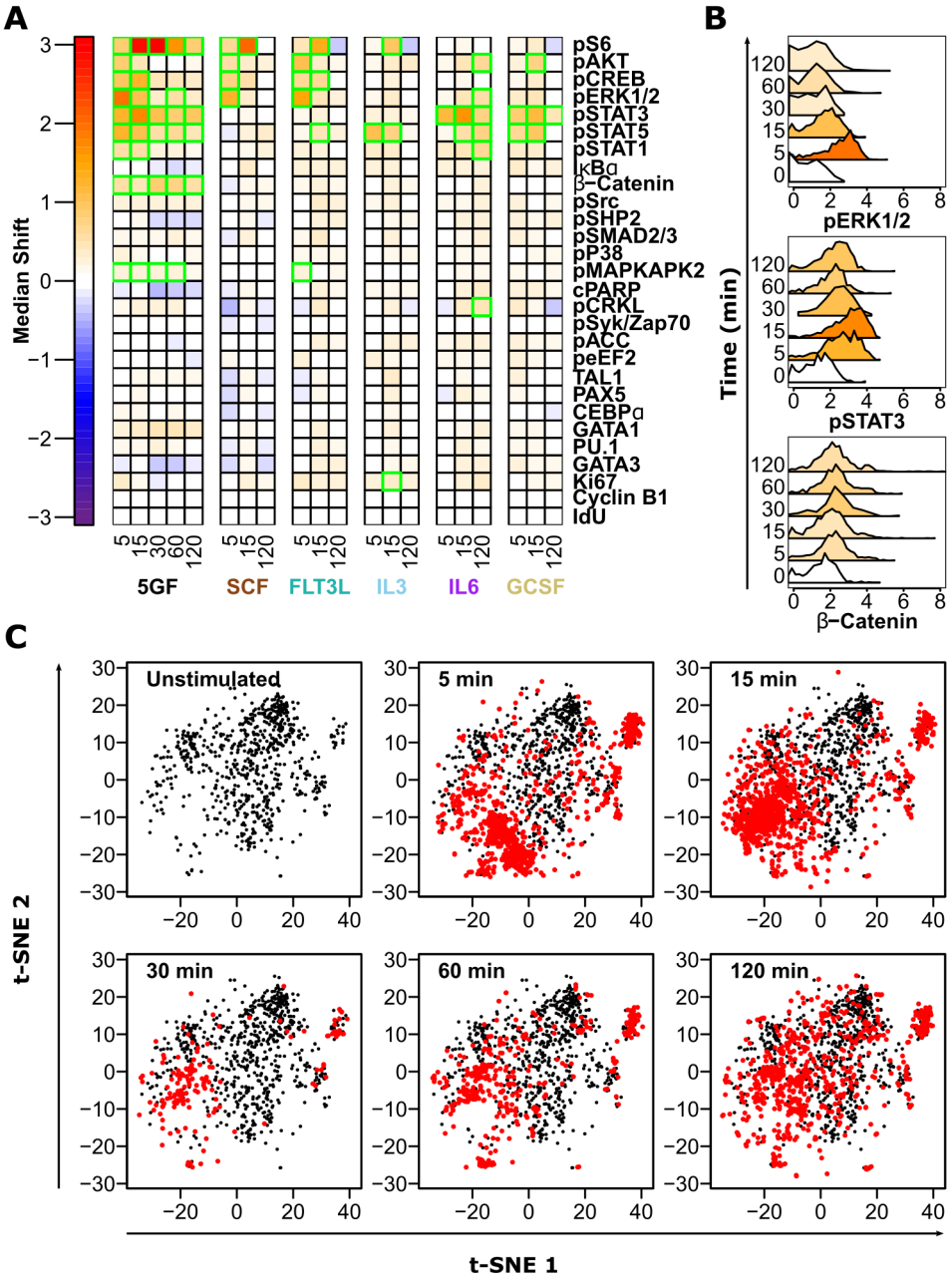


**Figure 3.7 Different GFs alone and in combination activate different signaling responses in CD49f$^+$ cells.** A) Median asinh (signal intensity/5) differences in signal activation in CD49f$^+$cells, compared to unstimulated cells. Significant differences are highlighted with green boxes. B) Representative histograms of signal intensity over time for pERK1/2 (top) pSTAT3 (middle), and active (non-phosphorylated) β-catenin (bottom) following stimulation of CD49f$^+$ cells with 5 GFs. Histogram color is based on the median shift in the stimulated cells relative to the

unstimulated cells. C) Dimensionality reduction using t-SNE on all analyzed $CD49f^+$ cells given all surface and intracellular markers (41 parameters). Unstimulated cells are shown as black points at all times. $CD49f^+$ cells with indicated times of exposure to the 5 GFs are shown in red. Data are from a total of 11,742 $CD49f^+$ cells analyzed in 1.2 million $CD34^+$ cells.

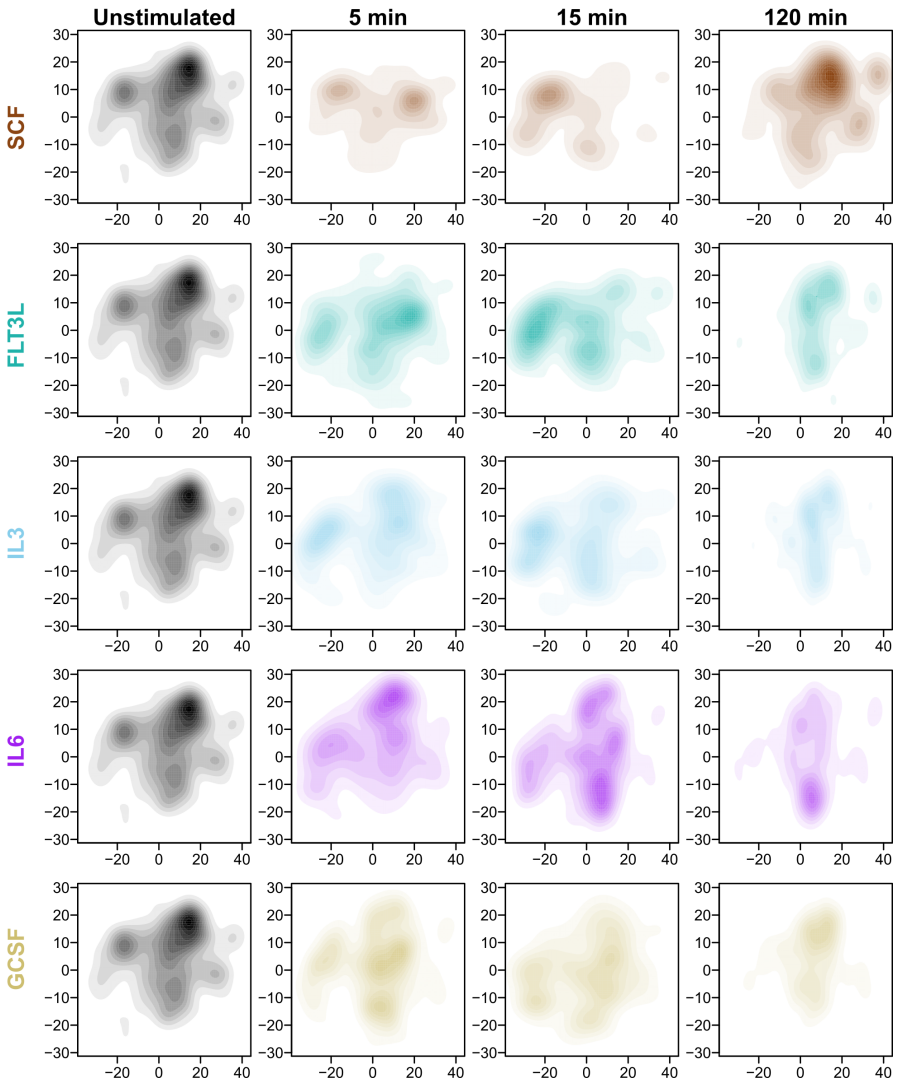


**Figure 3.8 Population distributions based on their molecular characteristics following stimulation with individual GFs.** Dimensionality reduction from a total space of all surface and intracellular markers (total of 41 parameters) using t-SNE on all CD49f$^{+}$ cells analyzed. Separate population densities are shown for CD49f$^{+}$ cells before and after exposure to each GF the for the indicated times.

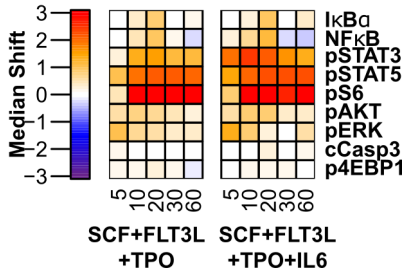


**Figure 3.9 Signal activation in alternative GF cocktails.** Median asinh (signal intensity/5) differences in signal activation in CD49f$^{+}$cells exposed to either SCF+FLT3L+TPO, or SCF+FLT3L+TPO+IL6. In this case, cells were left in SFM for 1 hour followed by stimulation for 5, 10, 20, 30, or 60 minutes as indicated. Unstimulated CD49f$^{+}$cells left in SFM for equivalent times were used to calculated signal differences.

# Chapter 4: Primitive human hematopoietic cells comprise a complex continuum of multiple functional states

## 4.1 Introduction

The hematopoietic system is one of the most intensively studied cellular hierarchies. In the mouse, it is now clear that the top of this hierarchy is composed of a variety of biologically distinct HSC types that share the defining feature of equivalent serial regenerative ability but are distinguished by their intrinsically different lineage potentialities (Benz et al., 2012; Dykstra et al., 2007; Lu et al., 2011; Muller-Sieburg et al., 2004; Sanjuan-Pla et al., 2013; Sieburg et al., 2006; Yamamoto et al., 2013). The coupling of *in vivo* repopulation assays and cell culture systems with flow cytometry has led to increasingly refined correlations between changes in cellular phenotypes and progressive restriction in their proliferative and differentiation capabilities (Akashi et al., 2000; Kent et al., 2009; Kondo et al., 1997; Morita et al., 2010; Osawa et al., 1996; Wilson et al., 2015). The assumed functional purity of these phenotypes has, in turn, been used to infer critical changes in their transcriptional profiles that reflect their altered functional properties (Lara-Astiaso et al., 2014; Petriv et al., 2010; Wilson et al., 2015). A growing body of evidence points to a similar multistep process characterizing human hematopoiesis (Cheung et al., 2013; Doulatov et al., 2010; Galy et al., 1995; Hao et al., 2001; Manz et al., 2002; Notta et al., 2011) and molecular profiling has also been performed on these populations (Chen et al., 2014; Laurenti et al., 2013; Notta et al., 2011). There is, however, a paucity of studies correlating the molecular and biological properties at the single cell level within each phenotype, particularly in the human system.

To address this gap, we used mass cytometry (Bendall et al., 2011b) to measure the levels of surface markers, active signaling intermediates, and cell cycle and transcriptional regulatory proteins in single cells from a spectrum of phenotypes across the human hematopoietic progenitor hierarchy and then combined this data together with the results of matched single-cell assays of progenitor and HSC activity. From these analyses, we discovered extensive overlap in the molecular properties of cells with many different phenotypes, as well as molecular and functional heterogeneity within every subset analyzed. Indeed, it was possible to show that a number of conventionally described phenotypes are actually composed of cells with distinct molecular and biological properties, including the identification of CD33 as a positive marker human HSCs capable of serial long-term repopulation, as distinct from those capable of only one regenerative cycle.

## 4.2 Methods

### 4.2.1 Umbilical cord blood

Anonymized heparinized umbilical cord blood (UCB) was obtained from normal full-term cesarian section deliveries in accordance with procedures approved by the Research Ethics Board of the University of British Columbia. Individual donor samples were then either stained directly or pooled when several were obtained on the same day as indicated. $CD34^+$ cells (>50%) were directly isolated by a 2-step procedure using reagents from STEMCELL Technologies, first to remove the bulk of the $CD11b^+$ monocytes, $CD3^+$ T-cells and $CD19^+$ B-cells along with the neutrophils and red cells using a RosetteSep™ strategy, followed by positive EasySep™ selection of the partially enriched $CD34^+$ cell population according to protocols recommended by the supplier. The highly $CD34^+$ cells thus obtained were then either used directly or first

cryopreserved in DMSO and FBS (STEMCELL Technologies) and subsequently thawed for later analyses by drop-wise addition of IMDM (STEMCELL Technologies) supplemented with FBS and 10 µg/mL DNase (Sigma-Aldrich).

### 4.2.2 Flow cytometry and index sorting

Thawed cells were suspended in blocking buffer consisting of HSBS supplemented with 5% human serum and 1.5 µg/mL anti-human CD32 antibody (Clone IV.3; STEMCELL Technologies). Cells were then stained for 1-2 hours on ice using either a panel designed to subset the progenitor compartment (Table 4.1), to subset the $CD49f^+$ population (Table 4.2), or to identify the $CD49f^+$ population and match to surface markers used in CyTOF analyses (Table 4.3).

For analyses of index sorted cells, single cells were sorted directly into the wells of Nunc™ 96-Well Polystyrene plates using a BD FACSAria™ Fusion sorter with index information (i.e., the fluorescence profile of the input cell) retained for later analysis. Full-Minus-One (FMO) controls were used to determine the threshold of positivity for CD90 and CD49f in relevant sorts.

### 4.2.3 Mass cytometric analysis

Fresh or thawed cells were suspended at $10^6$ cells/mL in HSBS+2% FBS. and then exposed to 5 µM Cisplatin (DVS Sciences) for 5 minutes on ice followed by 2 washes in HSBS+2% FBS (STEMCELL Technologies), re-suspension in 1 mL HSBS+2% FBS and fixation in 1.6% PFA (Electron Microscopy Sciences) for 10 minutes at room temperature. Cells

were then washed twice in PBS (STEMCELL Technologies) with 2% FBS and snap frozen on dry ice for later analysis.

Fixed cells were thawed and washed twice in 1x Barcode Perm Buffer (DVS Sciences) and re-suspended in 400 µL 1x Barcode Perm Buffer. Palladium (Pd) barcodes (DVS Sciences) listed in Table 4.4 were then added to each sample for 30 minutes on ice followed by 2 washes in Maxpar® Cell Staining Buffer (CSB; DVS Sciences). Samples were then pooled, re-suspended in 200 µL blocking buffer at a final cell concentration of $1.5x10^6$ cells/100 µL. Cells were then stained for 1 hour on ice with antibodies against the surface antigens listed in Table 4.5 and mixed every 15 minutes during this period. The cells were then washed with CSB, permeabilized by the addition of -80˚C methanol while vortexing to prevent clumping, immediately spun again and washed twice more in CSB to remove residual methanol. Cells were then stained with antibodies against intracellular markers (Table 4.5) for 1 hour on ice, again with mixing every 15 minutes. At the end of this period, cells were washed with CSB, and re-suspended in 0.5 µM $^{103}Rh$ in CSB at and left overnight at 4 ˚C in the dark. Cells were finally washed twice and resuspended in milli-Q 'ultrapure' $H_2O$ (Millipore) to a concentration $\leq 0.5x10^6$ cells/mL and EQ™ Four Element Calibration Beads (DVS Sciences) added at a concentration of $3.3x10^4$ beads/mL. Cells were then filtered and run on a CyTOF 2 (DVS Sciences) at a flow speed of 0.045 mL/minute, with a 30-second acquisition delay, and a 10-second detector stability delay.

### 4.2.4 *In vitro* assays of CFC and LTC-IC activity

For CFC assays, 50 µL of methyl-cellulose medium supplemented with 50 ng/mL SCF, 20 ng/mL each of GM-CSF, IL-3, IL-6, G-CSF, and 3 units/mL EPO (STEMCELL Technologies) was pre-loaded into the inner 60 wells of a flat bottom Nunc™ 96-well

polystyrene plate. Autoclaved distilled water was loaded into all outer wells to maintain high humidity while being kept in a humidified 37 ˚C incubator supplied with 5% $CO_2$ for 14-16 days. At the end of this period wells were imaged, and colony types assigned by a panel of the authors.

For LTC-IC assays, $5x10^4$ cell aliquots of irradiated M210B4 engineered to express human IL3 and G-CSF, *sl/sl* mouse fibroblasts engineered to express human SCF and IL3, and *sl/sl* mouse fibroblasts engineered to express human FLT3L,were seeded into the inner 60 collagen-coated flat bottom wells of a Nunc™ 96-well polystyrene plate preloaded with 100 µL MyeloCult™ H5100 (STEMCELL technologies) supplemented with $10^{-6}$ M hydrocortisone (Sigma-Aldrich) per well. Plates were maintained in a humidified 37 ˚C incubator with 5% $CO_2$ for a period of 6 weeks and scored weekly for the presence of non-adherent cells just prior to a half medium change. At the end of 6 weeks, 50 ng/mL SCF, 20 ng/mL each of GM-CSF, IL-3, IL-6, G-CSF, and 3 units/mL EPO, were added to each well, and incubation continued for an additional 14-16 days. At the end of this period, the contents of each well was imaged and assessed. Wells confluent with produced cells were scored as highly proliferative, those with >50 such cells but below confluence were scored as low proliferative clones. Wells in which obvious cell proliferation had been seen during the initial 6 weeks but no evidence of hematopoietic cells was seen at the final scoring was scored as transient and wells in which no evidence of hematopoietic cells was seen at any time were scored as negative.

### 4.2.5 Repopulation assays

Immunodeficient NRG mice used as recipients were bred and maintained in the Animal Resource Centre of the British Columbia Cancer Research Centre under SPF conditions and used according to protocols approved by the Animal Care Committee of the University of British

Columbia. All test cells were transplanted intravenously into mice pretreated with 900 cGy whole body $^{137}$Cs γ-irradiation delivered over 3 hours (based on preliminary experiments showing that this gives equivalent reconstitution of all lineages from transplanted human CD34$^{+}$ CB cells as is obtained in NSG mice given 315 cGy, unpublished data). Cell numbers for each injected phenotype in each experiment are listed in Table 4.6. BM was aspirated from alternating femurs of each primary recipient mouse 6, 12, and 20 weeks post transplant for analysis of the human cell numbers and types present. After 30 or 35 weeks, all primary mice were euthanized, both femurs, tibiae, and the pelvis harvested and crushed with a mortar and pestle, and the cells from all mice transplanted with the same input phenotype pooled for secondary transplantation. A proportion of each primary mouse BM pool from the final harvest was transplanted into similarly conditioned and followed secondary NRG recipients (10, 20 and 30 weeks post-transplant, Table 4.6).

### 4.2.6 Data analysis

All statistical testing was performed in R. Flow cytometry data was analyzed in R using a combination of the package 'flowCore' and custom scripts. For the CyTOF data, the sums were first taken for $^{112}$Cd and $^{113}$Cd as the eFluor-605 nanocrystal is detectable in both of these channels. Similarly, for all platinum channels ($^{190}$Pt, $^{192}$Pt, $^{194}$Pt, $^{195}$Pt, $^{196}$Pt, $^{198}$Pt), the data were separately summed to give a composite channel with better detection. We then used the 'compensate' function in the R package 'flowCore' to remove spillover from the combined $^{112/113}$Cd channel into the Palladium isotopes used in the barcoding as the nanocrystal spills into $^{110}$Pd. Values compensated to below zero were re-set to zero for downstream compatibility. Compensated files were then re-written and run through barcode deconvolution software (Zunder

et al., 2015b) with a Mahalanobis cutoff of 30 and a Separation cutoff of 0.1. Events were then gated for DNA content, viability (cisplatin$^{low/negative}$), and CD34 positivity. Population membership for all progenitor populations was determined for all remaining cells by manual gating.

We next used a t-SNE dimensionality reduction algorithm (Van der Maaten and Hinton, 2008) from the R package 'Rtsne' as a simple way of measuring overall molecular similarity between analyzed events (cells). This was performed using a combination of all surface (14 parameters) and intracellular markers (26 parameters) with the perplexity parameter set to 30, both with and without data scaling (mean set to 0, standard deviation set to 1, using the R function 'scale'). t-SNE analysis was also performed including only cells in the CD49f$^{+}$ (HSC) population with internal data scaling.

In addition, t-SNE analysis was also performed on 4 previously analyzed samples which had been exposed to SFM (IMDM supplemented with 10 mg/ml bovine serum albumin, 10 μg/ml insulin, 200 μg/ml transferrin, 40 μg/ml low-density lipoproteins, 100 U/ml penicillin, 100 μg/ml streptomycin, 2 mM glutamine [all from STEMCELL Technologies], and $10^{-4}$ M β-mercaptoethanol [Sigma]) for 3 hours (3 samples) or 1 hour (1 sample) and stained with a similar panel (but not palladium barcoded, as these were each stained and run months apart from one another). As before t-SNE was run on these (with and without data scaling) together with the other barcoded samples using the overlapping markers (38 parameters, HLA-DR and CD71 were excluded as these did not exist in the SFM-exposed data set).

Two dimensional kernel density estimations were performed on each sample, each progenitor population (ignoring samples) and on each progenitor population per-sample. To do so, the function 'kde2d' in the R package 'MASS' with the default gaussian kernel was used with

100 bins in each t-SNE dimension with boundaries extending to 20% past the data range. Following density estimation, each density distribution was converted to a probability density function (ie, total density sum = 1) by dividing each value in the density distribution by the sum of all values to obtain a normalized estimate of the overall molecular state of a given cell grouping. An estimate of the molecular similarity of any two populations was then obtained by calculating the overlap of any two probability density functions. This was done by calculating the total "non-overlap" by taking the sum of the absolute value of the residuals at each grid point and dividing this result by 2. As these values represent a probability density, the overall similarity could thus be calculated as 1-each difference.

Using the pair-wise overlap of cell populations, distance and similarity matrices were constructed. A hierarchical clustering algorithm (the R function 'hclust') was used to provide a simplified view of such relationships given the distance matrices. In order to test whether differences between progenitor populations were consistent between samples, a congruence among distance matrices (CADM) test (Campbell et al., 2011) was performed using the 'CADM.post' function in the R package 'ape'.

Mapping of functional progenitors to CyTOF data was performed by first scaling all $CD34^+$ cells from the index sort. Next a k-nearest neighbor algorithm (the 'knnx.index' function from the R package 'FNN') was used to determine the 10 nearest neighbors of each index-sorted progenitor within the total $CD34^+$ cells from the CyTOF data using the overlapping markers (CD45RA, CD71, CD45, CD123, CD34, CD33, CD49f, CD10, CD135, CD38, CD90, HLA-DR, CD133). The location on the t-SNE plot of that cell was then estimated by taking the mean in each t-SNE dimension of all 10 of its neighbors. The nearest neighbors of all cells of a given type were then used to calculate the total probability density of that cell type. A series of

Kruskal-Wallis tests were then used to compare the nearest neighbor pools of each cell type for each measured parameter. A FDR correction for multiple testing was then applied.

To analyze the index-sorted LTC-ICs, the data was normalized per plate and a k-nearest neighbors algorithm then used to match the cells to their 10 nearest neighbors (based on their levels of CD10, CD33, CD34, CD49f, CD90, CD114, and HLA-DR expression), but within the $CD49f^+$ population of the CyTOF data (scaled within $CD49f^+$). Approximate cell location and density were estimated as for the total $CD34^+$ subset analyses. A series of Wilcoxon Rank-Sum tests were then used to compare between the nearest neighbors of the highly proliferative LTC-ICs, and all other $CD49f^+$ cells from the CyTOF data that were not nearest neighbors of the highly proliferative LTC-ICs. Once again multiple testing was corrected using the FDR method.

## 4.3 Results

### 4.3.1 Data scaling reduces variability between samples and reveals differences between fresh, cryopreserved and briefly cultured cells

As a first step in the development of an unbiased approach to analyze the heterogeneity of $CD34^+$ UCB cells, we sought to determine their distribution spectra of 40 molecular features. These features consisted of 26 intracellular proteins as well as 14 markers detected on the cell surface. The latter included all of those now widely used to identify human CB HSCs and other major progenitor populations in the total $CD34^+$ subset (Figure 4.1). For this purpose, we analyzed a total of 12 $CD34^+$ CB samples in 4 separate runs. In one of these, we used a Palladium-based sample barcoding strategy (Behbehani et al., 2014; Zunder et al., 2015b) to enable 8 samples to be stained and analyzed simultaneously in the same tube, thereby minimizing technical variability (Behbehani et al., 2014; Zunder et al., 2015b). Three of these

were freshly obtained cells from a single donor. The other 5 were from different pools of CB collections (3-6 donors each) that had been cryopreserved and thawed prior to analysis. Overall we analyzed 280,298 $CD34^+$ events from these 8 samples combined (Table 4.7).

Figure 4.2 shows the extensive heterogeneity in the distributions obtained from the combined data after performing dimensionality reduction using t-SNE (Van der Maaten and Hinton, 2008) both with, and without data scaling. Scaling was introduced to prevent possible over-representation of a small number of highly expressed parameters in the reduced dimensions. Scaled data showed a median pair-wise overlap of 75% (IQR=67-78) compared to only 46% (IQR=40-62) in the raw (unscaled) data (paired Wilcoxon signed rank test $p<<0.001$, Figure 4.2A/B). This is consistent with the prediction that t-SNE distributions derived without scaling would be dominated by inter-sample heterogeneity. In contrast, the scaling largely abrogated these effects, while retaining the extent of heterogeneity in individual $CD34^+$ cells assessed for the 40 parameters included here. Interestingly, in the scaled data, cryopreserved and fresh samples were clearly distinguishable based on their similarity profiles, whereas these differences did not reach significance in the unscaled data (Wilcoxon rank sum test $p=0.002$ and 0.13 for scaled and unscaled data, respectively, Figure 4.2C/D).

To further test the robustness of these data, we repeated the analysis after including 4 additional samples that had been stained with an almost identical panel (38 of the 40 parameters) after a prior 1 or 3 hour exposure to SFM and run separately through the CyTOF months apart. Without scaling, data overlap with these samples was very low with an overall median pairwise overlap of 22 % (IQR 8-43, Figure 4.3A) and even less with the fresh or cryopreserved cells (median overlap 8 %, $p<<0.001$, Figure 4.3C), although the cultured cells showed greater similarity to one another (median pairwise overlap of 43%). However, data scaling markedly

increased the distribution overlap, to give an overall median overlap of 65% (IQR 58-76). The cultured samples were still more similar to one another (median in-group overlap of 79, IQR 73-80) than to cryopreserved and non-cryopreserved samples (median overlap of 57, IQR 52-61 (Figure 4.3B/D; $p<<0.001$). These latter results illustrate the large effects that sample source, handling and technical factors can have on the apparent molecular differences revealed by t-SNE distributions, precluding pooled analysis approaches and likewise the ability of pre-processing the data to substantially reduce these effects. We therefore opted to use the scaled data only for subsequent analyses.

### 4.3.2 Conventionally defined phenotypic subsets of $CD34^+$ CB cells are molecularly heterogeneous

We next assessed the molecular distributions of the 40 examined parameters within widely accepted $CD34^+$ progenitor populations to determine the extent of their heterogeneity and their, relatedness. Conventionally defined populations showed significantly different molecular distributions from one another along both t-SNE axes (Kruskal-Wallis rank sum test p values $<<0.001$ in both dimensions, Figure 4.4A). In spite of these average differences between recognized $CD34^+$ subsets, all of these populations also showed extensive overlap in their distributions of the molecular properties analyzed (median overlap of 45%, IQR 34-54%). Importantly, however, the distributions of a number of molecular features were consistent with their ascribed functional properties (Figure 4.5 and Figure 4.6). For example, on average, MEPs were found to express the transcription factor GATA1, which is associated with erythroid (Fujiwara et al., 1996) and megakaryocytic differentiation (Shivdasani et al., 1997), at a higher level than other progenitor populations. Analogously, C/EBPα, a transcription factor necessary

for granulocyte differentiation (Zhang et al., 1997, 1998), was expressed, on average, at a higher level in GMPs ($CD34^+CD38^+CD10^-CD45RA^+CD135^+$ cells) than in other subsets, and the same for PAX5, a transcription factor necessary for B-cell development (Nutt et al., 1999), in pre-B/NK progenitors and MLPs (Figure 4.5, Figure 4.6, all FDRs<<0.001). Interestingly, C/EBPα was also present in most pre-B/NK cells, and PAX5 in most GMPs. Together these results show that different progenitor populations can be discriminated in an expected fashion by some of their molecular features, but they are also not highly distinct from one another.

We then re-examined the hierarchical structure of these conventionally defined phenotypes based on the degree of pairwise overlap in the t-SNE distributions of all 40 parameters measured in them. All 8 samples in the first experiment showed significant congruence in the distance matrices thus obtained suggesting the observed relationships were reproducible (Holm-corrected CADM test p values ≤0.002). This remained the case when the 4 cultured samples were also included in the analysis, suggesting that the population differences recognized are robust even after the cells have been cultured in SFM (without GFs) for up to 3 hours (Figure 4.4B; Holm-corrected CADM test p values ≤0.01). CMPs and MEPs showed a high degree of overlap (median overlap of 63%, IQR = 60-64). Meanwhile, GMPs also had a high degree of overlap with pre-B/NK progenitors ($CD34^+CD38^+CD10^+CD45RA^+$ cells, median overlap of 61%), supporting the idea that many of these cells are more closely related to B-lymphoid progenitors than to progenitors of other myeloid lineages (Görgens et al., 2013).

Interestingly, we also found that all phenotypic populations were multi-modal, with significant deviations from unimodality in at least one t-SNE dimension (Hartigan's Dip test, FDRs < 0.01 in at least 1 dimension). This suggested that these phenotypically defined subpopulations are, themselves, composed of additional distinct sub-populations. Perhaps the

most striking example of this was the CMP subset, which contained 3 separate modes. Gating on each of these alone (Figure 4.7) showed that one consisted of cells expressing high levels of GATA1 and lower levels of PU.1 and C/EBPα, whereas the other 2 had opposite profiles (Figure 4.8A). These two subgroup could also be separated by their contrasting expression of CD114 (G-CSFR), CD33, CD133 which were higher in the myeloid modes, while CD71 was higher in the GATA1-expressing mode (Figure 4.8B). These results suggest that the 'CMP' population may actually be a mixture of MEP and GMP, and prospectively separable using additional surface markers.

### 4.3.3 Cells with different myeloid and erythroid differentiation properties also show distinct but overlapping molecular profiles

Combined measurement of functions unique to viable cells and their initial molecular state using mass cytometric analysis is not possible. Therefore to link these assessments we performed CFC assays on single, index-sorted $CD34^+$ cells that had been co-stained for a subset of the surface markers used in the mass cytomety experiments. We were then able to map the cells defined according to their cell outputs back onto the t-SNE plots. 491 of 660 single $CD34^+$ cells thus assessed, produced a colony of which 135 were large (>1000 cells) and 126 were small (50-1000 cells) GM colonies, 84 appeared to be pure erythroid colonies (>50 hemoglobinized cells), 139 contained mixtures of these lineages (Figure 4.9) and 7 were small colonies of cells with a blast-like morphology. Because these were rare and difficult to interpret, they were excluded from our subsequent analyses.

Several types of CFCs showed some distinct features, but in all cases, extensive overlap in their profiles were seen. For example, the median overlap between BFU-Es and CFU-GEMMs

was 81%, although their distributions were significantly different from one another (p values<0.01 in both t-SNE dimensions). In contrast, although the median overlap between high and low proliferative potential CFU-GMs was also 86%, their distributions were not significantly different from one another, in spite of significant differences from other progenitor types and cells that failed to grow or differentiate in the CFC assay (FDRs<<0.001 in at least 1 t-SNE dimension). When compared to accepted phenotypic subsets, BFU-Es and CFU-GEMMs were closely related to MEPs, and MPPs (Figure 4.10). CFU-GM colonies (regardless of their proliferative potential) were more closely related to CMPs than any other population, including GMPs (Figure 4.10).

Comparison of surface and intracellular markers between cells mapping to each functionally defined progenitor type also confirmed previously reported associations. For example, we found surface markers conventionally used for defining phenotype subsets, such as CD135 and CD45RA (Doulatov et al., 2010) were present at significantly different levels in different CFCs types (Figure 4.11). Similarly, CD133, recently reported to distinguish erythroid and granulopoietic progenitors (Görgens et al., 2013), also came up in our CFC data as significantly different in BFU-Es and CFU-GMs (Figure 4.11). We were also able to identify a number of expected differences in the intracellular markers associated with these functionally defined cells. These include a higher level of GATA1 in cells co-mapping with BFU-Es and slightly higher levels of PU.1 and C/EBPα in cells co-mapping with CFU-GMs. Together, these results demonstrate the power of our mapping strategy to identify meaningful differences in marker expression in functionally distinguished progenitors.

In addition to these previously identified differences, we also were able to detect a number of novel associations of specific properties with a defined functional potential. The most

obvious examples were the lower levels of CD34 and higher levels of CD71 associated with BFU-Es, and the higher levels of CD33 and CD114 (G-CSF receptor) associated with CFU-GMs as compared to BFU-Es. In addition we noted higher levels of phosphorylated STAT3 were associated with CFU-GMs as compared to BFU-Es and CFU-GEMMs, and higher levels of phosphorylated eEF2 were associated with BFU-Es as compared to CFU-GM (Figure 4.11). These point to differences in the basal signaling states of progenitors with restricted erythroid vs granulopoietic differentiation potentialities.

### 4.3.4 Identification of functionally and molecularly distinct subsets of HSCs in human CB

Molecular features of functionally defined HSCs are of particular interest because of their clinical relevance. However, the best available phenotype to isolate this population in its most enriched form, still only gives yields of ~10% functional purity (Notta et al., 2011). To search for possible subsets within this $CD49f^+$ phenotype with maximal sensitivity, we re-ran the t-SNE analyses using only cells in this subset. In parallel, we assayed 538 index sorted $CD49f^+$ cells for *in vitro* self-renewal capability. To do so we used a modified version of the LTC-IC assay in which we co-cultured single cells with stromal feeders for 6 weeks period, followed by the addition of GFs to stimulate further growth of cells present at that time. Wells were assessed visually another 2 weeks later (a total of 8 weeks after placing the cells in culture) for the presence of >50 cells. Using this approach, we found just over half (56%) of 538 $CD49f^+$ cells analyzed in this way in 4 independent experiments read out as positive in this assay. This included a total of 76 highly proliferative cells and 228 cells with low but persistent proliferative

potential. In the negative group were 93 cells with transient proliferative activity, and 141 cells that displayed no proliferative ability under these conditions (Figure 4.12).

We then mapped these cells also back to their nearest neighbors in the mass cytometry dataset using the overlap of the index sort information and the surface marker information from the mass cytometry data. The centers of density in t-SNE space were similar between all populations (Figure 4.13). Cells with the highest proliferative capacity did, however, map preferentially to a subset of the total $CD49f^+$ population and were significantly associated with high levels of CD34, CD90, and CD133 despite their having already been selected as $CD34^+$ and $CD90^+$. Additional markers associated with the highly proliferative LTC-IC were elevated levels of CD114 (G-CSFR) and CD33 (Figure 4.14), IκBα (suggesting low NFκB signaling), PU.1, phosphorylated CREB, eEF2 and a number of phosphorylated MAPK signaling intermediates, including P38, ERK1/2, MAPKAPK2, and AKT (Figure 4.14, Appendix B.2). Together these are consistent with the quiescent state of primitive hematopoietic cells, but also suggest tonic levels of pathway activation of a number of important downstream targets of GFs active on HSCs (see Chapter 3).

### 4.3.5 The most primitive human HSC reside in the $CD33^+$ sub-fraction of $CD49f^+$ cells

We then designed experiments to analyze the functional heterogeneity of the $CD49f^+$ compartment using a repopulation strategy. We first split the $CD49f^+$ compartment into 6 sub-fractions on the basis of their combined expression of CD45, CD33, and CD202b (Figure 4.15). Representative proportions of cells from each sub-fraction in 2 independent experiments (Table 4.6) were injected into irradiated NRG mice. All BM repopulating activity in primary animals was restricted to the $CD45^+CD33^{+/-}$ fractions of $CD49f^+$ cells (Figure 4.16). CD202b expression

on the initial cells did not substantially enrich for repopulating cells, although some repopulation was observed in this fraction (Figure 4.16). Interestingly, at 30-35 weeks post-transplant, we did not find any significant differences between the chimerism obtained from the $CD45^{+}CD33^{-}CD202b^{-}$ and $CD45^{+}CD33^{+}CD202b^{-}$ transplants and most of the observed repopulation was derived from these cells (t-test $p=0.24$). Secondary repopulating activity, however, was detected exclusively in the cells produced from the $CD45^{+}CD33^{+}CD202b^{-}$ subset (Fisher's test $p<0.001$, Figure 4.16) These findings demonstrate that HSC with durable self-renewal potential are restricted to the $CD33^{+}CD202b^{-}$ subset of $CD49f^{+}$ cells, consistent with the phenotypic properties associated with the highly proliferative LTC-ICs. These results also show that HSC repopulating capability is not only differentially distributed within the $CD49f^{+}$ population, but also that its durability can be associated with other molecular changes.

## 4.4 Discussion

Elucidation of the hierarchical structure of the hematopoietic differentiation process has been an evolving exercise spanning 5 decades (Eaves, 2015). Most recently have been results indicative of intrinsically perpetuated differences in lineage output potential at the HSC level (Dykstra et al., 2007; Muller-Sieburg et al., 2004); late links between B-cell and neutrophil differentiation (Doulatov et al., 2010; Görgens et al., 2013), and early links between HSCs and megakaryocytopoiesis (Sanjuan-Pla et al., 2013; Yamamoto et al., 2013). Here we have re-examined this issue using new technologies that enable large numbers of single cells to be analyzed in terms of dozens of molecular parameters coupled with the types and durabilities of their clonally tracked progeny outputs. We focused this study on the $CD34^{+}$ CB cell types using both the most recently defined phenotypes (Doulatov et al., 2010; Görgens et al., 2013) and a

more unbiased approach based on the relatedness of each cell analyzed within the multidimensional space defined by the collection of parameters assessed.

We found the molecular states of predefined phenotypes showed considerable agreement with existing literature. Hierarchical relationships between phenotypic populations based on molecular similarity also fit with many aspects of the currently accepted differentiation hierarchy. For example, we found that the GMP population appeared, on average, to be more closely related to Pre-B/NK progenitors than to other types of myeloid progenitors (Görgens et al., 2013). Interestingly, there was a surprising degree of difference between cells classified phenotypically as HSC and MPP, despite their similar surface profiles and even functional capabilities.

Within the HSC compartment, primitive functional capability was associated with a number of molecular differences. These included increased levels of active CREB, eEF2, and PU.1. The increased levels of phosphorylated eEF2 is indicative of inhibited protein synthesis (Browne and Proud, 2002), which may be related to the quiescent state of these cells (Becker et al., 1965; Bruce et al., 1966). Together these 3 features may be indicative of PKA signaling as all can be downstream targets (Delghandi et al., 2005; Diggle et al., 1998; Redpath and Proud, 1993). The elevated levels of PU.1 may also be related to a quiescent profile. PU.1 has been associated with cell cycle inhibition in mouse HSCs (Staber et al., 2013), and extended cell cycle times have also been associated with increased PU.1 accumulation in macrophages (Kueh et al., 2013). Interestingly, aside from the quiescent signature, significant activation of AKT, ERK1/2 and P38 was also observed, suggesting an activated signature. Additionally, significantly increased levels GATA1were also detected in HSCs, consistent with findings in the mouse where

the most durable HSCs are closely related to the megakaryocyte lineage (Sanjuan-Pla et al., 2013; Yamamoto et al., 2013).

In contrast, cells within historically defined (later types of) progenitor populations displayed a spread of molecular states, thus throwing into question the specific potentialities often assigned to them. Density estimates of the complete repertoire of properties showed that most preset phenotypes contained more than one center of density, indicative of multiple subpopulations within each phenotype. The three distinct centers of density present within the CMP population constitute a particularly overt example of this type of heterogeneity with one centre each defined by cells with the molecular properties of either erythroid or myeloid progenitors but not both in the same cell, illustrating discordancy between the acquisition of a unique phenotype and a further segregation of lineage options. This finding also highlights the importance of single cell measurements in determining in what cells bi-potency exists.

We also identified a surprising degree of overlap between the molecular states of pre-defined subsets of $CD34^{+}$ CB cells - even for CFCs that display different lineage outputs suggesting that this type of overlap was not an artifact of assessing phenotypically impure cell populations. If different progenitors represented unique and stable molecular states, as implied by current literature, transitions between them should be rare. One would therefore expect these states to be well resolved and distinct from one another in molecular space, with the cell density at any point in molecular space serving as an inverse estimate of inter-state barriers. The strong overlap in cell densities observed between historically defined subsets suggests that the barriers between differentiation states are much lower than previously conjectured (Figure 4.17) (Enver et al., 2009; Waddington and others, 1957).

A shallow differentiation landscape has important implications for HSC biology as it implies that shifts in lineage potentialities may be relatively easily achieved and be reversed. Consistent with such a model would be the possibility that finite transitions represent the outcomes of many gradual gains and losses of molecular characteristics before a new stable state is reached. The ability of GATA1 (Hirasawa et al., 2002; Kulessa et al., 1995) or STAT5 (Schuringa et al., 2004) over-expression to convert myeloid progenitors into erythroid and eosinophil progenitors suggests that such progenitor class alterations can indeed be accomplished in this way.

Within the HSC population, we observed a gradual loss of self-renewal potential despite similar molecular states. This was clearly demonstrated by the separation of cells with secondary repopulation capability from those with equivalent primary, but no secondary repopulation ability. In the mouse system, it has previously been shown that over-expression of NUP98-HOXA10 homeodomain was sufficient to increase the frequency of repopulating clones within a sorted HSC-enriched fraction, demonstrating that these could be induced to regain HSC activity (Sekulovic et al., 2011). Similarly, we have previously shown that culturing sorted E-SLAM cells (~50% pure mouse HSC(Kent et al., 2009)) in the correct GF environment was able to increase the frequency of cells able to repopulate recipient animals, albeit with shorter-term HSC (Wohrer et al., 2014). Together these results provide evidence that loss of the important regenerative ability of HSCs may also be relatively readily reversible if the right conditions can be found.

Here we combined protein measurements at single-cell resolution with high-throughput functional readouts in order to provide a map of the progenitor compartment in human $CD34^{+}$ CB cells. We reveal new molecular and functional heterogeneity between previously defined

phenotypes as well as substantial overlap in their properties. Together, these finding reveal a more complex and flatter molecular landscape of primitive stages of human hematopoietic cell differentiation than previously anticipated. Finally, we identify molecular characteristics of functionally defined human HSCs that allow those with durable self-renewal to be prospectively separated from those with long-term but time-limited (6 months) mature cell output ability.

**Table 4.1 Antibodies used in progenitor cell index sorts.**

| Antigen | Clone | Fluorophore |
|---|---|---|
| CD49f | GoH3 | eFluor450 |
| CD123 | 9F5 | Biotin |
| CD45RA | HI100 | eFluor605NC |
| HLA-DR | L243 | Brilliant Violet 650 |
| CD38 | HIT2 | Brilliant Violet 711 |
| CD71 | OKT9 | FITC |
| CD10 | HI10a | PerCP-Cy5.5 |
| CD135 | BV10A4H2 | PE |
| CD33 | WM53 | PE-CF549 |
| CD90 | 5E10 | PE-Cy7 |
| CD133 | AC133 | APC |
| CD34 | 581 | AF700 |
| CD45 | HI30 | APC-eFluor780 |

**Table 4.2 Antibody staining panel for bulk sub-setting of the CD49f compartment.**

| Antigen | Clone | Fluorophore |
|---|---|---|
| CD49f | GoH3 | eFluor450 |
| CD45 | 9.4 | FITC |
| CD34 | 4H11 | PerCP-eFluor710 |
| CD90 | 5E10 | PE |
| CD33 | WM53 | PE-Cy7 |
| CD202b | 33.1 (Ab33) | AF647 |
| CD38 | HIT2 | APC-eFluor780 or Brilliant Violet 605 |
| CD45RA | HI100 | APC-eFluor780 or eFluor605 |

**Table 4.3 Antibodies used in HSC index sorts.**

| Antigen | Clone | Fluorophore |
|---|---|---|
| CD114 | LMM741 | PE |
| CD33 | WM53 | PE-CF549 |
| CD90 | 5E10 | PE-Cy7 |
| CD49f | GoH3 | eFluor450 |
| CD11b | ICRF44 | Biotin |
| CD38 | HIT2 | FITC |
| CD45RA | HI100 | FITC |
| CD10 | CB-CALLA | APC |
| CD34 | 581 | AF700 |
| HLA-DR | L243 | Brilliant Violet 650 |

**Table 4.4 Sample cryo-preservation status, donor number, and palladium isotope labeling (1= presence, 0=absence)**

| Sample | Cryo-preserved | Number of Donors | $^{102}$Pd | $^{104}$Pd | $^{105}$Pd | $^{106}$Pd | $^{108}$Pd | $^{110}$Pd |
|---|---|---|---|---|---|---|---|---|
| UCB 6 | No | 1 | 1 | 1 | 1 | 0 | 0 | 0 |
| UCB 7 | No | 1 | 1 | 0 | 1 | 1 | 0 | 0 |
| UCB 8 | No | 1 | 1 | 0 | 1 | 0 | 1 | 0 |
| UCB 1 | Yes | 5 | 1 | 0 | 1 | 0 | 0 | 1 |
| UCB 2 | Yes | 3 | 0 | 1 | 1 | 1 | 0 | 0 |
| UCB 3 | Yes | 4 | 0 | 1 | 1 | 0 | 1 | 0 |
| UCB 4 | Yes | 6 | 0 | 1 | 1 | 0 | 0 | 1 |
| UCB 5 | Yes | 6 | 0 | 0 | 1 | 1 | 1 | 0 |

**Table 4.5 Antibodies used in the mass cytometric analyses.**

| Antigen | Clone | Supplier | Isotope | Concentration in 100 µL ($3x10^6$ cells) |
|---|---|---|---|---|
| **Intracellular** | | | | |
| pSHP2 (Y580) | D66F10 | DVS Sciences | 141Pr | 1 µL |
| GATA3 | D13C9 | CST | 142Nd | 0.4 µg |
| CRKL (pY207) | Polyclonal | DVS Sciences | 143Nd | 1 µL |
| SRC (pY418) | K98-37 | BD Biosciences | 145Nd | 0.05 µg |
| Acetyl-CoA Carboxylase (pS79) | Polyclonal | CST | 146Nd | 0.1 µg |
| Cyclin B1 | D5C10 | CST | 147Sm | 0.1 µg |
| PAX5 | D19F8 | CST | 148Nd | 0.2 µg |
| PU.1 | 9G7 | CST | 149Sm | 0.4 µg |
| STAT5 (pY694) | 47 | DVS Sciences | 150Nd | 1 µL |
| AKT (pS473) | D9E | DVS Sciences | 152Sm | 1 µL |
| STAT1 (pY701) | 58D6 | DVS Sciences | 153Eu | 1 µL |
| SMAD2/3 (pS465/S467)/(pS423/S425) | D6G10 | CST | 154Sm | 0.4 µg |
| p38 (pT180/Y182) | D3F9 | DVS Sciences | 156Gd | 1 µL |
| STAT3 (pY705) | 4/P-Stat3 | DVS Sciences | 158Gd | 1 µL |
| MAPKAPK2 (pT334) | 27B7 | DVS Sciences | 159Tb | 1 µL |
| IκBα | L35A5 | DVS Sciences | 164Dy | 1 µL |
| CREB (pS133) | 87G3 | DVS Sciences | 165Ho | 1 µL |
| β-Catenin (Non-phospho S33/S37/T41) | D13A1 | CST | 166Er | 0.4 µg |
| ERK1/2 (pT202/Y204) | D13.14.4E | DVS Sciences | 167Er | 1 µL |
| Ki67 | Ki67 | DVS Sciences | 168Er | 1 µL |
| pZAP70 (pY319)/SYK (pY352) | 17a | DVS Sciences | 171Yb | 1 µL |
| TAL1 | 5H1 | Abcam | 173Yb | 0.4 µg |
| C/EBPα | D56F10 | CST | 174Yb | 0.2 µg |
| S6 (pS235/S236) | N7-548 | DVS Sciences | 175Lu | 1 µL |
| GATA1 | D52H6 | CST | 176Yb | 0.4 µg |
| eEF2 (pT56) | Polyclonal | CST | 209Bi | 0.4 µg |
| **Surface** | | | | |
| CD71 | OKT9 | eBioscience | 139La | 0.2 µg |
| CD45 | HI30 | eBioscience | 115In | 0.2 µg |
| CD114 (GCSFR) | LMM741 | eBioscience | 144Nd | 0.4 µg |
| CD123 (IL3Ra) | 6H6 | eBioscience | 151Eu | 0.4 µg |
| CD34 | 4H11 | eBioscience | 155Gd | 0.2 µg |
| CD33 | WM53 | eBioscience | 157Gd | 0.4 µg |
| CD49f | eBioGoH3 | eBioscience | 160Gd | 0.1 µg |

| Antigen | Clone | Supplier | Isotope | Concentration in 100 µL ($3x10^6$ cells) |
|---|---|---|---|---|
| CD10 | SN5c | eBioscience | 161Dy | 0.2 µg |
| CD135 (FLT3) | BV10A4H2 | eBioscience | 162Dy | 0.4 µg |
| CD38 | HIT2 | eBioscience | 163Dy | 0.2 µg |
| CD90 | 5E10 | eBioscience | 169Tm | 0.4 µg |
| HLA-DR | L243 | BioLegend | 170Er | 0.4 µg |
| CD133 | AC133 | Miltenyi Biotec | 172Yb | 0.2 µg |
| CD45RA | HI100 | eBioscience | ef605NC | 1 µL |

**Table 4.6 Number of cells for each $CD34^+CD38^-CD45RA^-CD90^+CD49f^+$ subset injected per mouse.**

| | Cell number per 1° mouse | | Proportion of primary mouse per 2° mouse | |
|---|---|---|---|---|
| **Phenotype (within CD49f+)** | **Exp 1** | **Exp 2** | **Exp 1** | **Exp 2** |
| $CD45^-CD33^-$ | 16 | 4 | 0.2 | ND |
| $CD33^-CD202b^-$ | 207 | 212 | 0.4 | 0.4 |
| $CD33^-CD202b^+$ | 16 | 32 | 0.4 | 0.4 |
| $CD33^+CD202b^-$ | 210 | 151 | 0.4 | 0.4 |
| $CD33^+CD202b^+$ | 14 | 32 | 0.4 | 0.4 |
| $CD45^{++}CD33^{++}$ | 7 | 2 | 0.4 | ND |

ND=not done

**Table 4.7 Cell numbers per progenitor population associated with each sample.**

| Phenotype | Sample 1 | 2 | 3 | 4 | 5 | 6 | 7 | 8 |
|---|---|---|---|---|---|---|---|---|
| $CD34^+$ | 4004 | 1266 | 7460 | 7134 | 4582 | 47947 | 41338 | 166567 |
| $CD34^+CD38^-$ | 1640 | 693 | 2499 | 2495 | 1761 | 10583 | 8210 | 66163 |
| $CD34^+CD38^+$ | 1489 | 300 | 3007 | 2992 | 1703 | 28738 | 25906 | 58767 |
| **pre-B/NK**: $CD34^+CD38^+CD10^+CD45RA^+$ | 43 | 10 | 182 | 187 | 84 | 1250 | 914 | 1110 |
| **CMP**: $CD34^+CD38^+CD10^-$ $CD135^+CD45RA^-$ | 435 | 92 | 1227 | 927 | 530 | 12356 | 10419 | 23535 |
| **MEP**: $CD34^+CD38^+CD10^-$ $CD135^-CD45RA^-$ | 262 | 54 | 188 | 283 | 223 | 3957 | 4477 | 11580 |
| **GMP**: $CD34^+CD38^+CD10^-$ $CD135^+CD45RA^+$ | 426 | 80 | 766 | 988 | 509 | 6210 | 5756 | 12018 |
| **MLP**: $CD34^+CD38^-$ $CD10^+CD45RA^+$ | 230 | 104 | 454 | 561 | 321 | 1409 | 1552 | 5197 |
| **MPP**: $CD34^+CD38^-CD45RA^-$ $CD90^-CD49f^-$ | 436 | 182 | 139 | 332 | 333 | 1327 | 1172 | 13797 |
| **HSC**: $CD34^+CD38^-CD45RA^-$ $CD90^+CD49f^+$ | 38 | 12 | 308 | 134 | 67 | 884 | 366 | 1518 |

Phenotypes are based on (Doulatov et al., 2010; Notta et al., 2011)

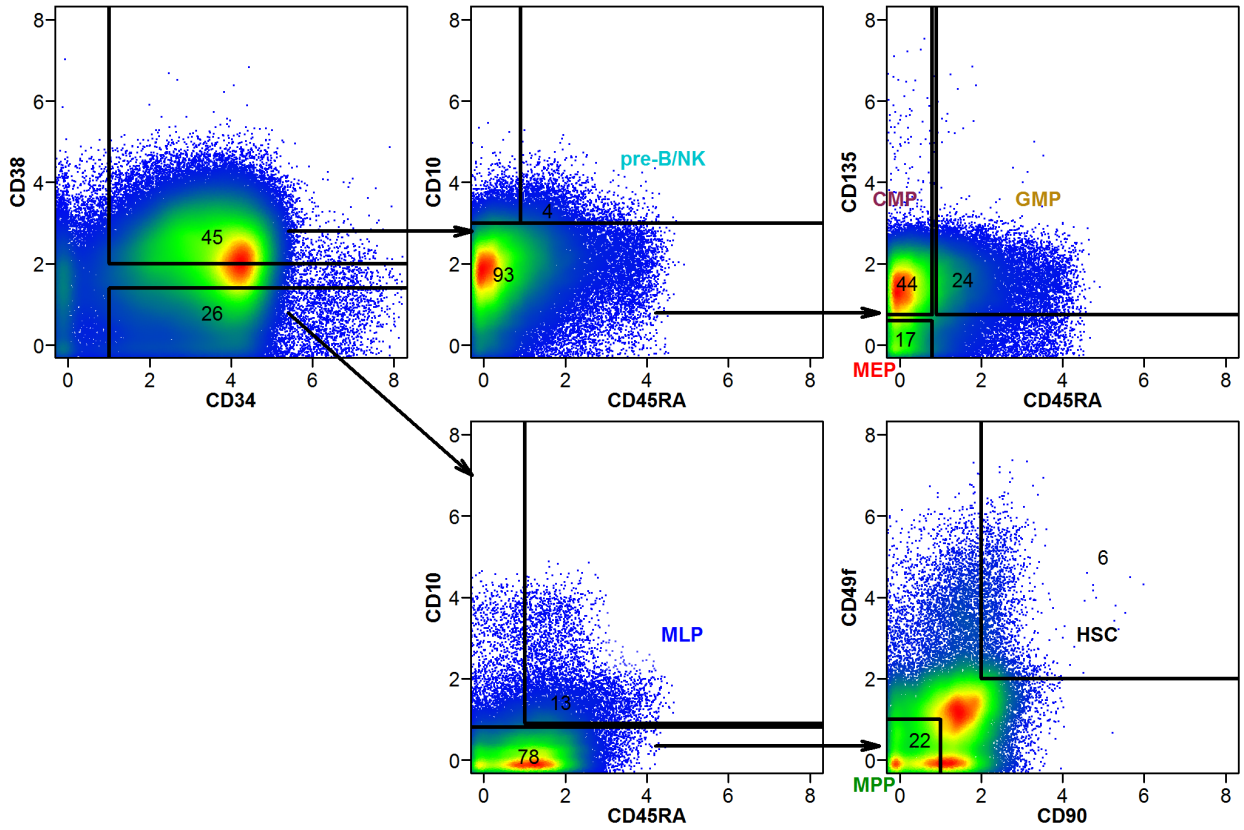


**Figure 4.1 Gating for progenitor populations from CyTOF data.** Plots represent cells pooled from all samples.

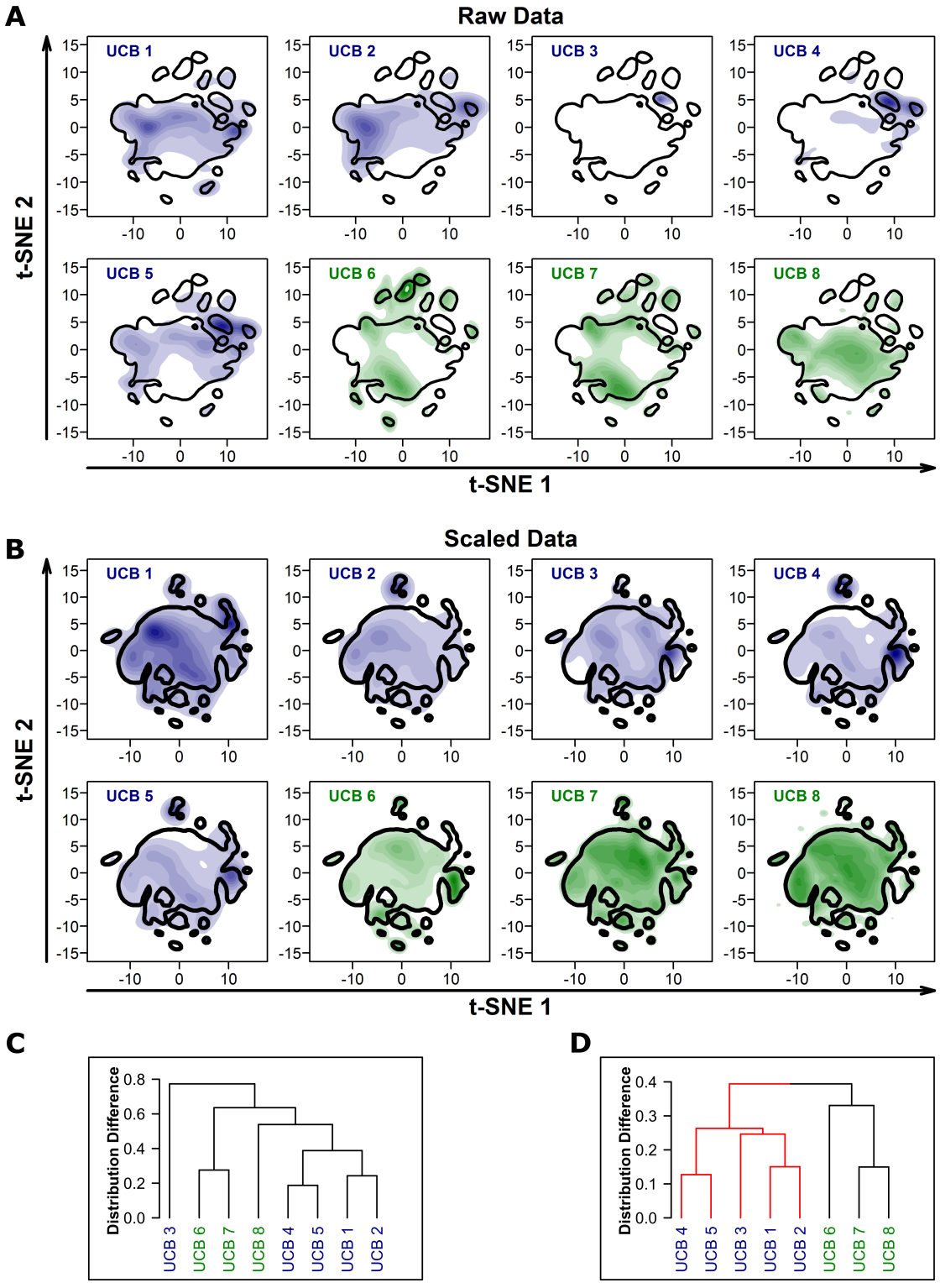


**Figure 4.2 Molecular overlap between samples with and without data scaling.** A/B) t-SNE distributions for each independent cord blood sample. Cryopreserved samples are shown in blue, while non-cryo-preserved samples

are shown in green. The $75^{th}$ quantile of the overall density distribution is shown in black. Data without scaling is shown in (A) and scaled data is shown in (B). C/D) Hierarchical clustering based on the pair-wise differences in density distributions for each sample using the raw (C), and scaled (D) data respectively.

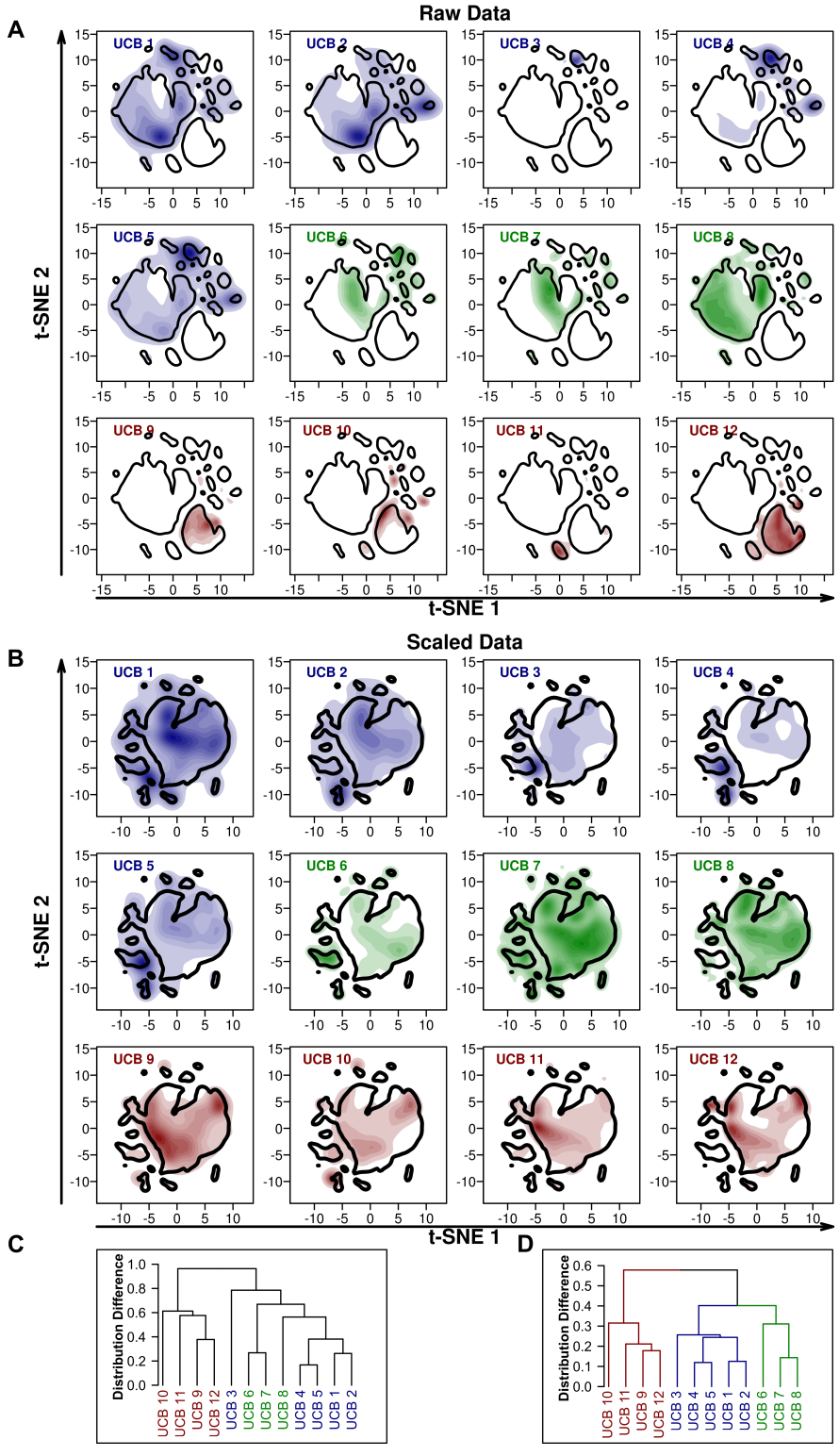


**Figure 4.3 Molecular overlap between samples including cells exposed to culture.** A/B) t-SNE distributions for each independent cord blood sample without (A) and with (B) data scaling. The 75$^{th}$ quantile of the overall density

distribution is shown in black. Cultured samples are shown in red, cryopreserved samples are shown in blue, and non-cryo-preserved samples are shown in green C/D) Hierarchical clustering based on the pair-wise differences in density distributions for each sample using the raw (C), and scaled (D) data respectively.

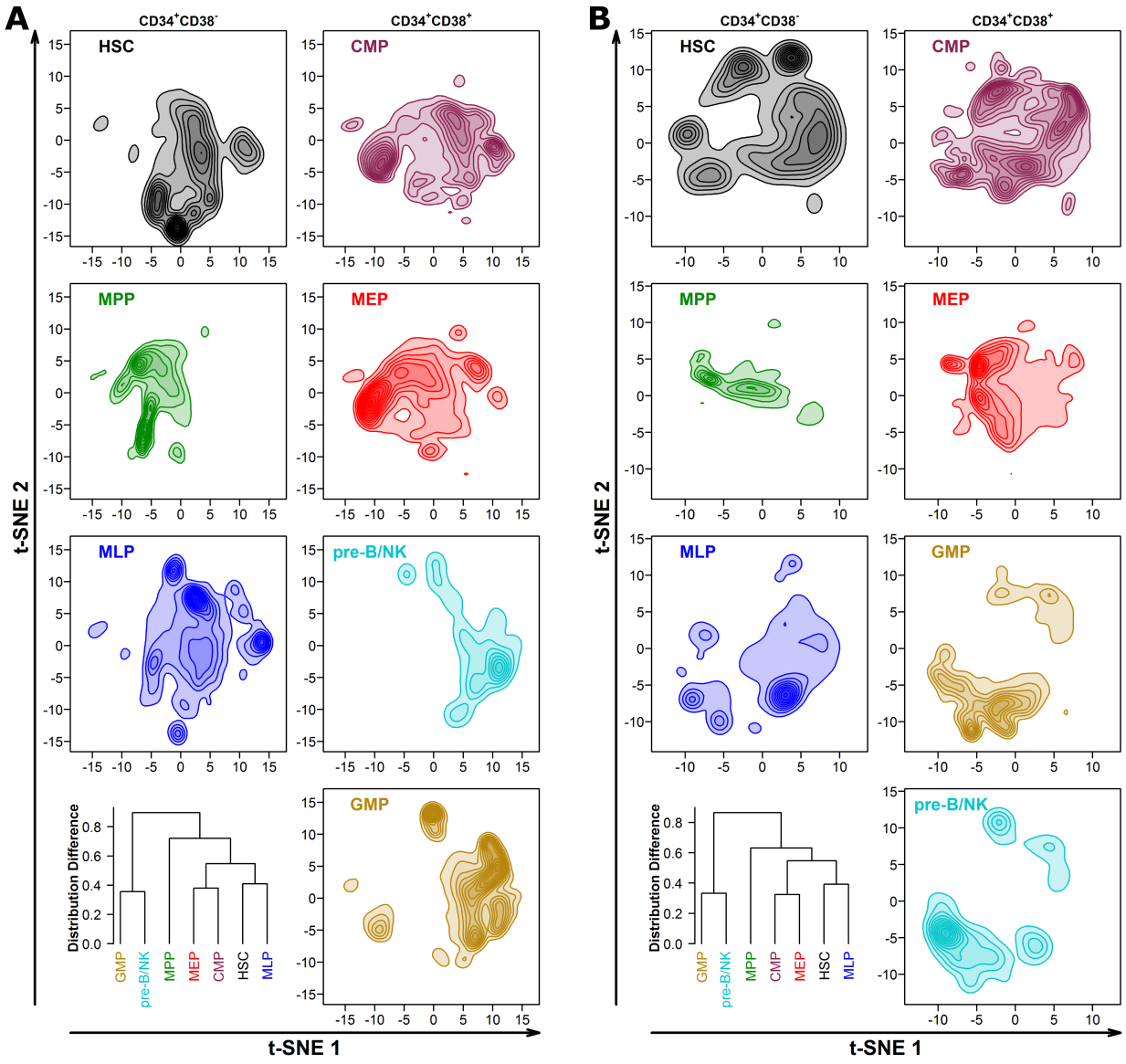


**Figure 4.4 Phenotypic progenitor distribution across molecular space.** t-SNE density distributions are shown based on the surface and intracellular characteristics of each phenotypic progenitor population. Distributions based on cryopreserved and non-preserved samples only are shown in (A). Distributions based on all samples, including SFM exposed samples are shown in (B). $CD34^{+}CD38^{-}$ populations are shown on the left while $CD34^{+}CD38^{+}$ populations are shown on the right in each case. A hierarchical clustering based on the pair-wise differences in density distributions is shown in the bottom left panels.

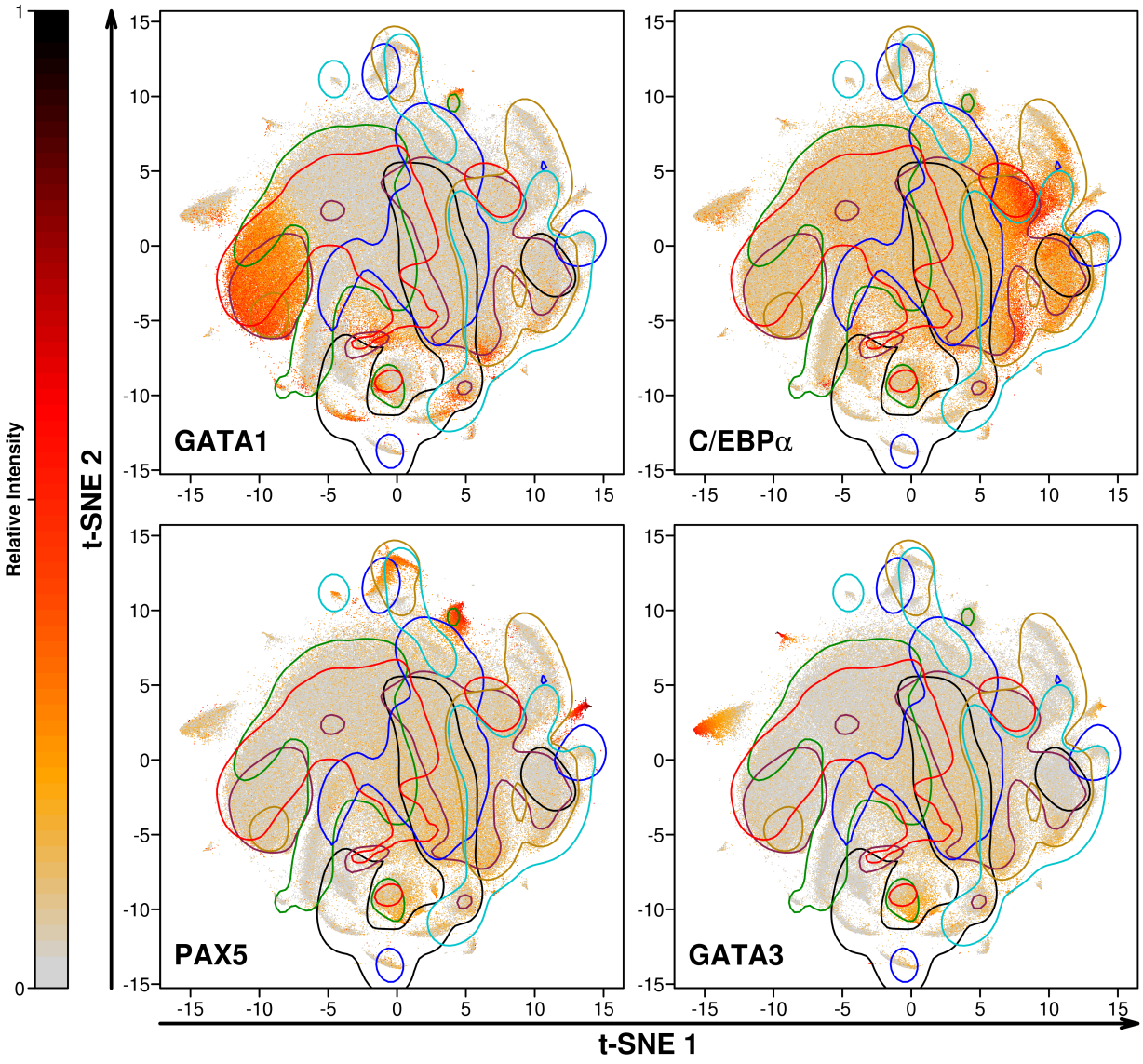


**Figure 4.5 Transcription factor levels across human progenitor molecular distribution.** t-SNE distributions of all analyzed CD34$^{+}$ cells are shown. Each cell is coloured based on relative transcription factor expression level within the total CD34$^{+}$ population. Contour lines are shown at the 90$^{th}$ quantile of the density distribution of cells from each phenotypic progenitor population. The contour for HSC is shown in black, MPP in green, MEP in red, GMP in brown, MLP in dark blue, and pre-B/NK in light blue.

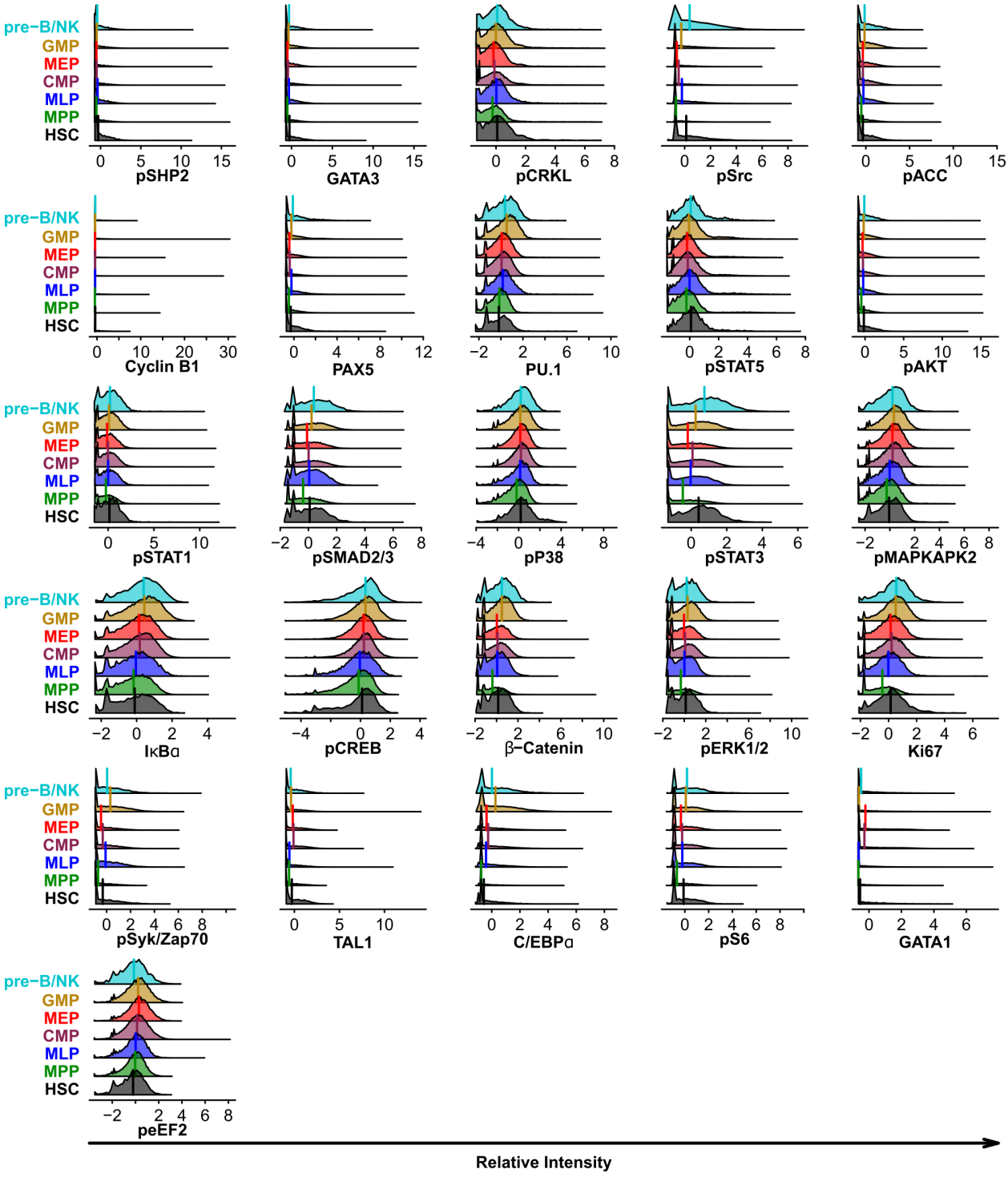


**Figure 4.6 Relative levels intracellular proteins in phenotypic progenitor populations.** Distributions of the scaled marker intensity are shown for each phenotypically defined progenitor population. Lines are drawn at median values.

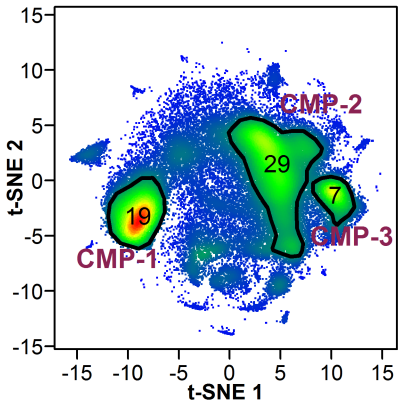


**Figure 4.7 Gating for CMP sub-populations.**

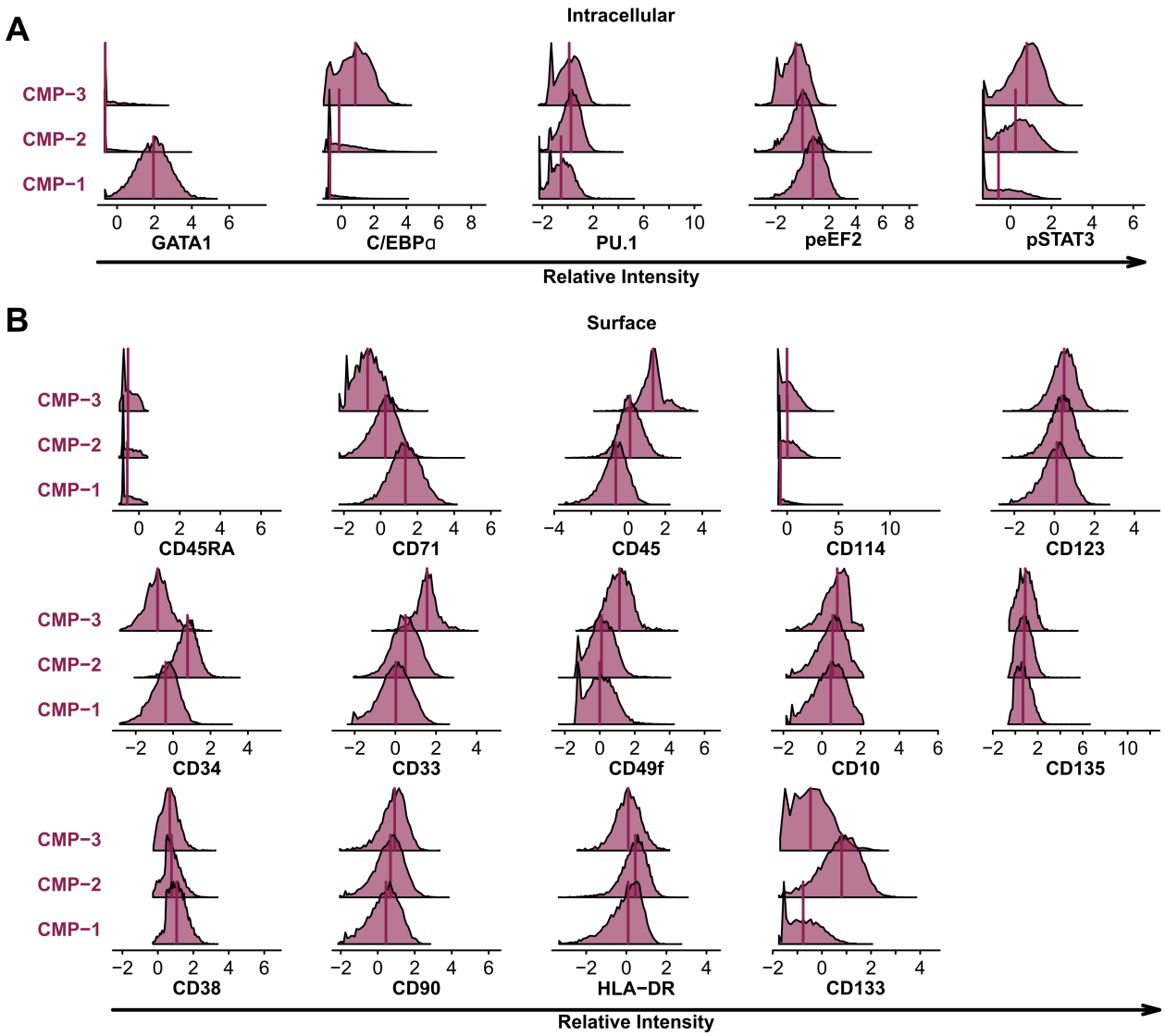


**Figure 4.8 Differences in molecular markers between CMP sub-populations.** A) Relative intensity is shown for a selection of analyzed transcription factor and signaling molecules for the three major CMP sub-populations. Median values are shown as lines. B) Relative intensity is shown for all analyzed surface for the three major CMP sub-populations. Median values are shown as lines.

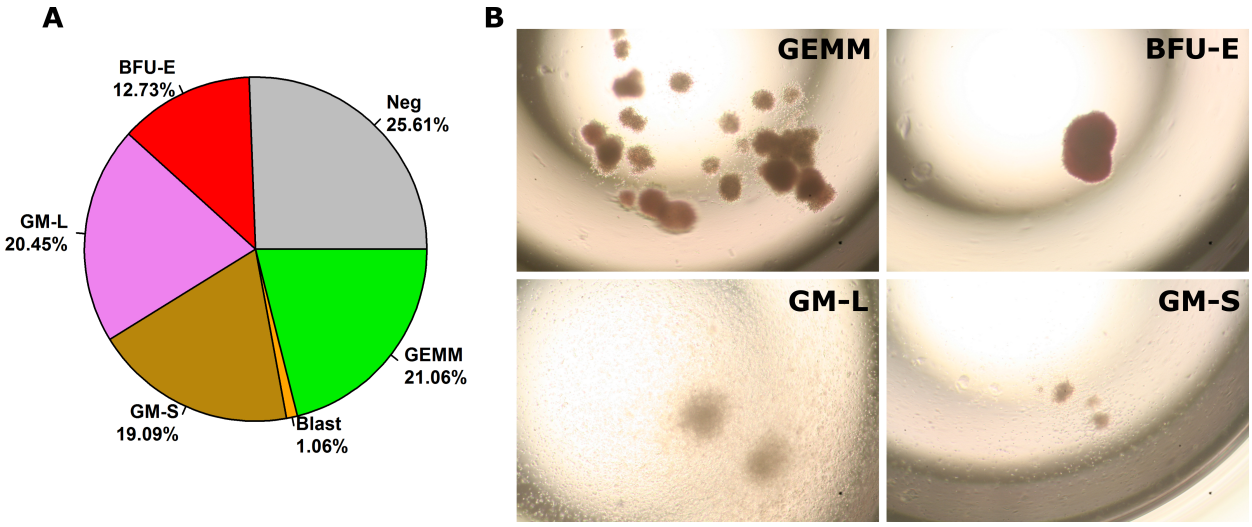


**Figure 4.9 Index sorted myeloid progenitor frequencies.** A) Frequency of myeloid progenitor colonies within $CD34^{+}$ observed following single cell index sorting. B) Example images of major colony types.

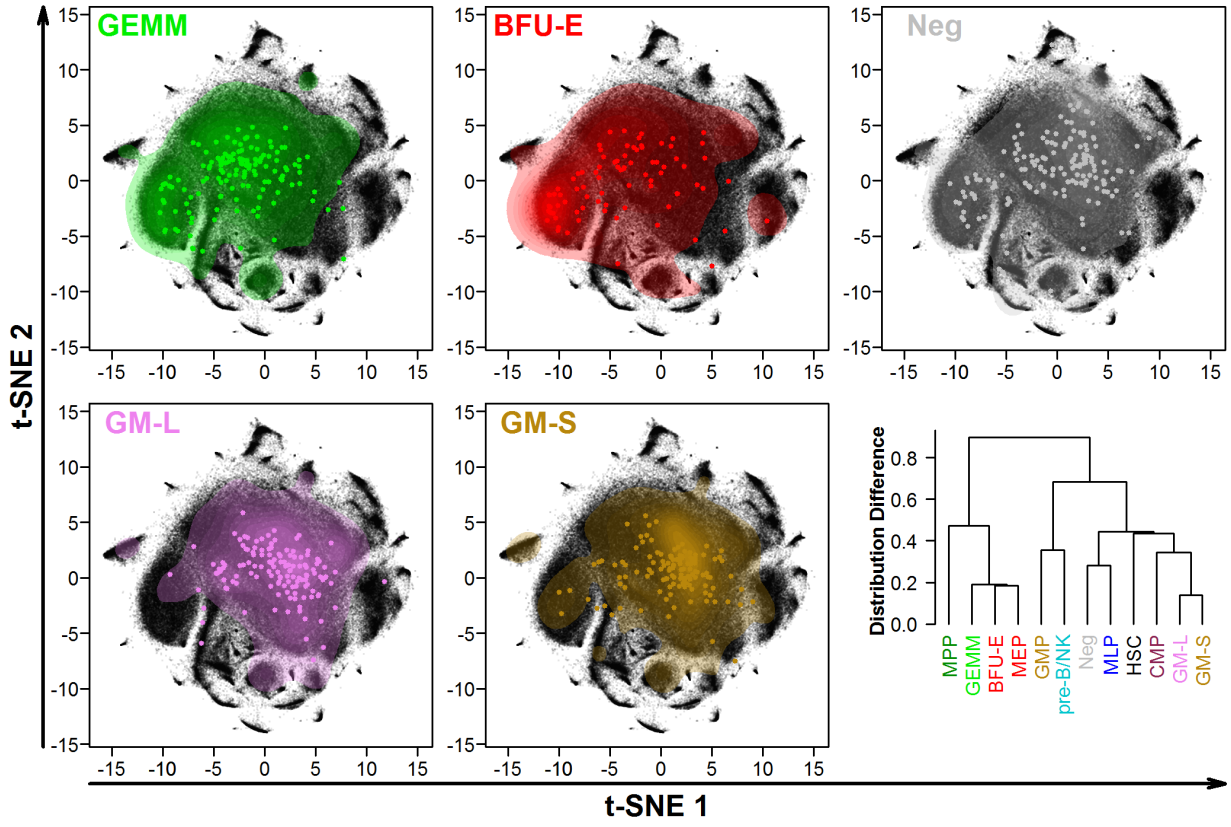


**Figure 4.10 Myeloid colony forming cell distribution in molecular space.** All CD34$^{+}$ cells analyzed by mass cytometry are shown as black points. The distribution of all nearest neighbours each given CFC type are shown as a translucent density. Estimated location of each CFC based on their 10 nearest neighbours are shown as points. Hierarchical clustering based on pair-wise differences in density distributions are shown for all CFC types as well as phenotypic progenitors.

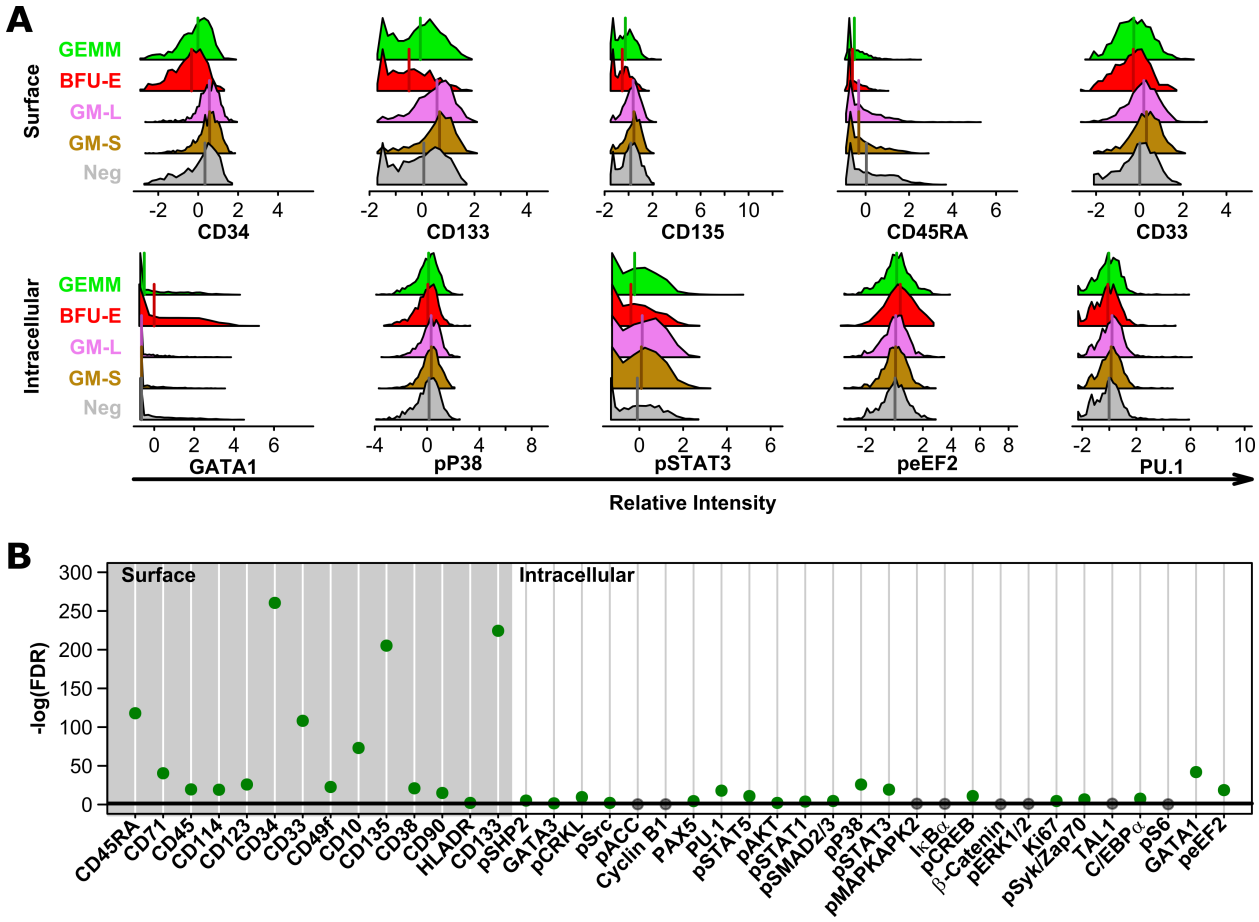


**Figure 4.11 Significant differences in surface and intracellular markers between myeloid colony forming cells.**

A) Relative marker intensities of the nearest neighbours for each myeloid CFC type. Median values are shown as lines. The top 5 most significant surface and intracellular differences are shown. B) Statistical differences between myeloid CFC expressed as $-\log_{10}$(FDR). Significant differences are shown as green circles. Non-significant differences are shown as grey circles.

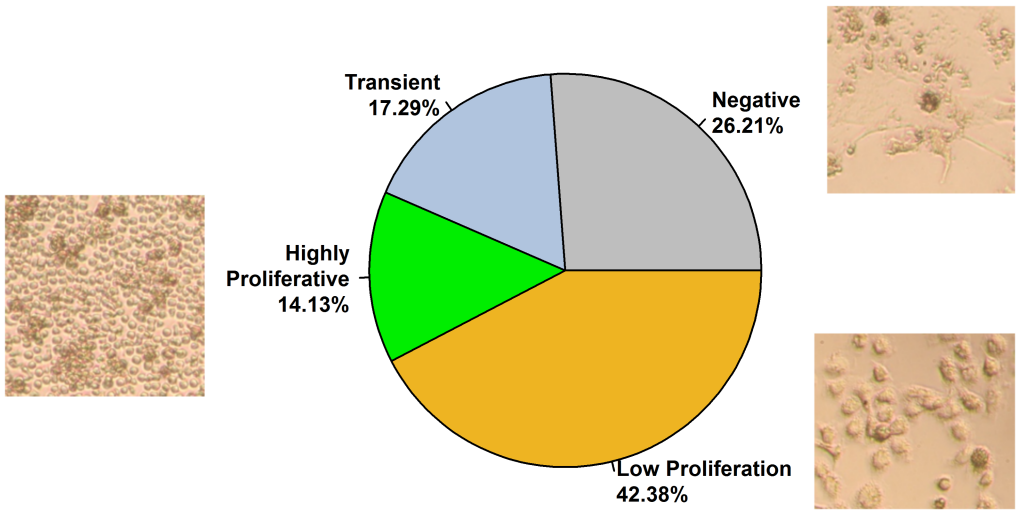


**Figure 4.12 Index sorted long-term culture initiating cell frequencies.** Frequency of LTC-IC within CD49f$^{+}$ cells observed following single cell index sorting. Example images are shown next to each type.

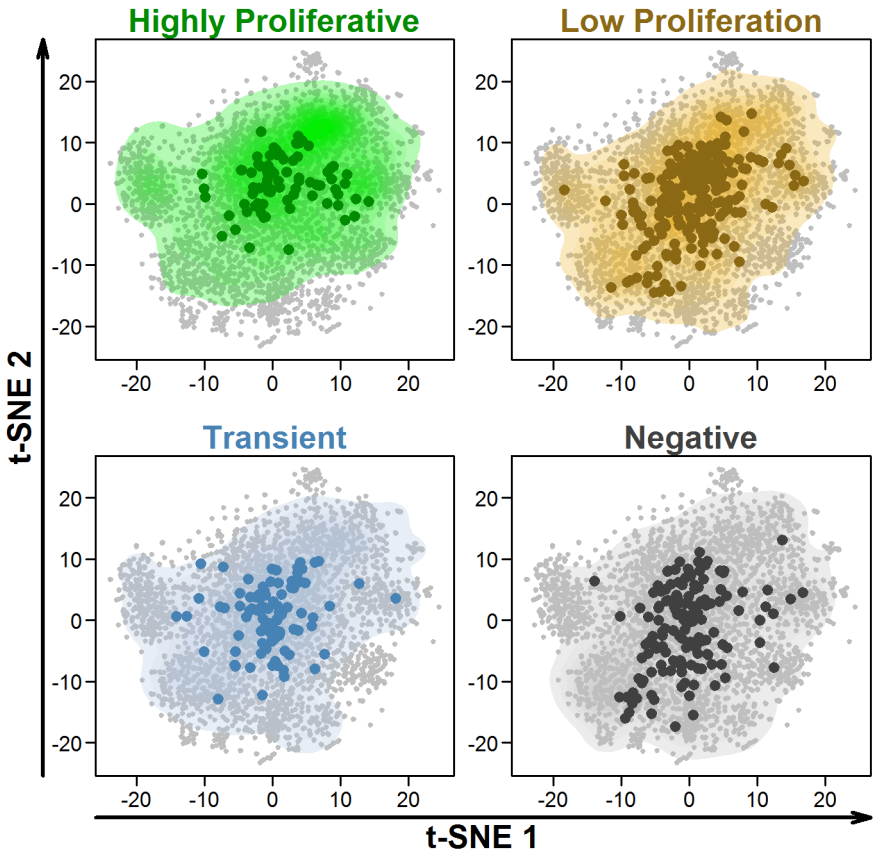


**Figure 4.13 Long-term culture initiating cell distribution in molecular space.** All CD49f$^{+}$ cells analyzed by mass cytometry are shown in light grey. The distribution of all nearest neighbours each given LTC-IC type are shown as a translucent density. Estimated location of each LTC-IC based on their 10 nearest neighbours are shown as points.

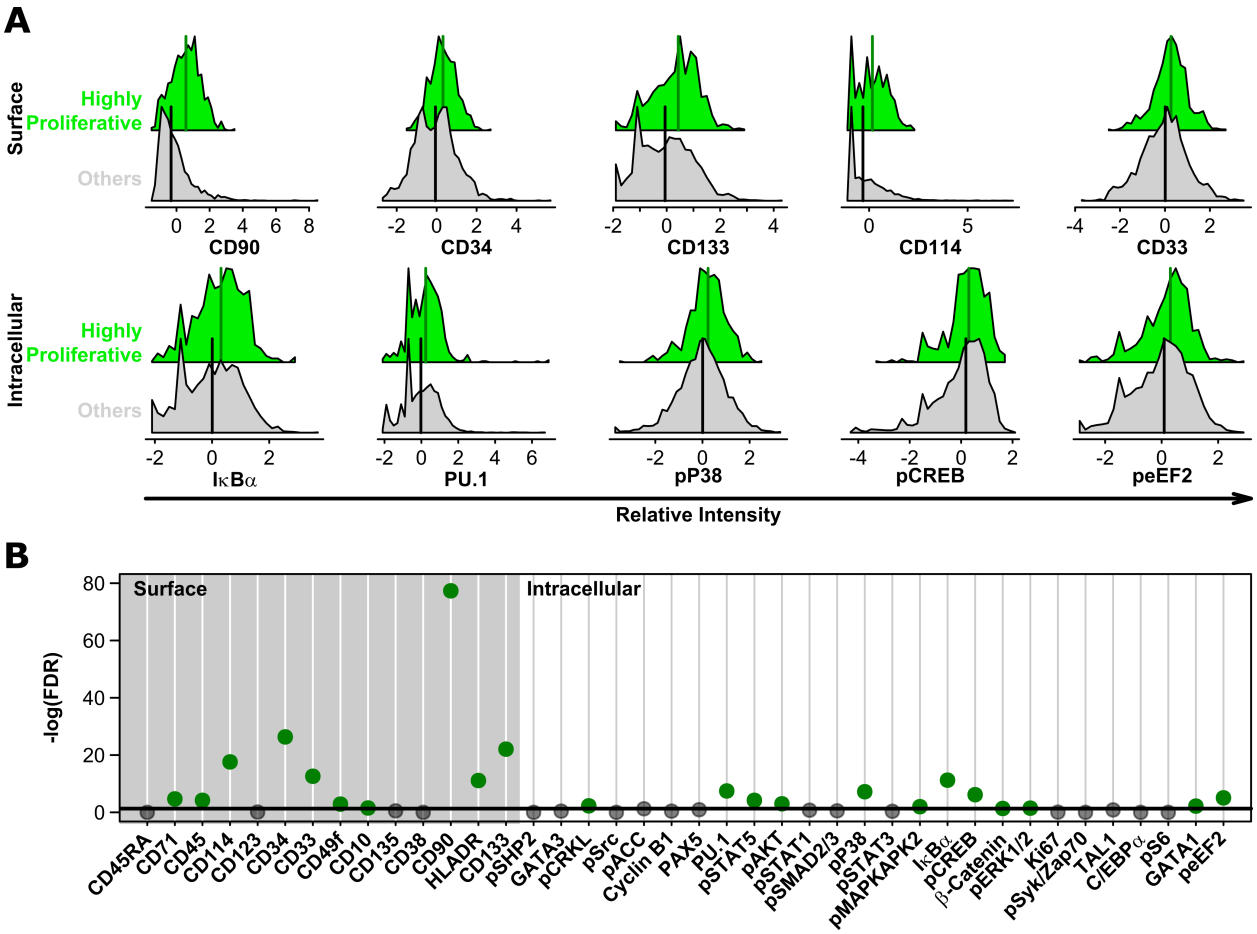


**Figure 4.14 Significant differences in surface and intracellular markers between highly proliferative long-term culture initiating cells and others.** A) Relative marker intensities of all nearest neighbours of highly proliferative LTC-IC or all other CD49f$^{+}$ cells measured by CyTOF. Median values are shown as lines. The top 5 most significant surface and intracellular differences are shown. B) Statistical differences expressed as -$\log_{10}$(FDR). Significant differences are shown as green circles. Non-significant differences are shown as grey circles.

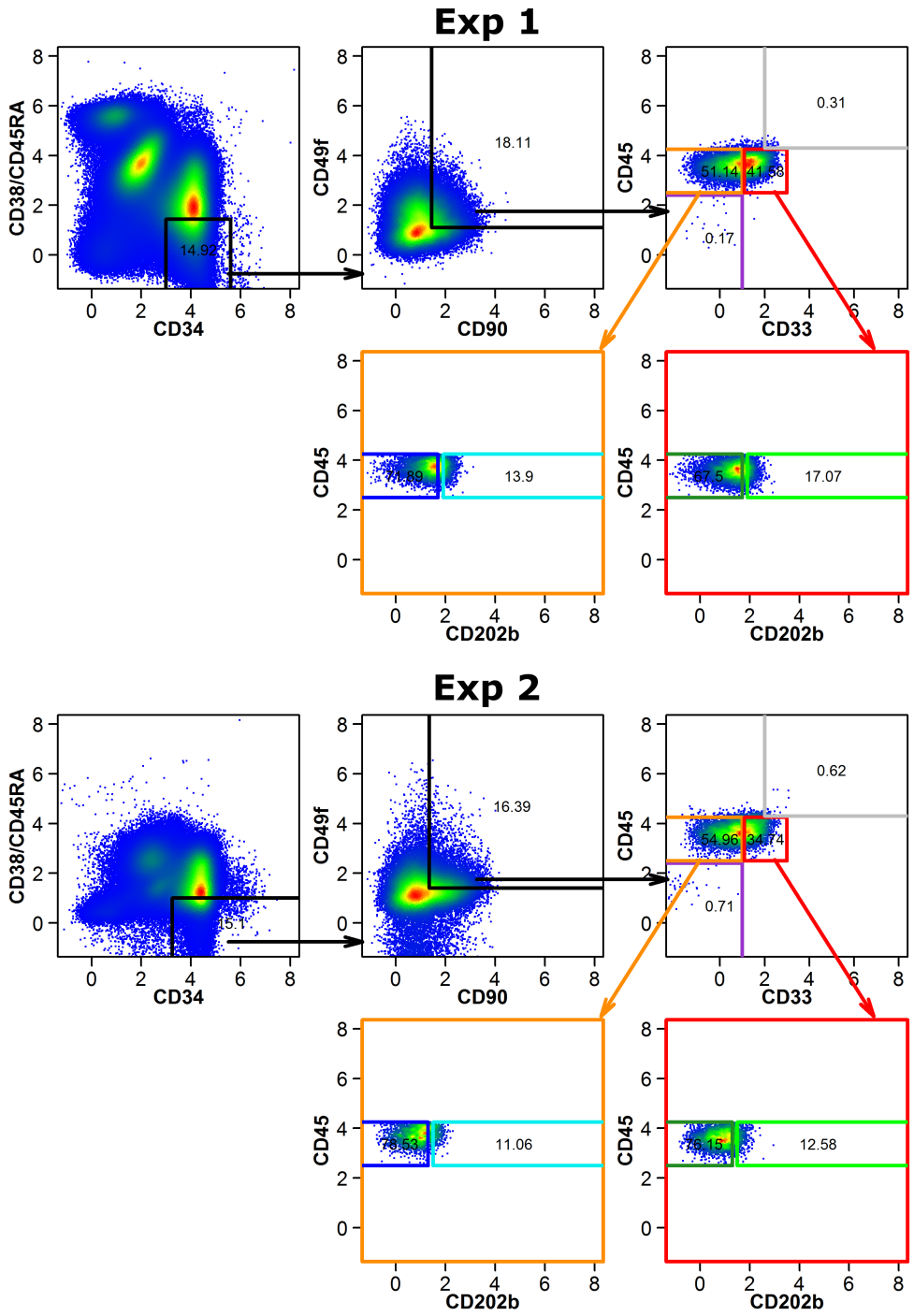


**Figure 4.15 Gating hierarchy for CD49f$^{+}$ subsets.**

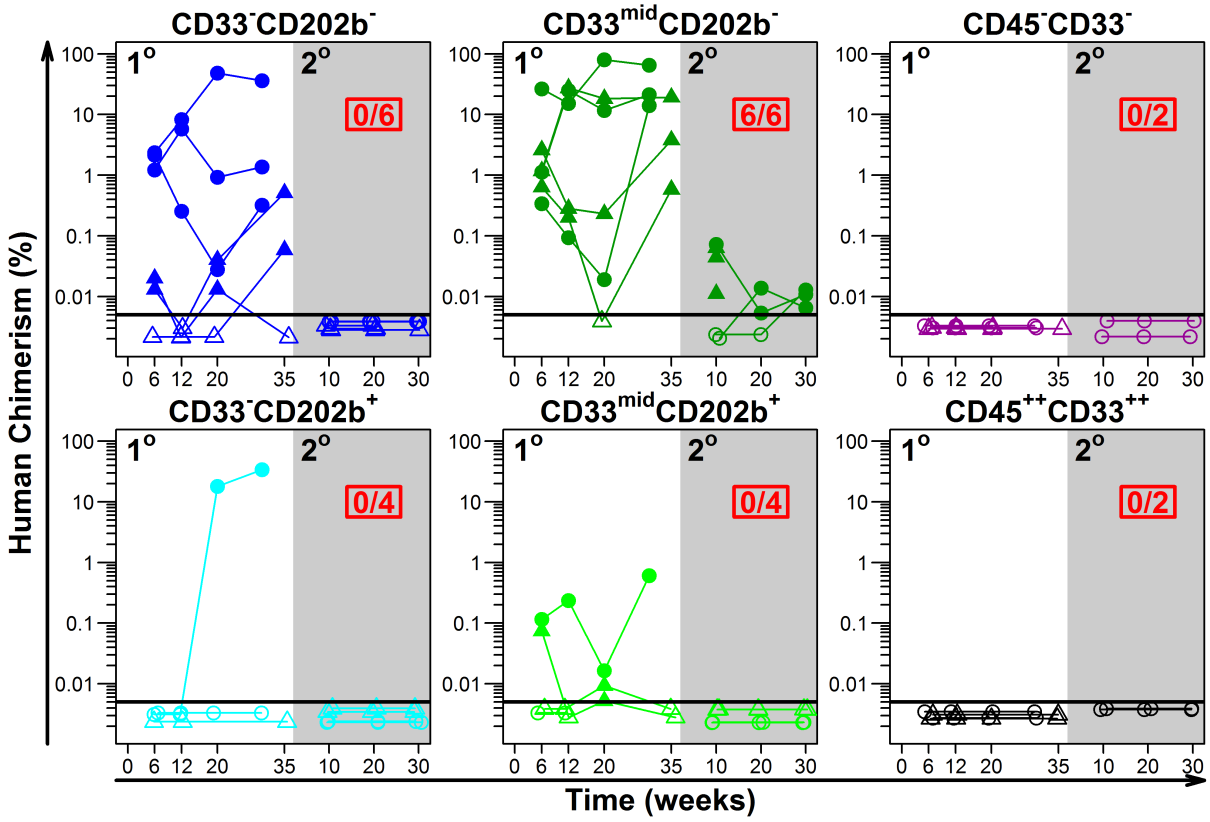


**Figure 4.16 Secondary repopulating activity is restricted to the CD33$^+$ sub-population of CD49f$^+$ cells.** Human chimerism levels are shown for each sub-fraction of CD34$^+$CD38$^-$CD45RA$^-$CD90$^+$CD49f$^+$. Mice from one experiment are shown as circles, while those from the other are shown as triangles. Threshold of detection is shown as a black line. Mice with chimerism below threshold of detection are shown as hollow points. Primary transplants are shown on a white background while secondary transplants are on a grey background. The number of secondary mice with above threshold of detection at any time point are highlighted in red.

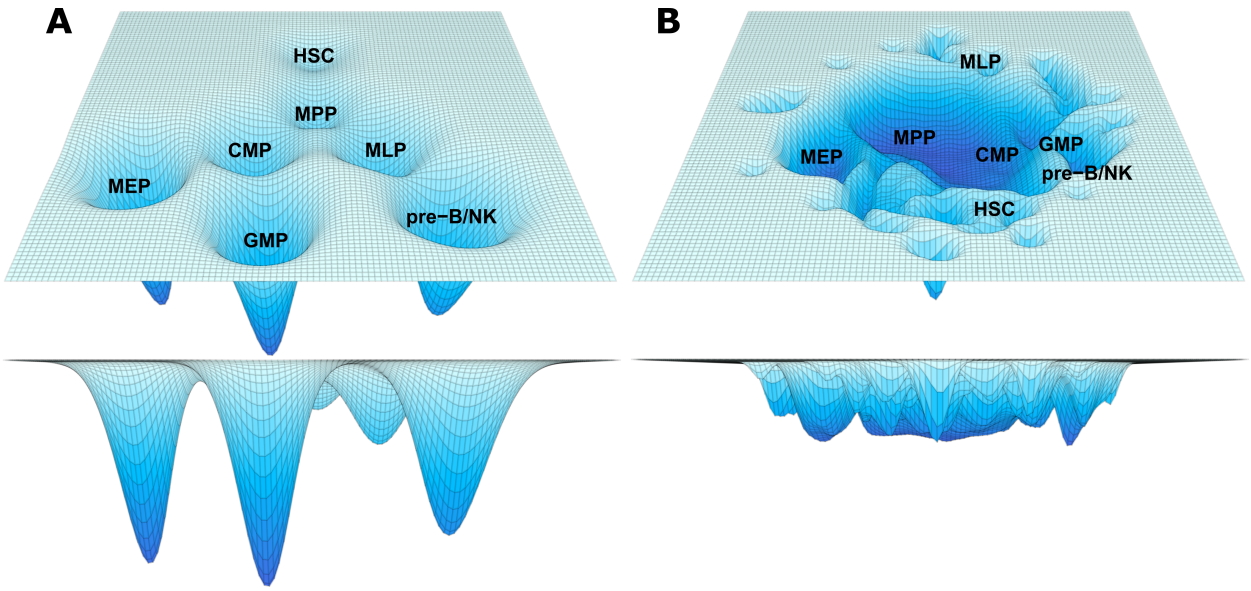


**Figure 4.17 Waddington landscapes of the human progenitor hierarchy.** A) A Waddington landscape of the hematopoietic progenitor hierarchy based on the classical model. Normal distributions were used to represent each population with relative numbers proportional to differentiation level. B) An estimation of the Waddington landscape of the hematopoietic progenitor hierarchy based on the observed data. The inverse of the cell density in t-SNE space was used to estimate the stability of different molecular states. Annotation was added based on phenotypic progenitor distributions. In both cases a top down view is shown above while a side view is shown below. Depths indicates relative stability.

# Chapter 5: Conclusions/implications/future directions and opportunities

## 5.1 Major contributions

The objective of this work was to elucidate the cellular and molecular programs involved in the control of specific HSC fate decisions. We have demonstrated that in both the human and the mouse, HSC survival, proliferation and maintenance of functional stem cell properties are controlled via distinct mechanisms. Further, we have defined new molecular relationships of cells with shared phenotypic and/or functional properties, identified additional surface markers thatmay aid in their future discrimination, and provided evidence that the molecular landscape of human hematopoietic progenitors is much flatter than previouslyanticipated.

Chapter 2 begins with work done together with Stefan Wohrer, wherein we investigated the differential regulation of mouse HSC survival, proliferation, and maintenance of HSC status. We begin by testing a number of different GF combinations which had previously been reported to allow HSC expansion (Audet et al., 2002; Huynh et al., 2008; Kent et al., 2008; Miller and Eaves, 1997; Oostendorp et al., 2002, 2005; Reya et al., 2003; Zhang et al., 2006a) using a more stringent definition of HSC than had been historically applied to this type of study. Using this approach, we were able to show that stromal support by the UG26-1B6 line is capable of maintaining durable HSC potential, and when combined with GFs that promote HSC proliferation resulted in an expansion of these HSCs with durable self-maintenance ability in vivo. By analyzing the individual progeny of split doublet HSCs, we obtained direct evidence that CM from the UG26 line together with GFs could promote symmetric self-renewal divisions of durable HSCs. Single-cell tracking showed that factors in UG26 CM were capable on their own of promoting HSC survival without stimulating their proliferation or loss of HSC functional

potential. In contrast, we found that SCF and IL11 could not fully maintain HSC status or survival, but stimulated the proliferation of every surviving HSC.

We next performed transcriptional analysis on ESLAM cells either fresh or following exposure to either SCF + IL11, UG26 CM alone, UG26 CM + SCF + IL11. By comparing the complement of receptors present in fresh ESLAM cells with the secreted proteins expressed in UG26-1B6, and cross-comparing that to pathways that were perturbed in the presence of UG26 CM, I identified a number of candidate GFs which could be responsible for the effects of UG26 CM. I then screened these candidates for their ability to promote ESLAM cell survival in the presence of SCF and IL11. This screen identified the combination of NGF and Col 1 as the most potent pro-survival factors, together mimicking the effects of the complete UG26 CM. Functional testing of these GFs then revealed that together they maintained durable HSC. Finally, I show that another combination of GFs are also capable of fully supporting the survival and proliferation of ESLAM cells, however, are not able to maintain durable HSC. Overall, these results combined to confirm, in the mouse, that HSC survival, proliferation, and stem cell status are regulated by mechanistically dissociable pathways.

In Chapter 3, I then describe the development of a culture strategy for maintaining *human* HSCs over an extended period in culture, and provide evidence that the survival, proliferation and maintenance of functional stem cell statusof  human HSC can likewise be dissociated. We also identifyied molecular intermediates that may mediate each of these GF-regulated programs. This involved initiating cultures with purified human $CD49f^{+}$ cells (~10% functional HSC; (Notta et al., 2011)), maintaining them in SFM plus a combination of 5 GFs (Zandstra et al., 1997) with periodic media addition and removal of mature cell outputs to minimize the output of inhibitory factors from an increasing concentration of mature cells (Csaszar et al 2012). Using

this strategy we were able to fully maintain input numbers of human HSCs over a 21-day period of culture despite massive concomitant outputs of mature cells. These results thus supercede reports that these same GFs induce a loss of human HSC activity within 9 days when less attention is given to the negative effects of co-produced mature cells (Bhatia et al., 1997). Given the beneficial effects of UG26 CM observed in Chapter 2 on mouse HSC expansion, we also tested the the effect of adding 50% UG26 CM to the 5 GFs in the human HSC expansion experiments. This resulted in a slight expansion of 20-week repopulating cell numbers, but no expansion of 12- or 30-week repopulating cells, and secondary repopulation was not detectable (albeit with lower starting cell equivalent doses compared with fresh or 5 GF cultured cells). The addition of UG26 CM to the 5 GFs thus did not provide the same substantial benefits as were observed in the mouse system.

Given that the 5GF combination had the ability to both maintain HSC functionality and induce their proliferation, we then sought to examine the roles of the component vs combined GFs on the survival and proliferation programs of human HSCs. Using powerful single-cell tracking techniques (Lecault et al., 2011), we found human HSC survival can be promoted by multiple GFs, but a combination is required to activate this program in every cell. We also found that induction of mitosis required exposure to at least 2 factors with SCF and IL3 showing the most potent combined activity. Surprisingly, assessment of the effects of these same GF combinations on maintenance of HSC repopulating ability over a 4-day period in culture showed little influence of GF response selectivity in contrast to the support of survival and proliferation. Together these results confirm that the regulation of human HSC survival, proliferation, and functional integrity, as for mouse HSC can be mechanistically dissociated.

Finally, I developed an antibody panel to assay the protein levels of >40 key surface and intracellular molecules in single cells via mass cytometry. We used this panel to analyze the signaling intermediates activated in cells exposed to each of the 5 GFs alone, or to all 5 in combination. This enabled members of the MAP kinase signaling cascade, together with STATs 3 and 5 to be identified as key immediate regulators of signaling that were activated by one or more GFs. Interestingly we also observed late-occurring effects including the suppression of apoptotic proteins and the activation of β-catenin (previously implicated in mouse HSC proliferation (Reya et al., 2003)) only in the 5 GF combination. Taken together, these findings suggest that the combinatorial effects of multiple GFs on the activation of survival and proliferation are mediated by a convergence of multiple, upstream signaling events.

In Chapter 4, I then attempted to re-examine the differentiation hierarchy found within human $CD34^+$ CB cells using an unbiased approach based on an assessment of 40 molecular parameters. This included the use of varying combinations of index sorting, high-throughput single-cell functional assays, and mass cytometry. With validated data processing, hematopoietic progenitors from independent donors showed remarkably reproducible molecular profiles. Population of different progenitors showed reproducibly distinct profiles, however, there was still a surprising degree of overlap between them. Moreover, this included the phenotype described as the HSC population, which, while relatively distinct from other subsets within the $CD34^+CD38^-$ population, was still found to strongly resemble many other more mature populations in its molecular state.

We further showed that all of the phenotypic populations were actually made up of more than one sub-population at a molecular level. In at least one case (the CMPs), the population appears to be a mixture of two different progenitor types which could then be separated using

additional surface markers. Within the CD49f$^{+}$ (HSC) compartment, we show that cells with primitive functional capacity have different levels of both a number of surface markers, as well as key molecular intermediates. Based on this result, we identify CD33, generally considered to be a marker of mature myeloid cells, as present on the most primitive HSCs with secondary repopulating capacity. Interestingly, the CD33$^{-}$ fraction also had robust primary repopulation, but lacked secondary activity at equivalent cell doses. This, together with the relative overlap in molecular profiles between progenitors, suggests that hematopoietic stem and progenitor function may actually be regulated by a surprisingly shallow molecular landscape.

## 5.2 Implications and future directions

### 5.2.1 The utility and limitations of surface phenotype in identification of cell populations

Surface markers have proven remarkably useful for isolating subsets of hematopoietic cells in a sterile and viable state so that their growth and differentiation responses to a variety of conditions can be defined. This, in turn, has led over the past 3 decades to the identification of phenotypes that are selectively enriched in progenitors that consistently display different proliferative, self-renewal and lineage output potentials (Akashi et al., 2000; Doulatov et al., 2010; Galy et al., 1995; Hao et al., 2001; Kent et al., 2009; Kondo et al., 1997; Manz et al., 2002; Morita et al., 2010; Notta et al., 2011; Osawa et al., 1996). The purities of the phenotypes obtained has prompted deep investigations of the molecular characteristics of many of these populations has and thereby helped contribute to our understanding of their functional properties (Chen et al., 2014; Lara-Astiaso et al., 2014; Laurenti et al., 2013; Notta et al., 2011; Petriv et al., 2010). In the present studies, some of the historically defined differential molecular characteristics of these phenotypes have been reproduced, confirming their utility.

One must be careful, however, as phenotypically defined populations are not functionally pure. In the mouse, HSCs defined by their repopulating activity in transplanted myelosuppressed recipients can now be enriched to a very high purity (Wilson et al., 2015). While significant advances have been made in the human system, the best purities achievable are still only ~10% for CB cells (Notta et al., 2011) (see also Chapter 3). As a result, any bulk measurement of this population will be dominated by other cells of unknown functional potential. Indeed, we have now provided formal evidence of marked heterogeneity in the molecular state of all currently accepted phenotypes of $CD34^+$ CB cells. In the case of human CMPs, we show that this phenotype appears to comprise 3 distinct subsets as inferred from their different molecular properties. One of these is suggestive of an erythroid progenitor and the other 2 are suggestive of granulopoietic progenitors, that could also be resolved by their differential expression of additional surface markers. Given this mixture of functional and molecular properties of the so-named CMPs, it is not surprising that bulk measurements applied to these would give them a a profile expected of cells with both functional capabilities. These findings highlight the importance of measuring molecular states in single cells.

By combining our molecular analysis with single cell functional assays, we were able to identify additional characteristics of the most primitive human HSC. Interestingly, cells with the most potent regenerative ability appear to be separable from those with still strong but not as potent capabilities by the use of CD33. The very similarity of these cells may allow deeper analyses of their molecular properties to identify some of the key regulators of normal human HSC regenerative capacity that have thus far remained elusive. The expression of CD33 on the surface of the most primitive normal human HSCs, also has implications for the treatment of human AML as originally proposed by Taussig *et al.* (Taussig et al., 2005). CD33-specific

antibodies have recently been used to target AML experimentally (Pizzitola et al., 2014) and clinically (Thol and Schlenk, 2014). While this approach appears to have clinical utility, significant toxicities have also been observed (Thol and Schlenk, 2014). Interestingly, these appear to be due to primarily to loss of platelets or infection, consistent with a toxic effect on the primitive normal HSCs that, based on mouse data, are closely related to the megakaryocyte lineage (Sanjuan-Pla et al., 2013).

### 5.2.2 Towards a molecular description of lineage restriction in primitive human hematopoietic cells

Understanding the critical molecular characteristics that determine the functional repertoire of primitive hematopoietic cells remains an outstanding goal. Historic models have invoked the concept of sequential rounds of bifurcation in which the character of one or more lineages is retained or reinforced and self-renewal and alternate lineage potentials are lost (Reya et al., 2001). According to this type of hierarchical model, each change defines a distinct (later) molecular state. While our data did associate unique molecular characteristics with different phenotypes that appear to support such a model, we also noted substantial overlap in the molecular distributions of all of these. If we assume that cells are more likely to reside in stable "attractor" molecular states (Enver et al., 2009), than in unstable states, the distribution of cells within a progenitor hierarchy can be used to infer the extent of barriers that exist between different populations and hence their interrelationships (Figure 4.17). Application of such an analysis to the $CD34^+$ CB cells assessed here showed a much flatter landscape than the discrete stages anticipated from historic models.

The relatively low barriers observed between cell populations suggests that they may be amenable to change their functional properties given an appropriate manipulation, including the recovery of durable self-renewal potential. Indeed, our observation in Chapter 2 that the frequency of ESLAM cells capable of repopulating recipient animals can be increased simply by pre-culture in the correct conditions supports this prediction. The published evidence of an ability of NA10hd expression in mouse cells that do not possess innate HSC activity to acquire it (Sekulovic et al., 2011) serves as an even stronger demonstration that HSC properties can be regained by at least a portion of closely related cells. Given the ability of a hand full of TFs to fully reprogram even mature blood cells to an embryonic state (Riddell et al., 2014; Takahashi and Yamanaka, 2006), induced plasticity between closely related hematopoietic progenitors seems even more plausible. While exciting, this possibility is also troubling. How does one now define a cell if it can change its properties from one minute to the next? There are also substantial implications to understanding the relevance of cell-of-origin questions in human leukemia. Low molecular barriers between cell types with normal distinct functional properties raises the question of whether leukemogenic mutations may also change the functional state of a given cell much more readily than previously anticipated. Going forward, both of these issues merit deeper thought and careful investigation.

### 5.2.3 Implications for *ex vivo* human HSC expansion

Expansion of human HSCs for clinical purposes has also been a major goal in the field for many years. Interestingly, early clinical trials of bulk CB cells expanded in culture with many of the same GFs as investigated here (see Chapter 3) conferred no clinical benefit (McNiece et al., 2000; Shpall et al., 2002). By contrast, in another trial in which a crude progenitor

enrichment was performed prior to culture, some improvement in time to engraftment was reported (De Lima et al., 2008). These findings support the idea that mature cells may negatively impact HSC expansion (Csaszar et al., 2012). The culture strategy used in Chapter 3 that allowed maintenance of long-term HSC activity represents an even more extreme version of this idea.

In an interesting corollary, clinical trials that have tested of the outputs of crudely enriched $CD34^+$ cells cultured with GFs together with the small molecules SR1 or nicotinamide and final co-injection of minimally manipulated T cells or $CD34^-$ cells have shown somewhat more success (Horwitz et al., 2014; Wagner et al., 2014). In both of these cases, time to engraftment was improved, and longer-term engraftment by the cultured cells was observed (Horwitz et al., 2014; Wagner et al., 2014). These results suggests that in a clinical setting where multiple cords are present, a functioning T-cell component may be necessary to allow long-term cells to compete effectively with un-manipulated cord units.

Co-culture with stromal cells has also been attempted in a clinical setting. This showed benefits to early engraftment with late failure of the expanded cord (de Lima et al., 2012), suggesting that the cultures expanded cells with rapid but transient regenerative activity at the expense of long-term HSCs. This is interesting given the efficacy of the stromal UG26 line in maintaining long-term mouse HSC that we observed here (see Chapter 2). The stromal line used in our study was, however, carefully selected for its ability to promote the maintenance of long-term mouse HSC *in vitro* (Oostendorp et al., 2002, 2005). Thus the less promising results obtained clinically may reflect the possibility that not all stromal cell types will be useful. Defined factors and culture conditions would thus be substantially preferable.

Despite progress made in supporting self-renewal divisions of human HSC *in vitro*, a robust and high yield method still remains out of reach. Over-expression of NA10hd in the

mouse has demonstrated that highly efficient *in vitro* expansion of HSCs from that species is possible, with values nearing the theoretical limit based on the likely number of cell divisions executed (Ohta et al., 2007). Cognate effects on human cells even of this method, however, have been decidedly more modest (Sloma et al., 2013). To date, the best examples of human HSC expansion have been achieved using the small molecules SR1 or UM171 together with GFs (Boitano et al., 2010; Fares et al., 2014). Even these reports, however, assuming the xenograft models used for measurement truly reflect long-term HSCs show only 10-20 fold increases (Boitano et al., 2010; Fares et al., 2014). When compared to the near infinite expansion possible from ES/iPS cells, or even the expansion achievable in mouse HSCs using NA10hd, the results obtained to date with human cells pale in comparison. The question thus remains; why has human HSC expansion been so difficult to achieve?

There are a number of possible contributing factors for this. Most researchers use a few months *in vivo* as a surrogate for HSC potential. While this may be sufficient to separate cells with very short-term outputs from those able to produce mature blood cells for several months, even in the mouse, this latter definition is now being recognized as insufficient to identify HSCs with durable self-renewal ability as revealed in serial transplant experiments (Benveniste et al., 2010; Benz et al., 2012; Dykstra et al., 2007; Yamamoto et al., 2013). Mounting evidence from both human trials and monkey models suggests that the outputs of human HSCs don't stabilize until  more than a year post transplant (Aiuti et al. Science. 2013; Biffi et al. Nature. 2013; Kim et al. Cell Stem Cell. 2014). Our results in Chapter 4 are also consistent with this time frame. As a result, the vast majority of the literature claiming effects on human "HSCs" may not actually reflect effects on the cells of interest.

To make matters worse, human cells with short, intermediate, and long-term repopulation capabilities likely have different regulation and growth requirements. Clinical trials showing accelerated time to repopulation but loss of expanded cell chimerism later on (often at or beyond one year) poignantly illustrate this (Delaney et al., 2010; de Lima et al., 2012). This principle can be seen even in short-term experimental models, as the GF requirements for CFC expansion and LTC-IC expansion are different (Petzer et al., 1996a; Zandstra et al., 1997). A truly intriguing corollary of this is the disconnect between what constitutes 'expansion' as defined in clinical trials and what researchers are striving for in terms of HSC expansion. In clinical trials to date, the primary goal appears to be accelerated engraftment of neutrophils and platelets following transplant; both of which are likely primarily dependent on the numbers of cells with short term repopulating ability that are transplanted. Indeed, the design of many trials doesn't even allow long-term repopulation by the expanded cells to be assessed (de Lima et al., 2008; McNiece et al., 2000; Shpall et al., 2002).

Our findings that survival, proliferation, and maintenance of HSC status can be independently regulated offer an alternative method to developing HSC expansion strategies. The disconnect between survival, proliferation, and maintenance of HSC capabilities means that each of these properties might be independently optimized. If this could be combined with a molecular definition of cell state, such as we begun to investigate in Chapter 4, it would allow rapid rounds of parameter optimization with specific and clear endpoints. In this way a truly rational expansion strategy with a solid mechanistic base might be devised.

## 5.3 Concluding remarks

There are clearly many hurdles to overcome before an understanding of human HSC regulation sufficient to allow clinically useful expansion of these cells is within sight. However, progress in this area will undoubtedly be facilitated by the combined use of an increasing array of tools that enable single-cell measurements to be made and analyzed. The work presented in this thesis identifies some of the key biological programs underpinning HSC expansion that can be regulated independently, and begins to identify the molecular states of varying cell populations and the barriers between them.

We anticipate that future work to more fully define the molecular characteristics of single cells across the differentiation process will be of significant value. In addition, we need to understand how stable each of key properties are to perturbations such as those created by GF exposure in order to reliably use them as an endpoint for HSC functionality. It will also be of substantial interest to learn how to directly activate specific signaling pathways that are associated with survival, mitogenesis, self-renewal and lineage control in order to further dissect out the minimal required activation criteria and potentially improve activation efficiency. It is clear, however, that a deeper understanding of the fundamental cellular and molecular characteristics of HSCs will be a necessary foundation for transformative expansion strategies.

## Bibliography


Adolfsson, J., Månsson, R., Buza-Vidas, N., Hultquist, A., Liuba, K., Jensen, C.T., Bryder, D., Yang, L., Borge, O.-J., Thoren, L.A.M., et al. (2005). Identification of Flt3+ Lympho-Myeloid Stem Cells Lacking Erythro-Megakaryocytic Potential: A Revised Road Map for Adult Blood Lineage Commitment. Cell *121*, 295–306.

Aiuti, A., Biasco, L., Scaramuzza, S., Ferrua, F., Cicalese, M.P., Baricordi, C., Dionisio, F., Calabria, A., Giannelli, S., Castiello, M.C., et al. (2013). Lentiviral Hematopoietic Stem Cell Gene Therapy in Patients with Wiskott-Aldrich Syndrome. Science *341*, 1233151.

Akashi, K., Traver, D., Miyamoto, T., and Weissman, I.L. (2000). A clonogenic common myeloid progenitor that gives rise to all myeloid lineages. Nature *404*, 193–197.

Allsopp, R.C., Morin, G.B., DePinho, R., Harley, C.B., and Weissman, I.L. (2003). Telomerase is required to slow telomere shortening and extend replicative lifespan of HSCs during serial transplantation. Blood *102*, 517–520.

Amir, E.D., Davis, K.L., Tadmor, M.D., Simonds, E.F., Levine, J.H., Bendall, S.C., Shenfeld, D.K., Krishnaswamy, S., Nolan, G.P., and Pe'er, D. (2013). viSNE enables visualization of high dimensional single-cell data and reveals phenotypic heterogeneity of leukemia. Nat. Biotechnol. *31*, 545–552.

Antonchuk, J., Sauvageau, G., and Humphries, R.K. (2002). HOXB4-induced expansion of adult hematopoietic stem cells ex vivo. Cell *109*, 39–45.

Appelbaum, F.R., Forman, S.J., Negrin, R.S., and Blume, K.G. (2011). Thomas' Hematopoietic Cell Transplantation (John Wiley & Sons).

Audet, J., Miller, C.L., Eaves, C.J., and Piret, J.M. (2002). Common and distinct features of cytokine effects on hematopoietic stem and progenitor cells revealed by dose-response surface analysis. Biotechnol. Bioeng. *80*, 393–404.

Babovic, S., and Eaves, C.J. (2014). Hierarchical organization of fetal and adult hematopoietic stem cells. Exp. Cell Res. *329*, 185–191.

Bach, F., Albertini, R., Joo, P., Anderson, J., and Bortin, M. (1968). BONE-MARROW TRANSPLANTATION IN A PATIENT WITH THE WISKOTT-ALDRICH SYNDROME. The Lancet *292*, 1364–1366.

Bandura, D.R., Baranov, V.I., Ornatsky, O.I., Antonov, A., Kinach, R., Lou, X., Pavlov, S., Vorobiev, S., Dick, J.E., and Tanner, S.D. (2009). Mass cytometry: technique for real time single cell multitarget immunoassay based on inductively coupled plasma time-of-flight mass spectrometry. Anal. Chem. *81*, 6813–6822.

Bass, D.A., Parce, J.W., Dechatelet, L.R., Szejda, P., Seeds, M.C., and Thomas, M. (1983). Flow cytometric studies of oxidative product formation by neutrophils: a graded response to membrane stimulation. J. Immunol. Baltim. Md 1950 *130*, 1910–1917.

Baudet, A., Karlsson, C., Talkhoncheh, M.S., Galeev, R., Magnusson, M., and Larsson, J. (2012). RNAi screen identifies MAPK14 as a druggable suppressor of human hematopoietic stem cell expansion. Blood *119*, 6255–6258.

Becker, A.J., McCULLOCH, E.A., and Till, J.E. (1963). Cytological demonstration of the clonal nature of spleen colonies derived from transplanted mouse marrow cells. Nature *197*, 452–454.

Becker, A.J., Mcculloch, E.A., Siminovitch, L., and Till, J.E. (1965). The Effect of Differing Demands for Blood Cell Production on DNA Synthesis by Hemopoietic Colony-Forming Cells of Mice. Blood *26*, 296–308.

Behbehani, G.K., Bendall, S.C., Clutter, M.R., Fantl, W.J., and Nolan, G.P. (2012). Single-cell mass cytometry adapted to measurements of the cell cycle. Cytom. Part J. Int. Soc. Anal. Cytol. *81*, 552–566.

Behbehani, G.K., Thom, C., Zunder, E.R., Finck, R., Gaudilliere, B., Fragiadakis, G.K., Fantl, W.J., and Nolan, G.P. (2014). Transient partial permeabilization with saponin enables cellular barcoding prior to surface marker staining. Cytom. Part J. Int. Soc. Anal. Cytol. *85*, 1011–1019.

Bell, J.J., and Bhandoola, A. (2008). The earliest thymic progenitors for T cells possess myeloid lineage potential. Nature *452*, 764–767.

Bendall, S.C., Simonds, E.F., Qiu, P., Amir, E.D., Krutzik, P.O., Finck, R., Bruggner, R.V., Melamed, R., Trejo, A., Ornatsky, O.I., et al. (2011a). Single-Cell Mass Cytometry of Differential Immune and Drug Responses Across a Human Hematopoietic Continuum. Science *332*, 687–696.

Bendall, S.C., Simonds, E.F., Qiu, P., Amir, E.D., Krutzik, P.O., Finck, R., Bruggner, R.V., Melamed, R., Trejo, A., Ornatsky, O.I., et al. (2011b). Single-cell mass cytometry of differential immune and drug responses across a human hematopoietic continuum. Science *332*, 687–696.

Bendall, S.C., Nolan, G.P., Roederer, M., and Chattopadhyay, P.K. (2012). A deep profiler's guide to cytometry. Trends Immunol. *33*, 323–332.

Bendall, S.C., Davis, K.L., Amir, E.-A.D., Tadmor, M.D., Simonds, E.F., Chen, T.J., Shenfeld, D.K., Nolan, G.P., and Pe'er, D. (2014). Single-cell trajectory detection uncovers progression and regulatory coordination in human B cell development. Cell *157*, 714–725.

Benveniste, P., Frelin, C., Janmohamed, S., Barbara, M., Herrington, R., Hyam, D., and Iscove, N.N. (2010). Intermediate-Term Hematopoietic Stem Cells with Extended but Time-Limited Reconstitution Potential. Cell Stem Cell *6*, 48–58.

Benz, C., Copley, M.R., Kent, D.G., Wohrer, S., Cortes, A., Aghaeepour, N., Ma, E., Mader, H., Rowe, K., Day, C., et al. (2012). Hematopoietic Stem Cell Subtypes Expand Differentially during Development and Display Distinct Lymphopoietic Programs. Cell Stem Cell *10*, 273–283.

Bhatia, M., Bonnet, D., Kapp, U., Wang, J.C., Murdoch, B., and Dick, J.E. (1997). Quantitative analysis reveals expansion of human hematopoietic repopulating cells after short-term ex vivo culture. J. Exp. Med. *186*, 619–624.

Biffi, A., Montini, E., Lorioli, L., Cesani, M., Fumagalli, F., Plati, T., Baldoli, C., Martino, S., Calabria, A., Canale, S., et al. (2013). Lentiviral Hematopoietic Stem Cell Gene Therapy Benefits Metachromatic Leukodystrophy. Science *341*, 1233158.

Blasco, M.A. (2005). Telomeres and human disease: ageing, cancer and beyond. Nat. Rev. Genet. *6*, 611–622.

Bodenmiller, B., Zunder, E.R., Finck, R., Chen, T.J., Savig, E.S., Bruggner, R.V., Simonds, E.F., Bendall, S.C., Sachs, K., Krutzik, P.O., et al. (2012). Multiplexed mass cytometry profiling of cellular states perturbed by small-molecule regulators. Nat. Biotechnol. *30*, 858–867.

Boitano, A.E., Wang, J., Romeo, R., Bouchez, L.C., Parker, A.E., Sutton, S.E., Walker, J.R., Flaveny, C.A., Perdew, G.H., Denison, M.S., et al. (2010). Aryl Hydrocarbon Receptor Antagonists Promote the Expansion of Human Hematopoietic Stem Cells. Science *329*, 1345–1348.

Bonnet, D., Lemoine, F.M., Najman, A., and Guigon, M. (1995). Comparison of the inhibitory effect of AcSDKP, TNF-alpha, TGF-beta, and MIP-1 alpha on marrow-purified CD34+ progenitors. Exp. Hematol. *23*, 551–556.

Bortin, M.M. (1970). A compendium of reported human bone marrow transplants. Transplantation *9*, 571–587.

Bowie, M.B., McKnight, K.D., Kent, D.G., McCaffrey, L., Hoodless, P.A., and Eaves, C.J. (2006). Hematopoietic stem cells proliferate until after birth and show a reversible phase-specific engraftment defect. J. Clin. Invest. *116*, 2808–2816.

Bowie, M.B., Kent, D.G., Dykstra, B., McKnight, K.D., McCaffrey, L., Hoodless, P.A., and Eaves, C.J. (2007a). Identification of a new intrinsically timed developmental checkpoint that reprograms key hematopoietic stem cell properties. Proc. Natl. Acad. Sci. U. S. A. *104*, 5878–5882.

Bowie, M.B., Kent, D.G., Copley, M.R., and Eaves, C.J. (2007b). Steel factor responsiveness regulates the high self-renewal phenotype of fetal hematopoietic stem cells. Blood *109*, 5043–5048.

Bradley, T.R., and Metcalf, D. (1966). The growth of mouse bone marrow cells in vitro. Immunol. Cell Biol. *44*, 287–300.

Bröske, A.-M., Vockentanz, L., Kharazi, S., Huska, M.R., Mancini, E., Scheller, M., Kuhl, C., Enns, A., Prinz, M., Jaenisch, R., et al. (2009). DNA methylation protects hematopoietic stem cell multipotency from myeloerythroid restriction. Nat. Genet. *41*, 1207–1215.

Browne, G.J., and Proud, C.G. (2002). Regulation of peptide-chain elongation in mammalian cells. Eur. J. Biochem. FEBS *269*, 5360–5368.

Broxmeyer, H.E., Douglas, G.W., Hangoc, G., Cooper, S., Bard, J., English, D., Arny, M., Thomas, L., and Boyse, E.A. (1989). Human umbilical cord blood as a potential source of transplantable hematopoietic stem/progenitor cells. Proc. Natl. Acad. Sci. U. S. A. *86*, 3828–3832.

Bruce, W.R., Meeker, B.E., and Valeriote, F.A. (1966). Comparison of the Sensitivity of Normal Hematopoietic and Transplanted Lymphoma Colony-Forming Cells to Chemotherapeutic Agents Administered In Vivo. J. Natl. Cancer Inst. *37*, 233–245.

Buckner, C.D., Epstein, R.B., Rudolph, R.H., Clift, R.A., Storb, R., and Thomas, E.D. (1970). Allogeneic Marrow Engraftment Following Whole Body Irradiation in a Patient with Leukemia. Blood *35*, 741–750.

Busch, K., Klapproth, K., Barile, M., Flossdorf, M., Holland-Letz, T., Schlenner, S.M., Reth, M., Höfer, T., and Rodewald, H.-R. (2015). Fundamental properties of unperturbed haematopoiesis from stem cells in vivo. Nature *518*, 542–546.

Buske, C., Feuring-Buske, M., Abramovich, C., Spiekermann, K., Eaves, C.J., Coulombel, L., Sauvageau, G., Hogge, D.E., and Humphries, R.K. (2002). Deregulated expression of HOXB4 enhances the primitive growth activity of human hematopoietic cells. Blood *100*, 862–868.

Bystrykh, L.V., de Haan, G., and Verovskaya, E. (2014). Barcoded vector libraries and retroviral or lentiviral barcoding of hematopoietic stem cells. Methods Mol. Biol. Clifton NJ *1185*, 345–360.

Campbell, V., Legendre, P., and Lapointe, F.-J. (2011). The performance of the Congruence Among Distance Matrices (CADM) test in phylogenetic analysis. BMC Evol. Biol. *11*, 64.

Cartier, N., Hacein-Bey-Abina, S., Bartholomae, C.C., Veres, G., Schmidt, M., Kutschera, I., Vidaud, M., Abel, U., Dal-Cortivo, L., Caccavelli, L., et al. (2009). Hematopoietic Stem Cell Gene Therapy with a Lentiviral Vector in X-Linked Adrenoleukodystrophy. Science *326*, 818–823.

Cashman, J.D., and Eaves, C.J. (1999). Human Growth Factor–Enhanced Regeneration of Transplantable Human Hematopoietic Stem Cells in Nonobese Diabetic/Severe Combined Immunodeficient Mice. Blood *93*, 481–487.

Cashman, J., Dykstra, B., Clark-Lewis, I., Eaves, A., and Eaves, C. (2002). Changes in the Proliferative Activity of Human Hematopoietic Stem Cells in NOD/SCID Mice and

Enhancement of Their Transplantability after In Vivo Treatment with Cell Cycle Inhibitors. J. Exp. Med. *196*, 1141–1150.

Cashman, J.D., Eaves, A.C., Raines, E.W., Ross, R., and Eaves, C.J. (1990). Mechanisms that regulate the cell cycle status of very primitive hematopoietic cells in long-term human marrow cultures. I. Stimulatory role of a variety of mesenchymal cell activators and inhibitory role of TGF-beta. Blood *75*, 96–101.

Cashman, J.D., Lapidot, T., Wang, J.C.Y., Doedens, M., Shultz, L.D., Lansdorp, P., Dick, J.E., and Eaves, C.J. (1997). Kinetic Evidence of the Regeneration of Multilineage Hematopoiesis From Primitive Cells in Normal Human Bone Marrow Transplanted Into Immunodeficient Mice. Blood *89*, 4307–4316.

Cashman, J.D., Eaves, C.J., Sarris, A.H., and Eaves, A.C. (1998). MCP-1, not MIP-1alpha, is the endogenous chemokine that cooperates with TGF-beta to inhibit the cycling of primitive normal but not leukemic (CML) progenitors in long-term human marrow cultures. Blood *92*, 2338–2344.

Cavazzana-Calvo, M., Payen, E., Negre, O., Wang, G., Hehir, K., Fusil, F., Down, J., Denaro, M., Brady, T., Westerman, K., et al. (2010). Transfusion independence and HMGA2 activation after gene therapy of human β-thalassaemia. Nature *467*, 318–322.

Celebi, B., Mantovani, D., and Pineault, N. (2011). Effects of extracellular matrix proteins on the growth of haematopoietic progenitor cells. Biomed. Mater. Bristol Engl. *6*, 055011.

Challen, G.A., Boles, N.C., Chambers, S.M., and Goodell, M.A. (2010). Distinct hematopoietic stem cell subtypes are differentially regulated by TGF-beta1. Cell Stem Cell *6*, 265–278.

Chen, L., Kostadima, M., Martens, J.H.A., Canu, G., Garcia, S.P., Turro, E., Downes, K., Macaulay, I.C., Bielczyk-Maczynska, E., Coe, S., et al. (2014). Transcriptional diversity during lineage commitment of human blood progenitors. Science *345*, 1251033.

Chen, M.J., Yokomizo, T., Zeigler, B.M., Dzierzak, E., and Speck, N.A. (2009). Runx1 is required for the endothelial to haematopoietic cell transition but not thereafter. Nature *457*, 887–891.

Chen, X., Skutt-Kakaria, K., Davison, J., Ou, Y.-L., Choi, E., Malik, P., Loeb, K., Wood, B., Georges, G., Torok-Storb, B., et al. (2012). G9a/GLP-dependent histone H3K9me2 patterning during human hematopoietic stem cell lineage commitment. Genes Dev. *26*, 2499–2511.

Cheung, A.M.S., Leung, D., Rostamirad, S., Dhillon, K., Miller, P.H., Droumeva, R., Brinkman, R.R., Hogge, D., Roy, D.C., and Eaves, C.J. (2012). Distinct but phenotypically heterogeneous human cell populations produce rapid recovery of platelets and neutrophils after transplantation. Blood *119*, 3431–3439.

Cheung, A.M.S., Nguyen, L.V., Carles, A., Beer, P., Miller, P.H., Knapp, D.J.H.F., Dhillon, K., Hirst, M., and Eaves, C.J. (2013). Analysis of the clonal growth and differentiation dynamics of primitive barcoded human cord blood cells in NSG mice. Blood *122*, 3129–3137.

Christianson, S.W., Greiner, D.L., Hesselton, R.A., Leif, J.H., Wagar, E.J., Schweitzer, I.B., Rajan, T.V., Gott, B., Roopenian, D.C., and Shultz, L.D. (1997). Enhanced human CD4+ T cell engraftment in beta2-microglobulin-deficient NOD-scid mice. J. Immunol. *158*, 3578–3586.

Ciau-Uitz, A., Monteiro, R., Kirmizitas, A., and Patient, R. (2014). Developmental hematopoiesis: ontogeny, genetic programming and conservation. Exp. Hematol. *42*, 669–683.

Colvin, G.A., Lambert, J.-F., Abedi, M., Hsieh, C.-C., Carlson, J.E., Stewart, F.M., and Quesenberry, P.J. (2004). Murine marrow cellularity and the concept of stem cell competition: geographic and quantitative determinants in stem cell biology. Leukemia *18*, 575–583.

Copley, M.R., Babovic, S., Benz, C., Knapp, D.J.H.F., Beer, P.A., Kent, D.G., Wohrer, S., Treloar, D.Q., Day, C., Rowe, K., et al. (2013). The Lin28b–let-7–Hmga2 axis determines the higher self-renewal potential of fetal haematopoietic stem cells. Nat. Cell Biol. *15*, 916–925.

Cornils, K., Bartholomae, C.C., Thielecke, L., Lange, C., Arens, A., Glauche, I., Mock, U., Riecken, K., Gerdes, S., von Kalle, C., et al. (2013). Comparative clonal analysis of reconstitution kinetics after transplantation of hematopoietic stem cells gene marked with a lentiviral SIN or a γ-retroviral LTR vector. Exp. Hematol. *41*, 28–38.e3.

Cosgun, K.N., Rahmig, S., Mende, N., Reinke, S., Hauber, I., Schäfer, C., Petzold, A., Weisbach, H., Heidkamp, G., Purbojo, A., et al. (2014). Kit Regulates HSC Engraftment across the Human-Mouse Species Barrier. Cell Stem Cell *15*, 227–238.

Crissman, H.A., and Steinkamp, J.A. (1973). Rapid, simultaneous measurement of DNA, protein, and cell volume in single cells from large mammalian cell populations. J. Cell Biol. *59*, 766–771.

Crissman, H.A., Darzynkiewicz, Z., Tobey, R.A., and Steinkamp, J.A. (1985). Correlated measurements of DNA, RNA, and protein in individual cells by flow cytometry. Science *228*, 1321–1324.

Croft, D., O'Kelly, G., Wu, G., Haw, R., Gillespie, M., Matthews, L., Caudy, M., Garapati, P., Gopinath, G., Jassal, B., et al. (2011). Reactome: a database of reactions, pathways and biological processes. Nucleic Acids Res. *39*, D691–D697.

Csaszar, E., Kirouac, D.C., Yu, M., Wang, W., Qiao, W., Cooke, M.P., Boitano, A.E., Ito, C., and Zandstra, P.W. (2012). Rapid Expansion of Human Hematopoietic Stem Cells by Automated Control of Inhibitory Feedback Signaling. Cell Stem Cell *10*, 218–229.

Cumano, A., Ferraz, J.C., Klaine, M., Di Santo, J.P., and Godin, I. (2001). Intraembryonic, but Not Yolk Sac Hematopoietic Precursors, Isolated before Circulation, Provide Long-Term Multilineage Reconstitution. Immunity *15*, 477–485.

De Koning, J., Van Bekkum, D.W., Dicke, K.A., Dooren, L.J., Van Rood, J.J., and Rádl, J. (1969). TRANSPLANTATION OF BONE-MARROW CELLS AND FETAL THYMUS IN AN INFANT WITH LYMPHOPENIC IMMUNOLOGICAL DEFICIENCY. The Lancet *293*, 1223–1227.

Delaney, C., Heimfeld, S., Brashem-Stein, C., Voorhies, H., Manger, R.L., and Bernstein, I.D. (2010). Notch-mediated expansion of human cord blood progenitor cells capable of rapid myeloid reconstitution. Nat. Med. *16*, 232–236.

Delghandi, M.P., Johannessen, M., and Moens, U. (2005). The cAMP signalling pathway activates CREB through PKA, p38 and MSK1 in NIH 3T3 cells. Cell. Signal. *17*, 1343–1351.

De Lima, M., McMannis, J.D., Saliba, R., Worth, L., Kebriaei, P., Popat, U., Qazilbash, M., Jones, R., Giralt, S., de Padua Silva, L., et al. (2008). Double Cord Blood Transplantation (CBT) with and without Ex-Vivo Expansion (EXP): A Randomized, Controlled Study. ASH Annu. Meet. Abstr. *112*, 154.

Devine, S.M., Flomenberg, N., Vesole, D.H., Liesveld, J., Weisdorf, D., Badel, K., Calandra, G., and DiPersio, J.F. (2004). Rapid mobilization of CD34+ cells following administration of the CXCR4 antagonist AMD3100 to patients with multiple myeloma and non-Hodgkin's lymphoma. J. Clin. Oncol. Off. J. Am. Soc. Clin. Oncol. *22*, 1095–1102.

Dexter, T.M., Allen, T.D., and Lajtha, L.G. (1977). Conditions controlling the proliferation of haemopoietic stem cells in vitro. J. Cell. Physiol. *91*, 335–344.

Dick, J.E., Magli, M.C., Huszar, D., Phillips, R.A., and Bernstein, A. (1985). Introduction of a selectable gene into primitive stem cells capable of long-term reconstitution of the hemopoietic system of W/Wv mice. Cell *42*, 71–79.

Dieterlen-Lievre, par F. (1975). On the origin of haemopoietic stem cells in the avian embryo: an experimental approach. J. Embryol. Exp. Morphol. *33*, 607–619.

Diggle, T.A., Redpath, N.T., Heesom, K.J., and Denton, R.M. (1998). Regulation of protein-synthesis elongation-factor-2 kinase by cAMP in adipocytes. Biochem. J. *336 ( Pt 3)*, 525–529.

Ding, L., and Morrison, S.J. (2013). Haematopoietic stem cells and early lymphoid progenitors occupy distinct bone marrow niches. Nature *495*, 231–235.

Domen, J., Cheshier, S.H., and Weissman, I.L. (2000). The role of apoptosis in the regulation of hematopoietic stem cells: Overexpression of Bcl-2 increases both their number and repopulation potential. J. Exp. Med. *191*, 253–264.

Doulatov, S., Notta, F., Eppert, K., Nguyen, L.T., Ohashi, P.S., and Dick, J.E. (2010). Revised map of the human progenitor hierarchy shows the origin of macrophages and dendritic cells in early lymphoid development. Nat. Immunol. *11*, 585–593.

Doulatov, S., Notta, F., Laurenti, E., and Dick, J.E. (2012). Hematopoiesis: A Human Perspective. Cell Stem Cell *10*, 120–136.

Duffy, D.C., McDonald, J.C., Schueller, O.J., and Whitesides, G.M. (1998). Rapid Prototyping of Microfluidic Systems in Poly(dimethylsiloxane). Anal. Chem. *70*, 4974–4984.

Durand, C., Robin, C., Bollerot, K., Baron, M.H., Ottersbach, K., and Dzierzak, E. (2007). Embryonic stromal clones reveal developmental regulators of definitive hematopoietic stem cells. Proc. Natl. Acad. Sci. U. S. A. *104*, 20838–20843.

Dykstra, B., Ramunas, J., Kent, D., McCaffrey, L., Szumsky, E., Kelly, L., Farn, K., Blaylock, A., Eaves, C., and Jervis, E. (2006). High-resolution video monitoring of hematopoietic stem cells cultured in single-cell arrays identifies new features of self-renewal. Proc. Natl. Acad. Sci. U. S. A. *103*, 8185–8190.

Dykstra, B., Kent, D., Bowie, M., McCaffrey, L., Hamilton, M., Lyons, K., Lee, S.-J., Brinkman, R., and Eaves, C. (2007). Long-Term Propagation of Distinct Hematopoietic Differentiation Programs In Vivo. Cell Stem Cell *1*, 218–229.

Eaves, C.J. (2015). Hematopoietic stem cells: concepts, definitions and the new reality. Blood blood – 2014–12 – 570200.

Eaves, C.J., and Eaves, A.C. (2006). Anatomy and physiology of hematopoiesis. In Childhood Leukemias, (Cambridge University Press),.

Eilken, H.M., Nishikawa, S.-I., and Schroeder, T. (2009). Continuous single-cell imaging of blood generation from haemogenic endothelium. Nature *457*, 896–900.

Ema, H., Takano, H., Sudo, K., and Nakauchi, H. (2000). In vitro self-renewal division of hematopoietic stem cells. J. Exp. Med. *192*, 1281–1288.

Emmrich, S., Rasche, M., Schöning, J., Reimer, C., Keihani, S., Maroz, A., Xie, Y., Li, Z., Schambach, A., Reinhardt, D., et al. (2014). miR-99a/100∼125b tricistrons regulate hematopoietic stem and progenitor cell homeostasis by shifting the balance between TGFβ and Wnt signaling. Genes Dev. *28*, 858–874.

Enver, T., Pera, M., Peterson, C., and Andrews, P.W. (2009). Stem cell states, fates, and the rules of attraction. Cell Stem Cell *4*, 387–397.

Ergen, A.V., Boles, N.C., and Goodell, M.A. (2012). Rantes/Ccl5 influences hematopoietic stem cell subtypes and causes myeloid skewing. Blood *119*, 2500–2509.

Fares, I., Chagraoui, J., Gareau, Y., Gingras, S., Ruel, R., Mayotte, N., Csaszar, E., Knapp, D.J.H.F., Miller, P., Ngom, M., et al. (2014). Pyrimidoindole derivatives are agonists of human hematopoietic stem cell self-renewal. Science *345*, 1509–1512.

Fialkow, P.J., Martin, P.J., Najfeld, V., Penfold, G.K., Jacobson, R.J., and Hansen, J.A. (1981a). Evidence for a multistep pathogenesis of chronic myelogenous leukemia. Blood *58*, 158–163.

Fialkow, P.J., Singer, J.W., Adamson, J.W., Vaidya, K., Dow, L.W., Ochs, J., and Moohr, J.W. (1981b). Acute nonlymphocytic leukemia: heterogeneity of stem cell origin. Blood *57*, 1068–1073.

Fialkow, P.J., Singer, J.W., Raskind, W.H., Adamson, J.W., Jacobson, R.J., Bernstein, I.D., Dow, L.W., Najfeld, V., and Veith, R. (1987). Clonal development, stem-cell differentiation, and clinical remissions in acute nonlymphocytic leukemia. N. Engl. J. Med. *317*, 468–473.

Fienberg, H.G., Simonds, E.F., Fantl, W.J., Nolan, G.P., and Bodenmiller, B. (2012). A platinum-based covalent viability reagent for single-cell mass cytometry. Cytom. Part J. Int. Soc. Anal. Cytol. *81*, 467–475.

Fleming, W.H., Alpern, E.J., Uchida, N., Ikuta, K., Spangrude, G.J., and Weissman, I.L. (1993). Functional heterogeneity is associated with the cell cycle status of murine hematopoietic stem cells. J. Cell Biol. *122*, 897–902.

Florian, M.C., Dörr, K., Niebel, A., Daria, D., Schrezenmeier, H., Rojewski, M., Filippi, M.-D., Hasenberg, A., Gunzer, M., Scharffetter-Kochanek, K., et al. (2012). Cdc42 activity regulates hematopoietic stem cell aging and rejuvenation. Cell Stem Cell *10*, 520–530.

Ford, C.E., Hamerton, J.L., Barnes, D.W., and Loutit, J.F. (1956). Cytological identification of radiation-chimaeras. Nature *177*, 452–454.

Fraser, C.C., Eaves, C.J., Szilvassy, S.J., and Humphries, R.K. (1990). Expansion in vitro of retrovirally marked totipotent hematopoietic stem cells. Blood *76*, 1071–1076.

Fraser, C.C., Szilvassy, S.J., Eaves, C.J., and Humphries, R.K. (1992). Proliferation of totipotent hematopoietic stem cells in vitro with retention of long-term competitive in vivo reconstituting ability. Proc. Natl. Acad. Sci. U. S. A. *89*, 1968–1972.

Frelin, C., Herrington, R., Janmohamed, S., Barbara, M., Tran, G., Paige, C.J., Benveniste, P., Zuñiga-Pflücker, J.-C., Souabni, A., Busslinger, M., et al. (2013). GATA-3 regulates the self-renewal of long-term hematopoietic stem cells. Nat. Immunol. *14*, 1037–1044.

Fujiwara, Y., Browne, C.P., Cunniff, K., Goff, S.C., and Orkin, S.H. (1996). Arrested development of embryonic red cell precursors in mouse embryos lacking transcription factor GATA-1. Proc. Natl. Acad. Sci. U. S. A. *93*, 12355–12358.

Galy, A., Travis, M., Cen, D., and Chen, B. (1995). Human T, B, natural killer, and dendritic cells arise from a common bone marrow progenitor cell subset. Immunity *3*, 459–473.

García, R., Aguiar, J., Alberti, E., de la Cuétara, K., and Pavón, N. (2004). Bone marrow stromal cells produce nerve growth factor and glial cell line-derived neurotrophic factors. Biochem. Biophys. Res. Commun. *316*, 753–754.

Gartner, S., and Kaplan, H.S. (1980). Long-term culture of human bone marrow cells. Proc. Natl. Acad. Sci. U. S. A. *77*, 4756–4759.

Gatti, R., Meuwissen, H., Allen, H., Hong, R., and Good, R. (1968). IMMUNOLOGICAL RECONSTITUTION OF SEX-LINKED LYMPHOPENIC IMMUNOLOGICAL DEFICIENCY. The Lancet *292*, 1366–1369.

Geissler, E.N., and Russell, E.S. (1983). Analysis of the hematopoietic effects of new dominant spotting (W) mutations of the mouse. I. Influence upon hematopoietic stem cells. Exp. Hematol. *11*, 452–460.

Genovese, G., Kähler, A.K., Handsaker, R.E., Lindberg, J., Rose, S.A., Bakhoum, S.F., Chambert, K., Mick, E., Neale, B.M., Fromer, M., et al. (2014). Clonal hematopoiesis and blood-cancer risk inferred from blood DNA sequence. N. Engl. J. Med. *371*, 2477–2487.

Gentleman, R.C., Carey, V.J., Bates, D.M., Bolstad, B., Dettling, M., Dudoit, S., Ellis, B., Gautier, L., Ge, Y., Gentry, J., et al. (2004). Bioconductor: open software development for computational biology and bioinformatics. Genome Biol. *5*, R80.

Gerber, H.-P., Malik, A.K., Solar, G.P., Sherman, D., Liang, X.H., Meng, G., Hong, K., Marsters, J.C., and Ferrara, N. (2002). VEGF regulates haematopoietic stem cell survival by an internal autocrine loop mechanism. Nature *417*, 954–958.

Glimm, H., Eisterer, W., Lee, K., Cashman, J., Holyoake, T.L., Nicolini, F., Shultz, L.D., von Kalle, C., and Eaves, C.J. (2001). Previously undetected human hematopoietic cell populations with short-term repopulating activity selectively engraft NOD/SCID-β2 microglobulin–null mice. J. Clin. Invest. *107*, 199–206.

Glimm, H., Schmidt, M., Fischer, M., Schwarzwaelder, K., Wissler, M., Klingenberg, S., Prinz, C., Waller, C.F., Lange, W., Eaves, C.J., et al. (2005). Efficient marking of human cells with rapid but transient repopulating activity in autografted recipients. Blood *106*, 893–898.

Goessling, W., Allen, R.S., Guan, X., Jin, P., Uchida, N., Dovey, M., Harris, J.M., Metzger, M.E., Bonifacino, A.C., Stroncek, D., et al. (2011). Prostaglandin E2 enhances human cord blood stem cell xenotransplants and shows long-term safety in preclinical nonhuman primate transplant models. Cell Stem Cell *8*, 445–458.

Görgens, A., Radtke, S., Möllmann, M., Cross, M., Dürig, J., Horn, P.A., and Giebel, B. (2013). Revision of the Human Hematopoietic Tree: Granulocyte Subtypes Derive from Distinct Hematopoietic Lineages. Cell Rep. *3*, 1539–1552.

Graf, T., and Enver, T. (2009). Forcing cells to change lineages. Nature *462*, 587–594.

Grosselin, J., Sii-Felice, K., Payen, E., Chretien, S., Tronik-Le Roux, D., and Leboulch, P. (2013). Arrayed lentiviral barcoding for quantification analysis of hematopoietic dynamics. Stem Cells Dayt. Ohio *31*, 2162–2171.

Grün, D., Kester, L., and van Oudenaarden, A. (2014). Validation of noise models for single-cell transcriptomics. Nat. Methods *11*, 637–640.

Guenechea, G., Gan, O.I., Dorrell, C., and Dick, J.E. (2001). Distinct classes of human stem cells that differ in proliferative and self-renewal potential. Nat. Immunol. *2*, 75–82.

Guezguez, B., Campbell, C.J.V., Boyd, A.L., Karanu, F., Casado, F.L., Di Cresce, C., Collins, T.J., Shapovalova, Z., Xenocostas, A., and Bhatia, M. (2013). Regional localization within the bone marrow influences the functional capacity of human HSCs. Cell Stem Cell *13*, 175–189.

de Haan, G., Weersing, E., Dontje, B., van Os, R., Bystrykh, L.V., Vellenga, E., and Miller, G. (2003). In vitro generation of long-term repopulating hematopoietic stem cells by fibroblast growth factor-1. Dev. Cell *4*, 241–251.

Hao, Q.-L., Zhu, J., Price, M.A., Payne, K.J., Barsky, L.W., and Crooks, G.M. (2001). Identification of a novel, human multilymphoid progenitor in cord. Blood *97*, 3683–3690.

Harkey, M.A., Kaul, R., Jacobs, M.A., Kurre, P., Bovee, D., Levy, R., and Blau, C.A. (2007). Multiarm high-throughput integration site detection: limitations of LAM-PCR technology and optimization for clonal analysis. Stem Cells Dev. *16*, 381–392.

Harrison, D.E. (1979). Mouse erythropoietic stem cell lines function normally 100 months: loss related to number of transplantations. Mech. Ageing Dev. *9*, 427–433.

Harrison, D.E., and Zhong, R.K. (1992). The same exhaustible multilineage precursor produces both myeloid and lymphoid cells as early as 3-4 weeks after marrow transplantation. Proc. Natl. Acad. Sci. U. S. A. *89*, 10134–10138.

Hashimshony, T., Wagner, F., Sher, N., and Yanai, I. (2012). CEL-Seq: single-cell RNA-Seq by multiplexed linear amplification. Cell Rep. *2*, 666–673.

Himburg, H.A., Muramoto, G.G., Daher, P., Meadows, S.K., Russell, J.L., Doan, P., Chi, J.-T., Salter, A.B., Lento, W.E., Reya, T., et al. (2010). Pleiotrophin regulates the expansion and regeneration of hematopoietic stem cells. Nat. Med. *16*, 475–482.

Hiramatsu, H., Nishikomori, R., Heike, T., Ito, M., Kobayashi, K., Katamura, K., and Nakahata, T. (2003). Complete reconstitution of human lymphocytes from cord blood CD34+ cells using the NOD/SCID/γcnull mice model. Blood *102*, 873–880.

Hirasawa, R., Shimizu, R., Takahashi, S., Osawa, M., Takayanagi, S., Kato, Y., Onodera, M., Minegishi, N., Yamamoto, M., Fukao, K., et al. (2002). Essential and instructive roles of GATA factors in eosinophil development. J. Exp. Med. *195*, 1379–1386.

Hogan, C.J., Shpall, E.J., McNulty, O., McNiece, I., Dick, J.E., Shultz, L.D., and Keller, G. (1997). Engraftment and Development of Human CD34+-Enriched Cells From Umbilical Cord Blood in NOD/LtSz-scid/scid Mice. Blood *90*, 85–96.

Hogan, C.J., Shpall, E.J., and Keller, G. (2002). Differential long-term and multilineage engraftment potential from subfractions of human CD34+ cord blood cells transplanted into NOD/SCID mice. Proc. Natl. Acad. Sci. U. S. A. *99*, 413–418.

Holyoake, T.L., Nicolini, F.E., and Eaves, C.J. (1999). Functional differences between transplantable human hematopoietic stem cells from fetal liver, cord blood, and adult marrow. Exp. Hematol. *27*, 1418–1427.

Horwitz, M.E., Chao, N.J., Rizzieri, D.A., Long, G.D., Sullivan, K.M., Gasparetto, C., Chute, J.P., Morris, A., McDonald, C., Waters-Pick, B., et al. (2014). Umbilical cord blood expansion with nicotinamide provides long-term multilineage engraftment. J. Clin. Invest. *124*, 3121–3128.

Hsu, P.D., Lander, E.S., and Zhang, F. (2014). Development and applications of CRISPR-Cas9 for genome engineering. Cell *157*, 1262–1278.

Hu, G., Xu, J., Deng, Z., Feng, J., and Jin, Y. (2011). Supernatant of bone marrow mesenchymal stromal cells induces peripheral blood mononuclear cells possessing mesenchymal features. Int. J. Biol. Sci. *7*, 364–375.

Huang, J., Nguyen-McCarty, M., Hexner, E.O., Danet-Desnoyers, G., and Klein, P.S. (2012). Maintenance of hematopoietic stem cells through regulation of Wnt and mTOR pathways. Nat. Med. *18*, 1778–1785.

Huynh, H., Iizuka, S., Kaba, M., Kirak, O., Zheng, J., Lodish, H.F., and Zhang, C.C. (2008). Insulin-like growth factor-binding protein 2 secreted by a tumorigenic cell line supports ex vivo expansion of mouse hematopoietic stem cells. Stem Cells Dayt. Ohio *26*, 1628–1635.

Inoki, K., Li, Y., Zhu, T., Wu, J., and Guan, K.-L. (2002). TSC2 is phosphorylated and inhibited by Akt and suppresses mTOR signalling. Nat. Cell Biol. *4*, 648–657.

Iscove, N.N., and Nawa, K. (1997). Hematopoietic stem cells expand during serial transplantation in vivo without apparent exhaustion. Curr. Biol. CB *7*, 805–808.

Islam, S., Kjällquist, U., Moliner, A., Zajac, P., Fan, J.-B., Lönnerberg, P., and Linnarsson, S. (2011). Characterization of the single-cell transcriptional landscape by highly multiplex RNA-seq. Genome Res. *21*, 1160–1167.

Islam, S., Zeisel, A., Joost, S., La Manno, G., Zajac, P., Kasper, M., Lönnerberg, P., and Linnarsson, S. (2014). Quantitative single-cell RNA-seq with unique molecular identifiers. Nat. Methods *11*, 163–166.

Ito, K., Carracedo, A., Weiss, D., Arai, F., Ala, U., Avigan, D.E., Schafer, Z.T., Evans, R.M., Suda, T., Lee, C.-H., et al. (2012). A PML–PPAR-δ pathway for fatty acid oxidation regulates hematopoietic stem cell maintenance. Nat. Med. *18*, 1350–1358.

Ito, M., Hiramatsu, H., Kobayashi, K., Suzue, K., Kawahata, M., Hioki, K., Ueyama, Y., Koyanagi, Y., Sugamura, K., Tsuji, K., et al. (2002). NOD/SCID/γ mouse: an excellent recipient mouse model for engraftment of human cells. Blood *100*, 3175–3182.

Jacobberger, J.W., Fogleman, D., and Lehman, J.M. (1986). Analysis of intracellular antigens by flow cytometry. Cytometry *7*, 356–364.

Jacobsen, F.W., Stokke, T., and Jacobsen, S.E. (1995). Transforming growth factor-beta potently inhibits the viability-promoting activity of stem cell factor and other cytokines and induces apoptosis of primitive murine hematopoietic progenitor cells. Blood *86*, 2957–2966.

Jacobson, L.O., Simmons, E.L., Marks, E.K., and Eldredge, J.H. (1951). Recovery from radiation injury. Science *113*, 510–511.

Jaiswal, S., Fontanillas, P., Flannick, J., Manning, A., Grauman, P.V., Mar, B.G., Lindsley, R.C., Mermel, C.H., Burtt, N., Chavez, A., et al. (2014). Age-related clonal hematopoiesis associated with adverse outcomes. N. Engl. J. Med. *371*, 2488–2498.

Jaitin, D.A., Kenigsberg, E., Keren-Shaul, H., Elefant, N., Paul, F., Zaretsky, I., Mildner, A., Cohen, N., Jung, S., Tanay, A., et al. (2014). Massively parallel single-cell RNA-seq for marker-free decomposition of tissues into cell types. Science *343*, 776–779.

Jones, R.J., Barber, J.P., Vala, M.S., Collector, M.I., Kaufmann, S.H., Ludeman, S.M., Colvin, O.M., and Hilton, J. (1995). Assessment of aldehyde dehydrogenase in viable cells. Blood *85*, 2742–2746.

Jordan, C.T., and Guzman, M.L. (2004). Mechanisms controlling pathogenesis and survival of leukemic stem cells. Oncogene *23*, 7178–7187.

Kale, V.P. (2004). Differential activation of MAPK signaling pathways by TGF-beta1 forms the molecular mechanism behind its dose-dependent bidirectional effects on hematopoiesis. Stem Cells Dev. *13*, 27–38.

Kale, V.P., and Vaidya, A.A. (2004). Molecular mechanisms behind the dose-dependent differential activation of MAPK pathways induced by transforming growth factor-beta1 in hematopoietic cells. Stem Cells Dev. *13*, 536–547.

Karlsson, G., Blank, U., Moody, J.L., Ehinger, M., Singbrant, S., Deng, C.-X., and Karlsson, S. (2007). Smad4 is critical for self-renewal of hematopoietic stem cells. J. Exp. Med. *204*, 467–474.

Keller, G., Paige, C., Gilboa, E., and Wagner, E.F. (1985). Expression of a foreign gene in myeloid and lymphoid cells derived from multipotent haematopoietic precursors. Nature *318*, 149–154.

Kent, D., Dykstra, B., and Eaves, C. (2007). Isolation and assessment of long-term reconstituting hematopoietic stem cells from adult mouse bone marrow. Curr. Protoc. Stem Cell Biol. *Chapter 2*, Unit 2A.4.

Kent, D.G., Dykstra, B.J., Cheyne, J., Ma, E., and Eaves, C.J. (2008). Steel factor coordinately regulates the molecular signature and biologic function of hematopoietic stem cells. Blood *112*, 560–567.

Kent, D.G., Copley, M.R., Benz, C., Wöhrer, S., Dykstra, B.J., Ma, E., Cheyne, J., Zhao, Y., Bowie, M.B., Zhao, Y., et al. (2009). Prospective isolation and molecular characterization of hematopoietic stem cells with durable self-renewal potential. Blood *113*, 6342–6350.

Kharas, M.G., Lengner, C.J., Al-Shahrour, F., Bullinger, L., Ball, B., Zaidi, S., Morgan, K., Tam, W., Paktinat, M., Okabe, R., et al. (2010). Musashi-2 regulates normal hematopoiesis and promotes aggressive myeloid leukemia. Nat. Med. *16*, 903–908.

Kim, S., Kim, N., Presson, A.P., Metzger, M.E., Bonifacino, A.C., Sehl, M., Chow, S.A., Crooks, G.M., Dunbar, C.E., An, D.S., et al. (2014). Dynamics of HSPC Repopulation In Non-human Primates Revealed by A Decade-Long Clonal-Tracking Study. Cell Stem Cell *14*, 473–485.

Kivioja, T., Vähärautio, A., Karlsson, K., Bonke, M., Enge, M., Linnarsson, S., and Taipale, J. (2012). Counting absolute numbers of molecules using unique molecular identifiers. Nat. Methods *9*, 72–74.

Kondo, M., Weissman, I.L., and Akashi, K. (1997). Identification of Clonogenic Common Lymphoid Progenitors in Mouse Bone Marrow. Cell *91*, 661–672.

Kraemer, P.M., Petersen, D.F., and Van Dilla, M.A. (1971). DNA constancy in heteroploidy and the stem line theory of tumors. Science *174*, 714–717.

Krishnaswamy, S., Spitzer, M.H., Mingueneau, M., Bendall, S.C., Litvin, O., Stone, E., Pe'er, D., and Nolan, G.P. (2014). Systems biology. Conditional density-based analysis of T cell signaling in single-cell data. Science *346*, 1250689.

Krutzik, P.O., and Nolan, G.P. (2003). Intracellular phospho-protein staining techniques for flow cytometry: monitoring single cell signaling events. Cytom. Part J. Int. Soc. Anal. Cytol. *55*, 61–70.

Krutzik, P.O., Clutter, M.R., and Nolan, G.P. (2005). Coordinate analysis of murine immune cell surface markers and intracellular phosphoproteins by flow cytometry. J. Immunol. Baltim. Md 1950 *175*, 2357–2365.

Kueh, H.Y., Champhekar, A., Champhekhar, A., Nutt, S.L., Elowitz, M.B., and Rothenberg, E.V. (2013). Positive feedback between PU.1 and the cell cycle controls myeloid differentiation. Science *341*, 670–673.

Kulessa, H., Frampton, J., and Graf, T. (1995). GATA-1 reprograms avian myelomonocytic cell lines into eosinophils, thromboblasts, and erythroblasts. Genes Dev. *9*, 1250–1262.

Kumano, K., Chiba, S., Kunisato, A., Sata, M., Saito, T., Nakagami-Yamaguchi, E., Yamaguchi, T., Masuda, S., Shimizu, K., Takahashi, T., et al. (2003). Notch1 but not Notch2 is essential for generating hematopoietic stem cells from endothelial cells. Immunity *18*, 699–711.

Kunisaki, Y., Bruns, I., Scheiermann, C., Ahmed, J., Pinho, S., Zhang, D., Mizoguchi, T., Wei, Q., Lucas, D., Ito, K., et al. (2013). Arteriolar niches maintain haematopoietic stem cell quiescence. Nature *502*, 637–643.

Kurth, I., Franke, K., Pompe, T., Bornhäuser, M., and Werner, C. (2011). Extracellular matrix functionalized microcavities to control hematopoietic stem and progenitor cell fate. Macromol. Biosci. *11*, 739–747.

Lacombe, J., Herblot, S., Rojas-Sutterlin, S., Haman, A., Barakat, S., Iscove, N.N., Sauvageau, G., and Hoang, T. (2010). Scl regulates the quiescence and the long-term competence of hematopoietic stem cells. Blood *115*, 792–803.

Lapidot, T., Pflumio, F., Doedens, M., Murdoch, B., Williams, D.E., and Dick, J.E. (1992). Cytokine stimulation of multilineage hematopoiesis from immature human cells engrafted in SCID mice. Science *255*, 1137–1141.

Lara-Astiaso, D., Weiner, A., Lorenzo-Vivas, E., Zaretsky, I., Jaitin, D.A., David, E., Keren-Shaul, H., Mildner, A., Winter, D., Jung, S., et al. (2014). Chromatin state dynamics during blood formation. Science *345*, 943–949.

Laurenti, E., Doulatov, S., Zandi, S., Plumb, I., Chen, J., April, C., Fan, J.-B., and Dick, J.E. (2013). The transcriptional architecture of early human hematopoiesis identifies multilevel control of lymphoid commitment. Nat. Immunol. *14*, 756–763.

Laurenti, E., Frelin, C., Xie, S., Ferrari, R., Dunant, C.F., Zandi, S., Neumann, A., Plumb, I., Doulatov, S., Chen, J., et al. (2015). CDK6 Levels Regulate Quiescence Exit in Human Hematopoietic Stem Cells. Cell Stem Cell *16*, 302–313.

Lecault, V., Vaninsberghe, M., Sekulovic, S., Knapp, D.J.H.F., Wohrer, S., Bowden, W., Viel, F., McLaughlin, T., Jarandehei, A., Miller, M., et al. (2011). High-throughput analysis of single hematopoietic stem cell proliferation in microfluidic cell culture arrays. Nat. Methods *8*, 581–586.

Lechman, E.R., Gentner, B., van Galen, P., Giustacchini, A., Saini, M., Boccalatte, F.E., Hiramatsu, H., Restuccia, U., Bachi, A., Voisin, V., et al. (2012). Attenuation of miR-126 Activity Expands HSC In Vivo without Exhaustion. Cell Stem Cell *11*, 799–811.

Ledran, M.H., Krassowska, A., Armstrong, L., Dimmick, I., Renström, J., Lang, R., Yung, S., Santibanez-Coref, M., Dzierzak, E., Stojkovic, M., et al. (2008). Efficient hematopoietic

differentiation of human embryonic stem cells on stromal cells derived from hematopoietic niches. Cell Stem Cell *3*, 85–98.

Lee, H.W., Blasco, M.A., Gottlieb, G.J., Horner, J.W., Greider, C.W., and DePinho, R.A. (1998). Essential role of mouse telomerase in highly proliferative organs. Nature *392*, 569–574.

Lemischka, I.R., Raulet, D.H., and Mulligan, R.C. (1986). Developmental potential and dynamic behavior of hematopoietic stem cells. Cell *45*, 917–927.

Li, Y., Qi, X., Liu, B., and Huang, H. (2015). The STAT5–GATA2 Pathway Is Critical in Basophil and Mast Cell Differentiation and Maintenance. J. Immunol. *194*, 4328–4338.

Liles, W.C., Broxmeyer, H.E., Rodger, E., Wood, B., Hübel, K., Cooper, S., Hangoc, G., Bridger, G.J., Henson, G.W., Calandra, G., et al. (2003). Mobilization of hematopoietic progenitor cells in healthy volunteers by AMD3100, a CXCR4 antagonist. Blood *102*, 2728–2730.

de Lima, M., McMannis, J., Gee, A., Komanduri, K., Couriel, D., Andersson, B.S., Hosing, C., Khouri, I., Jones, R., Champlin, R., et al. (2008). Transplantation of ex vivo expanded cord blood cells using the copper chelator tetraethylenepentamine: a phase I/II clinical trial. Bone Marrow Transplant. *41*, 771–778.

de Lima, M., McNiece, I., Robinson, S.N., Munsell, M., Eapen, M., Horowitz, M., Alousi, A., Saliba, R., McMannis, J.D., Kaur, I., et al. (2012). Cord-blood engraftment with ex vivo mesenchymal-cell coculture. N. Engl. J. Med. *367*, 2305–2315.

Liu, X., Zheng, H., Yu, W.-M., Cooper, T.M., Bunting, K.D., and Qu, C.-K. (2015). Maintenance of mouse hematopoietic stem cells ex vivo by reprogramming cellular metabolism. Blood *125*, 1562–1565.

Liu, Y., Liu, F., Yu, H., Zhao, X., Sashida, G., Deblasio, A., Harr, M., She, Q.-B., Chen, Z., Lin, H.-K., et al. (2012). Akt Phosphorylates the Transcriptional Repressor Bmi1 to Block Its Effects on the Tumor-Suppressing Ink4a-Arf Locus. Sci. Signal. *5*, ra77–ra77.

Lorenz, E., Uphoff, D., Reid, T.R., and Shelton, E. (1951). Modification of irradiation injury in mice and guinea pigs by bone marrow injections. J. Natl. Cancer Inst. *12*, 197–201.

Lou, X., Zhang, G., Herrera, I., Kinach, R., Ornatsky, O., Baranov, V., Nitz, M., and Winnik, M.A. (2007). Polymer-based elemental tags for sensitive bioassays. Angew. Chem. Int. Ed Engl. *46*, 6111–6114.

Lu, M., Kawamoto, H., Katsube, Y., Ikawa, T., and Katsura, Y. (2002). The Common Myelolymphoid Progenitor: A Key Intermediate Stage in Hemopoiesis Generating T and B Cells. J. Immunol. *169*, 3519–3525.

Lu, R., Neff, N.F., Quake, S.R., and Weissman, I.L. (2011). Tracking single hematopoietic stem cells in vivo using high-throughput sequencing in conjunction with viral genetic barcoding. Nat. Biotechnol. *29*, 928–933.

Lujan, E., Zunder, E.R., Ng, Y.H., Goronzy, I.N., Nolan, G.P., and Wernig, M. (2015). Early reprogramming regulators identified by prospective isolation and mass cytometry. Nature *521*, 352–356.

Lutolf, M.P., Doyonnas, R., Havenstrite, K., Koleckar, K., and Blau, H.M. (2009). Perturbation of single hematopoietic stem cell fates in artificial niches. Integr. Biol. Quant. Biosci. Nano Macro *1*, 59–69.

Magli, M.C., Iscove, N.N., and Odartchenko, N. (1982). Transient nature of early haematopoietic spleen colonies. Nature *295*, 527–529.

Majeti, R., Park, C.Y., and Weissman, I.L. (2007). Identification of a Hierarchy of Multipotent Hematopoietic Progenitors in Human Cord Blood. Cell Stem Cell *1*, 635–645.

Manz, M.G., Miyamoto, T., Akashi, K., and Weissman, I.L. (2002). Prospective isolation of human clonogenic common myeloid progenitors. Proc. Natl. Acad. Sci. *99*, 11872–11877.

Martin, F.H., Suggs, S.V., Langley, K.E., Lu, H.S., Ting, J., Okino, K.H., Morris, C.F., McNiece, I.K., Jacobsen, F.W., and Mendiaz, E.A. (1990). Primary structure and functional expression of rat and human stem cell factor DNAs. Cell *63*, 203–211.

Matsuoka, S., Tsuji, K., Hisakawa, H., Xu, M., Ebihara, Y., Ishii, T., Sugiyama, D., Manabe, A., Tanaka, R., Ikeda, Y., et al. (2001). Generation of definitive hematopoietic stem cells from murine early yolk sac and paraaortic splanchnopleures by aorta-gonad-mesonephros region–derived stromal cells. Blood *98*, 6–12.

Maximow, A. (1909). The Lymphocyte as a stem cell common to different blood elements in embryonic development and during the post-fetal life of mammals. Folia Haematol. *VIII*, 125–134.

McCulloch, E.A., Siminovitch, L., Till, J.E., Russell, E.S., and Bernstein, S.E. (1965). The cellular basis of the genetically determined hemopoietic defect in anemic mice of genotype Sl-Sld. Blood *26*, 399–410.

McIntosh, B.E., Brown, M.E., Duffin, B.M., Maufort, J.P., Vereide, D.T., Slukvin, I.I., and Thomson, J.A. (2015). Nonirradiated NOD,B6.SCID Il2rγ−/− KitW41/W41 (NBSGW) Mice Support Multilineage Engraftment of Human Hematopoietic Cells. Stem Cell Rep. *4*, 171–180.

McKenzie, J.L., Gan, O.I., Doedens, M., and Dick, J.E. (2005). Human short-term repopulating stem cells are efficiently detected following intrafemoral transplantation into NOD/SCID recipients depleted of CD122+ cells. Blood *106*, 1259–1261.

McNiece, I., Jones, R., Bearman, S.I., Cagnoni, P., Nieto, Y., Franklin, W., Ryder, J., Steele, A., Stoltz, J., Russell, P., et al. (2000). Ex vivo expanded peripheral blood progenitor cells provide rapid neutrophil recovery after high-dose chemotherapy in patients with breast cancer. Blood *96*, 3001–3007.

Medvinsky, A., and Dzierzak, E. (1996). Definitive Hematopoiesis Is Autonomously Initiated by the AGM Region. Cell *86*, 897–906.

Mercier, F.E., Ragu, C., and Scadden, D.T. (2012). The bone marrow at the crossroads of blood and immunity. Nat. Rev. Immunol. *12*, 49–60.

Miller, C.L., and Eaves, C.J. (1997). Expansion in vitro of adult murine hematopoietic stem cells with transplantable lympho-myeloid reconstituting ability. Proc. Natl. Acad. Sci. U. S. A. *94*, 13648–13653.

Miller, P.H., Cheung, A.M.S., Beer, P.A., Knapp, D.J.H.F., Dhillon, K., Rabu, G., Rostamirad, S., Humphries, R.K., and Eaves, C.J. (2013). Enhanced normal short-term human myelopoiesis in mice engineered to express human-specific myeloid growth factors. Blood *121*, e1–e4.

Mingueneau, M., Krishnaswamy, S., Spitzer, M.H., Bendall, S.C., Stone, E.L., Hedrick, S.M., Pe'er, D., Mathis, D., Nolan, G.P., and Benoist, C. (2014). Single-cell mass cytometry of TCR signaling: amplification of small initial differences results in low ERK activation in NOD mice. Proc. Natl. Acad. Sci. U. S. A. *111*, 16466–16471.

Moignard, V., Macaulay, I.C., Swiers, G., Buettner, F., Schütte, J., Calero-Nieto, F.J., Kinston, S., Joshi, A., Hannah, R., Theis, F.J., et al. (2013). Characterization of transcriptional networks in blood stem and progenitor cells using high-throughput single-cell gene expression analysis. Nat. Cell Biol. *15*, 363–372.

Moore, M.A.S., and Metcalf, D. (1970). Ontogeny of the Haemopoietic System: Yolk Sac Origin of In Vivo and In Vitro Colony Forming Cells in the Developing Mouse Embryo*. Br. J. Haematol. *18*, 279–296.

Moore, M. a. S., and Owen, J.J.T. (1965). Chromosome Marker Studies on the Development of the Haemopoietic System in the Chick Embryo. Nature *208*, 956–990.

Moore, K.A., Ema, H., and Lemischka, I.R. (1997). In vitro maintenance of highly purified, transplantable hematopoietic stem cells. Blood *89*, 4337–4347.

Morita, Y., Ema, H., and Nakauchi, H. (2010). Heterogeneity and hierarchy within the most primitive hematopoietic stem cell compartment. J. Exp. Med. *207*, 1173–1182.

Morrison, S.J., Wright, D.E., and Weissman, I.L. (1997). Cyclophosphamide/granulocyte colony-stimulating factor induces hematopoietic stem cells to proliferate prior to mobilization. Proc. Natl. Acad. Sci. U. S. A. *94*, 1908–1913.

Mossadegh-Keller, N., Sarrazin, S., Kandalla, P.K., Espinosa, L., Stanley, E.R., Nutt, S.L., Moore, J., and Sieweke, M.H. (2013). M-CSF instructs myeloid lineage fate in single haematopoietic stem cells. Nature *497*, 239–243.

Motte-Mohs, R.N.L., Herer, E., and Zúñiga-Pflücker, J.C. (2005). Induction of T-cell development from human cord blood hematopoietic stem cells by Delta-like 1 in vitro. Blood *105*, 1431–1439.

Muller-Sieburg, C.E., Cho, R.H., Karlsson, L., Huang, J.-F., and Sieburg, H.B. (2004). Myeloid-biased hematopoietic stem cells have extensive self-renewal capacity but generate diminished lymphoid progeny with impaired IL-7 responsiveness. Blood *103*, 4111–4118.

Nakano, T., Kodama, H., and Honjo, T. (1994). Generation of lymphohematopoietic cells from embryonic stem cells in culture. Science *265*, 1098–1101.

Newell, E.W., Sigal, N., Bendall, S.C., Nolan, G.P., and Davis, M.M. (2012). Cytometry by time-of-flight shows combinatorial cytokine expression and virus-specific cell niches within a continuum of CD8+ T cell phenotypes. Immunity *36*, 142–152.

Nguyen, L.V., Makarem, M., Carles, A., Moksa, M., Kannan, N., Pandoh, P., Eirew, P., Osako, T., Kardel, M., Cheung, A.M.S., et al. (2014). Clonal analysis via barcoding reveals diverse growth and differentiation of transplanted mouse and human mammary stem cells. Cell Stem Cell *14*, 253–263.

Nicolini, F.E., Holyoake, T.L., Cashman, J.D., Chu, P.P.Y., Lambie, K., and Eaves, C.J. (1999). Unique Differentiation Programs of Human Fetal Liver Stem Cells Shown Both In Vitro and In Vivo in NOD/SCID Mice. Blood *94*, 2686–2695.

North, T.E., Goessling, W., Walkley, C.R., Lengerke, C., Kopani, K.R., Lord, A.M., Weber, G.J., Bowman, T.V., Jang, I.-H., Grosser, T., et al. (2007). Prostaglandin E2 regulates vertebrate haematopoietic stem cell homeostasis. Nature *447*, 1007–1011.

Notta, F., Doulatov, S., Laurenti, E., Poeppl, A., Jurisica, I., and Dick, J.E. (2011). Isolation of Single Human Hematopoietic Stem Cells Capable of Long-Term Multilineage Engraftment. Science *333*, 218–221.

Nowell, P.C., Cole, L.J., Habermeyer, J.G., and Roan, P.L. (1956). Growth and Continued Function of Rat Marrow Cells in X-radiated Mice. Cancer Res. *16*, 258–261.

Nutt, S.L., Heavey, B., Rolink, A.G., and Busslinger, M. (1999). Commitment to the B-lymphoid lineage depends on the transcription factor Pax5. Nature *401*, 556–562.

O'Donnell, E.A., Ernst, D.N., and Hingorani, R. (2013). Multiparameter flow cytometry: advances in high resolution analysis. Immune Netw. *13*, 43–54.

Ogawa, M., Matsuzaki, Y., Nishikawa, S., Hayashi, S., Kunisada, T., Sudo, T., Kina, T., Nakauchi, H., and Nishikawa, S. (1991). Expression and function of c-kit in hemopoietic progenitor cells. J. Exp. Med. *174*, 63–71.

Oh, I.-H., Lau, A., and Eaves, C.J. (2000). During ontogeny primitive (CD34+CD38−) hematopoietic cells show altered expression of a subset of genes associated with early cytokine and differentiation responses of their adult counterparts. Blood *96*, 4160–4168.

Ohishi, K., Varnum-Finney, B., and Bernstein, I.D. (2002). Delta-1 enhances marrow and thymus repopulating ability of human CD34(+)CD38(-) cord blood cells. J. Clin. Invest. *110*, 1165–1174.

Ohta, H., Sekulovic, S., Bakovic, S., Eaves, C.J., Pineault, N., Gasparetto, M., Smith, C., Sauvageau, G., and Humphries, R.K. (2007). Near-maximal expansions of hematopoietic stem cells in culture using NUP98-HOX fusions. Exp. Hematol. *35*, 817–830.

Okada, S., Nakauchi, H., Nagayoshi, K., Nishikawa, S., Miura, Y., and Suda, T. (1992). In vivo and in vitro stem cell function of c-kit- and Sca-1-positive murine hematopoietic cells. Blood *80*, 3044–3050.

Oostendorp, R.A.J., Harvey, K.N., Kusadasi, N., de Bruijn, M.F.T.R., Saris, C., Ploemacher, R.E., Medvinsky, A.L., and Dzierzak, E.A. (2002). Stromal cell lines from mouse aorta-gonads-mesonephros subregions are potent supporters of hematopoietic stem cell activity. Blood *99*, 1183–1189.

Oostendorp, R.A.J., Robin, C., Steinhoff, C., Marz, S., Bräuer, R., Nuber, U.A., Dzierzak, E.A., and Peschel, C. (2005). Long-term maintenance of hematopoietic stem cells does not require contact with embryo-derived stromal cells in cocultures. Stem Cells Dayt. Ohio *23*, 842–851.

Osawa, M., Hanada, K., Hamada, H., and Nakauchi, H. (1996). Long-term lymphohematopoietic reconstitution by a single CD34-low/negative hematopoietic stem cell. Science *273*, 242–245.

Osborne, G.W. (2011). Recent advances in flow cytometric cell sorting. Methods Cell Biol. *102*, 533–556.

Pang, W.W., Price, E.A., Sahoo, D., Beerman, I., Maloney, W.J., Rossi, D.J., Schrier, S.L., and Weissman, I.L. (2011). Human bone marrow hematopoietic stem cells are increased in frequency and myeloid-biased with age. Proc. Natl. Acad. Sci. U. S. A. *108*, 20012–20017.

Park, I., Qian, D., Kiel, M., Becker, M.W., Pihalja, M., Weissman, I.L., Morrison, S.J., and Clarke, M.F. (2003). Bmi-1 is required for maintenance of adult self-renewing haematopoietic stem cells. Nature *423*, 302–305.

Park, S.-M., Deering, R.P., Lu, Y., Tivnan, P., Lianoglou, S., Al-Shahrour, F., Ebert, B.L., Hacohen, N., Leslie, C., Daley, G.Q., et al. (2014). Musashi-2 controls cell fate, lineage bias, and TGF-β signaling in HSCs. J. Exp. Med. *211*, 71–87.

Pater, E. de, Kaimakis, P., Vink, C.S., Yokomizo, T., Yamada-Inagawa, T., Linden, R. van der, Kartalaei, P.S., Camper, S.A., Speck, N., and Dzierzak, E. (2013). Gata2 is required for HSC generation and survival. J. Exp. Med. *210*, 2843–2850.

Pearson, T., Shultz, L.D., Miller, D., King, M., Laning, J., Fodor, W., Cuthbert, A., Burzenski, L., Gott, B., Lyons, B., et al. (2008). Non-obese diabetic–recombination activating gene-1 (NOD–Rag 1 null) interleukin (IL)-2 receptor common gamma chain (IL 2 rγnull) null mice: a radioresistant model for human lymphohaematopoietic engraftment. Clin. Exp. Immunol. *154*, 270–284.

Petriv, O.I., Kuchenbauer, F., Delaney, A.D., Lecault, V., White, A., Kent, D., Marmolejo, L., Heuser, M., Berg, T., Copley, M., et al. (2010). Comprehensive microRNA expression profiling of the hematopoietic hierarchy. Proc. Natl. Acad. Sci. U. S. A. *107*, 15443–15448.

Petzer, A.L., Zandstra, P.W., Piret, J.M., and Eaves, C.J. (1996a). Differential cytokine effects on primitive (CD34+CD38-) human hematopoietic cells: novel responses to Flt3-ligand and thrombopoietin. J. Exp. Med. *183*, 2551–2558.

Petzer, A.L., Hogge, D.E., Landsdorp, P.M., Reid, D.S., and Eaves, C.J. (1996b). Self-renewal of primitive human hematopoietic cells (long-term-culture-initiating cells) in vitro and their expansion in defined medium. Proc. Natl. Acad. Sci. U. S. A. *93*, 1470–1474.

Pflumio, F., Izac, B., Katz, A., Shultz, L.D., Vainchenker, W., and Coulombel, L. (1996). Phenotype and function of human hematopoietic cells engrafting immune- deficient CB17-severe combined immunodeficiency mice and nonobese diabetic-severe combined immunodeficiency mice after transplantation of human cord blood mononuclear cells. Blood *88*, 3731–3740.

Picelli, S., Faridani, O.R., Björklund, A.K., Winberg, G., Sagasser, S., and Sandberg, R. (2014). Full-length RNA-seq from single cells using Smart-seq2. Nat. Protoc. *9*, 171–181.

Pizzitola, I., Anjos-Afonso, F., Rouault-Pierre, K., Lassailly, F., Tettamanti, S., Spinelli, O., Biondi, A., Biagi, E., and Bonnet, D. (2014). Chimeric antigen receptors against CD33/CD123 antigens efficiently target primary acute myeloid leukemia cells in vivo. Leukemia *28*, 1596–1605.

Ploemacher, R.E., Sluijs, J. van der, Voerman, J.S., and Brons, N.H. (1989). An in vitro limiting-dilution assay of long-term repopulating hematopoietic stem cells in the mouse. Blood *74*, 2755–2763.

Pluznik, D.H., and Sachs, L. (1965). The cloning of normal “Mast” cells in tissue culture. J. Cell. Comp. Physiol. *66*, 319–324.

Porter, S.N., Baker, L.C., Mittelman, D., and Porteus, M.H. (2014). Lentiviral and targeted cellular barcoding reveals ongoing clonal dynamics of cell lines in vitro and in vivo. Genome Biol. *15*, R75.

Powles, R., Mehta, J., Kulkarni, S., Treleaven, J., Millar, B., Marsden, J., Shepherd, V., Rowland, A., Sirohi, B., Tait, D., et al. (2000). Allogeneic blood and bone-marrow stem-cell transplantation in haematological malignant diseases: a randomised trial. Lancet Lond. Engl. *355*, 1231–1237.

Qiu, P., Simonds, E.F., Bendall, S.C., Gibbs, K.D., Bruggner, R.V., Linderman, M.D., Sachs, K., Nolan, G.P., and Plevritis, S.K. (2011). Extracting a cellular hierarchy from high-dimensional cytometry data with SPADE. Nat. Biotechnol. *29*, 886–891.

Ramsköld, D., Luo, S., Wang, Y.-C., Li, R., Deng, Q., Faridani, O.R., Daniels, G.A., Khrebtukova, I., Loring, J.F., Laurent, L.C., et al. (2012). Full-length mRNA-Seq from single-cell levels of RNA and individual circulating tumor cells. Nat. Biotechnol. *30*, 777–782.

Rebel, V.I., Miller, C.L., Eaves, C.J., and Lansdorp, P.M. (1996). The repopulation potential of fetal liver hematopoietic stem cells in mice exceeds that of their liver adult bone marrow counterparts. Blood *87*, 3500–3507.

Redpath, N.T., and Proud, C.G. (1993). Cyclic AMP-dependent protein kinase phosphorylates rabbit reticulocyte elongation factor-2 kinase and induces calcium-independent activity. Biochem. J. *293 ( Pt 1)*, 31–34.

Reya, T., Morrison, S.J., Clarke, M.F., and Weissman, I.L. (2001). Stem cells, cancer, and cancer stem cells. Nature *414*, 105–111.

Reya, T., Duncan, A.W., Ailles, L., Domen, J., Scherer, D.C., Willert, K., Hintz, L., Nusse, R., and Weissman, I.L. (2003). A role for Wnt signalling in self-renewal of haematopoietic stem cells. Nature *423*, 409–414.

Riddell, J., Gazit, R., Garrison, B.S., Guo, G., Saadatpour, A., Mandal, P.K., Ebina, W., Volchkov, P., Yuan, G.-C., Orkin, S.H., et al. (2014). Reprogramming Committed Murine Blood Cells to Induced Hematopoietic Stem Cells with Defined Factors. Cell *157*, 549–564.

Rizo, A., Olthof, S., Han, L., Vellenga, E., de Haan, G., and Schuringa, J.J. (2009). Repression of BMI1 in normal and leukemic human CD34(+) cells impairs self-renewal and induces apoptosis. Blood *114*, 1498–1505.

Robb, L., Lyons, I., Li, R., Hartley, L., Köntgen, F., Harvey, R.P., Metcalf, D., and Begley, C.G. (1995). Absence of yolk sac hematopoiesis from mice with a targeted disruption of the scl gene. Proc. Natl. Acad. Sci. U. S. A. *92*, 7075–7079.

Robertson, J.D., Gale, R.E., Wynn, R.F., Dougal, M., Linch, D.C., Testa, N.G., and Chopra, R. (2000). Dynamics of telomere shortening in neutrophils and T lymphocytes during ageing and the relationship to skewed X chromosome inactivation patterns. Br. J. Haematol. *109*, 272–279.

Roederer, M. (2001). Spectral compensation for flow cytometry: visualization artifacts, limitations, and caveats. Cytometry *45*, 194–205.

Rossi, D.J., Bryder, D., Zahn, J.M., Ahlenius, H., Sonu, R., Wagers, A.J., and Weissman, I.L. (2005). Cell intrinsic alterations underlie hematopoietic stem cell aging. Proc. Natl. Acad. Sci. U. S. A. *102*, 9194–9199.

Rufer, N., Dragowska, W., Thornbury, G., Roosnek, E., and Lansdorp, P.M. (1998). Telomere length dynamics in human lymphocyte subpopulations measured by flow cytometry. Nat. Biotechnol. *16*, 743–747.

Ryan, M.A., Nattamai, K.J., Xing, E., Schleimer, D., Daria, D., Sengupta, A., Köhler, A., Liu, W., Gunzer, M., Jansen, M., et al. (2010). Pharmacological inhibition of EGFR signaling enhances G-CSF-induced hematopoietic stem cell mobilization. Nat. Med. *16*, 1141–1146.

Sachs, K., Perez, O., Pe'er, D., Lauffenburger, D.A., and Nolan, G.P. (2005). Causal protein-signaling networks derived from multiparameter single-cell data. Science *308*, 523–529.

Samokhvalov, I.M., Samokhvalova, N.I., and Nishikawa, S. (2007). Cell tracing shows the contribution of the yolk sac to adult haematopoiesis. Nature *446*, 1056–1061.

Sanjuan-Pla, A., Macaulay, I.C., Jensen, C.T., Woll, P.S., Luis, T.C., Mead, A., Moore, S., Carella, C., Matsuoka, S., Jones, T.B., et al. (2013). Platelet-biased stem cells reside at the apex of the haematopoietic stem-cell hierarchy. Nature *502*, 232–236.

Sarrazin, S., Mossadegh-Keller, N., Fukao, T., Aziz, A., Mourcin, F., Vanhille, L., Kelly Modis, L., Kastner, P., Chan, S., Duprez, E., et al. (2009). MafB restricts M-CSF-dependent myeloid commitment divisions of hematopoietic stem cells. Cell *138*, 300–313.

Sauvageau, G., Thorsteinsdottir, U., Eaves, C.J., Lawrence, H.J., Largman, C., Lansdorp, P.M., and Humphries, R.K. (1995). Overexpression of HOXB4 in hematopoietic cells causes the selective expansion of more primitive populations in vitro and in vivo. Genes Dev. *9*, 1753–1765.

Schmidt, M., Schwarzwaelder, K., Bartholomae, C., Zaoui, K., Ball, C., Pilz, I., Braun, S., Glimm, H., and von Kalle, C. (2007). High-resolution insertion-site analysis by linear amplification-mediated PCR (LAM-PCR). Nat. Methods *4*, 1051–1057.

Schuringa, J.J., Chung, K.Y., Morrone, G., and Moore, M.A.S. (2004). Constitutive activation of STAT5A promotes human hematopoietic stem cell self-renewal and erythroid differentiation. J. Exp. Med. *200*, 623–635.

Sekulovic, S., Gasparetto, M., Lecault, V., Hoesli, C.A., Kent, D.G., Rosten, P., Wan, A., Brookes, C., Hansen, C.L., Piret, J.M., et al. (2011). Ontogeny stage-independent and high-level clonal expansion in vitro of mouse hematopoietic stem cells stimulated by an engineered NUP98-HOX fusion transcription factor. Blood *118*, 4366–4376.

Senn, J.S., McCulloch, E.A., and Till, J.E. (1967). COMPARISON OF COLONY-FORMING ABILITY OF NORMAL AND LEUKÆMIC HUMAN MARROW IN CELL CULTURE. The Lancet *290*, 597–598.

Shibata, F., Goto-Koshino, Y., Morikawa, Y., Komori, T., Ito, M., Fukuchi, Y., Houchins, J.P., Tsang, M., Li, D.Y., Kitamura, T., et al. (2009). Roundabout 4 is expressed on hematopoietic stem cells and potentially involved in the niche-mediated regulation of the side population phenotype. Stem Cells Dayt. Ohio *27*, 183–190.

Shivdasani, R.A., Mayer, E.L., and Orkin, S.H. (1995). Absence of blood formation in mice lacking the T-cell leukaemia oncoprotein tal-1/SCL. Nature *373*, 432–434.

Shivdasani, R.A., Fujiwara, Y., McDevitt, M.A., and Orkin, S.H. (1997). A lineage-selective knockout establishes the critical role of transcription factor GATA-1 in megakaryocyte growth and platelet development. EMBO J. *16*, 3965–3973.

Shpall, E.J., Quinones, R., Giller, R., Zeng, C., Baron, A.E., Jones, R.B., Bearman, S.I., Nieto, Y., Freed, B., Madinger, N., et al. (2002). Transplantation of ex vivo expanded cord blood. Biol. Blood Marrow Transplant. J. Am. Soc. Blood Marrow Transplant. *8*, 368–376.

Sieburg, H.B., Cho, R.H., Dykstra, B., Uchida, N., Eaves, C.J., and Muller-Sieburg, C.E. (2006). The hematopoietic stem compartment consists of a limited number of discrete stem cell subsets. Blood *107*, 2311–2316.

Siminovitch, L., Mcculloch, E.A., and Till, J.E. (1963). THE DISTRIBUTION OF COLONY-FORMING CELLS AMONG SPLEEN COLONIES. J. Cell. Physiol. *62*, 327–336.

Sitnicka, E., Ruscetti, F.W., Priestley, G.V., Wolf, N.S., and Bartelmez, S.H. (1996). Transforming growth factor beta 1 directly and reversibly inhibits the initial cell divisions of long-term repopulating hematopoietic stem cells. Blood *88*, 82–88.

Sloma, I., Imren, S., Beer, P.A., Zhao, Y., Lecault, V., Leung, D., Raghuram, K., Brimacombe, C., Lambie, K., Piret, J., et al. (2013). Ex vivo expansion of normal and chronic myeloid leukemic stem cells without functional alteration using a NUP98HOXA10homeodomain fusion gene. Leukemia *27*, 159–169.

Smith-Berdan, S., Nguyen, A., Hassanein, D., Zimmer, M., Ugarte, F., Ciriza, J., Li, D., García-Ojeda, M.E., Hinck, L., and Forsberg, E.C. (2011). Robo4 cooperates with CXCR4 to specify hematopoietic stem cell localization to bone marrow niches. Cell Stem Cell *8*, 72–83.

Smyth, G.K., Michaud, J., and Scott, H.S. (2005). Use of within-array replicate spots for assessing differential expression in microarray experiments. Bioinforma. Oxf. Engl. *21*, 2067–2075.

Souroullas, G.P., Salmon, J.M., Sablitzky, F., Curtis, D.J., and Goodell, M.A. (2009). Adult hematopoietic stem and progenitor cells require either Lyl1 or Scl for survival. Cell Stem Cell *4*, 180–186.

Spangrude, G.J., Heimfeld, S., and Weissman, I.L. (1988). Purification and characterization of mouse hematopoietic stem cells. Science *241*, 58–62.

Staber, P.B., Zhang, P., Ye, M., Welner, R.S., Nombela-Arrieta, C., Bach, C., Kerenyi, M., Bartholdy, B.A., Zhang, H., Alberich-Jordà, M., et al. (2013). Sustained PU.1 levels balance cell-cycle regulators to prevent exhaustion of adult hematopoietic stem cells. Mol. Cell *49*, 934–946.

Stark, C., Breitkreutz, B.-J., Reguly, T., Boucher, L., Breitkreutz, A., and Tyers, M. (2006). BioGRID: a general repository for interaction datasets. Nucleic Acids Res. *34*, D535–D539.

Su, R.J., Zhang, X.B., Li, K., Yang, M., Li, C.K., Fok, T.F., James, A.E., Pong, H., and Yuen, P.M.P. (2002). Platelet-derived growth factor promotes ex vivo expansion of CD34+ cells from human cord blood and enhances long-term culture-initiating cells, non-obese diabetic/severe combined immunodeficient repopulating cells and formation of adherent cells. Br. J. Haematol. *117*, 735–746.

Subramanian, A., Tamayo, P., Mootha, V.K., Mukherjee, S., Ebert, B.L., Gillette, M.A., Paulovich, A., Pomeroy, S.L., Golub, T.R., Lander, E.S., et al. (2005). Gene set enrichment analysis: a knowledge-based approach for interpreting genome-wide expression profiles. Proc. Natl. Acad. Sci. U. S. A. *102*, 15545–15550.

Sun, J., Ramos, A., Chapman, B., Johnnidis, J.B., Le, L., Ho, Y.-J., Klein, A., Hofmann, O., and Camargo, F.D. (2014). Clonal dynamics of native haematopoiesis. Nature *514*, 322–327.

Sutherland, D.J., Till, J.E., and McCulloch, E.A. (1970). A kinetic study of the genetic control of hemopoietic progenitor cells assayed in culture and in vivo. J. Cell. Physiol. *75*, 267–274.

Sutherland, H.J., Eaves, C.J., Lansdorp, P.M., Thacker, J.D., and Hogge, D.E. (1991). Differential regulation of primitive human hematopoietic cells in long-term cultures maintained on genetically engineered murine stromal cells. Blood *78*, 666–672.

Suzuki, T., Yokoyama, Y., Kumano, K., Takanashi, M., Kozuma, S., Takato, T., Nakahata, T., Nishikawa, M., Sakano, S., Kurokawa, M., et al. (2006). Highly efficient ex vivo expansion of human hematopoietic stem cells using Delta1-Fc chimeric protein. Stem Cells Dayt. Ohio *24*, 2456–2465.

Szilvassy, S.J., Humphries, R.K., Lansdorp, P.M., Eaves, A.C., and Eaves, C.J. (1990). Quantitative assay for totipotent reconstituting hematopoietic stem cells by a competitive repopulation strategy. Proc. Natl. Acad. Sci. U. S. A. *87*, 8736–8740.

Tajima, S., Tsuji, K., Ebihara, Y., Sui, X., Tanaka, R., Muraoka, K., Yoshida, M., Yamada, K., Yasukawa, K., Taga, T., et al. (1996). Analysis of interleukin 6 receptor and gp130 expressions and proliferative capability of human CD34+ cells. J. Exp. Med. *184*, 1357–1364.

Takahashi, K., and Yamanaka, S. (2006). Induction of Pluripotent Stem Cells from Mouse Embryonic and Adult Fibroblast Cultures by Defined Factors. Cell *126*, 663–676.

Tang, F., Barbacioru, C., Wang, Y., Nordman, E., Lee, C., Xu, N., Wang, X., Bodeau, J., Tuch, B.B., Siddiqui, A., et al. (2009). mRNA-Seq whole-transcriptome analysis of a single cell. Nat. Methods *6*, 377–382.

Tanner, S.D., Ornatsky, O., Bandura, D.R., and Baranov, V.I. (2007). Multiplex bio-assay with inductively coupled plasma mass spectrometry: Towards a massively multivariate single-cell technology. Spectrochim. Acta Part B At. Spectrosc. *62*, 188–195.

Taussig, D.C., Pearce, D.J., Simpson, C., Rohatiner, A.Z., Lister, T.A., Kelly, G., Luongo, J.L., Danet-Desnoyers, G.-A.H., and Bonnet, D. (2005). Hematopoietic stem cells express multiple myeloid markers: implications for the origin and targeted therapy of acute myeloid leukemia. Blood *106*, 4086–4092.

Thol, F., and Schlenk, R.F. (2014). Gemtuzumab ozogamicin in acute myeloid leukemia revisited. Expert Opin. Biol. Ther. *14*, 1185–1195.

Thomas, E.D. (1993). Bone marrow transplantation - past, present and future. In Nobel Lectures, Physiology Or Medicine: 1981-1990, T. Frängsmyr, and J.E. Lindsten, eds. (World Scientific), pp. 576–584.

Thomas, E.D., Lochte, H.L., Cannon, J.H., Sahler, O.D., and Ferrebee, J.W. (1959). SUPRALETHAL WHOLE BODY IRRADIATION AND ISOLOGOUS MARROW TRANSPLANTATION IN MAN*. J. Clin. Invest. *38*, 1709–1716.

Thorsen, T., Maerkl, S.J., and Quake, S.R. (2002). Microfluidic Large-Scale Integration. Science *298*, 580–584.

Till, J.E., and McCulloch, E.A. (1961). A direct measurement of the radiation sensitivity of normal mouse bone marrow cells. Radiat. Res. *14*, 213–222.

Trowbridge, J.J., Snow, J.W., Kim, J., and Orkin, S.H. (2009). DNA Methyltransferase 1 Is Essential for and Uniquely Regulates Hematopoietic Stem and Progenitor Cells. Cell Stem Cell *5*, 442–449.

Umemoto, T., Yamato, M., Ishihara, J., Shiratsuchi, Y., Utsumi, M., Morita, Y., Tsukui, H., Terasawa, M., Shibata, T., Nishida, K., et al. (2012). Integrin-αvβ3 regulates thrombopoietin-mediated maintenance of hematopoietic stem cells. Blood *119*, 83–94.

Unger, M.A., Chou, H.-P., Thorsen, T., Scherer, A., and Quake, S.R. (2000). Monolithic Microfabricated Valves and Pumps by Multilayer Soft Lithography. Science *288*, 113–116.

Van der Maaten, L., and Hinton, G. (2008). Visualizing data using t-SNE. J. Mach. Learn. Res. *9*, 85.

Vermes, I., Haanen, C., Steffens-Nakken, H., and Reutelingsperger, C. (1995). A novel assay for apoptosis. Flow cytometric detection of phosphatidylserine expression on early apoptotic cells using fluorescein labelled Annexin V. J. Immunol. Methods *184*, 39–51.

Vieira, P., and Cumano, A. (2004). Differentiation of B lymphocytes from hematopoietic stem cells. Methods Mol. Biol. Clifton NJ *271*, 67–76.

Wada, H., Masuda, K., Satoh, R., Kakugawa, K., Ikawa, T., Katsura, Y., and Kawamoto, H. (2008). Adult T-cell progenitors retain myeloid potential. Nature *452*, 768–772.

Waddington, C.H., and others (1957). The strategy of the genes. A discussion of some aspects of theoretical biology. With an appendix by H. Kacser. Strategy Genes Discuss. Some Asp. Theor. Biol. Append. H Kacser ix+ – 262.

Wagers, A.J., and Weissman, I.L. (2006). Differential expression of alpha2 integrin separates long-term and short-term reconstituting Lin-/loThy1.1(lo)c-kit+ Sca-1+ hematopoietic stem cells. Stem Cells Dayt. Ohio *24*, 1087–1094.

Wagner, J.E., Brunstein, C., McKenna, D., Sumstad, D., Maahs, S., Laughlin, M., Perry, M.S., Boitano, A.E., Cooke, M.P., and Bleul, C.C. (2014). StemRegenin-1 (SR1) Expansion Culture Abrogates the Engraftment Barrier Associated with Umbilical Cord Blood Transplantation (UCBT). Blood *124*.

Walter, D., Lier, A., Geiselhart, A., Thalheimer, F.B., Huntscha, S., Sobotta, M.C., Moehrle, B., Brocks, D., Bayindir, I., Kaschutnig, P., et al. (2015). Exit from dormancy provokes DNA-damage-induced attrition in haematopoietic stem cells. Nature *520*, 549–552.

Wang, J., Sun, Q., Morita, Y., Jiang, H., Gross, A., Lechel, A., Hildner, K., Guachalla, L.M., Gompf, A., Hartmann, D., et al. (2012). A differentiation checkpoint limits hematopoietic stem cell self-renewal in response to DNA damage. Cell *148*, 1001–1014.

Watts, K.L., Zhang, X., Beard, B.C., Chiu, S.Y., Trobridge, G.D., Humphries, R.K., and Kiem, H.-P. (2011). Differential effects of HOXB4 and NUP98-HOXA10hd on hematopoietic repopulating cells in a nonhuman primate model. Hum. Gene Ther. *22*, 1475–1482.

Willert, K., Brown, J.D., Danenberg, E., Duncan, A.W., Weissman, I.L., Reya, T., Yates, J.R., and Nusse, R. (2003). Wnt proteins are lipid-modified and can act as stem cell growth factors. Nature *423*, 448–452.

Wilson, A., Laurenti, E., Oser, G., van der Wath, R.C., Blanco-Bose, W., Jaworski, M., Offner, S., Dunant, C.F., Eshkind, L., Bockamp, E., et al. (2008). Hematopoietic Stem Cells Reversibly Switch from Dormancy to Self-Renewal during Homeostasis and Repair. Cell *135*, 1118–1129.

Wilson, N.K., Kent, D.G., Buettner, F., Shehata, M., Macaulay, I.C., Calero-Nieto, F.J., Sánchez Castillo, M., Oedekoven, C.A., Diamanti, E., Schulte, R., et al. (2015). Combined Single-Cell Functional and Gene Expression Analysis Resolves Heterogeneity within Stem Cell Populations. Cell Stem Cell *16*, 712–724.

Wineman, J., Moore, K., Lemischka, I., and Müller-Sieburg, C. (1996). Functional heterogeneity of the hematopoietic microenvironment: rare stromal elements maintain long-term repopulating stem cells. Blood *87*, 4082–4090.

Woehrer, S., Miller, C.L., and Eaves, C.J. (2013). Long-term culture-initiating cell assay for mouse cells. Methods Mol. Biol. Clifton NJ *946*, 257–266.

Wohrer, S., Knapp, D.J.H.F., Copley, M.R., Benz, C., Kent, D.G., Rowe, K., Babovic, S., Mader, H., Oostendorp, R.A.J., and Eaves, C.J. (2014). Distinct Stromal Cell Factor Combinations Can Separately Control Hematopoietic Stem Cell Survival, Proliferation, and Self-Renewal. Cell Rep. *7*, 1956–1967.

Wu, A.M., Till, J.E., Siminovitch, L., and McCulloch, E.A. (1967). A cytological study of the capacity for differentiation of normal hemopoietic colony-forming cells. J. Cell. Physiol. *69*, 177–184.

Wu, A.M., Till, J.E., Siminovitch, L., and McCulloch, E.A. (1968). Cytological Evidence for a Relationship Between Normal Hematopoietic Colony-Forming Cells and Cells of the Lymphoid System. J. Exp. Med. *127*, 455–464.

Wu, C., Jares, A., Winkler, T., Xie, J., Metais, J.-Y., and Dunbar, C.E. (2013). High efficiency restriction enzyme-free linear amplification-mediated polymerase chain reaction approach for tracking lentiviral integration sites does not abrogate retrieval bias. Hum. Gene Ther. *24*, 38–47.

Xie, H., Xu, J., Hsu, J.H., Nguyen, M., Fujiwara, Y., Peng, C., and Orkin, S.H. (2014a). Polycomb repressive complex 2 regulates normal hematopoietic stem cell function in a developmental-stage-specific manner. Cell Stem Cell *14*, 68–80.

Xie, M., Lu, C., Wang, J., McLellan, M.D., Johnson, K.J., Wendl, M.C., McMichael, J.F., Schmidt, H.K., Yellapantula, V., Miller, C.A., et al. (2014b). Age-related mutations associated with clonal hematopoietic expansion and malignancies. Nat. Med. *20*, 1472–1478.

Yamamoto, R., Morita, Y., Ooehara, J., Hamanaka, S., Onodera, M., Rudolph, K.L., Ema, H., and Nakauchi, H. (2013). Clonal Analysis Unveils Self-Renewing Lineage-Restricted Progenitors Generated Directly from Hematopoietic Stem Cells. Cell *154*, 1112–1126.

Yamazaki, S., Iwama, A., Takayanagi, S., Eto, K., Ema, H., and Nakauchi, H. (2009). TGF-beta as a candidate bone marrow niche signal to induce hematopoietic stem cell hibernation. Blood *113*, 1250–1256.

Yeager, A.M., Kaizer, H., Santos, G.W., Saral, R., Colvin, O.M., Stuart, R.K., Braine, H.G., Burke, P.J., Ambinder, R.F., Burns, W.H., et al. (1986). Autologous Bone Marrow Transplantation in Patients with Acute Nonlymphocytic Leukemia, Using ex Vivo Marrow Treatment with 4-Hydroperoxycyclophosphamide. N. Engl. J. Med. *315*, 141–147.

Yellaboina, S., Dudekula, D.B., and Ko, M.S. (2008). Prediction of evolutionarily conserved interologs in Mus musculus. BMC Genomics *9*, 465.

Yoshikawa, Y., Ikebuchi, K., Ohkawara, J., Hirayama, F., Yamaguchi, M., Sato, N., Mori, K.J., Kasai, M., and Sekiguchi, S. (1999). A clonal culture assay for human cord blood lymphohematopoietic progenitors. Hum. Immunol. *60*, 75–82.

Yuan, J., Nguyen, C.K., Liu, X., Kanellopoulou, C., and Muljo, S.A. (2012). Lin28b Reprograms Adult Bone Marrow Hematopoietic Progenitors to Mediate Fetal-Like Lymphopoiesis. Science *335*, 1195–1200.

Zandstra, P.W., Conneally, E., Petzer, A.L., Piret, J.M., and Eaves, C.J. (1997). Cytokine manipulation of primitive human hematopoietic cell self-renewal. Proc. Natl. Acad. Sci. U. S. A. *94*, 4698–4703.

Zandstra, P.W., Conneally, E., Piret, J.M., and Eaves, C.J. (1998). Ontogeny-associated changes in the cytokine responses of primitive human haemopoietic cells. Br. J. Haematol. *101*, 770–778.

Zhang, C.C., and Lodish, H.F. (2004). Insulin-like growth factor 2 expressed in a novel fetal liver cell population is a growth factor for hematopoietic stem cells. Blood *103*, 2513–2521.

Zhang, C.C., Kaba, M., Ge, G., Xie, K., Tong, W., Hug, C., and Lodish, H.F. (2006a). Angiopoietin-like proteins stimulate ex vivo expansion of hematopoietic stem cells. Nat. Med. *12*, 240–245.

Zhang, D.E., Zhang, P., Wang, N.D., Hetherington, C.J., Darlington, G.J., and Tenen, D.G. (1997). Absence of granulocyte colony-stimulating factor signaling and neutrophil development in CCAAT enhancer binding protein alpha-deficient mice. Proc. Natl. Acad. Sci. U. S. A. *94*, 569–574.

Zhang, P., Iwama, A., Datta, M.W., Darlington, G.J., Link, D.C., and Tenen, D.G. (1998). Upregulation of interleukin 6 and granulocyte colony-stimulating factor receptors by transcription factor CCAAT enhancer binding protein alpha (C/EBP alpha) is critical for granulopoiesis. J. Exp. Med. *188*, 1173–1184.

Zhang, X.-B., Beard, B.C., Beebe, K., Storer, B., Humphries, R.K., and Kiem, H.-P. (2006b). Differential effects of HOXB4 on nonhuman primate short- and long-term repopulating cells. PLoS Med. *3*, e173.

Zhang, Y., Harada, A., Bluethmann, H., Wang, J.B., Nakao, S., Mukaida, N., and Matsushima, K. (1995). Tumor necrosis factor (TNF) is a physiologic regulator of hematopoietic progenitor cells: increase of early hematopoietic progenitor cells in TNF receptor p55-deficient mice in vivo and potent inhibition of progenitor cell proliferation by TNF alpha in vitro. Blood *86*, 2930–2937.

Zovein, A.C., Hofmann, J.J., Lynch, M., French, W.J., Turlo, K.A., Yang, Y., Becker, M.S., Zanetta, L., Dejana, E., Gasson, J.C., et al. (2008). Fate Tracing Reveals the Endothelial Origin of Hematopoietic Stem Cells. Cell Stem Cell *3*, 625–636.

Zsebo, K.M., Williams, D.A., Geissler, E.N., Broudy, V.C., Martin, F.H., Atkins, H.L., Hsu, R.Y., Birkett, N.C., Okino, K.H., and Murdock, D.C. (1990a). Stem cell factor is encoded at the Sl locus of the mouse and is the ligand for the c-kit tyrosine kinase receptor. Cell *63*, 213–224.

Zsebo, K.M., Wypych, J., McNiece, I.K., Lu, H.S., Smith, K.A., Karkare, S.B., Sachdev, R.K., Yuschenkoff, V.N., Birkett, N.C., and Williams, L.R. (1990b). Identification, purification, and biological characterization of hematopoietic stem cell factor from buffalo rat liver--conditioned medium. Cell *63*, 195–201.

Zunder, E.R., Lujan, E., Goltsev, Y., Wernig, M., and Nolan, G.P. (2015a). A continuous molecular roadmap to iPSC reprogramming through progression analysis of single-cell mass cytometry. Cell Stem Cell *16*, 323–337.

Zunder, E.R., Finck, R., Behbehani, G.K., Amir, E.-A.D., Krishnaswamy, S., Gonzalez, V.D., Lorang, C.G., Bjornson, Z., Spitzer, M.H., Bodenmiller, B., et al. (2015b). Palladium-based mass tag cell barcoding with a doublet-filtering scheme and single-cell deconvolution algorithm. Nat. Protoc. *10*, 316–333.

# Appendices

## Appendix A

### A.1 REACTOME pathways (n=250) with significantly altered transcript expression in ESLAM cells maintained in S+11+UG26 CM.

| Pathway | Gene No. | P value |
|---|---|---|
| ADP SIGNALLING THROUGH P2Y PURINOCEPTOR 1 | 25 | 9.9999E-06 |
| APOPTOSIS | 122 | 9.9999E-06 |
| AUTODEGRADATION OF CDH1 BY CDH1 APC | 53 | 9.9999E-06 |
| AXON GUIDANCE | 156 | 9.9999E-06 |
| BRANCHED CHAIN AMINO ACID CATABOLISM | 17 | 9.9999E-06 |
| CD28 DEPENDENT VAV1 PATHWAY | 11 | 9.9999E-06 |
| CDC20 PHOSPHO APC MEDIATED DEGRADATION OF CYCLIN A | 59 | 9.9999E-06 |
| CDT1 ASSOCIATION WITH THE CDC6 ORC ORIGIN COMPLEX | 48 | 9.9999E-06 |
| CELL CYCLE CHECKPOINTS | 104 | 9.9999E-06 |
| CELL CYCLE MITOTIC | 292 | 9.9999E-06 |
| CELL SURFACE INTERACTIONS AT THE VASCULAR WALL | 89 | 9.9999E-06 |
| CENTROSOME MATURATION | 67 | 9.9999E-06 |
| CITRIC ACID CYCLE | 18 | 9.9999E-06 |
| CLATHRIN DERIVED VESICLE BUDDING | 56 | 9.9999E-06 |
| COSTIMULATION BY THE CD28 FAMILY | 60 | 9.9999E-06 |
| CYCLIN E ASSOCIATED EVENTS DURING G1 S TRANSITION | 54 | 9.9999E-06 |
| DARPP32 EVENTS | 25 | 9.9999E-06 |
| DIABETES PATHWAYS | 292 | 9.9999E-06 |
| DNA REPAIR | 98 | 9.9999E-06 |
| DNA REPLICATION PRE INITIATION | 71 | 9.9999E-06 |
| DOUBLE STRAND BREAK REPAIR | 21 | 9.9999E-06 |
| DOWN STREAM SIGNAL TRANSDUCTION | 35 | 9.9999E-06 |
| DOWNSTREAM TCR SIGNALING | 36 | 9.9999E-06 |
| ELECTRON TRANSPORT CHAIN | 56 | 9.9999E-06 |
| ELONGATION AND PROCESSING OF CAPPED TRANSCRIPTS | 109 | 9.9999E-06 |
| FORMATION AND MATURATION OF MRNA TRANSCRIPT | 127 | 9.9999E-06 |
| FORMATION OF A POOL OF FREE 40S SUBUNITS | 40 | 9.9999E-06 |
| FORMATION OF ATP BY CHEMIOSMOTIC COUPLING | 10 | 9.9999E-06 |
| FORMATION OF PLATELET PLUG | 180 | 9.9999E-06 |
| FORMATION OF THE TERNARY COMPLEX AND SUBSEQUENTLY THE 43S COMPLEX | 27 | 9.9999E-06 |

| Pathway | Gene No. | P value |
|---|---|---|
| FURTHER PLATELET RELEASATE | 22 | 9.9999E-06 |
| G1 S TRANSITION | 95 | 9.9999E-06 |
| G2 M TRANSITION | 79 | 9.9999E-06 |
| GENE EXPRESSION | 341 | 9.9999E-06 |
| GENERIC TRANSCRIPTION PATHWAY | 35 | 9.9999E-06 |
| GLOBAL GENOMIC NER | 32 | 9.9999E-06 |
| GLUCONEOGENESIS | 27 | 9.9999E-06 |
| GLUCOSE METABOLISM | 51 | 9.9999E-06 |
| GLUCOSE REGULATION OF INSULIN SECRETION | 130 | 9.9999E-06 |
| GLYCOGEN BREAKDOWN GLYCOGENOLYSIS | 15 | 9.9999E-06 |
| GLYCOLYSIS | 19 | 9.9999E-06 |
| GOLGI ASSOCIATED VESICLE BIOGENESIS | 50 | 9.9999E-06 |
| GRB2 SOS PROVIDES LINKAGE TO MAPK SIGNALING FOR INTERGRINS | 15 | 9.9999E-06 |
| GTP HYDROLYSIS AND JOINING OF THE 60S RIBOSOMAL SUBUNIT | 50 | 9.9999E-06 |
| HEMOSTASIS | 264 | 9.9999E-06 |
| HIV INFECTION | 169 | 9.9999E-06 |
| HIV LIFE CYCLE | 98 | 9.9999E-06 |
| HIV1 TRANSCRIPTION INITIATION | 38 | 9.9999E-06 |
| HOST INTERACTIONS OF HIV FACTORS | 109 | 9.9999E-06 |
| INFLUENZA LIFE CYCLE | 80 | 9.9999E-06 |
| INFLUENZA VIRAL RNA TRANSCRIPTION AND REPLICATION | 44 | 9.9999E-06 |
| INSULIN SYNTHESIS AND SECRETION | 72 | 9.9999E-06 |
| INTEGRATION OF ENERGY METABOLISM | 198 | 9.9999E-06 |
| INTEGRIN CELL SURFACE INTERACTIONS | 80 | 9.9999E-06 |
| LATE PHASE OF HIV LIFE CYCLE | 87 | 9.9999E-06 |
| LOSS OF NLP FROM MITOTIC CENTROSOMES | 60 | 9.9999E-06 |
| M G1 TRANSITION | 57 | 9.9999E-06 |
| MEMBRANE TRAFFICKING | 73 | 9.9999E-06 |
| METABLISM OF NUCLEOTIDES | 70 | 9.9999E-06 |
| METABOLISM OF CARBOHYDRATES | 109 | 9.9999E-06 |
| METABOLISM OF PROTEINS | 153 | 9.9999E-06 |
| MITOTIC PROMETAPHASE | 89 | 9.9999E-06 |
| MRNA 3 END PROCESSING | 22 | 9.9999E-06 |
| MRNA PROCESSING | 31 | 9.9999E-06 |
| MRNA SPLICING | 83 | 9.9999E-06 |
| MRNA SPLICING MINOR PATHWAY | 32 | 9.9999E-06 |
| NCAM SIGNALING FOR NEURITE OUT GROWTH | 67 | 9.9999E-06 |
| NCAM1 INTERACTIONS | 43 | 9.9999E-06 |
| NUCLEAR IMPORT OF REV PROTEIN | 29 | 9.9999E-06 |
| NUCLEOTIDE EXCISION REPAIR | 47 | 9.9999E-06 |
| OPIOID SIGNALLING | 82 | 9.9999E-06 |
| ORC1 REMOVAL FROM CHROMATIN | 59 | 9.9999E-06 |

| Pathway | Gene No. | P value |
|---|---|---|
| OTHER SEMAPHORIN INTERACTIONS | 15 | 9.9999E-06 |
| P38MAPK EVENTS | 13 | 9.9999E-06 |
| P53 INDEPENDENT DNA DAMAGE RESPONSE | 39 | 9.9999E-06 |
| PEPTIDE CHAIN ELONGATION | 31 | 9.9999E-06 |
| PLATELET ACTIVATION | 161 | 9.9999E-06 |
| PLATELET ACTIVATION TRIGGERS | 58 | 9.9999E-06 |
| PLATELET DEGRANULATION | 82 | 9.9999E-06 |
| PREFOLDIN MEDIATED TRANSFER OF SUBSTRATE TO CCT TRIC | 24 | 9.9999E-06 |
| PROCESSING OF CAPPED INTRON CONTAINING PRE MRNA | 113 | 9.9999E-06 |
| PYRUVATE METABOLISM AND TCA CYCLE | 35 | 9.9999E-06 |
| REGULATION OF APC ACTIVATORS BETWEEN G1 S AND EARLY ANAPHASE | 66 | 9.9999E-06 |
| REGULATION OF BETA CELL DEVELOPMENT | 62 | 9.9999E-06 |
| REGULATION OF GENE EXPRESSION IN BETA CELLS | 48 | 9.9999E-06 |
| REGULATION OF INSULIN SECRETION | 180 | 9.9999E-06 |
| REGULATION OF INSULIN SECRETION BY GLUCAGON LIKE PEPTIDE 1 | 59 | 9.9999E-06 |
| REGULATION OF ORNITHINE DECARBOXYLASE | 43 | 9.9999E-06 |
| REV MEDIATED NUCLEAR EXPORT OF HIV1 RNA | 30 | 9.9999E-06 |
| RHO GTPASE CYCLE | 120 | 9.9999E-06 |
| RNA POL II CTD PHOSPHORYLATION AND INTERACTION WITH CE | 25 | 9.9999E-06 |
| RNA POLYMERASE I CHAIN ELONGATION | 20 | 9.9999E-06 |
| RNA POLYMERASE I PROMOTER ESCAPE | 20 | 9.9999E-06 |
| RNA POLYMERASE I TRANSCRIPTION INITIATION | 24 | 9.9999E-06 |
| RNA POLYMERASE I TRANSCRIPTION TERMINATION | 21 | 9.9999E-06 |
| RNA POLYMERASE II TRANSCRIPTION | 78 | 9.9999E-06 |
| S PHASE | 98 | 9.9999E-06 |
| SCF BETA TRCP MEDIATED DEGRADATION OF EMI1 | 44 | 9.9999E-06 |
| SCF SKP2 MEDIATED DEGRADATION OF P27 P21 | 48 | 9.9999E-06 |
| SEMA3A PAK DEPENDENT AXON REPULSION | 13 | 9.9999E-06 |
| SEMA4D IN SEMAPHORIN SIGNALING | 28 | 9.9999E-06 |
| SEMA4D INDUCED CELL MIGRATION AND GROWTH CONE COLLAPSE | 23 | 9.9999E-06 |
| SEMAPHORIN INTERACTIONS | 63 | 9.9999E-06 |
| SHC MEDIATED SIGNALLING | 12 | 9.9999E-06 |
| SIGNALING BY PDGF | 63 | 9.9999E-06 |
| SIGNALING BY TGF BETA | 15 | 9.9999E-06 |
| SIGNALING BY WNT | 54 | 9.9999E-06 |
| SIGNALING IN IMMUNE SYSTEM | 294 | 9.9999E-06 |
| SIGNALLING BY NGF | 208 | 9.9999E-06 |
| SIGNALLING TO ERKS | 34 | 9.9999E-06 |
| SIGNALLING TO RAS | 26 | 9.9999E-06 |
| SNRNP ASSEMBLY | 45 | 9.9999E-06 |
| SOS MEDIATED SIGNALLING | 13 | 9.9999E-06 |

| Pathway | Gene No. | P value |
|---|---|---|
| SYNTHESIS OF DNA | 84 | 9.9999E-06 |
| TCR SIGNALING | 53 | 9.9999E-06 |
| TIE2 SIGNALING | 18 | 9.9999E-06 |
| TRAF6 MEDIATED INDUCTION OF THE ANTIVIRAL CYTOKINE IFN ALPHA BETA CASCADE | 52 | 9.9999E-06 |
| TRANSCRIPTION | 146 | 9.9999E-06 |
| TRANSCRIPTION OF THE HIV GENOME | 57 | 9.9999E-06 |
| TRANSLATION | 64 | 9.9999E-06 |
| TRANSLATION INITIATION COMPLEX FORMATION | 33 | 9.9999E-06 |
| TRANSMISSION ACROSS CHEMICAL SYNAPSES | 127 | 9.9999E-06 |
| TRANSPORT OF MATURE MRNA DERIVED FROM AN INTRON CONTAINING TRANSCRIPT | 39 | 9.9999E-06 |
| TRKA SIGNALLING FROM THE PLASMA MEMBRANE | 102 | 9.9999E-06 |
| VIF MEDIATED DEGRADATION OF APOBEC3G | 42 | 9.9999E-06 |
| VIRAL MRNA TRANSLATION | 30 | 9.9999E-06 |
| VPR MEDIATED NUCLEAR IMPORT OF PICS | 30 | 9.9999E-06 |
| PP2A MEDIATED DEPHOSPHORYLATION OF KEY METABOLIC FACTORS | 10 | 9.9999E-06 |
| SYNTHESIS AND INTERCONVERSION OF NUCLEOTIDE DI AND TRIPHOSPHATES | 18 | 9.9999E-06 |
| TRANSPORT OF RIBONUCLEOPROTEINS INTO THE HOST NUCLEUS | 28 | 9.9999E-06 |
| GLUCOSE TRANSPORT | 37 | 9.9999E-06 |
| MRNA DECAY BY 5 TO 3 EXORIBONUCLEASE | 12 | 9.9999E-06 |
| REGULATION OF GLUCOKINASE BY GLUCOKINASE REGULATORY PROTEIN | 28 | 9.9999E-06 |
| STABILIZATION OF P53 | 41 | 9.9999E-06 |
| DEPOLARIZATION OF THE PRESYNAPTIC TERMINAL TRIGGERS THE OPENING OF CALCIUM CHANNELS | 12 | 9.9999E-06 |
| INHIBITION OF INSULIN SECRETION BY ADRENALINE NORADRENALINE | 30 | 9.9999E-06 |
| MRNA DECAY BY 3 TO 5 EXORIBONUCLEASE | 10 | 9.9999E-06 |
| NEP NS2 INTERACTS WITH THE CELLULAR EXPORT MACHINERY | 28 | 9.9999E-06 |
| RNA POLYMERASE I III AND MITOCHONDRIAL TRANSCRIPTION | 82 | 9.9999E-06 |
| TRANSPORT OF THE SLBP INDEPENDENT MATURE MRNA | 31 | 9.9999E-06 |
| SMOOTH MUSCLE CONTRACTION | 23 | 9.9999E-06 |
| METABOLISM OF MRNA | 42 | 9.9999E-06 |
| METABOLISM OF RNA | 87 | 9.9999E-06 |
| MITOTIC M M G1 PHASES | 150 | 9.9999E-06 |
| APCDC20 MEDIATED DEGRADATION OF CYCLIN B | 16 | 1.99998E-05 |
| CHAPERONIN MEDIATED PROTEIN FOLDING | 45 | 1.99998E-05 |
| FORMATION OF TUBULIN FOLDING INTERMEDIATES BY CCT TRIC | 17 | 1.99998E-05 |
| INACTIVATION OF APC VIA DIRECT INHIBITION OF THE | 18 | 1.99998E-05 |

| Pathway | Gene No. | P value |
|---|---|---|
| APCOMPLEX | | |
| GRB2 EVENTS IN EGFR SIGNALING | 13 | 2.99997E-05 |
| HIV1 TRANSCRIPTION ELONGATION | 39 | 2.99997E-05 |
| P75 NTR RECEPTOR MEDIATED SIGNALLING | 78 | 2.99997E-05 |
| RNA POLYMERASE I PROMOTER CLEARANCE | 49 | 2.99997E-05 |
| SEMA3A PLEXIN REPULSION SIGNALING BY INHIBITING INTEGRIN ADHESION | 13 | 2.99997E-05 |
| DUAL INCISION REACTION IN GG NER | 20 | 3.99996E-05 |
| SIGNAL AMPLIFICATION | 31 | 5.99994E-05 |
| LYSOSOME VESICLE BIOGENESIS | 22 | 6.99993E-05 |
| MTOR SIGNALLING | 26 | 6.99993E-05 |
| MUSCLE CONTRACTION | 50 | 8.99991E-05 |
| MAP KINASES ACTIVATION IN TLR CASCADE | 44 | 0.000109999 |
| METABOLISM OF AMINO ACIDS | 152 | 0.000119999 |
| TRANSCRIPTION COUPLED NER | 42 | 0.000129999 |
| PHOSPHORYLATION OF THE APC | 16 | 0.000149999 |
| DUAL INCISION REACTION IN TC NER | 27 | 0.000159998 |
| RNA POLYMERASE III TRANSCRIPTION TERMINATION | 16 | 0.000159998 |
| TOLL RECEPTOR CASCADES | 83 | 0.000209998 |
| G ALPHA 12 13 SIGNALLING EVENTS | 54 | 0.000259997 |
| HORMONE BIOSYNTHESIS | 48 | 0.000289997 |
| TOLL LIKE RECEPTOR 3 CASCADE | 58 | 0.000339997 |
| EXTENSION OF TELOMERES | 26 | 0.000369996 |
| CONVERSION FROM APC CDC20 TO APC CDH1 IN LATE ANAPHASE | 17 | 0.000419996 |
| CYCLIN A1 ASSOCIATED EVENTS DURING G2 M TRANSITION | 14 | 0.000419996 |
| MYOGENESSIS | 28 | 0.000419996 |
| CRMPS IN SEMA3A SIGNALING | 15 | 0.000689993 |
| ENERGY DEPENDENT REGULATION OF MTOR BY LKB1 AMPK | 17 | 0.000689993 |
| PURINE RIBONUCLEOSIDE MONOPHOSPHATE BIOSYNTHESIS | 11 | 0.000729993 |
| REGULATION OF AMPK ACTIVITY VIA LKB1 | 14 | 0.000949991 |
| SIGNALLING TO P38 VIA RIT AND RIN | 14 | 0.00099999 |
| SHC RELATED EVENTS | 14 | 0.00104999 |
| ACTIVATION OF ATR IN RESPONSE TO REPLICATION STRESS | 37 | 0.001199988 |
| NEURORANSMITTER RECEPTOR BINDING AND DOWNSTREAM TRANSMISSION IN THE POSTSYNAPTIC CELL | 81 | 0.001329987 |
| P130CAS LINKAGE TO MAPK SIGNALING FOR INTEGRINS | 15 | 0.001429986 |
| IRS RELATED EVENTS | 78 | 0.001439986 |
| COLLAGEN MEDIATED ACTIVATION CASCADE | 22 | 0.001879981 |
| PD1 SIGNALING | 19 | 0.002419976 |
| DNA STRAND ELONGATION | 30 | 0.002529975 |

| Pathway | Gene No. | P value |
|---|---|---|
| ACTIVATION OF NMDA RECEPTOR UPON GLUTAMATE BINDING AND POSTSYNAPTIC EVENTS | 35 | 0.002779972 |
| POST NMDA RECEPTOR ACTIVATION EVENTS | 31 | 0.00297997 |
| ACTIVATION OF KAINATE RECEPTORS UPON GLUTAMATE BINDING | 32 | 0.003079969 |
| UNFOLDED PROTEIN RESPONSE | 18 | 0.003359966 |
| COPI MEDIATED TRANSPORT | 10 | 0.003579964 |
| IONOTROPIC ACTIVITY OF KAINATE RECEPTORS | 12 | 0.003679963 |
| G BETA GAMMA SIGNALLING THROUGH PI3KGAMMA | 25 | 0.004239958 |
| ASSOCIATION OF TRIC CCT WITH TARGET PROTEINS DURING BIOSYNTHESIS | 29 | 0.004539955 |
| FRS2 MEDIATED ACTIVATION | 16 | 0.004679953 |
| SIGNALING BY EGFR | 46 | 0.004809952 |
| MAPK TARGETS NUCLEAR EVENTS MEDIATED BY MAP KINASES | 30 | 0.005239948 |
| FANCONI ANEMIA PATHWAY | 14 | 0.005269947 |
| NOREPINEPHRINE NEUROTRANSMITTER RELEASE CYCLE | 12 | 0.005859941 |
| UNWINDING OF DNA | 11 | 0.006569934 |
| G PROTEIN ACTIVATION | 28 | 0.007599924 |
| HOMOLOGOUS RECOMBINATION REPAIR | 15 | 0.007729923 |
| POST CHAPERONIN TUBULIN FOLDING PATHWAY | 14 | 0.007929921 |
| INNATE IMMUNITY SIGNALING | 102 | 0.008489915 |
| FORMATION OF THE EARLY ELONGATION COMPLEX | 30 | 0.008569914 |
| ERKS ARE INACTIVATED | 12 | 0.008609914 |
| G PROTEIN BETA GAMMA SIGNALLING | 28 | 0.00895991 |
| THROMBOXANE SIGNALLING THROUGH TP RECEPTOR | 23 | 0.009259907 |
| CYTOSOLIC TRNA AMINOACYLATION | 23 | 0.009319907 |
| THROMBIN SIGNALLING THROUGH PROTEINASE ACTIVATED RECEPTORS | 27 | 0.009469905 |
| ACTIVATION OF THE PRE REPLICATIVE COMPLEX | 29 | 0.009619904 |
| SIGNALING BY VEGF | 11 | 0.009619904 |
| INTEGRIN ALPHAIIBBETA3 SIGNALING | 23 | 0.009699903 |
| CAM PATHWAY | 25 | 0.009899901 |
| POST TRANSLATIONAL PROTEIN MODIFICATION | 39 | 0.009939901 |
| CELL DEATH SIGNALLING VIA NRAGE NRIF AND NADE | 58 | 0.0100299 |
| NOTCH HLH TRANSCRIPTION PATHWAY | 13 | 0.010729893 |
| PLC BETA MEDIATED EVENTS | 37 | 0.011629884 |
| G1 PHASE | 16 | 0.012059879 |
| ACTIVATION OF THE AP1 FAMILY OF TRANSCRIPTION FACTORS | 10 | 0.012179878 |
| NUCLEAR EVENTS KINASE AND TRANSCRIPTION FACTOR ACTIVATION | 24 | 0.014819852 |
| CD28 CO STIMULATION | 29 | 0.01495985 |
| RECRUITMENT OF NUMA TO MITOTIC CENTROSOMES | 9 | 0.015909841 |
| INTRINSIC PATHWAY FOR APOPTOSIS | 28 | 0.016219838 |
| EARLY PHASE OF HIV LIFE CYCLE | 11 | 0.016759832 |

| Pathway | Gene No. | P value |
|---|---|---|
| REGULATION OF LIPID METABOLISM BY PEROXISOME PROLIFERATOR ACTIVATED RECEPTOR ALPHA | 59 | 0.017239828 |
| METABOLISM OF NITRIC OXIDE | 12 | 0.017549825 |
| ACTIVATED AMPK STIMULATES FATTY ACID OXIDATION IN MUSCLE | 17 | 0.018879811 |
| STEROID HORMONE BIOSYNTHESIS | 12 | 0.020779792 |
| GLUCAGON TYPE LIGAND RECEPTORS | 33 | 0.020829792 |
| G2 M CHECKPOINTS | 42 | 0.021099789 |
| PURINE METABOLISM | 30 | 0.023589764 |
| RNA POLYMERASE III TRANSCRIPTION | 32 | 0.024209758 |
| PLC GAMMA1 SIGNALLING | 34 | 0.024369756 |
| RNA POLYMERASE III TRANSCRIPTION INITIATION FROM TYPE 3 PROMOTER | 21 | 0.025379746 |
| EGFR DOWNREGULATION | 22 | 0.026479735 |
| NRAGE SIGNALS DEATH THROUGH JNK | 47 | 0.026749733 |
| ERK MAPK TARGETS | 21 | 0.02903971 |
| TAT MEDIATED HIV1 ELONGATION ARREST AND RECOVERY | 28 | 0.030679693 |
| ADP SIGNALLING THROUGH P2Y PURINOCEPTOR 12 | 21 | 0.030729693 |
| STEROID HORMONES | 19 | 0.030919691 |
| PI3K AKT SIGNALLING | 37 | 0.031249688 |
| G BETA GAMMA SIGNALLING THROUGH PLC BETA | 20 | 0.031289687 |
| CTLA4 INHIBITORY SIGNALING | 21 | 0.035129649 |
| ACTIVATION OF RAC | 14 | 0.035659643 |
| RAS ACTIVATION UOPN CA2+ INFUX THROUGH NMDA RECEPTOR | 17 | 0.036129639 |
| ACTIVATION OF CHAPERONES BY IRE1 ALPHA | 9 | 0.042199578 |
| POLYMERASE SWITCHING | 13 | 0.042259577 |
| MTORC1 MEDIATED SIGNALLING | 10 | 0.044689553 |
| CD28 DEPENDENT PI3K AKT SIGNALING | 19 | 0.046469535 |
| RNA POLYMERASE III CHAIN ELONGATION | 11 | 0.047679523 |

## A.2 Secreted factor mRNAs (n=172) produced by UG26 cells with predicted interactions with the products of genes expressed by activated ESLAM cells.

| Entrez Gene ID | Gene Symbol | Mean Intensity($Log_2$) | Receptor(s) |
|---|---|---|---|
| 16785 | Rpsa | 13.23 | Atp5b, Csf2ra, Itga6, Kdelr1 |
| 16852 | Lgals1 | 13.20 | Cd7, Lgals3bp, Susd2 |
| 16952 | Anxa1 | 12.77 | Fpr1, Trpm7 |
| 15481 | Hspa8 | 12.59 | Grb2, Irs1, Cxcr4, Ripk2,Ncor1,Tnfrsf1a, Tnfrsf1b, Cd40, Traf1, Traf2, Atp9b, Ripk3, Kdelr1, Myd88 |
| 16854 | Lgals3 | 12.42 | Lgals3bp, Cubn, Ncoa3 |

| | | | |
|---|---|---|---|
| 14683 | Gnas | 12.32 | Grin2b |
| 23980 | Pebp1 | 12.29 | Adrbk1, Ppard, Nr2c2 |
| 17319 | Mif | 12.22 | Cd74, Tnfrsf14 |
| 14456 | Gas6 | 12.18 | Mertk, Tyro3 |
| 12261 | C1qbp | 12.14 | Gab1, Gabrb1, Tnfrsf1a, Tnfrsf1b, Traf1, Ripk3 |
| 22166 | Txn1 | 12.12 | Nr3c1 |
| 12631 | Cfl1 | 12.11 | Grb2 |
| 15519 | Hsp90aa1 | 12.03 | Alk, Ahr, Aip, Ar, Asgr1, Arntl, Esr1, Nr3c1, Nr3c2, Kdr, Ppara, Tnfrsf1a, Nr2c2, Traf1, Traf2, Ripk3, Ripk2 |
| 227753 | Gsn | 11.86 | Ar, Grb2, Grin2b |
| 12306 | Anxa2 | 11.85 | Grb2 |
| 14219 | Ctgf | 11.85 | Erbb4, Lrp1, Itga5 |
| 14115 | Fbln2 | 11.77 | Itgb3, Nsd1 |
| 18787 | Serpine1 | 11.74 | Lrp2, Lrp1, Thbd, Vtn, Lrp1b |
| 21858 | Timp2 | 11.70 | Itga3, Pgrmc1 |
| 18073 | Nid1 | 11.55 | Itgav, Itgb3, Lgals3bp, Ptprf, Notch1 |
| 12010 | B2m | 11.45 | Fcgrt, Tfrc |
| 19156 | Psap | 11.37 | Celsr1 |
| 21825 | Thbs1 | 11.01 | Cd36, Scarb2, Lrp1, Lrp5, Itgb3, Tnfrsf11b |
| 12317 | Calr | 10.96 | Ar, Nr3c1, Itga2b, Itga3, Itgav, Lrp1 |
| 12847 | Copa | 10.88 | Pdgfrb, Mtnr1b |
| 20315 | Cxcl12 | 10.78 | Cxcr4, Cxcr7, Dpp4 |
| 12827 | Col4a2 | 10.78 | Cd44, Cd93, Antxr2 |
| 21859 | Timp3 | 10.69 | Kdr |
| 12826 | Col4a1 | 10.68 | Cd44, Cd93 |
| 14828 | Hspa5 | 10.65 | Atp5b, Scarb2, Htr3a, Ldlr, Grb2, Gria1, Tnfrsf1a, Tnfrsf1b, Traf2, Mtnr1b, Ripk3, Myd88 |
| 12833 | Col6a1 | 10.61 | Cd44, Lgals3bp |
| 20296 | Ccl2 | 10.52 | Ccr2 |
| 12842 | Col1a1 | 10.47 | Cd44, Cd36, Itga2, Itga5, Cd93, Ddr2 |
| 231887 | Pdap1 | 10.39 | Pdgfrb |
| 13024 | Ctla2a | 10.29 | Tinagl1 |
| 16423 | Cd47 | 10.29 | Itgav, P2ry2 |
| 14751 | Gpi1 | 10.25 | Amfr |
| 12331 | Cap1 | 10.18 | Traf3 |
| 13722 | Aimp1 | 10.17 | Slc20a1 |
| 17387 | Mmp14 | 10.13 | Lrp1, Itgav |
| 12832 | Col5a2 | 10.06 | Cd44 |
| 14205 | Figf | 9.97 | Kdr, Flt4, Itga9 |
| 13003 | Vcan | 9.97 | Itga4 |
| 21814 | Tgfbr3 | 9.96 | Acvr2a, Tgfbr2, Tgfbr1 |
| 56348 | Hsd17b12 | 9.93 | Slc7a1 |
| 14268 | Fn1 | 9.91 | Cd44 |
| 14313 | Fst | 9.85 | Spsb1 |
| 16007 | Cyr61 | 9.74 | Itgav |
| 12977 | Csf1 | 9.67 | Csf1r, Celsr3, Slc7a1, Myd88 |
| 20306 | Ccl7 | 9.63 | Ccr2, Ccr1, Ccr1l1 |

| | | | |
|---|---|---|---|
| 226519 | Lamc1 | 9.47 | Cd44, Sv2a, Sv2b, Sv2c |
| 14825 | Cxcl1 | 9.31 | Cxcr2 |
| 21923 | Tnc | 9.28 | Itga9, Itga5, Itgb6, Ptprb, Itga8 |
| 12843 | Col1a2 | 9.26 | Cd44, Cd36, Itga2, Itga2b, Itgb3, Cd93 |
| 57914 | Crlf2 | 9.23 | Il7r |
| 19242 | Ptn | 9.23 | Alk, Gnb2l1, Ptprb, Ptprz1, Ryr1 |
| 22341 | Vegfc | 9.20 | Kdr, Flt4 |
| 14423 | Galnt1 | 9.18 | Ptprf |
| 21826 | Thbs2 | 9.13 | Cd36 |
| 15530 | Hspg2 | 9.08 | Itga2 |
| 16779 | Lamb2 | 9.00 | Cd44, Sv2a, Sv2b, Sv2c |
| 20377 | Sfrp1 | 8.92 | Fzd6 |
| 12834 | Col6a2 | 8.87 | Cd44 |
| 16323 | Inhba | 8.76 | Acvr2a, Acvr2b, Acvr1, Tgfbr3 |
| 12830 | Col4a5 | 8.75 | Cd44, Cd93 |
| 53381 | Prdx4 | 8.71 | Atp5b |
| 19039 | Lgals3bp | 8.65 | Phb2 |
| 54635 | Pdgfc | 8.63 | Pdgfra |
| 12159 | Bmp4 | 8.59 | Bmpr1a, Bmpr1b, Bmpr2 |
| 16412 | Itgb1 | 8.56 | Ptch2 |
| 76737 | Creld2 | 8.54 | Chrna4, Chrnb2 |
| 22340 | Vegfb | 8.50 | Flt1, Nrp1 |
| 110611 | Hdlbp | 8.49 | Gnb2l1, Ptch2 |
| 12831 | Col5a1 | 8.42 | Cd44, Lgals3bp |
| 20348 | Sema3c | 8.41 | Nrp1 |
| 19128 | Pros1 | 8.41 | Tyro3 |
| 18590 | Pdgfa | 8.40 | Pdgfra |
| 16777 | Lamb1 | 8.39 | Cd44, Sv2a, Sv2b, Sv2c |
| 14178 | Fgf7 | 8.38 | Fgfr3, Fgfr4, Nrp1 |
| 13138 | Dag1 | 8.23 | Grb2, Rapsn, Musk |
| 11883 | Arsa | 8.23 | Bmpr2 |
| 12931 | Crlf1 | 8.22 | Cntfr |
| 13874 | Ereg | 8.19 | Erbb4 |
| 14600 | Ghr | 8.14 | Grb2, Irs1, Ncoa6 |
| 18208 | Ntn1 | 8.09 | Adora2b, Dcc, Neo1, Unc5c |
| 56213 | Htra1 | 7.98 | Grb2 |
| 17311 | Kitl | 7.89 | Kit |
| 21803 | Tgfb1 | 7.85 | Acvrl1, Itgav, Itgb6, Tgfbr1, Tgfbr2, Tgfbr3, Vtn |
| 16956 | Lpl | 7.85 | Lrp2, Lrp1 |
| 13614 | Edn1 | 7.85 | Ednra, Ednrb |
| 17295 | Met | 7.81 | Grb2, Gab1, Ptprb, Ptprj, Spsb1, Itgb4, Plxnb1 |
| 11535 | Adm | 7.76 | Calcrl, Gpr182 |
| 12837 | Col8a1 | 7.71 | Itga1, Itga2, Efemp2 |
| 22418 | Wnt5a | 7.70 | Fzd1, Fzd5, Ror2, Lrp6, Ryk |
| 13038 | Ctsk | 7.70 | Fgfr3 |
| 15200 | Hbegf | 7.63 | Erbb4 |

| | | | |
|---|---|---|---|
| 17388 | Mmp15 | 7.53 | Lrp1 |
| 12064 | Bdnf | 7.52 | Esr1, Sort1 |
| 114249 | Npnt | 7.49 | Itga8 |
| 16835 | Ldlr | 7.40 | Ldlrap1, Lrpap1, Flt1 |
| 12825 | Col3a1 | 7.36 | Cd44, Ddr2 |
| 433375 | Creg1 | 7.33 | Igf2r |
| 11486 | Ada | 7.27 | Adora1, Adora2a, Adora2b, Dpp4, Drd1a, Grb2, Nr3c1 |
| 20563 | Slit2 | 7.26 | Robo2 |
| 16880 | Lifr | 7.23 | Cntfr, Il31ra |
| 12822 | Col18a1 | 7.23 | Kdr, Itga5 |
| 20564 | Slit3 | 7.17 | Robo2 |
| 30878 | Apln | 7.14 | Aplnr |
| 15925 | Ide | 7.13 | Ar, Nr3c1 |
| 100952 | Emilin1 | 7.11 | Tgfbr2 |
| 16194 | Il6ra | 7.00 | Erap1 |
| 16403 | Itga6 | 6.99 | Cd36, Grb2, Itgb4 |
| 19206 | Ptch1 | 6.97 | Smo |
| 11826 | Aqp1 | 6.94 | Trip6, Efemp2 |
| 67573 | Loxl4 | 6.89 | Trip13 |
| 21827 | Thbs3 | 6.88 | Cd36 |
| 12475 | Cd14 | 6.87 | Tlr3, Itgb2, Lgals3bp, Tlr4, Tlr2, Itgam |
| 20210 | Saa3 | 6.71 | Fpr1 |
| 20350 | Sema3f | 6.68 | Nrp1 |
| 11491 | Adam17 | 6.66 | Erbb4, Notch1, Ptpn3 |
| 94216 | Col4a6 | 6.65 | Cd44, Cd93 |
| 16190 | Il4ra | 6.64 | Gnb2l1, Il13ra1, Irs1, Irs2, Cd40 |
| 18049 | Ngf | 6.62 | Sort1, Ngfr, Ntrk1 |
| 20300 | Ccl25 | 6.59 | Ccr9, Ccr10, Ccbp2 |
| 22417 | Wnt4 | 6.57 | Fzd6 |
| 56708 | Clcf1 | 6.54 | Cntfr, Crlf1 |
| 21808 | Tgfb2 | 6.48 | Tgfbr1, Tgfbr2, Tgfbr3, Vtn |
| 21802 | Tgfa | 6.37 | Erbb4, Rhbdf1 |
| 12835 | Col6a3 | 6.30 | Cd44 |
| 20312 | Cx3cl1 | 6.28 | Cx3cr1 |
| 14172 | Fgf18 | 6.23 | Fgfr3, Fgfr4 |
| 20349 | Sema3e | 6.21 | Plxnd1 |
| 13848 | Ephb6 | 6.19 | Grb2, Ephb1 |
| 22339 | Vegfa | 6.14 | Flt1, Kdr, Grin2b |
| 16173 | Il18 | 6.14 | Il1rl2, Il18rap, Il18r1 |
| 16819 | Lcn2 | 6.11 | Lrp2 |
| 53623 | Gria3 | 6.10 | Gria2 |
| 22403 | Wisp2 | 6.07 | Igf1r, Igf2r |
| 22413 | Wnt2 | 6.04 | Fzd1, Fzd9 |
| 17087 | Ly96 | 6.02 | Tlr4, Tlr2 |
| 20310 | Cxcl2 | 5.95 | Cxcr2 |
| 20440 | St6gal1 | 5.94 | Cd22 |

| | | | |
|---|---|---|---|
| 21809 | Tgfb3 | 5.89 | Acvrl1, Tgfbr1, Tgfbr2, Tgfbr3 |
| 18133 | Nov | 5.84 | Notch1 |
| 22042 | Tfrc | 5.79 | Gabarap |
| 16975 | Lrp8 | 5.75 | Grin1 |
| 20660 | Sorl1 | 5.67 | Lrpap1 |
| 11815 | Apod | 5.63 | Lepr, Atp5b, Scarb2 |
| 14566 | Gdf9 | 5.40 | Acvr2a, Bmpr1a, Bmpr1b, Bmpr2 |
| 21950 | Tnfsf9 | 5.24 | Tnfrsf9, Traf1, Traf2 |
| 13214 | Defb1 | 5.23 | Ccr6 |
| 19143 | St14 | 5.19 | F2rl1 |
| 16193 | Il6 | 5.14 | Il6ra, Hrh1 |
| 17082 | Il1rl1 | 5.13 | Myd88 |
| 13636 | Efna1 | 5.10 | Epha1, Epha2, Epha3, Epha4, Epha6, Epha7, Epha8, Ephb1, Tgfbr1 |
| 53867 | Col5a3 | 4.91 | Cd44 |
| 16180 | Il1rap | 4.88 | Irak1, Il1r1 |
| 16878 | Lif | 4.85 | Lifr |
| 20750 | Spp1 | 4.68 | Itga9, Itga5, Itgav |
| 16196 | Il7 | 4.60 | Il7r |
| 18591 | Pdgfb | 4.31 | Pdgfra, Pdgfrb |
| 16169 | Il15ra | 4.30 | Traf2, Il2rb |
| 16000 | Igf1 | 4.26 | Igf1r, Igsf1 |
| 53603 | Tslp | 4.05 | Il7r, Crlf2 |
| 11600 | Angpt1 | 3.90 | Itga5, Tek |
| 12223 | Btc | 3.90 | Erbb4, Egfr |
| 11602 | Angpt4 | 3.76 | Tek |
| 71785 | Pdgfd | 3.38 | Pdgfrb |
| 53604 | Zpbp | 3.34 | Zp2 |
| 110312 | Pmch | 3.24 | Mchr1 |
| 12156 | Bmp2 | 3.22 | Acvr1, Bmpr1b, Bmpr2, Bmpr1a |
| 13645 | Egf | 3.19 | Egfr, Erbb3, Grb2, Vtn |

## Appendix B

**B.1 Additional relative marker intensities of the nearest neighbours for each myeloid CFC type.** Median values are shown as lines. All markers that were not in the top 5 surface or intracellular are shown (significance testing and top 5 marks are shown in Figure 4.11). Differences there did not reach significance are marked with "NS". Surface markers are shown in (A) while intracellular markers are shown in (B).

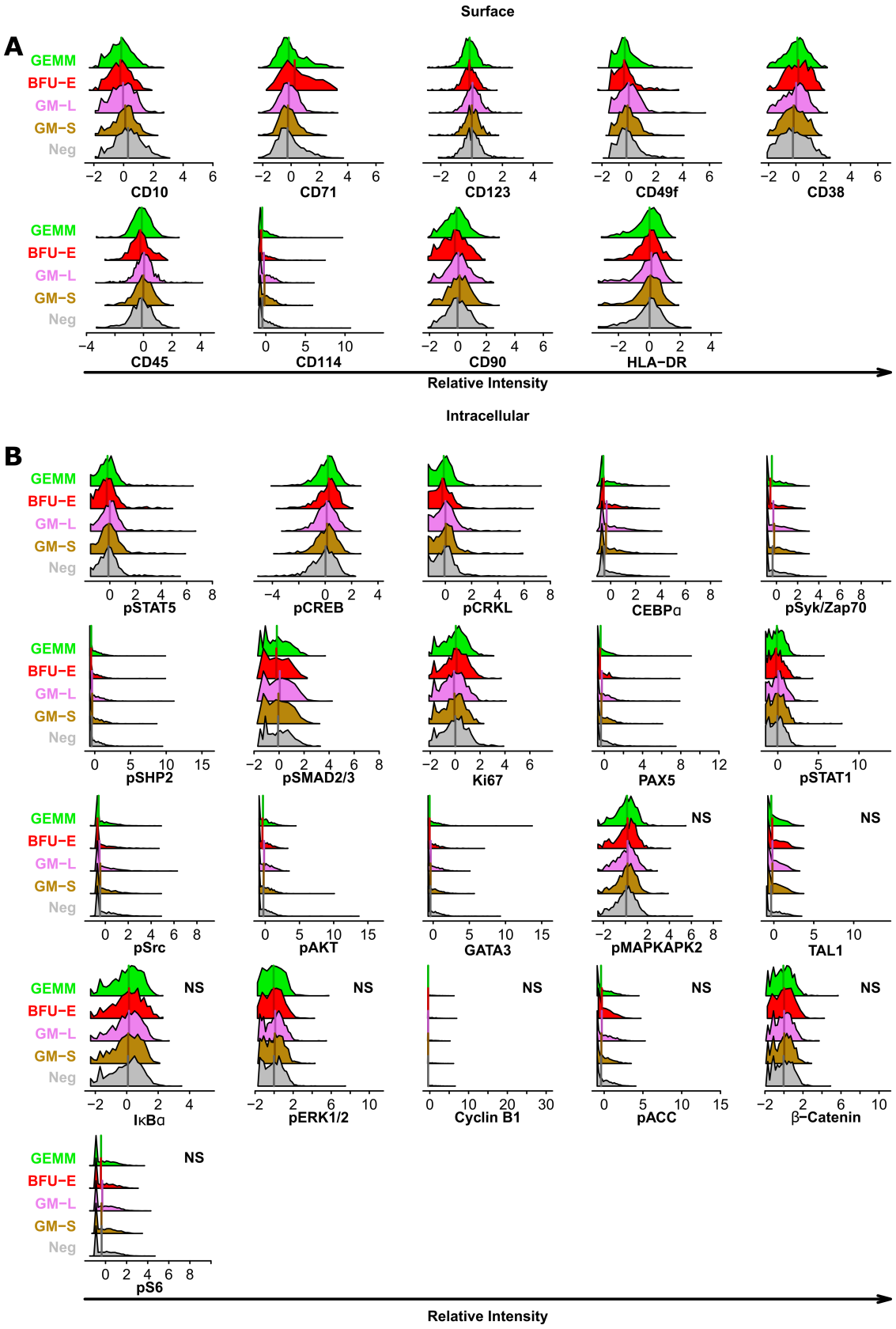
A
Surface
GEMM
BFU-E
GM-L
GM-S
Neg
CD10
CD71
CD123
CD49f
CD38
CD45
CD114
CD90
HLA-DR
Relative Intensity
B
Intracellular
pSTAT5
pCREB
pCRKL
CEBPα
pSyk/Zap70
pSHP2
pSMAD2/3
Ki67
PAX5
pSTAT1
pSrc
pAKT
GATA3
pMAPKAPK2
TAL1
IκBα
pERK1/2
Cyclin B1
pACC
β-Catenin
pS6
NS
Relative Intensity

## B.2 Additional relative marker intensities of the nearest neighbours of highly proliferative LTC-IC compared to all others.

Median values are shown as lines. All markers that were not in the top 5 surface or intracellular are shown (significance testing and top 5 marks are shown in Figure 4.14). Differences there did not reach significance are marked with "NS". Surface markers are shown in (A) while intracellular markers are shown in (B).

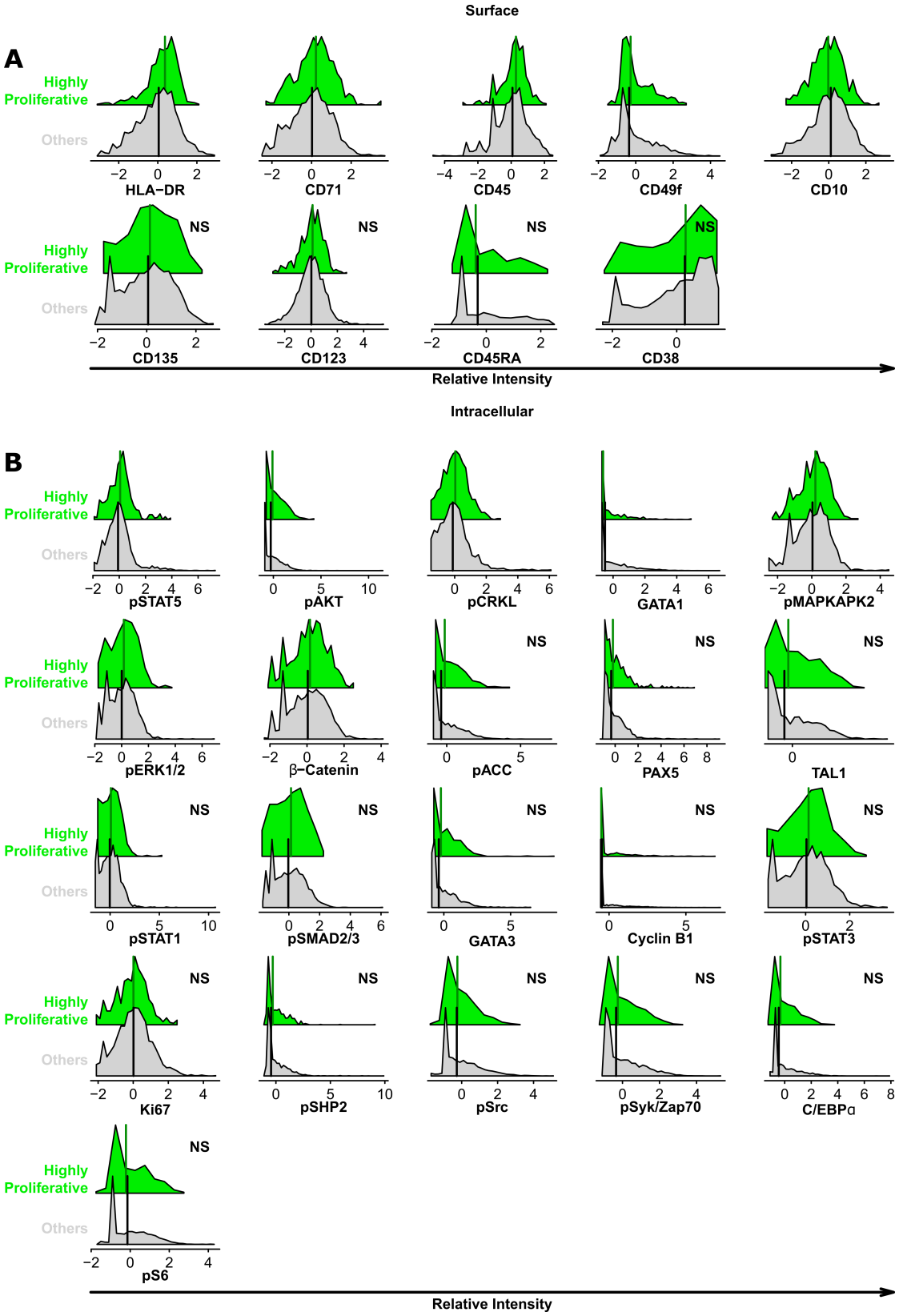
Surface
A
Highly Proliferative
Others
HLA−DR
CD71
CD45
CD49f
CD10
NS
CD135
CD123
CD45RA
CD38
Relative Intensity
Intracellular
B
pSTAT5
pAKT
pCRKL
GATA1
pMAPKAPK2
pERK1/2
β−Catenin
pACC
PAX5
TAL1
pSTAT1
pSMAD2/3
GATA3
Cyclin B1
pSTAT3
Ki67
pSHP2
pSrc
pSyk/Zap70
C/EBPα
pS6
Relative Intensity